

National Aeronautics and Space Administration  
John F. Kennedy Space Center



# Research and Technology 2004 Annual Report

NASA Technical  
Memorandum 2004-211535

Explore. Discover. Understand.

# **Research and Technology 2004 Annual Report**

**John F. Kennedy Space Center**

## Foreword

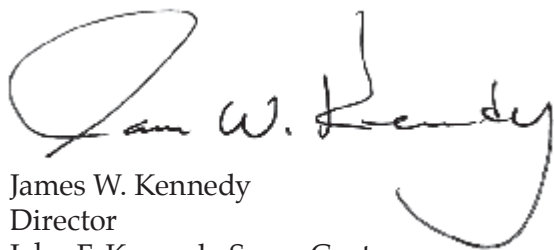
While the Agency undergoes change regularly, one thing remains the same—NASA's revolutionary and innovative approach to research and technology. Our NASA family, with the technologies we develop and apply, builds the solid Kennedy Space Center (KSC) foundation that enables endless possibilities.

Successful technology development and application projects are critical to KSC. When advanced technologies are infused in our systems, the outcomes are dramatically safer, more efficient, and more responsive spaceport and range operations for our customers. The KSC research and technology team includes a wide variety of partnerships among civil servants, contractors, academic institutions, and commercial industries.

KSC focuses its research and development activities on a list of KSC high-priority technology needs defined by our primary stakeholders, including current operational programs, future programs, and enabling technical programs. We focus and align our technology investments, personnel investments, new project proposals, and strategic partnerships with the technology needs most important to our stakeholders in order to maximize benefits for the Agency and the Nation.

Transformational spaceport and range technologies are required to enable new spacecraft processing and launch capabilities involving common, shared-usage equipment applicable to many different vehicles and payloads. These advanced technologies will benefit any Earth spaceport, lunar base, or Mars base.

This report highlights the successful results of KSC's stellar research and technology work during 2004. Dr. Dave Bartine, KSC Chief Technologist, is responsible for publication of this report and is the point of contact for any desired information. Contact him at 321-867-7069 or <David.E.Bartine@nasa.gov>.



James W. Kennedy  
Director  
John F. Kennedy Space Center

# CONTENTS

<b>Command, Control, and Monitoring Technologies .....</b>	<b>1</b>
Ground Camera Photogrammetry: 3-D Debris Trajectory Analysis .....	2
Ground Camera 3-D FOD Tracking Software .....	4
Particle Beam Propulsion: Simulations of an Electrostatic Sail Concept .....	6
First-Order Image Charge Calculator for Conducting Spheres .....	8
Implementation of an Automatic Particle Counter Using an Acoustic Transducer .....	10
Identifying and Quantifying Toxic Vapors Using an Electronic Nose .....	12
Small Gas Analyzer for NASA and Commercial Applications .....	14
Real-Time POSIX Threads for Linux .....	16
Electrostatic Radiation Shielding .....	18
Scaling Device Software for Measuring the Size of Remote Objects .....	20
Utilizing MIL-STD-1553B Digital Data Bus Devices Across an IEEE-1394A Serial Bus .....	22
 <b>Fluid System Technologies .....</b>	 <b>25</b>
Parameter Estimation of Spacecraft Fuel Slosh Mode .....	26
Color-Indicating Wipe for Cleaning Hypergolic Propellant .....	28
Highly Selective Membranes for Gas Separations .....	30
Solid Xenon Storage for Next-Generation Xenon Ion In-Space Propulsion .....	32
Highly Reliable Liquid Oxygen (LOX) Pump for Vehicle Loading .....	34
 <b>Range Technologies .....</b>	 <b>37</b>
Hexagonal Fractal Multiband Antenna .....	38
Aircraft Attitude Drift Correction Using a Heading-Based Reset Function .....	40
Passive Millimeter Wave Imaging .....	42
Effect of Clouds on Optical Imaging of the Space Shuttle During the Ascent Phase: A Statistical Analysis Based on a 3-D Model .....	44
Space-Based Telemetry and Range Safety (STARS) 2004 .....	46
Iridium Flight Modem .....	48
Autonomous Flight Safety System (AFSS) – Phase III .....	50
Latest Enhancements for the Microwave Scanning Beam Landing System (MSBLS) Flight Inspection System .....	52
Real-Time Telemetry Display System (RTTDS) .....	54
Advanced Data Description Exchange Services for Heterogeneous Vehicle and Spaceport Control and Monitoring Systems .....	56
Emerging Communication Technology (ECT) .....	58
Four-Channel IRIG-106 Telemetry Decoder on a PC-104 Plus Card .....	60
 <b>Spaceport Structures and Materials .....</b>	 <b>63</b>
Pressure Dependence of Insulator-Insulator Contact Charging .....	64
Electro-Optic Method of Surface Charge Measurement .....	66



## CONTENTS (continued)

Polyimide Wire Insulation Repair Material .....	68
Medium-Velocity-Contact Electrification Experiments With Martian Regolith Simulant .....	70
Development of the Dust Particle Analyzer To Characterize the Size and Charge of Particles Suspended in the Martian Atmosphere .....	72
Self-Assembled Monolayers on Aluminum 2024-T3 .....	74
Prediction of the Long-Term Corrosion Performance of Candidate Alloys for Launch Pad Applications Using dc Electrochemical Techniques .....	76
Electrochemical Impedance Spectroscopy of Alloys in a Simulated Space Shuttle Launch Environment .....	78
Nanotechnology for the Protection of Reinforcing Steel in Concrete Structures.....	80
Single-Coat / Rapid-Cure Protective Coatings for Lining Tanks on U.S. Navy Ships .....	82
Innovative High-Temperature Noise Reduction Materials .....	84
Paschen Breakdown Experiments in a Simulated Martian Atmosphere .....	86
A Wearable Electrostatic Hazard Detection System.....	88
Development of Rocket Acoustic Prediction Tool (RAPT) .....	90
Moisture-Resistant Thermal Protection System (TPS) Materials .....	92
<b>Process and Human Factors Engineering Technologies .....</b>	<b>95</b>
Toolkit for Enabling Adaptive Modeling and Simulation (TEAMS) .....	96
Human Factors Investigation Refinements.....	98
Schedule and Activity Generator/Estimator (SAGE).....	100
Generic Simulation Environment for Modeling Future Launch Operations (GEM-FLO) .....	102
Shuttle Operations Simulations .....	104
Shuttle Operations Root Cause Analysis Database.....	106
Integrated Human Factors Toolkit Comparison Matrix.....	108
AreaAdvisor – Spatial, Real-Time Resources Intelligence .....	110
System Reliability of Multielement Integrated Testing (MEIT) .....	112
Wing Leading-Edge Structural Subsystems and Reinforced Carbon-Carbon (RCC) Orbiter Processing Facility (OPF) Area/ Access Enhancements.....	114
TAL Site Heat Shield Removal Study.....	116
A Discrete-Event Simulation Model for Spaceport Operations (SPACESIM) .....	118
Virtual Testbed for Spaceport Models.....	120
NASA Faculty Fellowship Program (NFFP) 3-D Modeling.....	122
External Tank 3-D Model Creation Techniques .....	124
Orbiter Wing Tip Alignment Tool.....	126

## CONTENTS (continued)

<b>Biological Sciences.....</b>	<b>129</b>
Advanced Life Support Research: Systems Analysis of Waste .....	130
Advanced Life Support Research: Systems Analysis of Clothing .....	132
Porous Tube Insert Module (PTIM) Assembly and Integration: A Modular Tray Supporting Both Porous Tube and Substrate Nutrient Delivery Systems for Plant Studies in Space .....	134
Plant Lighting Systems.....	136
Bioluminescent Monitoring of Opportunistic Pathogens in the Spacecraft Environment.....	138
Sensing and Control System Development in Support of the Water Offset Nutrient Delivery ExpeRiment (WONDER) .....	140
Challenges Utilizing Nonmetallic Materials in the Development of the Advanced Biological Research System (ABRS) .....	142
Transgenic Arabidopsis Gene Expression System (TAGES) Imaging System (TIS).....	144
Role of Finite-Element Analysis Techniques in the Development of Life Science Payloads .....	146
Denitrification Composter To Stabilize Space Mission Trash.....	148
Development of a VOC Filter Cartridge for Biological Experiments in Space .....	150
Advanced Life Support (ALS) Project: International Space Station (ISS) Baseline Environmental Crop Studies .....	152
Evaluation of an Aerobic Rotational Membrane System for the Treatment of Graywater Waste Streams....	154
In Situ Heavy-Metal Contaminant Removal Using Emulsified Iron .....	156
 <b>Appendix A: KSC High-Priority Technology Needs .....</b>	 <b>159</b>
 <b>Appendix B: Florida Space Research and Education Grant Program.....</b>	 <b>164</b>
 <b>Index.....</b>	 <b>167</b>

# Primary Stakeholders for KSC Technology



**Shuttle Processing**



**Launch Services Program**



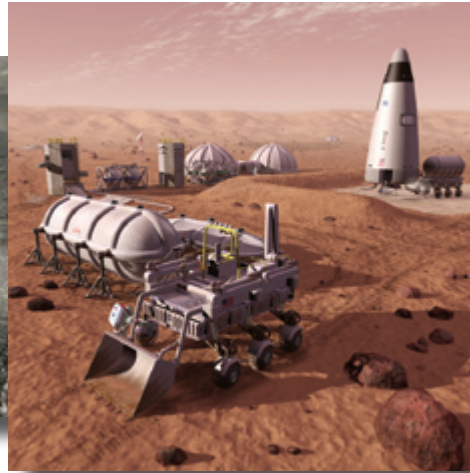
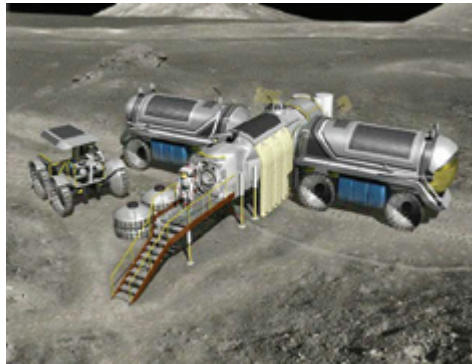
**International Space Station/  
Payload Processing**



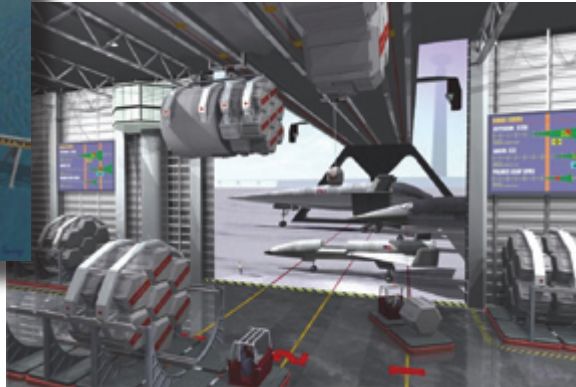


# Development and Application Activities

## Human and Robotic Exploration



## Future Spaceports and Ranges



## Enabling Technical Programs

- Safety and Mission Assurance
- Institutional Facilities and Equipment
- Information Technology and Communication Services

# Introduction

The John F. Kennedy Space Center's (KSC) outstanding record of achievements has earned it an honored place in history and an essential role in Space Transportation Systems of today and tomorrow. KSC is increasing the momentum in technology development for current and future spaceports. KSC's dual mission includes space launch operations and spaceport and range technology development. KSC's technology development and application efforts support NASA's goals of increased safety, reduced cost of space access, and rapid expansion of commercial markets by infusing spaceport technologies into all facets of current and future Space Transportation Systems.

KSC's background as the nation's premier launch site creates an ideal environment for spaceport and range technology development and applications. KSC's knowledge, expertise, facilities, and equipment provide technologies and processes to customers who propose to build and operate spaceports on Earth, lunar bases, Mars bases, and beyond. KSC has three strategic lines of business: Spaceport Operations, Spaceport Design and Systems Development, and Spaceport and Range Technology and Science. These strategic lines of business are illustrated on the facing page. KSC has unparalleled expertise in designing, building, and operating a spaceport with all of its complex technologies and systems.

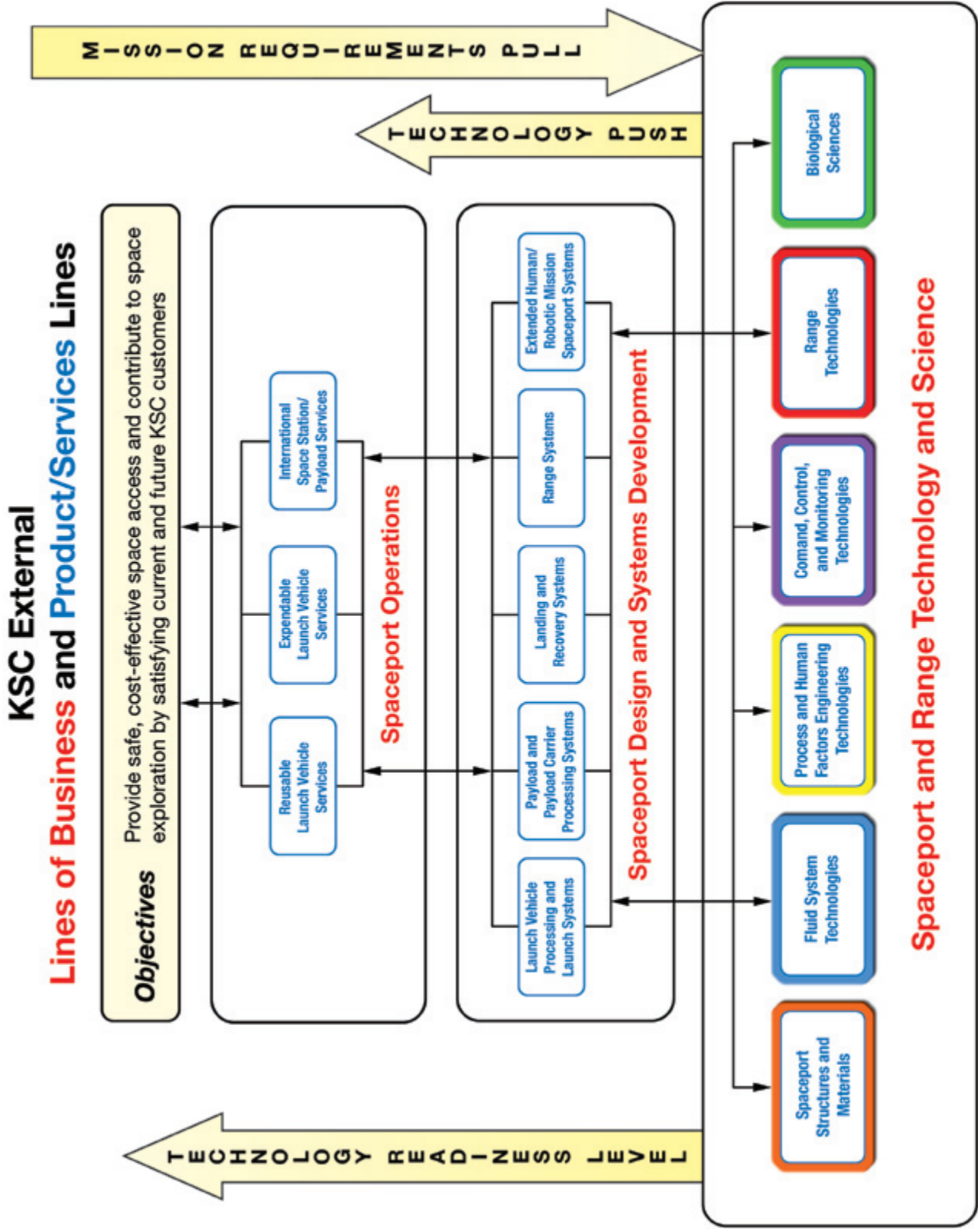
KSC technology development activities are categorized by six Spaceport Technology and Science Product Lines – Fluid System Technologies; Spaceport Structures and Materials; Process and Human Factors Engineering Technologies; Command, Control, and Monitoring Technologies; Range Technologies; and Biological Sciences. This report is organized by KSC's six Spaceport Technology and Science Product Lines.

The primary stakeholders for spaceport and range technologies are current operational programs and future programs. These stakeholders are illustrated on pages vi and vii. KSC aggressively seeks industry participation and collaboration in its research and technology development initiatives. KSC also seeks to transfer its expertise and technology to the commercial sector and academic community. Programs and commercialization opportunities available to American industries and other institutional organizations are described in the Technology Transfer Office Internet Web site at <<http://technology.ksc.nasa.gov>>. Electronic versions of the KSC Research and Technology Reports can be found at <<http://rtreport.ksc.nasa.gov>>.



KSC focuses its research and development activities on a list of KSC High-Priority Technology (HPT) Needs defined by our primary stakeholders, including current operational programs, future programs, and enabling technical programs. We focus and align our technology investments, personnel investments, new project proposals, and strategic partnerships with the technology needs most important to our stakeholders in order to maximize benefits for the Agency and the nation. The reports of research and technologies for 2004 that support the KSC HPT Needs display the HPT icon. The full list of KSC HPT Needs appears in Appendix A.





# Command, Control, and Monitoring Technologies

Command, Control, and Monitoring (CCM) Technologies help enable future affordable, responsive, and safe spaceports. These spaceports can be Government-owned, commercial, orbital, or nonterrestrial. The goal is to reduce the cost of access to space while increasing safety. CCM Technologies can help in this role through the reduction and elimination of unique interface and infrastructure requirements. As we move away from a one-for-one cardinality between launch vehicle and ground infrastructure toward a truly many-to-many paradigm, we must shift our thinking about how we process and launch spacecraft. Spacecraft will have to become smarter and be in control of their spaceport processing, requesting needed services from the spaceport, as opposed to the smart spaceport telling the vehicle that it is now OK to fly. We must strive to remove complexity not only in the design but also in how information is presented to humans, wherever they may be in the loop, and provide decision support. Increases in processing requirements throughout the spaceport will drive advancements in the communication infrastructure, capability, and security. Finally, when dealing with human spaceflight, we need to support robust, fault-tolerant designs in both the software and hardware systems. The technology focus areas that will drive the roadmap toward that ultimate vision include the following:

- Sensors and Data Acquisition
- Spaceport Processing and Health Maintenance
- Advanced Software and Computing Architectures
- Simulation and Situational Awareness

*For more information regarding Command, Control, and Monitoring Technologies, please contact David Kruhm ([David.A.Kruhm@nasa.gov](mailto:David.A.Kruhm@nasa.gov)), YA-D5, (321) 867-6742, or Robert Waterman ([Robert.D.Waterman@nasa.gov](mailto:Robert.D.Waterman@nasa.gov)), YA, (321) 867-6680.*

# Ground Camera Photogrammetry: 3-D Debris Trajectory Analysis



Resource/  
Personnel/FOD  
ID & Tracking

Routine analysis of launch video images is critical to Space Shuttle operations at Kennedy Space Center. Specifically, there is an important need to quantitatively determine the location, speed, and direction of movement of foreign object debris (FOD) in the vicinity of the vehicle during the first few minutes of ascent. A 3-D FOD trajectory analysis is accomplished by acquiring image data from multiple cameras that view simultaneous events, such as FOD trajectory. A minimum of two cameras viewing an event from two different perspectives, where the angle between the camera view lines is in the approximate range of 15 to 165 degrees, provides the necessary data to determine an estimate of the  $(x,y,z)$  position of an object of unknown origin. Measuring the 3-D position of an object moving relative to a fixed background in a set of sequential image frames directly leads to an estimate of object position, velocity, and acceleration. The technical approach to this problem is based on the principles of 3-D photogrammetry, a well-known technique in the field of aerial surveying and 3-D computer-aided design (CAD)/computer-aided engineering (CAE) modeling.

The current mathematical method developed for this application is based on a non-recursive numerical technique that relies on a matrix inversion. The computational speed improvement is several orders of magnitude (100 or 1,000 times improvement) over a previous method used.

$$\begin{pmatrix} m \\ n \end{pmatrix} = \left\{ \begin{pmatrix} R_x & R_y & R_z \end{pmatrix} \begin{pmatrix} x \\ y \\ z \end{pmatrix} + 1 \right\}^{-1} \left\{ \begin{pmatrix} a_x & b_x & c_x \\ a_y & b_y & c_y \end{pmatrix} \cdot \begin{pmatrix} x \\ y \\ z \end{pmatrix} + \begin{pmatrix} m_0 \\ n_0 \end{pmatrix} \right\} + \begin{pmatrix} m_c \\ n_c \end{pmatrix} \quad (1)$$

Equation (1) represents a generalized camera model, where the unknown camera parameters are  $a_x, b_x, c_x, a_y, b_y, c_y, R_x, R_y, R_z, m_0$ , and  $n_0$ . The constants  $(m_c, n_c)$  are the image coordinates of the camera optical axis, usually corresponding to the center of the image. An error function  $E = E(a_x, b_x, c_x, a_y, b_y, c_y, R_x, R_y, R_z, m_0, n_0)$  can be formed from the camera model, Equation (1), using reference points visible in the camera image. Each of the  $k$ th reference points consists of five known values: three world coordinates,  $(x_k, y_k, z_k)$  and two image pixel coordinates  $(m_k, n_k)$ . The error function is a function of the 11 camera parameters. Finding the minimum of  $E$  provides an estimate of the optimum set of 11 parameters required by Equation (1). The most practical method of finding the minimum of  $E$  is to locate the point in the 11-dimensional parameter space where the gradient of  $E$  is equal to zero.

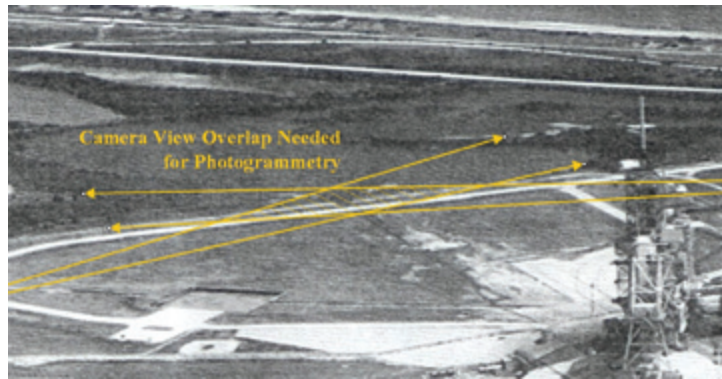
Consider multiple cameras viewing the same object at the unknown position  $(x,y,z)$ . Synchronized (or temporally interpolated) image data from two or more cameras can be combined, again using an error minimization strategy. In this case, an error function  $E(x,y,z)$  can be defined by summing the difference terms for all cameras. The unknown coordinates can be found by setting the gradient of  $E$  to zero and finding the solution. Setting the gradient of  $E$  to zero leads to the solution of the unknown position  $(x,y,z)$ .

## Key accomplishments:

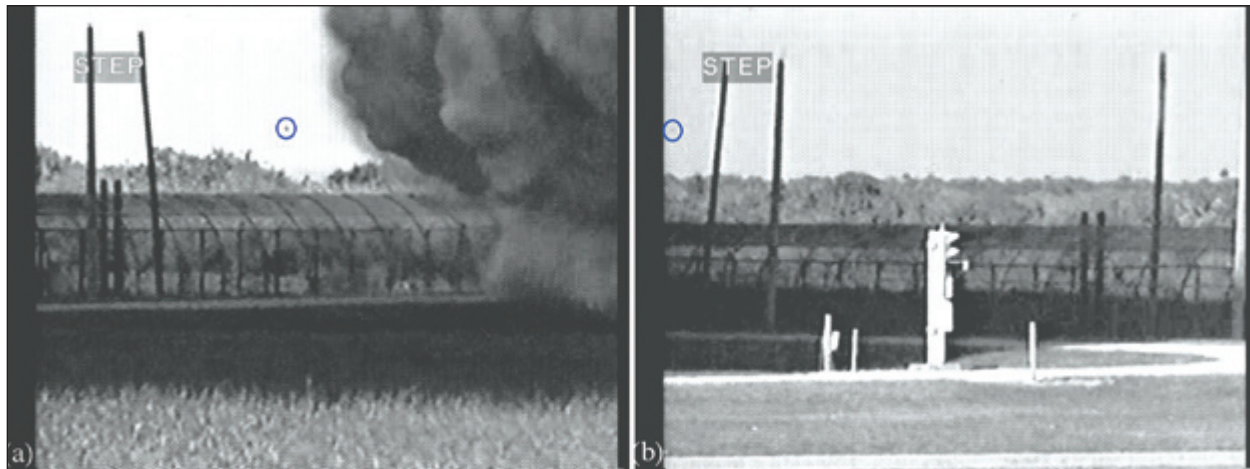
- Developed a generalized camera math model, valid for both near and far fields.
- Implemented a nonrecursive solution based on a linear error function.

Contact: Dr. R.C. Youngquist ([Robert.C.Youngquist@nasa.gov](mailto:Robert.C.Youngquist@nasa.gov)), YA-C3-E, (321) 867-1829

Participating Organization: ASRC Aerospace (Dr. J.E. Lane and S.J. Klinko)



Camera view lines for launch pad perimeter fence FOD trajectory analysis.



Perimeter fence section study: (a) view from camera 1; (b) view from camera 2 (blue circles show unknown debris object viewed by two cameras).



## Ground Camera 3-D FOD Tracking Software



Resource/  
Personnel/FOD  
ID & Tracking

A stand-alone 3-D foreign object debris (FOD) trajectory analysis software package was developed at Kennedy Space Center to analyze Shuttle launch film and video images using methods of 3-D photogrammetry (see *Ground Camera Photogrammetry: 3-D Debris Trajectory Analysis*).

The software methodology depends on obtaining sequential image frames of the FOD event. The frames can be in almost any standard image file format (bmp, jpg, tif, dpx, etc.). Image frames for two or more different points of view are needed to process the FOD event. The points of view must be located at an angle between 15 and 165 degrees relative to each other when viewing the FOD event.

The software user manual describes the operation and proper use of the 3-D FOD Vision Trajectory Location Software. The software is referred to simply as FOD Vision. As a test of FOD Vision, the software processed scanned film and video images from ground cameras E212 and ET208 of the launch of STS-107. However, before running the software, a reference point database is created from Shuttle computer-aided design (CAD) structure data of the Orbiter, External Tank, and Solid Rocket Boosters. Approximately seven reference points of key features are entered into the database, as shown in Figure 1. The software then calculates camera model parameters and stores the values for later use.

Once the camera model parameters are determined for each camera (there is no real limit on the number of cameras used), "image stitching" is performed to merge the multiple camera views into a single 3-D solution. Precise measurements are achieved by first synchronizing camera data using a linear trajectory interpolation algorithm, operating on each 2-D image. This process is performed automatically by the software. Trajectory values are finally calculated, including position and velocity, as well as approximate FOD size, as shown in Figure 2.

### Key accomplishments:

- A stand-alone FOD trajectory analysis software package was developed to perform 3-D photogrammetry analysis.
- This software was delivered to the NASA Film Analysis Laboratory for evaluation and comparison to other COTS software products.

### Key milestone:

- The software will be evaluated against other COTS software, such as RealViz, and may become an operational Film Analysis Laboratory tool in the future.

Contact: Dr. R.C. Youngquist ([Robert.C.Youngquist@nasa.gov](mailto:Robert.C.Youngquist@nasa.gov)), YA-C3-E, (321) 867-1829

Participating Organization: ASRC Aerospace (S.J. Klinko and Dr. J.E. Lane)



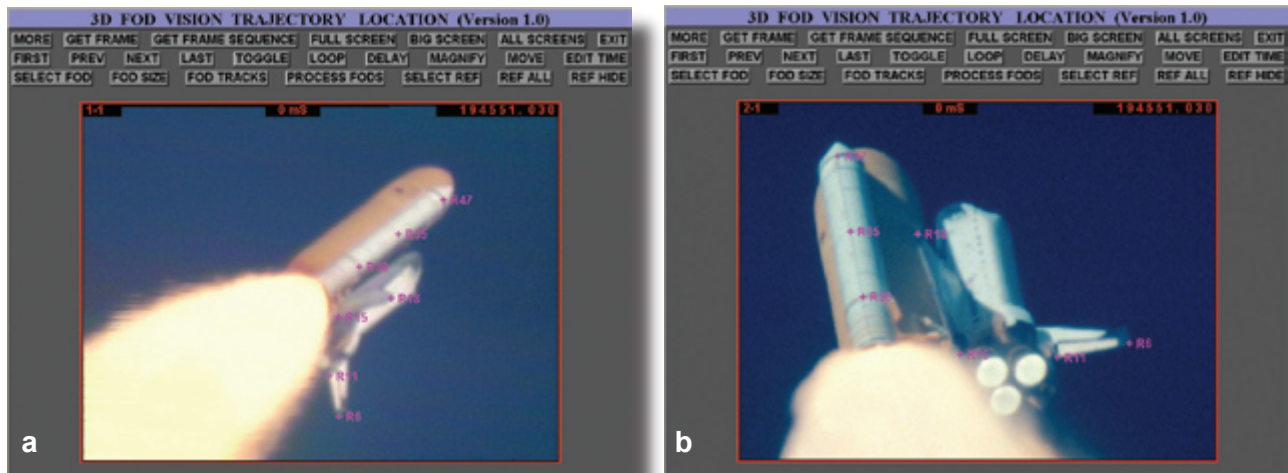


Figure 1. Vehicle reference point placement from camera views (a) E212 and (b) ET208.

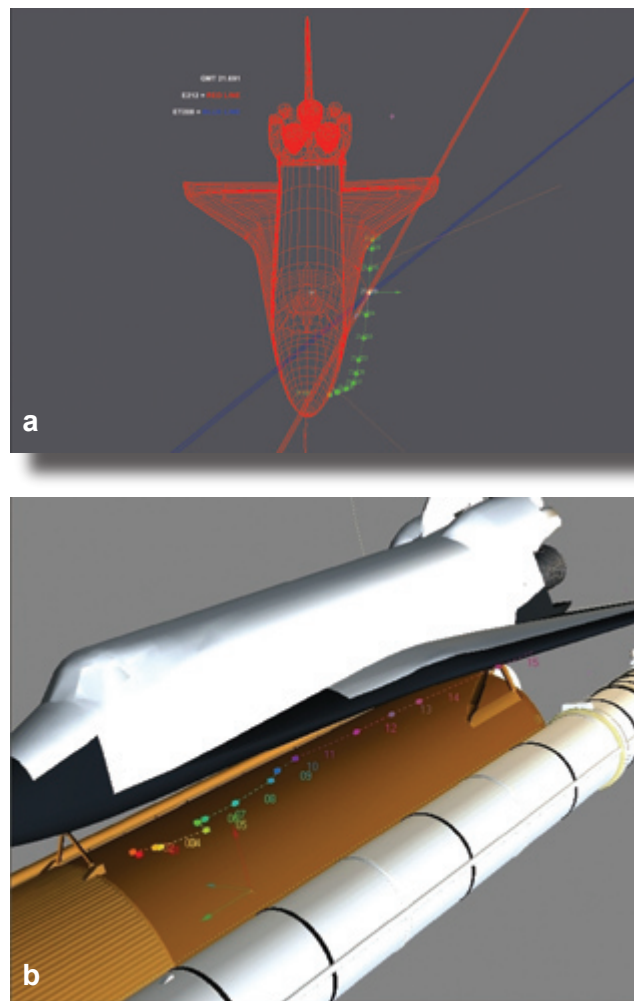


Figure 2. Two separate results of trajectory analysis: (a) presented to NASA Film Analysis Laboratory as part of the Columbia Accident Investigation Board and (b) results from FOD Vision.

## Particle Beam Propulsion: Simulations of an Electrostatic Sail Concept

An interplanetary propulsion system has been proposed that uses a finely focused particle beam, originating from a charged-particle generator on the Moon's surface. The beam pushes a spacecraft using the coulomb forces of the charged particle against a cluster of charged spheres attached to the spacecraft. Spherical geometry was studied since it is much easier to simulate. However, the shape of an operational electrostatic sail may resemble something very different.

The spacecraft is accelerated by means of the momentum transfer of the charged particles, scattered by the electric field of the electrostatic sail. Momentum transfer from a charged particle with velocity  $\mathbf{u}$ , can be computed by assuming conservation of the 4-momentum vector,  $\mathbf{P}$ :

$$\mathbf{P} = m_0 \gamma(u) \begin{pmatrix} u_x \\ u_y \\ u_z \\ 1 \end{pmatrix} \quad (1a)$$

where

$$\gamma(u) = (1 - \mathbf{u} \cdot \mathbf{u} / c^2)^{-1/2} \quad \mathbf{u} = \begin{pmatrix} u_x \\ u_y \\ u_z \end{pmatrix} \quad (1b)$$

and  $m_0$  is the rest mass of the particle.

The momentum transferred to the spacecraft for classical scattering (i.e., no energy loss due to radiation) is given by:

$$\Delta \mathbf{P} = \mathbf{P} - \mathbf{P}' = m_0 \begin{pmatrix} \gamma(u)u_x - \gamma(u')u'_x \\ \gamma(u)u_y - \gamma(u')u'_y \\ \gamma(u)u_z - \gamma(u')u'_z \\ \gamma(u) - \gamma(u') \end{pmatrix} \quad (2)$$

where the unprimed vector corresponds to the initial 4-momentum in the far field (i.e., outside the influence of the electrostatic spheres), and the primed vector corresponds to the final 4-momentum, after scattering, again in the far field. Note that far field is defined by the math model and software implementation as any point where the position vector  $\mathbf{r}$  of the particle satisfies  $|\mathbf{r}| \geq R_0$ .  $R_0$  is a model simulation constant.

The FORTRAN software implementation computes and logs the 3-momentum transferred to the spacecraft in a file named Pxfer.dat, where the 3-momentum is the first three components in Equation (2). The reported value of the 3-momentum  $\Delta \mathbf{p}$  is computed as the sum of all  $N$  particles in a run:

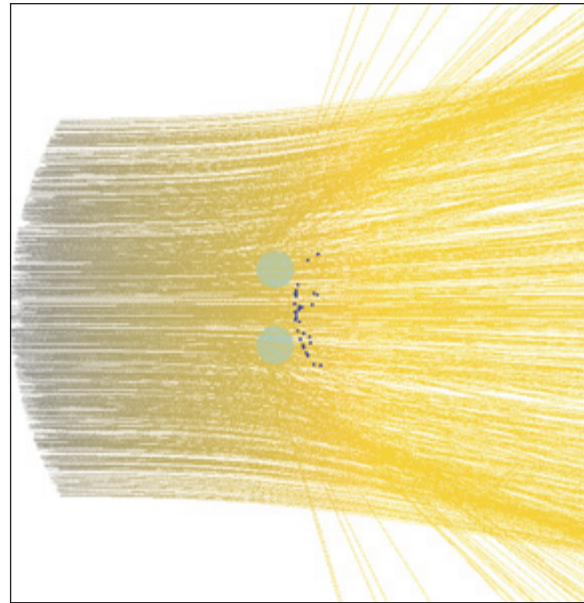
$$\Delta \mathbf{p} = m_0 \sum_{k=1}^N [\gamma(u_k) \mathbf{p}_k - \gamma(u'_k) \mathbf{p}'_k] \quad (3)$$

## Key accomplishments:

- Developed a simulation of the momentum transfer due to charged particles scattered by a cluster of electrostatic sails.
- Devised a simple concept of steering based on controlling the voltage to parts of the sail.

Contact: Dr. R.C. Youngquist ([Robert.C.Youngquist@nasa.gov](mailto:Robert.C.Youngquist@nasa.gov)), YA-C3-E, (321) 867-1829

Participating Organizations: ASRC Aerospace (Dr. J.E. Lane) and YA-C3-E (P.T. Metzger)



Simulation of charged-particle flux from a focused particle beam, scattered by electrostatic sails.

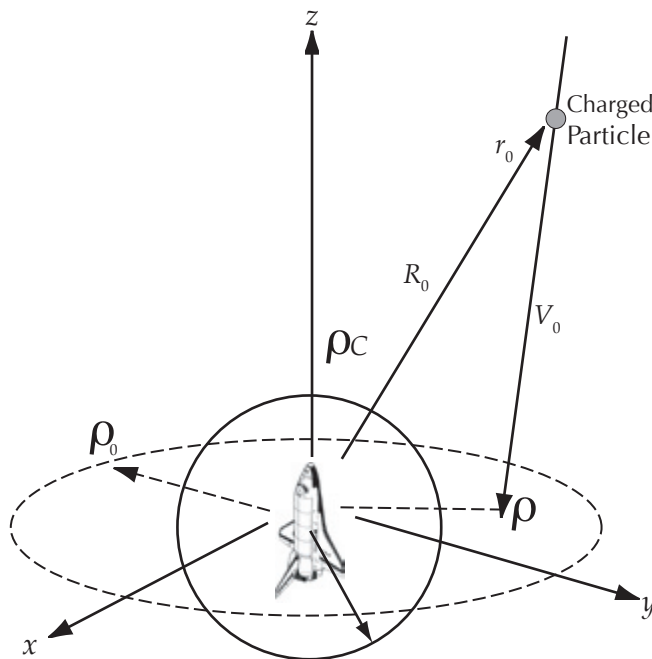
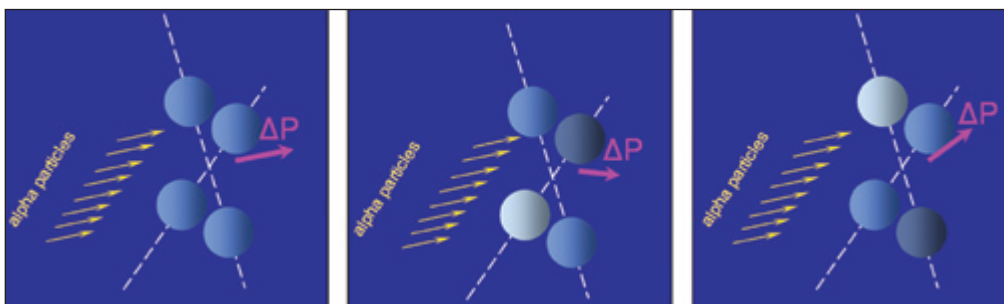


Diagram of charged particle intersecting sphere of influence of electrostatic sails (spheres).



Particle beam propulsion steering via asymmetric sphere voltages.



Steering achieved by modifying the momentum vector as a function of sphere voltages.

# First-Order Image Charge Calculator for Conducting Spheres



Radiation  
Protection  
Technologies

Using a first-order set of image charges, the voltage potential distribution due to interaction and spatial proximity of a cluster of conducting spheres is modified so that the error is reduced. The error is defined as the difference between the specified voltages on the sphere surfaces and the computed voltage from the point charge distribution on the sphere surfaces. This technique leads to a valuable improvement in the simulation accuracy of electrostatic shields and electrostatic sails. Image charge correction applied to the system of conducting spheres results in a configuration as depicted in the figures.

In the numerical/math model of the electrostatic radiation shield and beam propulsion sails, it was initially assumed that the electric field and voltage potential could be described by an equivalent single-point charge at the center of each conducting sphere. This assumption is reasonable when the spheres are separated by at least three diameters. Otherwise, the approximation rapidly degenerates as the intersphere spacing decreases.

The electric field potential, Equation (1), becomes a double summation over all  $N$  spheres, where there are  $N^2$  total charges,  $N$  zeroth-order charges, and  $N(N - 1)$  first-order image charges. The potential on the surface of sphere  $k$  can be expressed as

$$V_k = \frac{1}{4\pi\epsilon_0} \sum_{i=1}^N \left[ \frac{q_i}{|R_k \mathbf{e} + \mathbf{r}_k - \mathbf{r}_i|} + \sum_{\substack{j=1 \\ j \neq i}}^N \frac{q_{ij}}{|R_k \mathbf{e} + \mathbf{r}_k - \mathbf{r}_{ij}|} \right] = \sum_{i=1}^N C_{ki} q_i \quad (1)$$

where  $\mathbf{e}$  is any unit vector and

$$C_{ki} = \frac{1}{4\pi\epsilon_0} \sum_{j=1}^N \left[ \frac{1}{|R_k \mathbf{e} + \mathbf{r}_k - \mathbf{r}_i|} - \sum_{\substack{j=1 \\ j \neq i}}^N \frac{R_j}{|\mathbf{r}_j - \mathbf{r}_i| \cdot |R_k \mathbf{e} + \mathbf{r}_k - \mathbf{r}_{ij}|} \right] \quad (2)$$

where the image charge parameters are given by the following relations:

$$q_{ij} = -\frac{R_i}{|\mathbf{r}_i - \mathbf{r}_j|} q_j \quad \mathbf{r}_{ij} = \mathbf{r}_i - R_i^2 \frac{\mathbf{r}_i - \mathbf{r}_j}{|\mathbf{r}_i - \mathbf{r}_j|^2} \quad (3)$$

Since all charges are unknowns, the goal is to eliminate all  $q$ 's from Equation (1), which can also be expressed in matrix form as  $\mathbf{V} = \mathbf{C} \cdot \mathbf{q}$ , and then solving for  $\mathbf{q}$ :

$$\mathbf{q} = \mathbf{C}^{-1} \cdot \mathbf{V} \quad (4)$$

where  $\mathbf{V}$  is a vector of length  $N$  of sphere voltages  $V_k$ ,  $\mathbf{q}$  is a vector of length  $N$  of zeroth-order charges  $q_i$ , and  $\mathbf{C}$  is an  $N \times N$  array as described by Equation (2).

Since  $\mathbf{e}$  is a random unit vector,  $\mathbf{C}$  according to Equation (2) will not have a unique value. A better estimate of  $\mathbf{C}$  is obtained by averaging Equation (2) over many random unit vectors,  $\mathbf{e}_i$ :

$$C_{ki} = \frac{1}{4\pi\epsilon_0} \frac{1}{M} \sum_{l=1}^M \left[ \frac{1}{|R_k \mathbf{e}_l + \mathbf{r}_k - \mathbf{r}_i|} - \sum_{\substack{j=1 \\ j \neq i}}^N \frac{1}{|R_k \mathbf{e}_l + \mathbf{r}_k - \mathbf{r}_{ji}|} \frac{R_j}{|\mathbf{r}_j - \mathbf{r}_i|} \right] \quad (5)$$

Key accomplishment:

- A method to improve the numerical computation of the electric field potential due to a cluster of electrostatic conducting spheres was devised and successfully implemented in KSC's Electrostatic Radiation Shield model.

Key milestone:

- This method based on first-order images chargers can be used in future simulations involving electrostatic radiation shield models, such as those needed to develop a lunar base shield configuration.

Contact: P.T. Metzger ([Philip.T.Metzger@nasa.gov](mailto:Philip.T.Metzger@nasa.gov)),  
YA-C3-E, (321) 867-6052

Participating Organizations: ASRC Aerospace (Dr. J.E. Lane) and YA-C3-E (Dr. R.C. Youngquist)

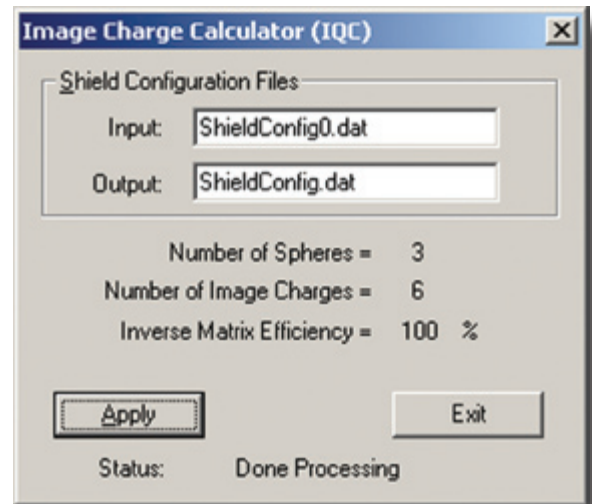


Image charge calculator GUI.

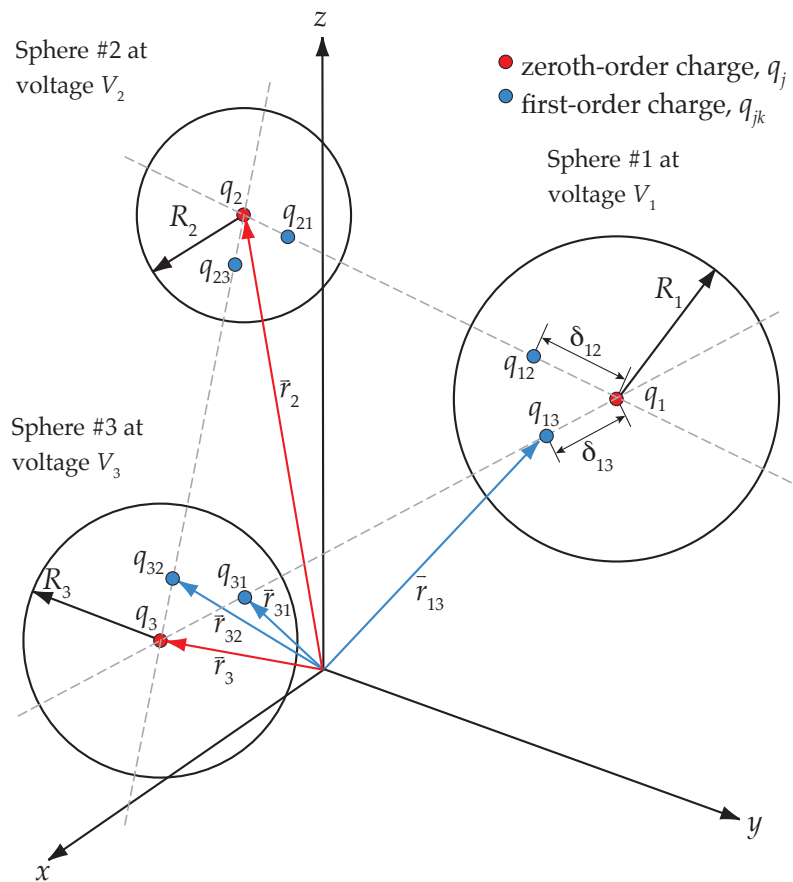


Image charge treatment of a system of conducting spheres.



# Implementation of an Automatic Particle Counter Using an Acoustic Transducer



Contamination  
Detection/Reduction/  
Cleaning

The objective of this research is to detect small (micron- and submicron-sized) airborne particles through acoustic means. Aerosol particle detection finds important applications in the commercial, military, and aerospace sectors and is of special importance in clean-room monitoring. To date, most particle detection and sizing have been done using costly laser-scattering devices or the more economical but relatively unreliable tape lift techniques. Researchers at KSC and the University of Central Florida (UCF) have developed a device able to detect airborne particles using an acoustic transducer. We will demonstrate the particle sizing and particle-concentration-measuring accuracy of the device compared to laser-scattering-based instruments.

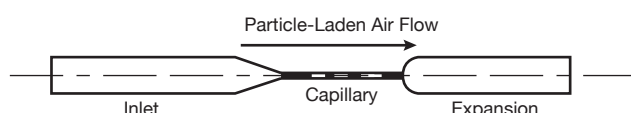


Figure 1. Acoustic transducer.

The acoustic transducer (Figure 1) is a small converging-diverging glass tube through which air is drawn. If the air is laden with particles and as the flow accelerates through the contracting inlet, the particles cannot follow the large change

in velocity because of their inertia, and vortices are generated as air flows over the particles. These vortices generate sound, which is amplified by the transducer inlet tube acting as an organ pipe. A microphone with the right sensitivity can be used to capture the sound emitted. The sound (which is distinctly audible) has been shown to contain the fundamental frequency (as well as the harmonics) of the air column inside the inlet portion of the transducer. The frequency and amplitude content of the microphone signal can be related to the size and, to some extent, shape of the particles.

The experimental setup and preliminary testing of the acoustic transducer have been completed (Figures 2 and 3). Two Plexiglas chambers are sealed and connected through the acoustic transducer. A vacuum is created in one chamber, and another chamber (containing all the instrumentation) is open to room air through a HEPA filter, which eliminates airborne room particles. A stream of dry air stirs and injects particles of known size (all particles are within 6 percent of the mean size) into the chamber. As particles pass through the transducer, they generate a high-frequency signal that decays within a few milliseconds (Figure 4). Notice that particles of different sizes generate signals with different amplitudes. For flows of sufficiently low particle concentration (which is the case in most applications), concentration can be calculated by counting the different signal peaks (Figure 4c) for a known air flow rate (redundantly measured in the experimental setup by a digital manometer and a rotameter).

Future experiments will use this setup to measure signals from spherical polystyrene latex (PSL) particles of known size using different transducers (i.e., different inlet lengths and capillary diameters) and thus generate a solid calibration set of data. The limits of the transducer in sizing submicron particles will be tested. Also, the transducer's ability to measure different concentrations will be determined. Previously, 15- $\mu\text{m}$  particles with concentrations down to 10 parts per liter were successfully measured by the acoustic transducer. Once calibration is performed, the setup will be opened to room air, signals will be collected from airborne room particles, and measurements will be checked against laser-scattering measurements of the same room air to determine the acoustic transducer accuracy. Ultimately, a fully automated

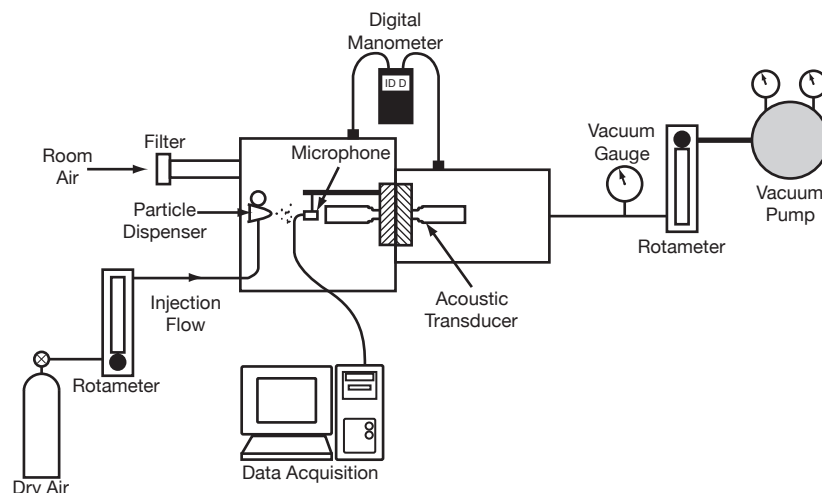


Figure 2. Experimental setup schematic.

air monitoring system will be sought where a single acoustic transducer will continuously provide particle size and concentration data from clean-room facilities. The system will be complete with online data logging services so that a time history of particle size distribution and concentration can be made available to laboratory managers.

#### Key accomplishments:

- Designed, fabricated, and tested vacuum chambers and instrumentation.
- Developed real-time data collection interface.
- Purchased TSI Aerodynamic Particle Sizer (APS 3321) for calibration and data comparison.
- Obtained proof-of-concept preliminary data.

#### Key milestones:

- Develop mathematical/Computational Fluid Dynamics codes to model two-phase flow through the acoustic transducer (October 2004).
- Collect data that could lead to empirical relationships between emitted sound power and particle diameter/size (October 2004).
- Present the project at selected aerosol monitoring conferences (2005).

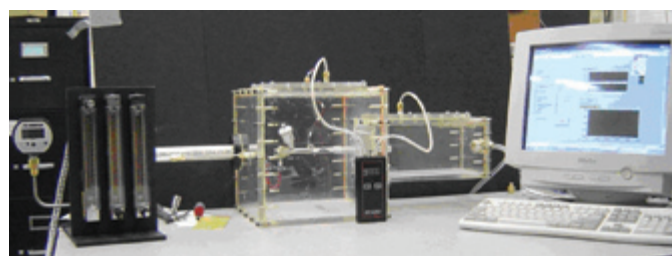


Figure 3. Acoustic transducer setup showing Plexiglas chambers, transducer, particle dispenser, rotameters, digital manometer, and data acquisition computer.

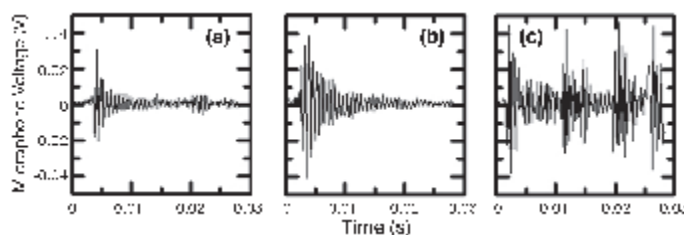


Figure 4. Microphone voltage signals gathered from acoustic transducer at a flow rate of 25 L/min. (a) 15- $\mu\text{m}$  particle; (b) 50- $\mu\text{m}$  particle; (c) signal train produced when several particles pass through the transducer.

Contact: G.F. Haddad ([George.F.Haddad@nasa.gov](mailto:George.F.Haddad@nasa.gov)), VA-F4, (321) 476-3658

Participating Organization: University of Central Florida (Dr. R.H. Chen and Dr. M. Chaos)

## Identifying and Quantifying Toxic Vapors Using an Electronic Nose



*Hazardous-Leak  
Detection & Isolation*

The ability to monitor the air quality in closed environments, such as those of the Shuttle, the International Space Station (ISS), and future human missions to Mars or the Moon, is important to ensure the health and safety of the astronauts. Postmission analyses of grab air samples from the Shuttle have confirmed the occasional presence of onboard volatile organic contaminants.

Contamination may also occur when astronauts bring dangerous levels of hypergols (hydrazine [HZ], monomethylhydrazine [MMH], and unsymmetrical dimethylhydrazine [UDMH]) into the airlock on their extravehicular activity (EVA) suits. When the airlock is pressurized, the contaminants are released in the airlock chamber, potentially contaminating the airlock and the breathing environment of the ISS or Shuttle, and thus causing a critical risk to crew and vehicle safety. Hypergols are very toxic and are suspected human carcinogens. In addition to hypergolic propellants, the ISS also uses ammonia in the cooling system, which is a corrosive toxic substance. Quick disconnect is used to replenish the ammonia, and leaks of ammonia are known to have happened.

On the ground, storage and transportation of hypergolic fuels present potentials for leaks and spills. Current technology can detect contamination down to 10 ppb but with a response time of 10 to 15 minutes.



*An Airsense e-nose controlled by a Palm handheld computer.*

A need therefore exists for a lightweight, low-power, miniature instrument that can monitor trace levels of contaminants in real time. In addition to identifying the contaminant, it is also important to quantify its concentration so appropriate action may be taken.

One promising technology is the electronic nose (e-nose). An e-nose consists of an array of nonspecific vapor sensors. In general, the sensor array is designed such that individual sensors respond to a broad range of chemicals, but with a unique sensitivity relative to the other sensors. The unique strengths of an e-nose are its small size, light weight, power efficiency, fast response, ease of use, and sensitivity to very low levels of contaminants. The e-nose is also very versatile; it can be “trained” to monitor many different contaminants and thus can detect the scenarios mentioned, as well as others, such as fire, that might compromise air quality in enclosed environments.

Previous research at KSC has demonstrated the ability of a COTS e-nose to detect hypergolic fuels and oxidizers, as well as a variety of volatile organic compounds, at concentrations near or below the 7-day space maximum allowable concentrations. Our research also showed that the pattern recognition procedures developed at KSC gave significantly better results than those provided by the COTS vendor.

Vapor identification is achieved by comparing the sensor response pattern of an unknown vapor to previously established patterns of known vapors using pattern recognition techniques. Statistical analysis methods are used for concentration estimation.

A prototype unit based on an Airsense e-nose was developed (see the figure). To reduce size, weight, and initial startup time, software was written to use a Palm handheld computer instead of the usual laptop as the user interface. The prototype has demonstrated a detection limit for Hz and MMH of 10 ppb with a response time of 90 seconds, a vapor identification success rate of over 95 percent, and a concentration estimation accuracy of  $\pm 5$  percent on average. It also demonstrated similar results with a variety of volatile organic compounds.

Key accomplishments:

- Developed algorithms that can identify vapors with 95 percent or better accuracy and quantify their concentrations to within  $\pm 5$  percent on average.
- Packaged a COTS e-nose, which normally requires a separate power supply and PC/laptop, into a portable unit (approximately 12 by 9 by 6 inches) with an 8-hour lithium battery and Palm handheld computer.

Contact: Dr. T.P. Griffin ([Timothy.P.Griffin@nasa.gov](mailto:Timothy.P.Griffin@nasa.gov)), YA-F2-C, (321) 867-6755

Participating Organization: ASRC Aerospace (Dr. B.R. Linnell)



## Small Gas Analyzer for NASA and Commercial Applications



*Hazardous-Leak  
Detection & Isolation*

A small mass spectrometer system initially designed at the Jet Propulsion Laboratory (JPL) and further developed by Intelligent Ion was evaluated at KSC. This system is small enough to fit inside a carry-on suitcase (Figures 1 and 2), yet has an analytical performance that approaches many benchtop mass spectrometer systems. Although still in the development phase, this system has very promising characteristics. These include a rapid setup time of 15 minutes (the time between unpacking the system and when the first scan can be taken); a dynamic range of approximately four orders of magnitude; a scan time of less than 1 second; and detection limits in the low ppm range for a wide variety of compounds, including common volatile organics and hydrazines. These characteristics make this unit one of the more promising systems in the emerging market of field-portable mass spectrometers.

Mass spectrometers not only are capable of quantifying compounds but can identify unknowns – even in a mixture. These systems can be very specific in component identification. This, coupled with a wide dynamic range, makes these analyzers very desirable. Unfortunately, mass spectrometers are generally very large and heavy, and developing field-portable units presents quite a challenge. It is important to NASA that the environments where personnel work and vehicles operate remain free of hazardous chemicals. Thus there is a need to develop systems capable of quantifying a vast mixture of airborne chemicals. With its ability to detect and monitor hydrazine and common volatile organic compounds (VOCs), this system promises to meet these needs. The table shows a short list of some representative compounds that are of interest to NASA as well as industry. Acetone and toluene are VOCs commonly found in manufactured equipment and are a concern in confined spaces, such as automobiles and spacecraft. Hydrazine (Hz), monomethylhydrazine (MMH), and unsymmetrical dimethylhydrazine (UDMH) are hazardous hypergolic fuels common to the aerospace industry. Representative spectra are shown in Figures 3 and 4.

*Detection limits for some representative compounds.*

Compound	Detection Limit (ppm)
Acetone	13.0
Toluene	0.1
Hz	23.0
MMH	3.0
UDMH	4.0

A new detector being developed will increase the sensitivity of the unit as well as improve the detection limits. A gas chromatograph (GC) interface is also being developed. The addition of a GC will provide better unknown identification in complex mixtures as well as improve detection limits. Improvements to the control software and user interface are an ongoing process to optimize system operation and reduce user interaction time required. This will reduce the labor costs associated with operating the system and reduce the human-factors errors.



### Key accomplishments:

- Detection of MMH and UDMH below 10 ppm in air.
- Detection of VOCs below 1 ppm in air.
- Scan time less than 1 second.
- Small and light for field portability.

### Key milestones:

- Installation of charge-coupled device detector.
- Coupling to GC.
- Software improvements.

Contact: Dr. T.P. Griffin ([Timothy.P.Griffin@nasa.gov](mailto:Timothy.P.Griffin@nasa.gov)), YA-F2-C, (321) 867-6755

Participating Organizations: Jet Propulsion Laboratory (J. Houseman), Intelligent Ion (G. Kibelka), and ASRC Aerospace (Dr. CR. Arkin)



Figure 1. System in operation.



Figure 2. The system is small and light for portability.

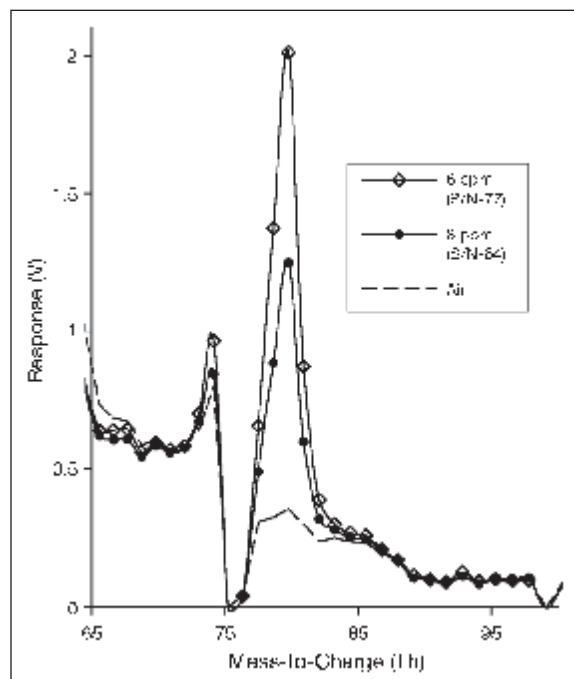


Figure 3. Toluene at various concentrations.

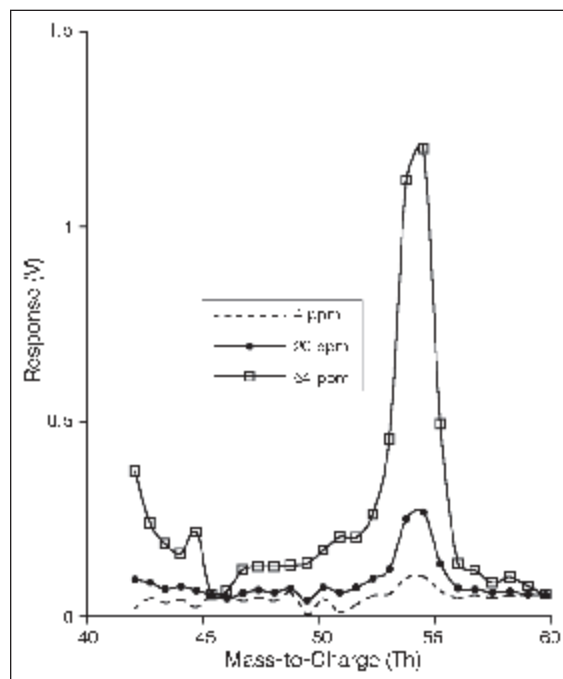


Figure 4. UDMH at various concentrations.

## Real-Time POSIX Threads for Linux



Seamless  
Command & Control  
Coordination

Successful implementation of the Exploration Program will require that NASA leverage and opportunistically facilitate cost-effective technologies. Control system development and life cycle costs must be reduced so early program deliverables do not impede later program deliverables. Tools to accomplish this will need to employ innovative architectures that can minimize the manpower required to configure and operate these control systems. Adoption of common tools, such as control systems and avionics testers, can reduce program costs through standard user applications and system applications. One of the largest life cycle costs of critical control systems is recertification. As the number of vendor products increases, the frequency of recertifications increases. Previous evaluations of mainstream open-source products have occurred before appropriate commercial momentum occurred. The open-source cost-shared model is actively supported by many companies as a formal part of their corporate product portfolio; therefore, NASA can safely invest in mainstream open-source products as part of a larger Government effort and have private industry pick up the majority of the long-term sustaining costs. The primary candidates are the Linux operating system, Linux native graphics interface, Apache Web server, and the MySQL relational database.

The goals of this project are to facilitate the use of cost-effective, open-source options for NASA software platforms and to promote the use of “open” national and international software standards for NASA projects. The Linux operating system is open-source <[www.kernel.org](http://www.kernel.org)> and is supported by companies such as Red Hat, Dell, IBM, HP, Sun, and Intel via Red Hat. POSIX is an Institute of Electrical and Electronics Engineers (IEEE), American National Standards Institute (ANSI), and International Standardization Organization standard for a Portable UNIX Operating System Interface. The use of open-source software, such as Linux, presents a tremendous opportunity to NASA for cost savings, while still meeting mission objectives for reliability and performance.

By writing programs to the POSIX interface standards, applications can be ported across multiple hardware and operating system platforms. For example, Microsoft Windows supports a subset of the POSIX standard as does Linux. The conclusion, then, is that coding to the POSIX standard provides the greatest benefits in terms of application longevity and portability. To save money, it is only necessary to examine the lowest-cost hardware/software combination that meets a project’s requirements and supports the subset of POSIX needed for the job.

One of the additions to POSIX to support the development of real-time embedded systems is the Threads interface. A “thread” in operating systems lingo is a lightweight process. The Threads Application Programming Interface (API) supports concurrent programming; that is, a program with many parallel or synchronized actions. The Threads API also supports methods for real-time concurrent programming.

Future NASA projects could benefit from the adoption of Linux as an implementation platform. However, the Linux POSIX Threads (PThreads) libraries do not support the real-time features needed for embedded applications. Thus, this project investigated the current state of real-time PThreads support in Linux and planned enhancements in areas where real-time functions were lacking. Coincidentally, the Windows Threads library also does not support the real-time POSIX features. More information on Threads programming can be found in *Programming with POSIX Threads* by David R. Butenhof.

In examining the “open” source code for IBM’s Next-Generation POSIX Threads (NGPT) Project, RedHat’s GNU C library Native POSIX Threads Library (NPTL), and the POSIX Threads

for Win32 Project, it was discovered that none of the projects implemented the priority protocols to address the priority inversion problem. Thus, on both the Windows and Linux platforms, there were no available solutions. Recently, the IBM project was canceled so as not to compete with NPTL, which was adopted as the Linux “standard.”

Both Windows and Linux had the further defect that thread priority was only “suggestive;” that is, two threads, one at priority 4 and the other at priority 5, would both execute simultaneously. Clearly, there was more than one problem to address, but since the priority protocols were not implemented at all as opposed to being poorly implemented, it was decided to address the protocols first.

The project began as simply an effort to fix current implementations, but it quickly became apparent that it would be necessary to implement a new POSIX Threads library from scratch with two major requirements. The first requirement was that priority-based programs had to execute correctly with the new library. “Correctly” just means the results are members of the set of all possible results from a valid interleaving of execution. The second requirement was that the library had to run on both Windows and Linux. Both requirements are unique and important. Neither is implemented by any current library.

The new POSIX Threads library has been implemented but only for private scope methods. The public scope methods depend on the UNIX “fork” system call and shared memory, which restricts their use to only Linux. The table lists the library’s prealpha test status for Win32.

Key accomplishments:

- The library contains 128 files and 5,873 lines of C code.
- The initial version of the library was implemented in 6 weeks.
- Two freely available test suites were used for validation: the NPTL suite contains 217 programs and the Win32 suite contains 93 programs.
- The library runs on both Fedora Core 2 Linux and Windows XP.
- An open-source Web site was created <<http://bcook.cs.GeorgiaSouthern.edu/pthreads>>.

Contact: E.J. Schafer ([Eric.J.Schafer@nasa.gov](mailto:Eric.J.Schafer@nasa.gov)), YA-D8, (321) 861-7674

Participating Organization: Georgia Southern University (Dr. R.P. Cook)

#### New Library Win32 test status 7/20/04

Test Name	Pass-Fail	Test Name	Pass-Fail	Test Name	Pass-Fail	Test Name	Pass-Fail	Test Name	Pass-Fail	Test Name	Pass-Fail
barrier1	P	cleanup3	P	delay2	P	mutex1r	P	mutex8r	P	self2	P
barrier2	P	condvar1	P	equal1	P	mutex2	P	once1	P	semaphore1	P
barrier3	P	condvar1b	P	earno1	F	mutex3	P	priority1	F	semaphore2	P
barrier4	P	condvar2	P	exception1	F	mutex3e	F	priority2	F	sizes	P
barrier5	P	condvar2b	P	exception2	F	Mutex3r	F	reuse1	P	spin1	P
barrier6	P	condvar3	P	exception3	F	mutex4	P	reuse2	P	spin2	P
cancel1	P	condvar3b	P	exit1	P	mutex5	P	rwlock1	P	spin3	P
cancel2	F	condvar3c	P	exit2	P	mutex6	P	rwlock2	P	spin4	P
cancel3	F	condvar3d	P	exit3	P	mutex6e	P	rwlock2b	P	tryentercs	F
cancel4	F	condvar4	P	exit4	F	mutex6es	F	rwlock3	P	tryentercs2	F
cancel5	F	condvar5	P	exit5	F	mutex6s	F	rwlock3b	P	tsd1	P
cancel6	F	condvar6	P	join0	P	mutex6n	P	rwlock4	P	valid1	P
cancel6a	F	condvar7	P	join1	P	mutex6r	P	rwlock4b	P	valid2	P
cancel6d	F	condvar8	P	join2	P	mutex7	P	rwlock5	P		
cancel7	F	condvar9	P	join3	F	mutex7e	P	rwlock5b	P		
cancel8	F	context1	F	kill1	P	mutex7n	P	Rwlock6	P		
cancel9	F	count1	P	loadfree	F	mutex7r	P	rwlock6b	P		
cleanup0	P	create1	P	mutex1	P	mutex8	P	rwlock6c	P		
cleanup1	P	create2	P	mutex1e	P	mutex8e	P	rwlock7	P		
cleanup2	P	delay1	P	mutex1n	P	mutex8n	P	self1	P		

## Electrostatic Radiation Shielding



Radiation Protection  
Technologies

Human exploration and development of the solar system are not possible without space radiation shielding to protect the crew and the spacecraft. The radiation damages biological tissues and causes either severe, immediate effects (death within a matter of weeks) or cumulative, long-term effects (increase of lifetime cancer risk).

Arbitrary electrostatic fields may be decomposed mathematically into an infinite superposition known as a “multipole expansion,” whose lowest-order term is the monopole component, followed by the dipole, quadrupole, etc. The components decrease in strength in inverse proportion to the distance. Therefore, it should be possible to assign different shielding functions to each term in a multipole expansion of the fields. For example, a very strong quadrupole term may dominate the physics closest to the spacecraft, while a weaker but farther-reaching monopole term dominates the physics farther away, thus producing “shells” of protection surrounding the spacecraft without the constraints of excessive mass and magnetic plasma containment proposed by other approaches.

The quadrupole term may be assigned to repel positively charged particles, including those at very high energy (protons and high-Z-energy particles encountered in smaller quantities), while the weaker monopole term may be assigned to repel the vast quantity of electrons that need only to be brushed away from the quadrupole-dominated region to prevent the electrostatic field from accelerating them into the spacecraft. On the other hand, the high-energy, positively charged particles and the much higher-quantity, lower-energy, positively charged particles (which are part of the solar wind) will both be repelled by the large quadrupole term dominating the region immediately around the spacecraft. Hence, it is possible for one multipole expansion to solve all parts of the shielding problem.

This arrangement can be easily deployed in space using lightweight structures. The charge that creates the electric field may be driven onto the surface of lightweight balloons that self-inflate under the coulomb force when the voltage is applied. That voltage may be created by simple electrostatic generators, such as a Van de Graaf machine. The current output from such a device is very low, but likewise, the influx of solar and galactic particles onto the balloons is also very low. It is therefore feasible for the generators to sustain the voltage. Tethers and lightweight, flexible rods may be sufficient to deploy the balloons around the spacecraft. Thus, the entire system is low-mass and depends only upon well-known technology. Some improvement is needed in the electrostatic generators to provide the level of voltage needed to protect against the largest solar flare protons and against the most significant flux of high-Z-energy particles, but this improvement seems achievable.

A model was written in Fortran to simulate the trajectories of high-energy charged particles in the presence of a set of charged balloons. Both isotropic and directional radiation versions were developed. See Figure 1 for a typical user interface and Figure 2 for the output of a simulation. The distribution of charges on the balloons was largely uniform as long as the spacing between balloons exceeded three times their diameter. A future model version is expected to more accurately predict the fields that result from the actual (nonuniform) charge distribution.

Shielding efficiency (the percentage reduction in the number of particles striking the protected region, as a function of particle energy) was calculated for a sample shield geometry using several different voltages on the spheres (Figure 3). The research indicates that asymmetrical



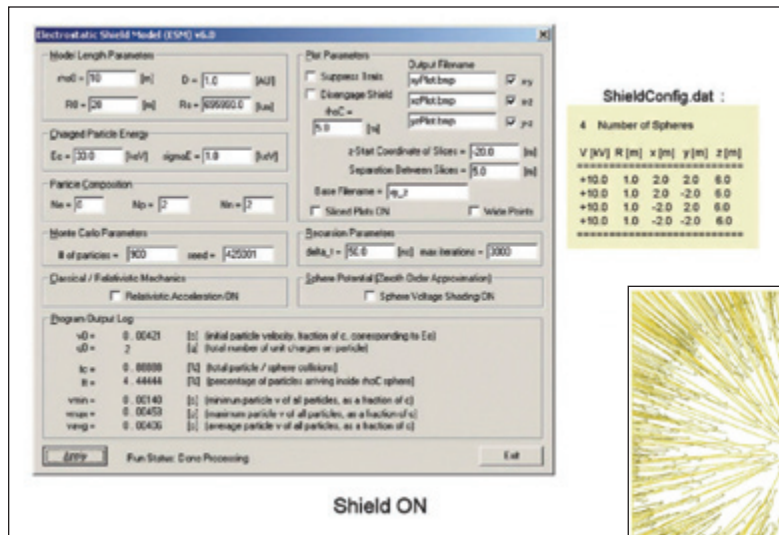


Figure 1. Radiation and beamed propulsion model user interface.

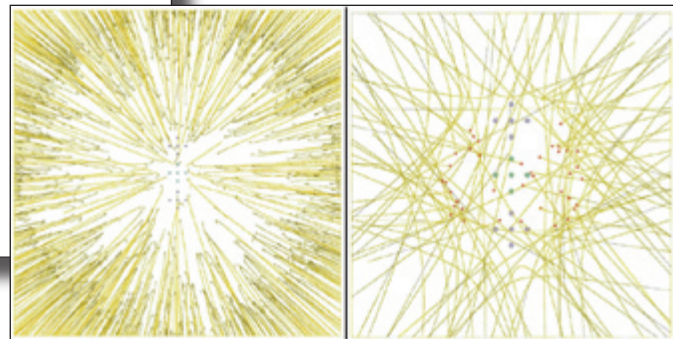


Figure 2. Views of 3-D particle trajectories for isotropic protons (left) and isotropic electrons (right) repelled over a wide region. Protons are repelled from the central region (the spacecraft). No particles reach the spacecraft.

electrostatic shielding is feasible if the electrostatic voltages are a factor of 40 greater than what is currently available using Van de Graaf generators on Earth. This seems achievable for two reasons. First, in space greater electric fields can be sustained because there is no risk of atmospheric ionization; therefore, multiple generators can be connected in series to increase the voltages, which is sufficient by itself to solve the problem. Second, until now there has been no motivation to improve electrostatics generators in a way that will support typical applications in space, where there is no atmosphere, no ever-present ground plane, and more spatial freedom. Consequently, this immature technology can be expected to advance rapidly.

Even if multipole electrostatics used in conjunction with passive shielding cannot stop the most energetic galactic cosmic ray (GCR) particles, the technology will provide a dramatic improvement over passive shielding alone, which cannot sufficiently reduce flux for the most powerful solar particle events (SPEs) without the addition of excessive mass. Electrostatics with very little mass will deflect the entire flux up to a particular energy level. It will also reduce the energy of those GCR particles that get through, thereby reducing secondary radiation. Thus, electrostatic protection against SPEs, coupled with passive shielding against the highest-energy GCR particles, may provide the optimal solution.

Contacts: Dr. R.C. Youngquist ([Robert.C.Youngquist@nasa.gov](mailto:Robert.C.Youngquist@nasa.gov)), YA-C3-E, (321) 867-1829; and P.T. Metzger, YA-C3-E, (321) 867-6052

Participating Organization: ASRC Aerospace (Dr. J.E. Lane)

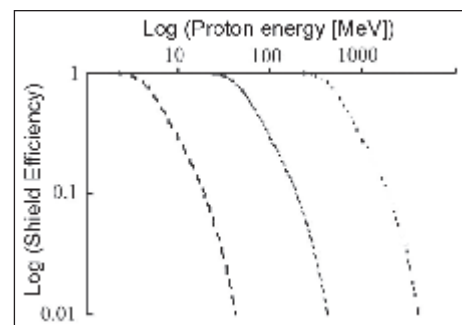


Figure 3. Shield efficiency versus proton energy (center line: nominal shield voltages, left line: 1/10 voltages, right line: 10 times voltages).

# Scaling Device Software for Measuring the Size of Remote Objects



Defect/Damage  
Location & Spacecraft  
Handling Systems

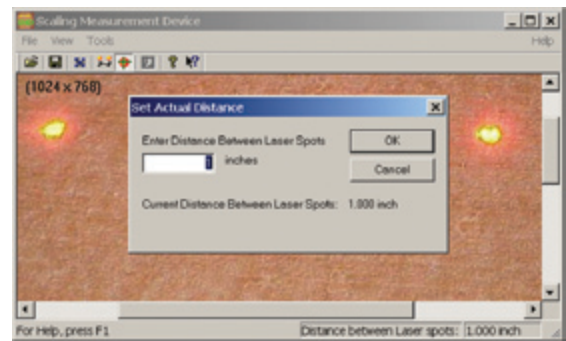
In many photographic situations, an object, such as a ruler, is placed in the field of view so the viewer will have an indication of the scale of the other objects in the photo. Sometimes this is not possible (for example, when photographing damage sites on the Shuttle's External Tank). Telephoto lenses can zoom in to see damage clearly, but the viewer cannot determine the scale of the damage because there is not a reference object in the image.

To address these limitations, a laser scaling device can be attached directly to a camera, which projects a known pattern into the field of view. When a photo is taken, the image of this pattern—currently a set of laser dots spaced by 1 inch—appears along with the image of the object under investigation. To effectively use the information provided by this device, a software package was written to allow a user to scale the objects seen in the photo. This software package has the following features:

- Fully uses the capabilities of the Windows operating system. For example, the .gif and .jpg image formats can now be brought into the software, whereas the previous version only allowed bitmap (.bmp) image formats.



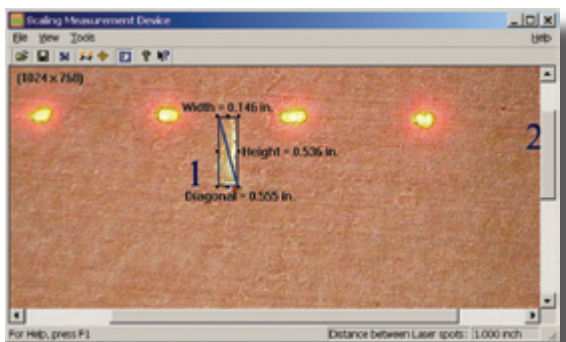
Basic appearance of the application after loading an image.



Set Actual Distance dialog window for the user to define actual physical distance between laser spots.



The application window showing markers placed on laser spots.



The application window showing the flexible measurement zone measuring a damaged area.

- Application was designed in a modular, object-oriented architecture driven by events. Events are handled via a message loop.
- Defines the application as a single document interface as opposed to a multidocument interface, reducing the need for unneeded “child” windows and extra graphical user interface (GUI) management by the user. Only one image is loaded at any one time.
- Provides an unlimited number of laser spot markers, enabling the operator to use any evenly spaced reference points in the image instead of only the laser spots.
- Provides the capability for unlimited uses of the application, enabling the user to load a new image without exiting the application. Each time another image is loaded all user-changed parameters are reset to their initial default values.
- Creates a flexible measurement zone capability in which the zone is placed with the first click and “rubberbands” to the second destination point showing the user in an animated fashion where the zone’s boundaries are as the mouse is dragged.
- Always shows the horizontal, vertical, and diagonal dimensions of the measurement zone and allows the zone to be moved and resized or re-created.
- Allows the user to set the reference distance to a new value without placing a new measurement zone.
- Displays the *Actual Distance Between Laser Spots* setting in the status bar.
- Expands the help section significantly by providing a Help Context button and provides a standard Windows help interface populated with image examples to explain the application’s functionality. These are hyperlinked where applicable.

Contacts: K.C. Ballard ([Kim.C.Ballard@nasa.gov](mailto:Kim.C.Ballard@nasa.gov)), YA-D5, (321) 867-6686; and Dr. R.C. Youngquist, YA-C2-E, (321) 867-1829

Participating Organizations: PH-H2 (J.E. Rivera), PH-A (C.G. Stevenson), and ASRC Aerospace (Dr. J.E. Lane, R.B. Cox, and W.D. Haskell)

## Utilizing MIL-STD-1553B Digital Data Bus Devices Across an IEEE-1394A Serial Bus



Communication  
Technology  
Upgrades

The objective of this project is to provide a migration path from the MIL-STD-1553B, Aircraft Internal Time Division Multiplex Data Bus, to an IEEE 1394A, High Performance Serial Bus, avionics architecture by developing a bridge that provides backward compatibility to MIL-STD-1553B legacy equipment on the IEEE 1394A bus. This allows the much higher performance and capable IEEE 1394A bus (referred to as the 1394 bus hereafter) to be used in next-generation spacecraft while maintaining compatibility with the legacy MIL-STD-1553B (referred to as the 1553 bus hereafter) equipment that is widely supported by the aerospace industry.

The 1394 and the 1553 buses have very different and incompatible architectures. As an example, the 1553 bus is a command-response bus with only one bus controller (BC), while the 1394 bus is a multimaster bus where all nodes can initiate transactions. The bridge is a requesting or target node in the 1394 bus and a bus controller or remote terminal in the 1553 bus. The bridge can also commingle with other high-performance devices on the 1394 bus (Figure 1). The bridge can read, write, and send mode code to any remote terminal from any requesting node on the 1394 bus.

A 1394 requesting node (e.g., a processor) can build a list frame that contains as many 1553 bus commands as possible in the bridge. The bridge will execute the list frame at the time and frequency specified by the requesting node. This capability will decouple the operations of the requesting node and the operations of the 1553 bus, and thus free the requesting node from tedious and time-consuming direct interactions with the bridge.

The bridge can support an architecture that has a 1394 bus backbone feeding up to eight 1553 buses on one isochronous channel. Since the 1394 bus has 64 isochronous channels, it can support up to 512 1553 buses. Each 1553 bus can support 32 devices; therefore, the architecture can potentially support a system that has 16,384 devices.

The requesting node on the 1394 bus sends the 1553 bus commands to the bridge via the 1394 bus packets. The 1553 bus commands are embedded in the data field of the 1394 bus. Upon receiving the 1394 packet, the bridge extracts the data field and decodes the commands. The commands will be executed as bus transactions on the 1553 bus. Upon the completion of the 1553 bus operations, the bridge gathers the results and sends them back to the requesting node on the 1394 bus. The bridge also sends status and other information to the requesting node via the 1394 bus packets (Figure 2). In addition to the 1553 bus commands, the 1394 requesting node can also send commands to set up the operations of the bridge and inquire about the internal status of the bridge.

Preliminary requirements of the 1394-1553 bridge were identified. The preliminary

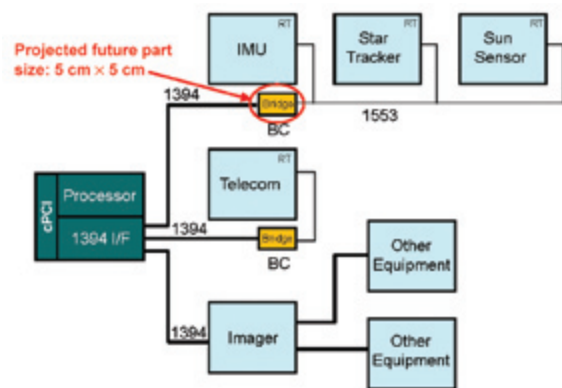


Figure 1. Bridge in 1394 bus.



system architecture is complete along with the preliminary set of bridge commands and statuses/responses. Hardware design is being done by SEAKR Engineering Inc. Layout of the prototype board is complete (Figure 3). SEAKR has selected VxWorks as the operating system.

The board support package needed for the hardware/software interface is being developed by SEAKR while software development is a Jet Propulsion Laboratory (JPL) activity. Major items to be developed include software architecture, application program interfaces (API), and test software.

#### Key accomplishments:

- Implemented prototype 1553 bus management commands and command timing characterization in a testbed.
- Defined bridge commands.
- Completed preliminary system architecture and prototype board layout.

#### Key milestones:

- 2002: Phase I STTR complete.
- 2004: Prototype board. Hardware/software integration.

Contact: I.H. Otero ([Ismael.H.Otero@nasa.gov](mailto:H.Otero@nasa.gov)), TA-D2-B,  
(321) 861-3726

Participating Organizations:  
SEAKR Engineering, Inc.  
(J. Carrol and M. Reynold) and  
JPL (S. Chau, T. Huynh, and  
L. Day)

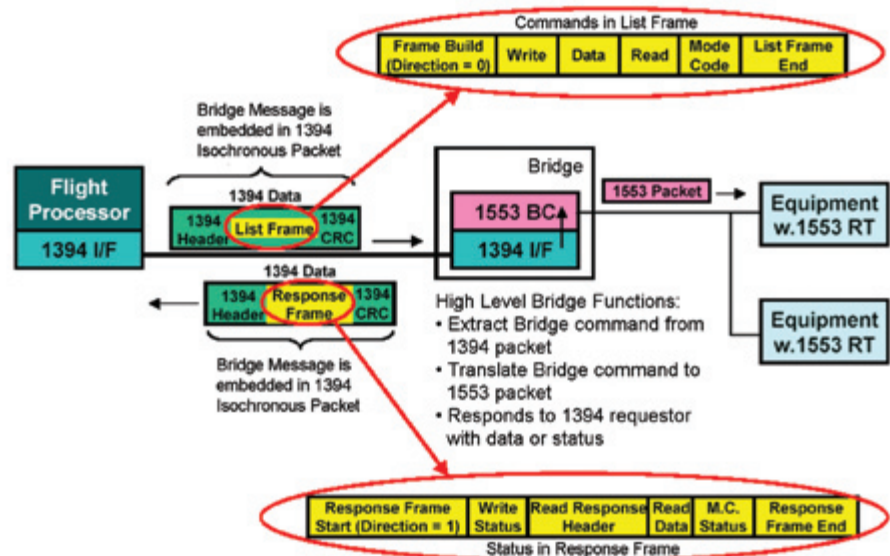


Figure 2. Architecture concept.

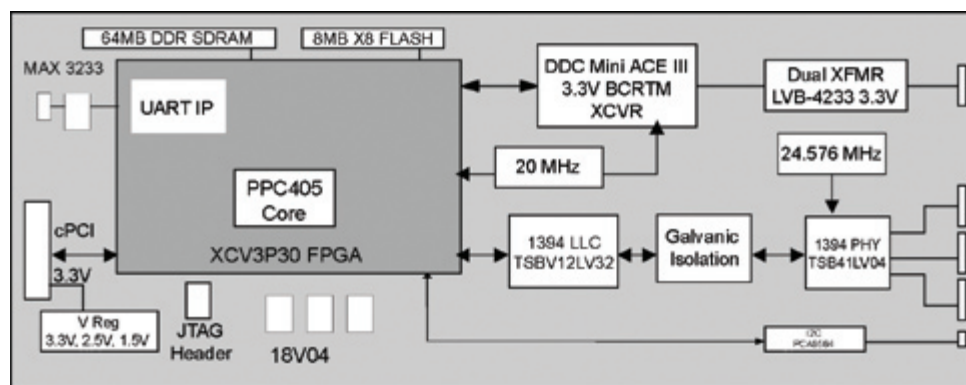


Figure 3. Prototype board layout.

# Fluid System Technologies

Fluid System Technologies help reduce the cost of access to space and increase safety by reducing the human oversight of servicing, reducing the waste streams, and reducing the number of hazardous operations and vehicle interfaces. Fluid System Technologies will support developing a better understanding of the fluid environment in all areas of spaceport activity through analysis and simulation. In addition, Fluid System Technologies will seek to develop the means to reduce thermal losses associated with cryogenic fuels, minimize maintenance and process monitoring costs, and provide for safe operation of the spaceport. A major goal of this technology product line is to create efficient technologies that can be quickly adapted to the changing fluid needs of future space vehicle elements and systems residing at the spaceport. The technology focus areas of the roadmap that drive technology development toward the ultimate vision include the following:

- Storage, Distribution, and Servicing Systems
- Production, Recovery, and Disposal Management Systems
- Vehicle Interface Systems
- Fluid Safety Systems
- Expendable Launch Vehicle (ELV)/ Reuseable Launch Vehicle (RLV) Thermal/ Fluids Environments and Management

*For more information regarding Fluid System Technologies, please contact Bill Notardonato ([Bill.Notardonato@nasa.gov](mailto:Bill.Notardonato@nasa.gov)), YA-D1, (321) 867-2613.*

## Parameter Estimation of Spacecraft Fuel Slosh Mode



Spacecraft  
Nutation  
Models

Fuel slosh in the upper stages of a spinning spacecraft during launch has been a long-standing concern for the success of a space mission. Energy loss through the movement of the liquid fuel in the fuel tank affects the gyroscopic stability of the spacecraft and leads to increased nutation (wobble) that can cause devastating control issues. The rate at which nutation develops (defined by Nutation Time Constant) can be tedious to calculate and largely inaccurate if done during the early stages of spacecraft design. Purely analytical means of predicting the influence of onboard liquids have been generally unsatisfactory. A strong need exists to identify and model the conditions of resonance between nutation motion and liquid modes and to understand the general characteristics of the types of liquid motion that cause problems in spinning spacecraft. A 3-D computerized model of the fuel slosh that accounts for any resonant modes found in ground-based testing will allow for increased accuracy in the overall modeling process. Attempts are being made to develop a more accurate model of the fuel slosh, using a more generalized 3-D computerized model incorporating masses, springs, and dampers as mechanical analogs. Parameters describing the model include the mass and inertia tensor of the moving fuel, spring constants, and damper coefficients. Refining and understanding the effects of these parameters should allow for a more accurate simulation of fuel slosh. The current research will focus on developing models of different complexity and estimating the model parameters that will ultimately provide a more realistic prediction of Nutation Time Constant obtained through simulation.



Figure 1. Full-scale testing of spacecraft fuel tanks using SSTR.

A computer simulation of the Spinning Slosh Test Rig (SSTR) incorporating a 3-D rotor model was developed using MATLAB software. The SSTR can subject a spacecraft test tank to a realistic nutation motion in which the spin rate and the nutation frequency can be varied independently, with the spin rate chosen to create a centrifugal acceleration large enough to ensure the configuration of the bladder and liquid in the tank is nearly identical to the zero-g configuration (Figure 1). The MATLAB model has the flexibility to include different parameters (inertia of moving fuel mass, translational and rotational stiffness, and damping in the three mutually perpendicular directions, offsets, etc.) in the parametric estimation process. The complexity of the 3-D rotor model depends on the parameters included in the estimation process. It is assumed more parameters will provide better response characteristics closer to reality. The parameter estimation procedure is illustrated in Figure 2. The nonlinear least squares algorithm is employed to minimize the residual. This minimization of residual is performed using the Newton's method for nonlinear least squares or the Levenberg-Marquardt modification to find the appropriate parameter values. This is accomplished through the LSQNONLIN algorithm of the optimization toolbox in MATLAB. Two illustrative examples are taken in this study: a simple mass-spring-damper model and a complex model of the SSTR. Figures 3 and 4 illustrate the results of the estimation process and provide a close agreement of the response between simulated experimental response and model response.

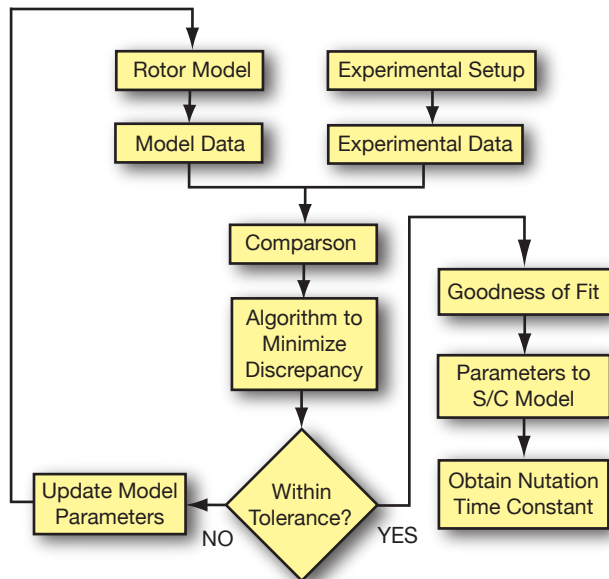


Figure 2. Parametric estimation process.

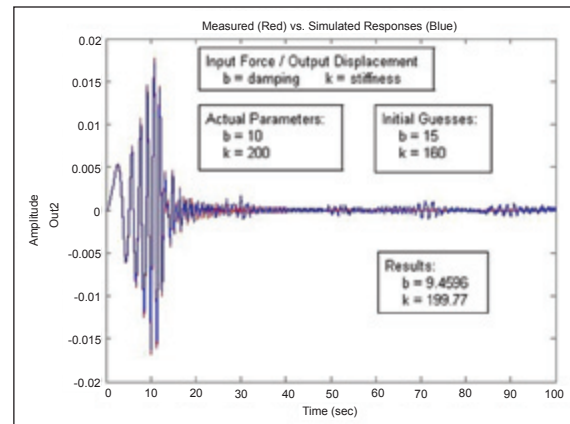


Figure 3. Comparison of measured (red) versus simulated (blue) responses for simple spring-mass-damper system model.

#### Key accomplishments:

- Developed a computerized 3-D MATLAB model (of varying complexity) of the fuel slosh.
- Illustrated the parameter estimation concept.
- Developed and validated two parameter estimation approaches (using code developed in-house and using The MathWorks Parameter Estimation Toolbox as a “black box”).
- Input the identified parameters into the spacecraft model to obtain the Nutation Time Constant.

#### Key milestones:

- Study the coupling effects between parameters of the model.
- Modify the model to include more than one mass to account for various resonant modes found during experimental testing.
- Seamlessly automate the overall parameter estimation process in MATLAB software.

Contact: J.E. Sudermann ([James.E.Sudermann@nasa.gov](mailto:James.E.Sudermann@nasa.gov)), VA-F3, (321) 476-3669

Participating Organizations: Embry-Riddle Aeronautical University (Dr. S. Gangadharan and J. Ristow) and The MathWorks, Inc. (Dr. B. Eryilmaz)

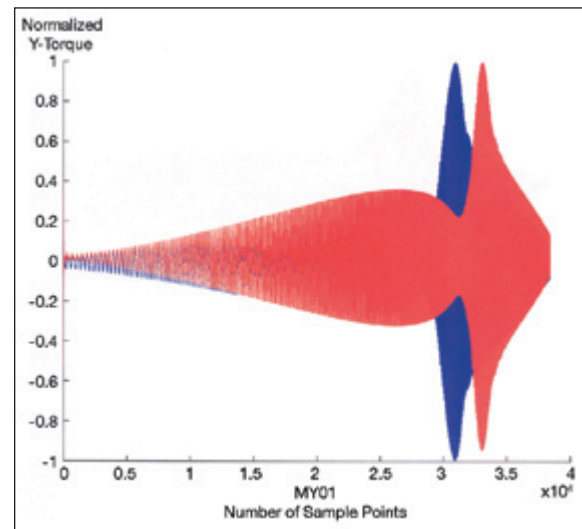


Figure 4. Measured (red) versus simulated (blue) responses for SSTR model.



## Color-Indicating Wipe for Cleaning Hypergolic Propellant



Contamination  
Detection/Reduction/  
Cleaning

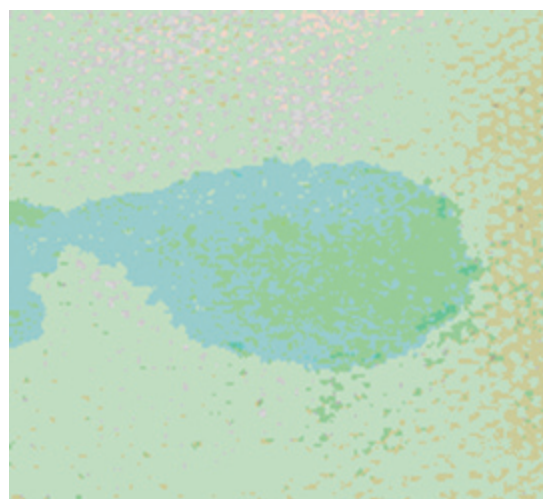
Large quantities of hypergolic propellant are used onboard the Shuttle in the Orbiter Maneuvering System (OMS) and Reaction Control System (RCS). During propellant loading operations, wipes are used to clean up any spills. The current wipe is made of polypropylene, a feutron felt material that does not absorb liquids very well.

At the KSC Applied Chemistry Laboratory, a new wipe has been developed. It is very absorbing; changes color to blue or pink when contacting fuel or oxidizer, respectively; and is made by coating an absorbing wipe with a color indicator.

Market search found a wipe (JNJ Industries, catalog no. 0327 UltraSorb) that can absorb liquid 10 times its weight. The wipe is a 13-inch square of rayon material coated with color indicator that has been tested for ignition and reactivity (method MTB-175-88) with hydrazine, monomethylhydrazine, and nitrogen tetroxide. The wipe has been tested for electrostatic discharge (ESD) property (triboelectric method MMA-1985-79 rev. 4). The ignition test measures temperature change for 10 minutes when a 2-inch square of material is in contact with 0.5 mL of propellants. The reactivity test documents changes of physical appearance after soaking a 4-inch square of material in 1.0 mL of propellants for 10 minutes. Materials are considered acceptable if there is no ignition and the temperature rise is no greater than 2.8 °C when exposed to liquid fuel. The ESD test grounds three samples, both sides, at 75±5 °F and relative humidity of 30 percent or 45 percent, and reports the highest 5-second voltage. Materials are considered acceptable if the highest voltage is no greater than 350 volts in magnitude regardless of polarity. The wipe was accepted as safe for hypergolic propellant application.



Wipe exposed to oxidizer.



Wipe exposed to fuel.

To prepare wipes, a stock color-indicating solution is made by dissolving 25 mg thymol blue, 62 mg methyl red, 250 mg bromothymol blue, and 500 mg phenolphthalein in 50 mL of 95 percent ethanol. Deionized water is added to make 1 L of solution. From the stock solution, a 10-percent solution is prepared and its pH adjusted to 11. In a rectangular dish, 10 wipes are placed in 1 L of the 10-percent solution until completely saturated. Excess solution is removed by squeezing the wipes between two plastic plates. Then, the wipes are dried in a clothes dryer at normal heat setting.

Adjusting the pH to 11 is necessary because the initial wipe material is acidic. To make a neutral wipe that is yellowish green, pH 11 was experimentally determined to be most suitable. In addition, the wipes need to be dried rather fast to prevent absorption of carbon dioxide, which will change the wipe to peach color. Yellowish green was selected for the wipe because it can clearly show a color change to blue with fuel and pink with oxidizer.

Once the wipes are coated with the indicator and stored in a plastic bag, they are ready for use. No maintenance is required. Using the wipes is very easy: just wipe the surface and observe a color change. If there is no color change, there is no exposure to liquid hypergolic propellants and the surface is clean. The used wipes can be stored in a sealed plastic bag for disposal.

End users have completed several rounds of field tests during hypergolic loading operation. The wipe has been well received for its ability to absorb and its color change that ensures the surface is clean.

*Contacts:* R.C. Young ([Rebecca.C.Young@nasa.gov](mailto:Rebecca.C.Young@nasa.gov)), YA-C3, (321) 867-8765; and T.A. Campbell, PH-G2, (321) 861-5114

*Participating Organization:* United Space Alliance (J.M. Hooper)

## Highly Selective Membranes for Gas Separations

The Extravehicular Mobility Unit (EMU) used for extravehicular activity (EVA) and for air revitalization for spacecraft environments is very complex. Lighter-weight and less complex EMUs would be more useful to astronauts in EVA. One method of reducing the weight of the EMU is to lower the weight and power requirements for the air revitalization system.

Current air revitalization systems utilize lithium hydroxide to scrub carbon dioxide from the EMU air supply. Approximately 2 kg of lithium hydroxide is consumed for every 8 hours of EVA, and the full canister weighs approximately 4 kg. A fan that circulates the air through the canister adds to the weight and power requirement. For a mission lasting 6 months (approximately 180 days), the full lithium hydroxide canisters alone would weigh over 2,000 kg.

The use of supported ionic liquid membranes for carbon dioxide separation has been reported in several patents and peer-reviewed journals. These membranes, however, suffer from various limitations, including stability and selectivity. At KSC we are currently developing technology that will eliminate (or greatly reduce) these limitations. The goals of this project are to develop a new class of microencapsulated membrane with high selectivity for carbon dioxide separation and to collect permeation data for these new membranes.

The design of the microencapsulated membranes is shown in Figure 1. A liquid with high carbon dioxide solubility is encapsulated in a polymer with high

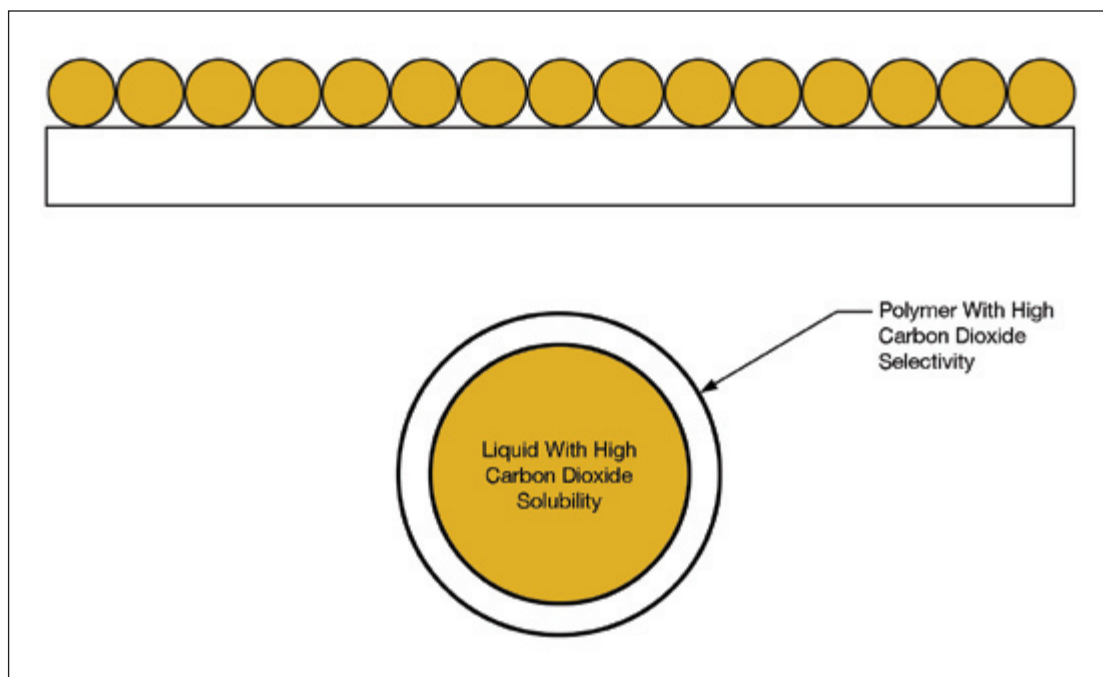


Figure 1. Cartoon of Microencapsulated Membrane.

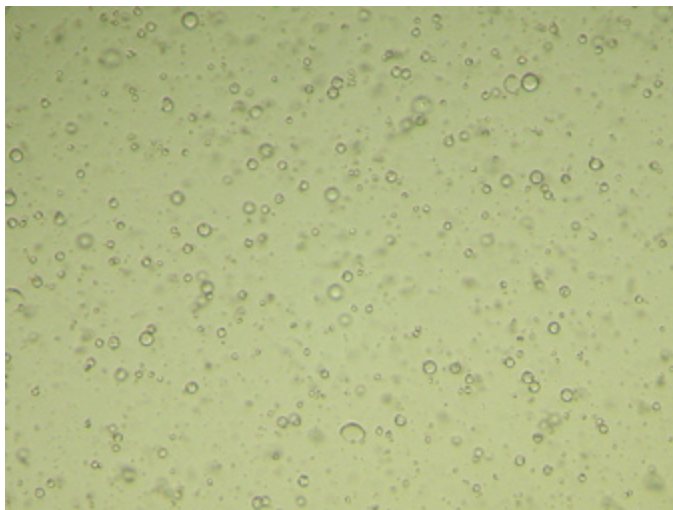


Figure 2. Microcapsules containing ionic liquid.

carbon dioxide/oxygen selectivity. These microparticles are then attached to a polymer substrate (membrane) with good carbon dioxide/oxygen selectivity. The substrate does not need to be the same as the polymer used to encapsulate the liquid. By using various polymers and substrates, a wide variety of selectivities for carbon dioxide/oxygen can be obtained.

The advantages of using a microencapsulated membrane are increased stability, wider temperature application, and selectivity. The increased stability is due to the encapsulation process, eliminating the “drying out” process that occurs in the liquid-supported membrane system. The right choice of liquid can offer greater operating ranges, from very low temperatures to relatively high temperatures (-50 to 400 °C). Selectivity can be changed by simply changing the polymer encapsulant or the substrate.

#### Key accomplishments:

- Determined carbon dioxide solubility for a wide variety of liquids.
- Prepared microcapsules containing tested liquids (Figure 2).
- Obtained preliminary data for liquid-supported membranes as a model system.

#### Key milestones:

- Prepare microcapsules containing various liquids with high levels of carbon dioxide solubility.
- Test permeability of newly prepared microencapsulated membranes.

Contact: Dr. C.F. Parrish ([Clyde.F.Parrish@nasa.gov](mailto:Clyde.F.Parrish@nasa.gov)), YA-C3, (321) 867-8763

Participating Organizations: ASRC Aerospace (Dr. T.L. Gibson, Dr. S.T. Jolley, and L. Fitzpatrick) and Florida Institute of Technology (Dr. M.J. Novak)



## Solid Xenon Storage for Next-Generation Xenon Ion In-Space Propulsion

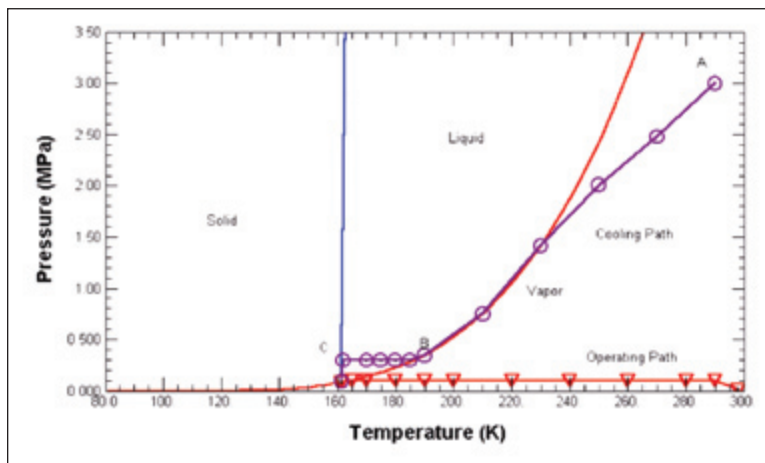
For more than 44 years, NASA has conducted an ion propulsion program. A number of experimental flight demonstrations were made for solar electric power (SEP) propulsion systems. Various sizes of thrusters were tested. Xenon propellant has achieved the highest specific impulse, the best mass/propellant ratio, and the highest efficiency among all the candidate propellants. The success of Deep Space 1 (DS1) further leads to the development of the NASA Evolution Xenon Thruster (NEXT) system (Domonskos et al. 2002) that has a larger-size (40-cm) thruster with higher specific mass (greater than 3.6 kg/kW), higher efficiencies at all power levels, and higher specific impulse than the NASA Solar Electric Propulsion Technology Application Readiness (NSTAR) thruster. The applications for this large system include Mars, Lunar Cargo Transporter, Gateway (L1), Nuclear Electric Propulsion (NEP) for Jupiter Icy Moon Orbiter (JIMO), etc. In both NSTAR and NEXT thruster systems, xenon is serviced on the ground and stored in space at a supercritical state that typically corresponds to much higher pressures with its temperature at an ambient condition. A typical pressure up to 4,500 psia is required to reach the desired mass storage. This storage mode not only imposes a high-pressure constraint to the material of the storage tank but also requires a complicated pressure control system to monitor and regulate the xenon propellant supply rate in space. In the design of many SEP and chemical/SEP hybrid space vehicles and their associated space systems for extended space exploration, a significantly large amount of xenon needs to be either stored on the spacecraft as its own propellant or stored as a payload cargo for use in replenishing other space vehicles in a space gateway. A payload of 30,000 kg of xenon, stored cryogenically and having a total mass of 21,500 kg, has been reported for both outbound and inbound propulsion of the transfer vehicle. The demand for even higher xenon mass for future space exploration could arise. It becomes very costly to store such a large mass of high-pressure, supercritical xenon with current technology.

A xenon liquefaction and storage system for spacecraft using xenon ion propulsion is proposed and analyzed. The benefit to this storage and feeding method is to supply more xenon in a given volume than high-pressure supercritical-state xenon storage. An estimated minimum 55-percent increase in storage mass for a given volume can be reached. This benefit is especially significant when a large quantity of xenon, on the order of 10,000 kg, is required for extended space exploration.

Through the NASA / American Society for Engineering Education (ASEE) Faculty Fellowship Program, this project outlines the issues associated with the development of a solid xenon cooler to implement the new system concept. A lumped, multiphase analytical model with phase change was developed, and

NSTAR and NEXT engine attributes.

Engine Attribute	NSTAR*	NEXT†
Input power, kW	2.29	6.85 (up to 8)
Specific impulse, s	3,280	4,100 (Max. 74,050)
Flow rate, mg/s	2.75	5.89
Thrust, mN	93	237
Efficiency at full power	62%	768%
Propellant throughout, kg	83 design, 140 demo	>300
Specific mass, kg/kW	3.6	>3.6
*Patterson et al. (1995); †Domonkos et al. (2002)		



Xenon phase diagram.

preliminary results are presented to identify the key design parameters that could lead to a low-cost, effective alternative to the xenon storage and feeding system in space. It is more energy-efficient to solidify xenon at a higher supply pressure. For the required xenon feed rate in a xenon ion thruster, the controllability is affected by the solid xenon surface area that may be subject to undesired heat gain. Operational issues associated with ground processing and storage, as well as flight usage, have been addressed. A further research plan and approaches to implement the plan are recommended.

Contact: W.U. Notardonato ([Bill.Notardonato@nasa.gov](mailto:Bill.Notardonato@nasa.gov)), YA-D1,  
(321) 867-2613

Participating Organization: Florida International University (Dr. Y.X. Tao)

## Highly Reliable Liquid Oxygen (LOX) Pump for Vehicle Loading



*Propellant Loading  
Servicing/Storage*

The current Shuttle LOX loading pumps have several maintenance issues that result in relatively low reliability. The proposed LOX pump system would mitigate NASA's reliability concerns in this critical application by virtue of the seal arrangement tested in Phase I and of each pump's ability to meet the current launch pad fill rates in the event of one unit's failure.

Phase I focused on reliability issues surrounding the primary sealing arrangement in the LOX pumps and demonstrated the feasibility of a noncontacting combination of a dynamic seal and a purged labyrinth seal set as a highly reliable sealing solution for the primary seal for LOX transfer pumps. This arrangement eliminates the present configuration wherein the face seal is a wearing component. Additionally, Phase I efforts produced a unique concept for a new LOX pumping system for vehicle loading operations. In the proposed new system, two pumps could operate in parallel, providing an increase in LOX transfer rate of 50 percent.

The Barber-Nichols, Inc. (BNI) common pump design using a single shaft to drive both the motor and pump impeller facilitates the use of a noncontacting, radial seal in this application. The current Shuttle LOX pump uses a bellows-type face seal arrangement, which is prone to bellows cracking, wear from fatigue, premature seal wear from freezing moisture on the face of the closed seal, and poor sealing from misalignment of seal mating rings. The current LOX pump configuration also utilizes a two-shaft system, with the pump drive shaft coupled to the motor shaft through a universal joint drive shaft. This system developed vibration issues that had detrimental effects on the seals in the pump. BNI's pump design will replace the seals and add reliability.

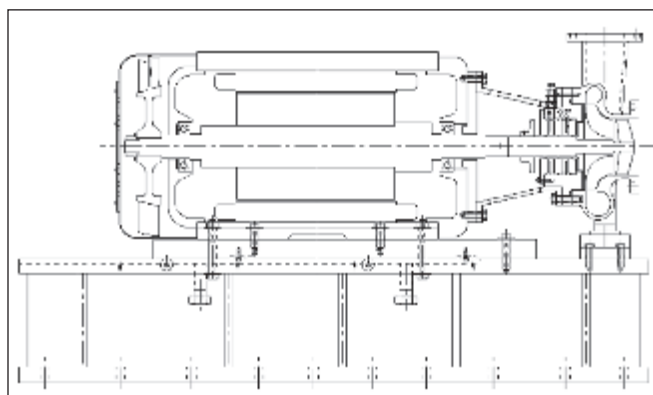
Phase II will include the design and manufacture of a complete pump system composed of two pumps, pump performance testing using water, and cryogenic testing at KSC's Advanced Technology Development Center (ATDC).

The proposed pumping system (incorporating the new seal arrangement) can be applied immediately to retrofit the existing Shuttle LOX loading pumps at KSC. The system was designed to have minimal impact to existing mechanical, piping, and electrical infrastructures used for vehicle loading at launch pads. Furthermore, there are a great number of LOX transfer pumps currently employed by NASA (e.g., Stennis Space Center) and in the Department of Defense that could be replaced by this more reliable pump. With some modifications, this pump concept could also be utilized by NASA to transfer liquid hydrogen or other propellants.

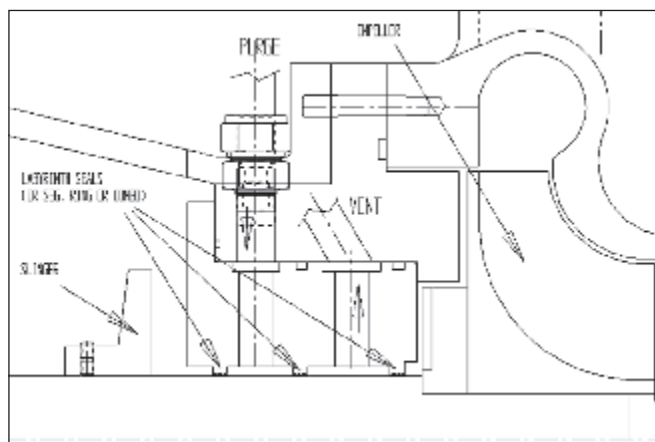
Technology developed in the Phase II effort can be applied to any low-viscosity, hazardous fluid pumping application. Potential markets include the chemical and petrochemical industry, where nearly all pumped fluids meet these criteria. Another large market for this pump technology would be in liquefied natural gas transfer and ship off-loading. Because it is not submersible, this pump would be more efficient and cost less to install and maintain. This large pump would offer an attractive alternative to submersible pumps and would be cost-competitive in this growing market. A smaller market that perhaps should be counted in long-term plans is that of commercial space vehicles. As more private space vehicle firms achieve success, this pump could be marketed to support the ground test and launch facilities of private and commercial space industries.

Contact: D.M. Pittman ([Donald.M.Pittman@nasa.gov](mailto:Donald.M.Pittman@nasa.gov)), YA-D1, (321) 867-6894

Participating Organization: Barber-Nichols, Inc. (M.E. Rottmund)



Preliminary LOX pump layout.



Close-up of seal area.



# Range Technologies

Range Technologies consist of unique facilities and equipment technologies that provide the control and measurement data necessary to ensure the safety of launch and test operations for the range/spaceport. Examples of these technologies include (1) data processing equipment for range safety analysis, communications systems for telemetry processing, reception, and destruct command systems; (2) sensor and instrumentation systems for vehicle tracking, such as radar systems and optical tracking displays; and (3) data communications management, distribution, and recording systems. Significant capital investment is required to build and maintain this capability and as a result, these assets have traditionally been slow to modernize or have limited flexibility to accommodate new requirements and vehicles. In addition, the cost associated with range system infrastructure is difficult to quantify.

Future range operations will require flexible range technologies that can incorporate the latest technological advances. It is expected to be largely space-based and will be seamlessly augmented with mobile, deployable, and/or ground-based assets. Minimal ground infrastructure will be required and will primarily be located at the launch head, reducing the operational cost. Self-healing autonomous ground and flight systems will become the norm. Range systems will have situational awareness and be intelligent enough to reconfigure autonomously when individual systems “drop out” or are unavailable. A National/Global Range Network with regional hubs is envisioned, which provides 24/7 coverage, is scalable to user requirements, and is seamlessly integrated into the national and global air space. The modernization activities will also ensure that future technology improvements will be able to adapt to different space flight hardware designs, and the degree of customization or reconfiguration for specific launch vehicles operations will be minimized. Multiple simultaneous test and launch operations by multiple vehicles from multiple spaceports are also envisioned.

With the goals and objectives of improving safety, improving range responsiveness (support more launches, reduce lead and turnaround time, and reduce delays), reducing variable launch and range costs, reducing cost of fixed infrastructure, and improving capacity and flexibility, the KSC team has stepped up to colead, with the Air Force Space Command, a national coalition called Advanced Range Technologies Working Group (ARTWG), which is identifying the next-generation range technology roadmaps for the next 25 years.

The seven range technology areas of focus include:

- Weather Measurement and Forecasting Technologies
- Tracking and Surveillance Technologies
- Telemetry Technologies
- Decision-Making Support Technologies
- Planning, Scheduling, and Coordination-of-Assets Technologies
- Range Command and Control Systems Technologies
- Communication Architecture Technologies

For more information regarding Range Technologies, please contact Richard Nelson ([Richard.A.Nelson@nasa.gov](mailto:Richard.A.Nelson@nasa.gov)), YA-D7, (321) 867-3332.

# Hexagonal Fractal Multiband Antenna



Seamless  
Command & Control  
Coordination

The explosive growth in the wireless industry has renewed interest in multiband antennas. The most recent multiband antenna development is the incorporation of fractal geometry into radiators. The Sierpinski gasket antenna is a prime example. Since the Sierpinski gasket has proven itself to be an excellent multiband antenna, other multiband antennas can similarly be constructed using fractal geometry.

The Sierpinski gasket or Sierpinski triangle antenna possesses resonant frequencies with a power of 2. This log periodic frequency behavior is the direct result of constructing the Sierpinski gasket with a scale factor of  $1/2$ . The triangles within the Sierpinski gasket antenna are interconnected to maintain conductivity and to preserve electrical self-similarity.

The hexagonal fractal is constructed by reducing a hexagon generator shape to one-third its former size and grouping six smaller hexagons together. This procedure is known as the Iterated Function System (IFS) and is described by the following matrix equation.

$$w \begin{bmatrix} x \\ y \end{bmatrix} = \begin{bmatrix} a & b \\ c & d \end{bmatrix} \begin{bmatrix} x \\ y \end{bmatrix} + \begin{bmatrix} e \\ f \end{bmatrix} \quad (1)$$

The first three hexagonal fractal iterations are displayed in Figure 1. The hexagonal fractal IFS coefficients are given in Table 1. The ideal coefficients are for fractals with touching vertices but no conductivity. The actual coefficients are for fractals with overlapping vertices and therefore conductivity. The hexagonal fractal antenna is implemented in the corner-fed dipole configuration with overlapping vertices to preserve the electrical self-similarity paramount in multiband design. When viewed from the corner input, it is apparent the hexagonal fractal presents similar scale lengths of one-third, and therefore it can generate resonant frequencies with a power of 3.

Table 1. IFS transformation coefficients for the hexagonal fractal (ideal and actual [in parenthesis] coefficients for the hexagonal fractal. Translational coefficients  $e$  and  $f$  are normalized to hexagon side length of 100 mm).

W	$a$	$b$	$c$	$d$	$e$	$f$
1	0.3333 (0.35)	0	0	0.3333 (0.35)	0.0	0.0
2	0.3333 (0.35)	0	0	0.3333 (0.35)	0.6667	0.0
3	0.3333 (0.35)	0	0	0.3333 (0.35)	-0.3333	0.578
4	0.3333 (0.35)	0	0	0.3333 (0.35)	1.0	0.578
5	0.3333 (0.35)	0	0	0.3333 (0.35)	0.0	1.155
6	0.3333 (0.35)	0	0	0.3333 (0.35)	0.6667	1.155

Table 2. Hexagonal fractal dipole antenna resonant frequency characteristics.

Fractal Iteration K2				
$n$	$F_n$ (GHz)	$S_{11}$ (dB)	BW (GHz)	$F_{n+1}/f_n$
1	0.263	-12.33	0.09	N/A
2	1.403	-21.88	0.19	5.33
3	4.263	-15.38	0.95	3.04

The first three iterations of the corner-fed hexagonal fractal dipole were measured and examined using the method of moments (MoM). The reflection coefficients for the first three iterations of the hexagonal fractal antenna are plotted in Figures 2, 3, and 4. Details of the resonant frequency are listed in Table 2 for the second iteration of the hexagonal fractal antenna. Aside from the first resonant frequency, hexagonal fractal antenna produces recurring resonant frequencies with a factor of about 3. An approximate resonance frequency relationship is given for the hexagonal fractal antenna,

$$f_n \approx \frac{0.468 \cdot c}{l \cdot \delta^{n-2}}, \quad 2 \leq n \leq k+1 \quad (2)$$

where  $c$  is the speed of light,  $l$  is the hexagon side length,  $\delta$  is the scale factor,  $n$  is the resonance, and  $k$  the fractal iteration.

The hexagonal fractal antenna is observed to possess multiband behavior similar to the Sierpinski gasket antenna. However, the hexagonal fractal antenna resonant frequencies repeat with a factor of 3, whereas the Sierpinski gasket antenna resonant frequencies repeat with a factor of 2 in frequency. This new fractal antenna allows flexibility in matching multiband operations in which a larger frequency separation is required.

This research was supported by the KSC Graduate Fellowship Program.

Contact: P.W. Tang ([Phillip.W.Tang@nasa.gov](mailto:Phillip.W.Tang@nasa.gov)), UB-G2, (321) 867-6413

Participating Organization: University of Central Florida (Dr. P.F. Wahid)

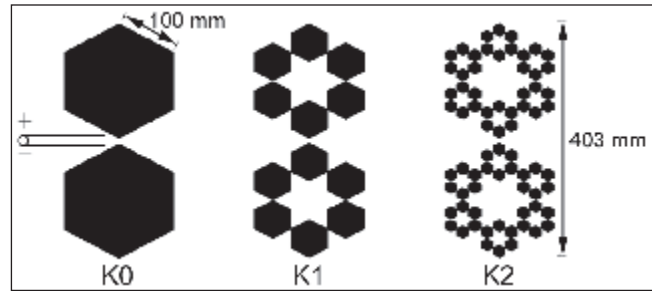


Figure 1. First three iterations of the hexagonal fractal.

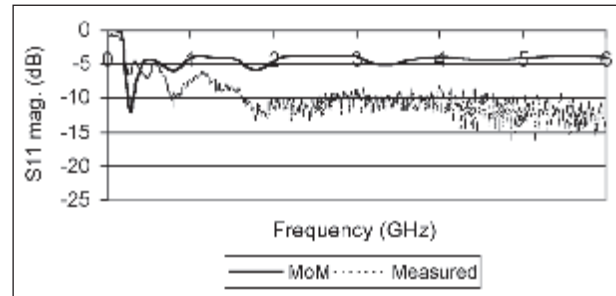


Figure 2. Zero-stage (K0) hexagonal fractal dipole reflection coefficient.

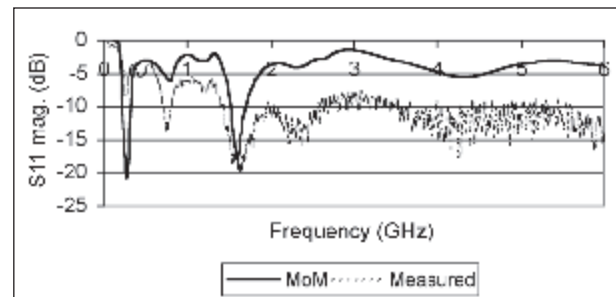


Figure 3. First-stage (K1) hexagonal fractal dipole reflection coefficient.

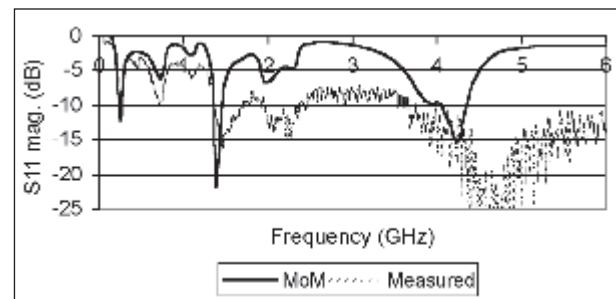


Figure 4. Second-stage (K2) hexagonal fractal dipole reflection coefficient.

# Aircraft Attitude Drift Correction Using a Heading-Based Reset Function



Space & Air Traffic  
Management  
System

Aircraft navigation attitude data consisting of yaw, pitch, and roll with respect to a specified initial orientation can be obtained from the body axes rotation rates using a numerical integration scheme. However, the results are known to drift and diverge in 30 seconds or less. Resetting the integrator using new and externally supplied yaw, pitch, and roll angles provides a means to correct the drift, but this is a difficult and time-consuming process.

A technique was developed at KSC that estimates the rotation rates based on the radar and/or GPS position and velocity data and automatically resets the integration. Seven test flights of the Space-Based Telemetry and Range Safety (STARS) project were flown on an F-15B at Dryden Flight Research Center during the summer of 2003. The test data recorded included the aircraft's position from ground-based tracking radar, the angular rotation rates about the aircraft's body axes, and onboard GPS position and velocity data. To perform a communications link margin analysis, the angular rate data was used to obtain the aircraft's orientation or "attitude." The tracking radar provided position information or "ephemeris" data. The combined attitude and ephemeris data files were loaded into Satellite Tool Kit to generate a complete 3-D animated simulation of the F-15B flight.

Unfortunately, the type of hardware used onboard the F-15B to measure the rotation rates was subject to large amounts of drift, especially during low-acceleration flight events. The fix for this drift was a manual re-creation of the attitude data by observing the flight videos or by estimating a best-guess attitude based on reasonable flight characteristics of the F-15B aircraft.

One obvious disadvantage of this manual method is that it is extremely time-consuming and tedious. In addition, based on position and velocity

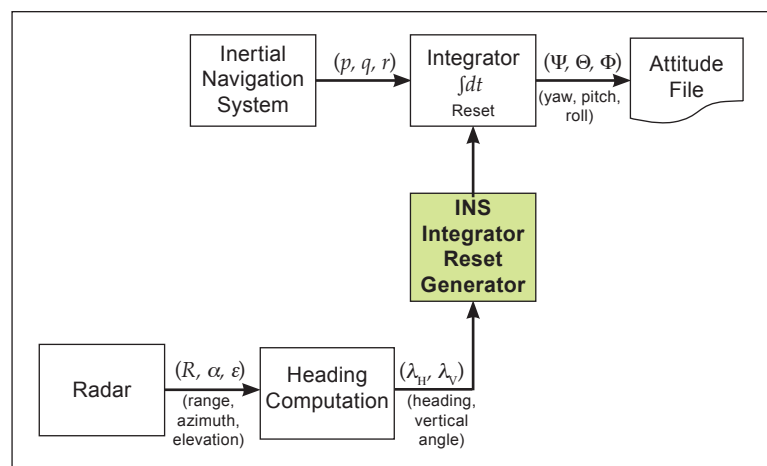


Figure 1. Inertial Navigation System attitude drift suppression using heading-based reset.



**Reset Condition:** Reset IF

$$\begin{cases} \frac{d\lambda_v / dt}{|\lambda_v|} < \gamma_1 \\ \text{OR} \\ |\lambda_v| < \gamma_2 \text{ AND } |\lambda_H| < \gamma_3 \end{cases}$$

Example:  
 $\lambda_1 = 0.01$   
 $\lambda_2 = 3$   
 $\lambda_3 = 1$

**Reset Angles:**

$$\begin{pmatrix} \Psi \\ \Theta \\ \Phi \end{pmatrix} = \begin{pmatrix} a_0 + a_1 \left| \frac{d\lambda_H}{dt} \right| + a_2 \bar{\lambda}_V \\ b \frac{d\lambda_H / dt}{|d\lambda_H / dt|^\beta} \end{pmatrix}$$

Example:  
 $a_0 = 6$   
 $a_1 = 0.5$   
 $a_2 = 2$   
 $b = 85$   
 $\beta = 0.7$

$a_0, a_1, a_2, b, \beta \longrightarrow \text{constants}$

Figure 2. Reset generator.

data alone, it may not always be obvious what a reasonable attitude should be. A better method was needed to generate the attitude data from the poor-quality rotation rate data.

Yaw, pitch, and roll angles can be obtained by integrating the rotation rates about the aircraft's body axes using a known initial orientation. The error in these angles can grow very quickly with time and often becomes unacceptable after only 30 seconds of level flight. The error is much less when the aircraft is undergoing very dynamic maneuvers with angular rates much greater than the noise level.

The new integration routine can reset the integration at any time by providing the numerical integration routine with a corrected set of attitude angles using heading and vertical velocity information obtained from either tracking radar or GPS data.

Key accomplishment:

- Developed a technique to estimate aircraft rotation rates based on radar and/or GPS position and velocity data. This algorithm automatically resets the numerical integration.

Contact: Dr. J.C. Simpson ([James.C.Simpson@nasa.gov](mailto:James.C.Simpson@nasa.gov)), YA-D7, (321) 867-6937

Participating Organization: ASRC Aerospace (Dr. J.E. Lane)

## Passive Millimeter Wave Imaging



Risk  
Assessment  
Tool

The fundamental imaging problem for missions carrying nuclear payload materials is the obscuring, billowing cloud of plume exhaust. To increase the efficiency of solid rocket motors, the exhaust particles in these clouds are very small. Unfortunately, with current exhaust particles being so small, high attenuation/obscuration occurs at both visible-light wavelengths and scanning laser beam wavelengths. This means that established viewing methods using optical or scanning laser beams no longer always meet Range Safety imaging requirements for new heavy launch vehicles at the launch facilities with upgraded water pad deluge systems.

A promising solution to this problem, now investigated over three consecutive projects, is Passive Millimeter Wavelength Imaging. Passive Millimeter Wavelength Imaging works because the physical objects naturally emit millimeter wave energies passively at all temperatures above absolute zero. No millimeter wave energy illumination is required; and unlike radar beams, no energy is radiated at the launch vehicle. Passive Millimeter Wavelength Imaging therefore holds great promise for providing enhanced observation capabilities for the current generation of heavy launch vehicles while remaining inherently safe for use around launch ordinance devices and other pyrotechnic devices.

This year, Phases II and III of the Passive Millimeter Wavelength Imaging project extended the theoretical and empirical understanding of applying this technology to launch situations. Accomplishments during Phase II included instrumenting and collecting actual launch vibration and acoustic data at an imager mounting location identified in Phase I.

The launch of the Spitzer Space Telescope from Launch Complex (LC) 17 at Cape Canaveral Air Force Station on August 25, 2003, provided the vibration data for this test. Analysis of the launch vibration and acoustic environment data collected during the Space Infrared Telescope Facility (SIRTF)/Spitzer launch was released in a Phase II final report. In addition, all the millimeter wave test equipment required for Phase III testing was procured.



*Solid-fuel rocket motor holder firing test.*

During Phase III activities conducted this year, a solid-fuel rocket motor holder and a millimeter wave attenuation measurement test chamber were designed and fabricated. Together, these enable accurate measurement of electromagnetic wave attenuation versus wavelength at various millimeter wavelengths in the presence of obscurants. Millimeter wavelength horn antennas and isolators, incorporated in waveguide, enable accurate test chamber propagation attenuation measurements through dry air, steam, water spray, and/or solid rocket motor plume exhaust clouds immediately after burning small amounts of ammonium perchlorate, magnesium, and aluminum-based solid rocket motor fuel inside the test chamber. This capability simulates actual solid rocket motor exhaust launch plumes well, thus enabling accurate millimeter wavelength obscuration attenuation measurements. The end result is accurate determination of the key specifica-

tions required for implementing and developing cost-effective operational Passive Millimeter Wavelength Imaging systems.

Tasks anticipated for the coming year are to procure or design a prototype imager based on the specifications determined through both theoretical and experimental results from Phases I, II, and III and to conduct a series of tests on an initial proof-of-concept imager.

Passive Millimeter Wavelength Imaging technology can be applied to a wider range of topics, including passive inspection of external Orbiter tanks on the launch pad and passive inspection of vehicles at guard station checkpoints.

#### Key accomplishments:

- Successfully characterized actual launch vibration and acoustic data at LC-17 and identified the environment an imager must be designed to survive.
- Researched key technical journals and papers.
- Designed and built a solid-fuel rocket motor holder and test chamber for measuring millimeter wavelength attenuation through launch plumes, steam, and water spray.
- Collected empirical data to improve theoretical models for estimating the performance limits of Passive Millimeter Wavelength Imaging in a launch environment.

#### Key milestones:

- 2002: Commenced research (October). Released Phase I final report, establishing theoretical limits (December).
- 2003: Instrumented LC-17 and measured vibration/acoustic environment during SIRTf launch (August). Released Phase II final report with data and analysis of vibration and acoustic environment during SIRTf launch (September). Held design review for test chamber design (December).
- 2004: Test chamber became operational for measuring millimeter wavelength attenuation through simulated launch plumes consisting of steam, smoke, and water spray (April).

Contact: A. Hongamen ([Alexis.Hongamen-1@nasa.gov](mailto:Alexis.Hongamen-1@nasa.gov)), YA-E2, (321) 867-3107

Participating Organizations: 45<sup>th</sup> Space Wing (C.D. Botts), ASRC Aerospace (Dr. G.L. Bastin, W.G. Harris, Dr. M. Kandula, T. Erdogan, J.B. Crisafulli, W.D. Haskell, K.A. Murtland, J.D. Polk, and M.M. Scott), YA-D7-E1 (J. Murray), YA-D7 (R.A. Nelson), and YA-C3-E (Dr. R.C. Youngquist)



Vehicle obscuration during launch.



# Effect of Clouds on Optical Imaging of the Space Shuttle During the Ascent Phase: A Statistical Analysis Based on a 3-D Model



Localized Weather  
Forecasting and  
Measurement

Clouds are highly effective in obscuring optical images of the Space Shuttle Launch Vehicle (SSLV) taken by ground-based and airborne tracking cameras. Because the imagery is used for quick-look and postflight engineering analysis, the Columbia Accident Investigation Board (CAIB) recommended the imaging system be upgraded to obtain at least three useful views of the SSLV from liftoff to at least Solid Rocket Booster (SRB) separation for return to flight.

In September 2003, the Applied Meteorology Unit (AMU) was tasked by the KSC Weather Office to identify and evaluate methods to determine if a sufficient number of SSLV imaging cameras will have a field of view unobstructed by weather. At that time, the KSC Weather Office advised that forecast guidance should be available at the end of the T-9-minute hold and be valid throughout the 5-minute launch window for International Space Station (ISS) missions. Since the lifetimes of individual cloud elements capable of obscuring optical views of the SSLV are typically 20 minutes or less, accurately observing and forecasting cloud obscuration over an extended network of cameras posed a significant challenge for the current state of observational and modeling techniques. Although a firm Go/No-Go indicator was highly desirable, a probabilistic assessment would be acceptable if a binary indicator was impossible or too costly to develop.

In October 2003, the AMU concluded a concept study that outlined two complementary methodologies: statistical and observational (Figure 1). The concept study recommended incorporating statistical results into the forecast guidance that since even the best numerical simulations based on real observations will never reach "truth."

After a review of the concept study by a team consisting of the Shuttle Launch Director, NASA Inter-center Photo Working Group, KSC Ice and Debris Team, KSC Weather Office, 45th Weather Squadron, and AMU, the statistical methodology was selected for further development. In November 2003, the

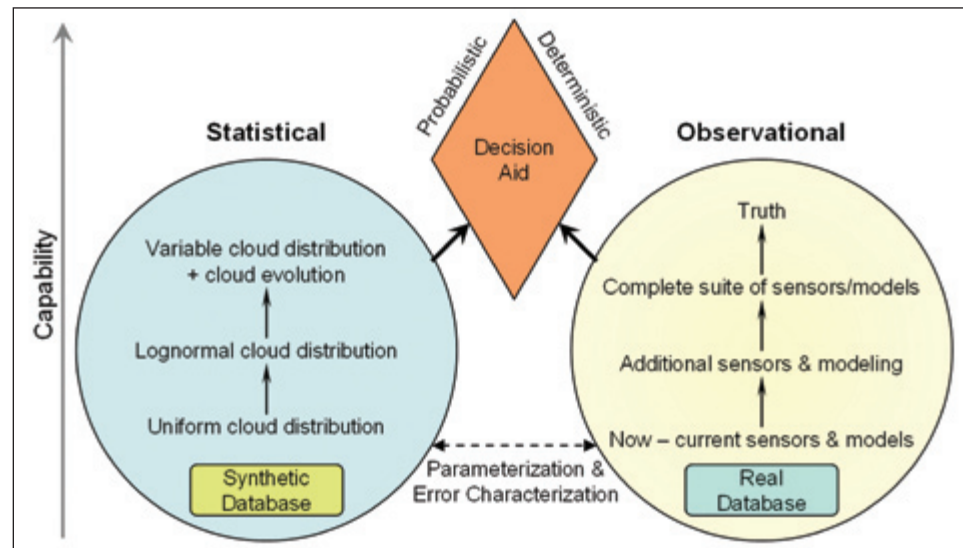


Figure 1. Hierarchy of potential methodologies showing increased capability with time. A statistical method is represented by the circle on the left, which illustrates increasing levels of complexity to simulate cloud fields. The statistical method could provide earliest capability for a Go/No-Go decision aid, if required, as a probabilistic tool. An observational method, represented by the circle on the right, illustrates increased capability gained through improved sensors and numerical simulations and modeling of near real-time data. The observational method has the potential to provide a more deterministic tool for a Go/No-Go decision aid, if required.



KSC Weather Office tasked the AMU to develop a model to forecast the probability that, at any time from launch to SRB separation, at least three of the Shuttle ascent imaging cameras will have a view of the vehicle unobstructed by cloud.

A computer simulation model (Figures 2 and 3) was developed and used to estimate the ability of a network of optical imaging cameras to obtain at least N simultaneous views of the SSLV from liftoff to SRB separation in the presence of clouds. The model generated line-of-sight (LOS) data for a prescribed camera network and vehicle ascent trajectory. The camera network and ascent trajectory were embedded in a 3-D field of randomly distributed clouds. The LOS from each camera to the launch vehicle was computed along the vehicle trajectory, and cloud obscuration was noted as a binary variable, either obscured or clear. The obscuration data was then analyzed to determine the percentage of time from liftoff to SRB separation that at least N simultaneous views of the launch vehicle were obtained by the camera network, where N ranged from 2 to 6. One thousand trials with randomly distributed clouds were analyzed for each of approximately 19 different cloud scenarios. The cloud scenarios had prescribed cloud bases, tops, and sizes, with cloud coverage ranging from clear to overcast by 1/8 increments.

#### Key accomplishments:

- 2003: Completed a concept study to identify and evaluate alternative methods for determining if a sufficient number of Shuttle launch imaging cameras will have a field of view unobstructed by weather.
- 2004: Developed a statistical cloud model to quantify the degree to which the upgrade of the optical imaging system would improve the probability of acquiring three simultaneous views of the SSLV from liftoff to SRB separation in the presence of clouds.

#### Key milestones:

- 2005: Implement an operational tool on the Meteorological Information and Data Display System in the Range Weather Operations facility to enable the Launch Weather Officer to quickly determine if existing cloud cover has the potential to obscure optical imaging of the SSLV.

Contacts: J.T. Madura ([John.T.Madura@nasa.gov](mailto:John.T.Madura@nasa.gov)), YA-D, (321) 867-0814; and Dr. F.J. Merceret, YA-D, (321) 867-0818

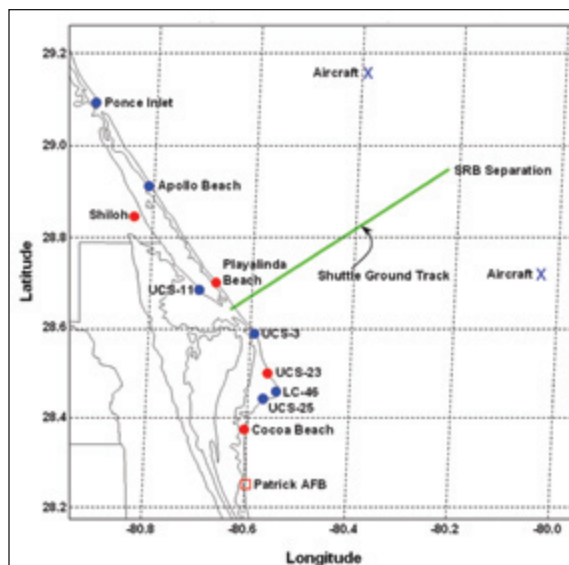


Figure 2. Configuration of long-range camera sites before upgrade (red) and after upgrade (red and blue). The airborne cameras are located 15 nautical miles NE and SW of the SRB separation point at an altitude of 65,000 ft.

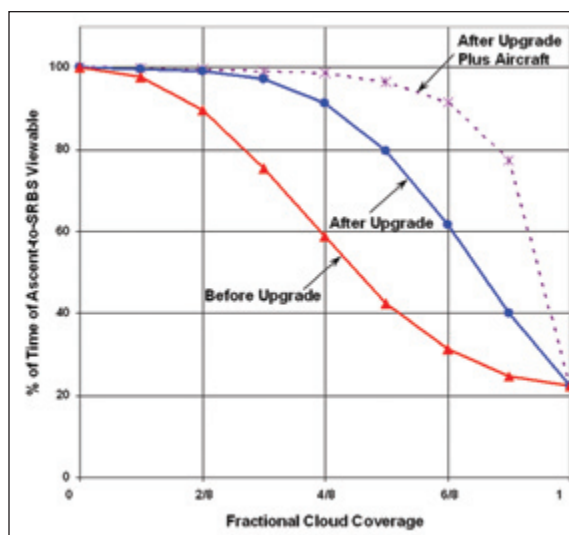


Figure 3. Fractional cloud cover versus percentage of time from liftoff to SRB separation that the launch vehicle was viewable simultaneously by at least three cameras for the network before upgrade (triangles), after upgrades without airborne cameras (circles), and after upgrade with airborne cameras (stars), for cloud bases at 8,000 ft and cloud thicknesses of 500 ft.

Participating Organizations: ENSCO, Inc. (D.A. Short, R.E. Lane, Jr., and W.H. Bauman, III) and 45th Weather Squadron (K.A. Winters)

## Space-Based Telemetry and Range Safety (STARS) 2004



TDRSS-Compatible  
Transceiver

This was a very busy and exciting year for the STARS project, a multicenter NASA project to determine the feasibility of using space-based assets, such as the Tracking and Data Relay Satellite System (TDRSS) and GPS, to increase flexibility and to reduce operational costs by decreasing the need for ground-based downrange assets and infrastructure.

There were seven successful test flights on an F-15B at Dryden Flight Research Center (DFRC) during June and July 2003. TDRSS was used for the space-based communications. Many maneuvers were performed and various configurations were tested as summarized in the table. Each flight lasted about an hour and resulted in large amounts of data for postflight analysis. The locations of the antennas on the aircraft are shown in the figure.

The Range Safety subsystem received low-rate flight termination signals and transmitted telemetry containing tracking data and health and status indicators. The Range User subsystem transmitted voice, video, and vehicle/payload data. All major test objectives were met. The success of STARS is attributed to the close working partnerships among many different NASA Centers, contractors, and the United States Air Force.

These test flights indicate that space-based communications can be used for both safety-critical and user data during the ascent phase of launch vehicles. This should result in significant cost savings after the initial development of the necessary systems. This demonstration also proved that a large team from many different organizations can work

### Flight profiles.

Flight	Date	TDRSS <sup>a</sup>	Maneuvers <sup>b</sup>	Comments
1	June 3	<ul style="list-style-type: none"> <li>RS – TDRS-W,S</li> <li>RU – TDRS-171 at 250 kbps</li> </ul>	<ul style="list-style-type: none"> <li>Straight and Level (turns)</li> <li>Dynamic (rolls, loops, POPUs, cloverleafs)</li> <li>Launch Vehicle Simulation</li> <li>(rapid ascent/descent)</li> </ul>	
2	June 13	<ul style="list-style-type: none"> <li>RS – TDRS-W,S</li> <li>RU – TDRS-171 at 500 kbps</li> </ul>	<ul style="list-style-type: none"> <li>Straight and Level (turns)</li> <li>Supersonic Level Flight</li> </ul>	
3	June 17	<ul style="list-style-type: none"> <li>RS – TDRS-171</li> <li>RU – TDRS-S,W at 125 kbps</li> </ul>	<ul style="list-style-type: none"> <li>Straight and Level (turns)</li> <li>Launch Vehicle Simulation (rapid ascent/descent)</li> </ul>	Flight recorder problems. No post-flight analysis performed.
4	June 19	<ul style="list-style-type: none"> <li>RS – TDRS-S</li> <li>RU – TDRS-W, 171 at 125 kbps</li> </ul>	<ul style="list-style-type: none"> <li>Dynamic (rolls)</li> <li>Slow (POPUs)</li> </ul>	No FTS commands transmitted.
5	June 24	<ul style="list-style-type: none"> <li>RS – TDRS-W</li> <li>RU – TDRS-171 at 250 kbps</li> </ul>	<ul style="list-style-type: none"> <li>Dynamic (rolls, loops, POPUs)</li> <li>Launch Vehicle Simulation (rapid ascent/descent)</li> <li>Supersonic Level Flight</li> </ul>	No Range Safety telemetry link. Frequency clearance not authorized.
6	July 9	<ul style="list-style-type: none"> <li>RS – TDRS-W</li> <li>RU – not used</li> </ul>	<ul style="list-style-type: none"> <li>Long-Distance Level Flight</li> <li>Straight and Level (turns)</li> </ul>	Only top RS antenna used. Filtered power to high-power amplifier for top antenna for first time.
7	July 15	<ul style="list-style-type: none"> <li>RS – TDRS-W</li> <li>RU – TDRS-171 at 125 kbps</li> </ul>	<ul style="list-style-type: none"> <li>Dynamic (rolls, loops, POPUs)</li> <li>Launch Vehicle Simulation (rapid ascent/descent)</li> </ul>	No STARS GPS. Filtered power to top/bottom RS transmit antennas.
<sup>a</sup> RS = Range Safety; RU = Range User <sup>b</sup> POPU = push-over–pull up				

together in overcoming technical and administrative challenges to successfully demonstrate new technology that will eventually make access to space easier and less expensive for everyone. The lessons learned from this initial set of test flights will carry over into the second set of test flights currently scheduled for early 2005, when a specially designed Ku-band phased-array antenna will be tested to increase the Range User data rates and the Range Safety system will communicate with multiple TDRSs simultaneously.

#### Key accomplishments:

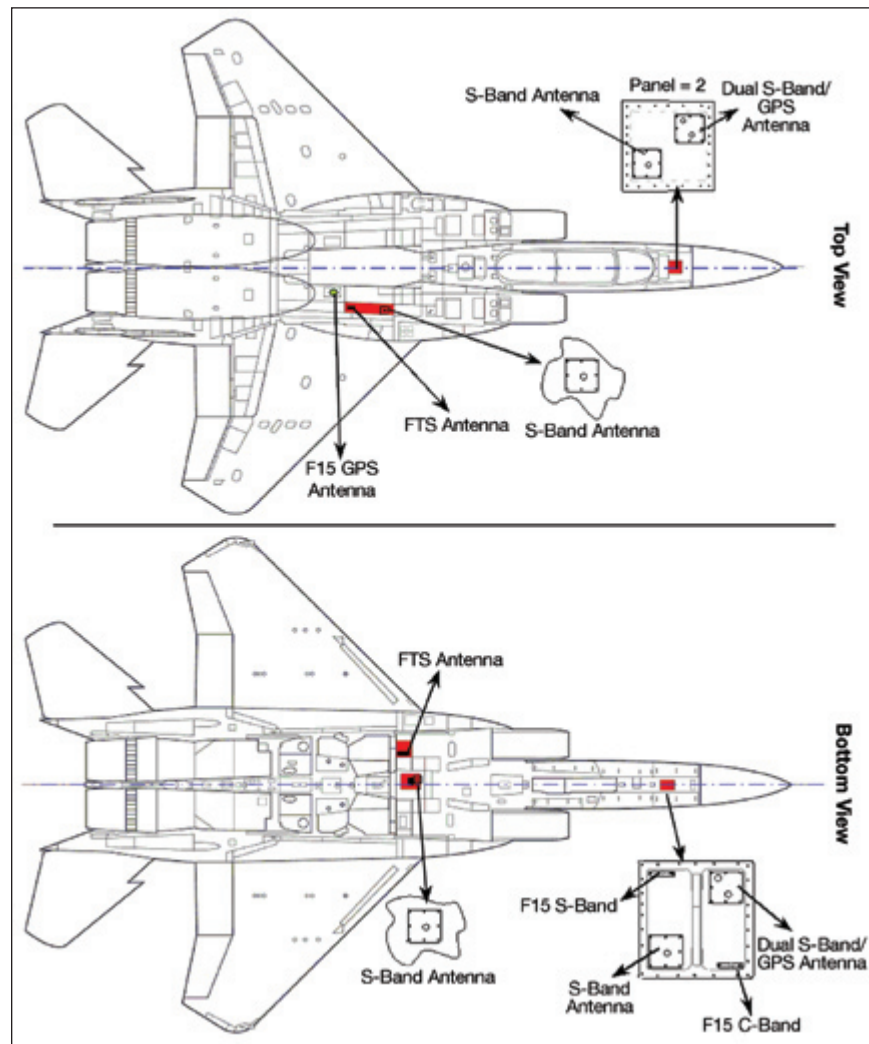
- Seven test flights on a NASA F-15B at DFRC.
- Extensive postflight analysis and Flight Demonstration 1 Final Report.
- Critical Design Review for Flight Demonstration 2.
- Integration of Range Safety processor, low-power transceiver, and GPS receiver into single unit for Flight Demonstration 2.

#### Key milestones:

- Summer 2004: Delivery of Flight Demonstration 2 flight hardware to DFRC.
- Spring 2005: Flight Demonstration 2 at DFRC.
- 2006: Flight Demonstration 3 on a hypersonic vehicle.

Contacts: L.M. Valencia  
([Lisa.M.Valencia@nasa.gov](mailto:Lisa.M.Valencia@nasa.gov)),  
YA-E6, (321) 861-7682; S.N.  
Bundick, Wallops Flight Facility,  
(757) 824-1424; and R.D.  
Sakahara, DFRC, (661) 276-2566

Participating Organizations:  
YA-D7 (E.C. Denson and Dr. J.C.  
Simpson), Goddard Space Flight  
Center (T.C. Sobchak), DFRC  
(D.E. Whiteman), General  
Dynamics (D.O. Glasscock), ITT  
(M. Harlacher and D.L. Wampler),  
NENS (M.A. Stager and J.A.  
Smith), RSO (J.L. Parks), and  
ASRC Aerospace (R.B. Birr)



Antenna locations on the F-15B.

# Iridium Flight Modem



Mission Data  
Feedback &  
Analysis

Development continued on the Flight Modem project that uses the Iridium global satellite communications system with commercial off-the-shelf communications equipment for low-rate, low-cost, two-way telemetry.

This year the applicability of Iridium Flight Modem for balloons was studied. Balloons are relatively slow-moving, low-altitude (less than 35 km) vehicles on which the antennas can be oriented upward, making them an excellent candidate for Iridium Flight Modem. However, balloons have special environmental concerns. Typical modems will function at temperatures as low as  $-10^{\circ}\text{C}$  without any modifications. With adequate insulation, tests indicate that typical modems will function at  $-70^{\circ}\text{C}$  for about 100 minutes—typical of a short-duration weather balloon operation. Long-duration balloons have both low- and high-temperature extremes and will require additional modifications. Smaller balloons also have restrictive size and weight requirements that are difficult to meet with the current hardware. Additional development is needed to satisfy these requirements.

There were two test flights of opportunity on sounding rockets during which the flight modem was integrated with a GPS receiver and transmitted a standard GPS position and velocity message. The first took place on

August 1, 2003, on a Terrier MK70-Improved Orion at Wallops Flight Facility (Figure 1). Interference between the flight modem and the onboard GPS receiver discovered during preflight testing led to the decision not to turn on the flight modem until after the high flight accelerations were over so that the onboard GPS receiver had the best chance to maintain lock with the GPS satellites. The modem did not start dialing until after the rocket had achieved its greatest speed at T+80 seconds. A connection was not established until T+285 seconds, and then only 14 seconds of flight modem data were transmitted. The entire flight lasted about 434 seconds. The connection was lost as the rocket started to descend, when it probably tumbled erratically, causing a loss of signal. The hardware was not recovered.

The second sounding rocket flight took place on April 13, 2004, on another Terrier MK70-Improved Orion at White Sands Complex (WSC). More filters were added to prevent radio frequency interference



Figure 1. Terrier Orion Rocket with Iridium Flight Modem onboard August 1, 2003.



problems. The flight modem sent data from liftoff to apogee of 120 km at T+161 seconds (the maximum altitude for guaranteed Iridium coverage is 150 km). The flight modem reacquired after the first parachute deployed at an altitude of about 4.5 km at T+338 seconds. Data was sent until the rocket hit the ground with a reported force of 50 g's. The Iridium link was maintained on impact, but the flight modem GPS dropped out for about 5 seconds. The flight modem continued to transmit for another 25 minutes. The position it was transmitting was within about 10 m of the rocket's location when it was found by the recovery team. All the hardware was recovered (Figure 2).

Iridium Flight Modem is an inexpensive and convenient method of sending two-way telemetry for aerospace applications. The Iridium system has an inherent reconnect time of as much as 20 to 30 seconds, so Iridium Flight Modem is most appropriate for relatively slow-moving vehicles such as aircraft or balloons that can tolerate these reconnect times.

#### Key accomplishments:

- 2001: Developed flight-ready prototype and performed initial ground-based demonstration.
- March through June 2002: Conducted four aircraft flight tests, improved software, increased data rates, tested different protocols, and measured data latency.
- July 2002: Developed prototype multiplexed dual modems.
- February 2003: Designed and built an integrated computer/modem box, updated operating system, and implemented real-time commanding and loss-less data compression scheme to increase data rate. Received integrated GPS receiver/modems for acceptance testing.
- March 2003: Conducted first unmanned aerial vehicle test on a model aircraft at KSC.
- October 2003: Performed environmental testing of integrated GPS receiver/modems.
- December 2003: Completed feasibility study.
- June 2003: Conducted sounding rocket flight 1 at WSC.
- April 2004: Conducted sounding rocket flight 2 at WSC.

#### Key milestones:

- Sounding rocket flight test report.
- Weather balloon flight test.

Contacts: Dr. J.C. Simpson ([James.C.Simpson@nasa.gov](mailto:James.C.Simpson@nasa.gov)), YA-D7, (321) 867-6937; A.J. Murray, YA-D7-E1, (321) 867-6673; and R.L. Wessells, Wallops Flight Facility, (757) 824-1297

Participating Organizations: ASRC Aerospace (W.D. Haskell and R.B. Birr) and NSROC (T. Gass)

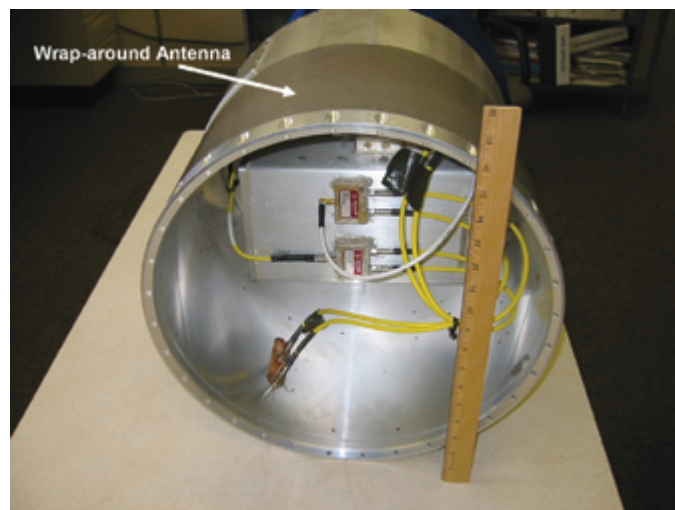


Figure 2. Postflight of Flight Modem hardware in second rocket.

## Autonomous Flight Safety System (AFSS) – Phase III



Integrated System  
Health Management  
Technologies

AFSS, a joint KSC–Wallops Flight Facility (WFF) project in its third phase of development, is an independent subsystem intended to be mounted onboard Expendable Launch Vehicles (ELVs). AFSS uses tracking and attitude data from redundant onboard sensors to autonomously make flight termination decisions using software-based rules implemented on redundant flight processors. The goals of this project are to increase capabilities by allowing launches from locations that do not have or cannot afford extensive ground-based Range Safety assets, to decrease range costs, and to decrease reaction time for special situations.

Phase III flight prototype development adds the following improvements to earlier phases:

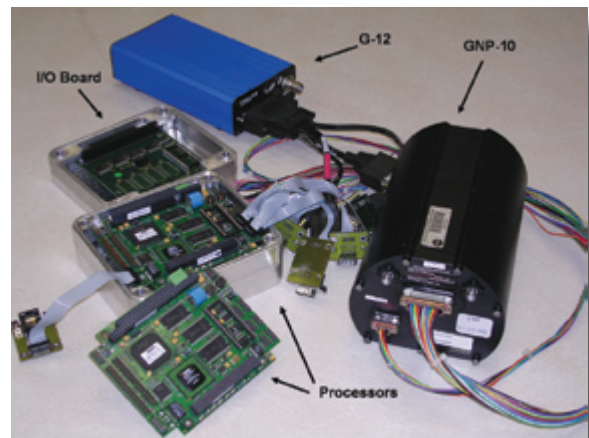
- Concept of Operations, more rigorous system-level requirements, and a baseline design
- Improved mission rule algorithms
- Multisensor / multiprocessor redundancy management approaches
- Flight-qualifiable hardware
- Extensive simulation testing
- Preliminary flight testing

Phase III AFSS is made up of redundant input sensors and redundant processors. The sensors are either GPS receivers or tightly coupled GPS/inertial measurement unit (IMU) sensors, and the flight processors are IBM Power PCs on PC104 boards running the VxWorks real-time operating system. Sensor solutions are checked for validity and compared with predetermined mission rules and boundaries established by the Range Safety authorities. The output of AFSS is a Monitor, Arm, Terminate, or Ready-to-Launch signal that is sent to the Command Switch Logic and Interlock Circuit (CSLIC), which interfaces with the termination system.

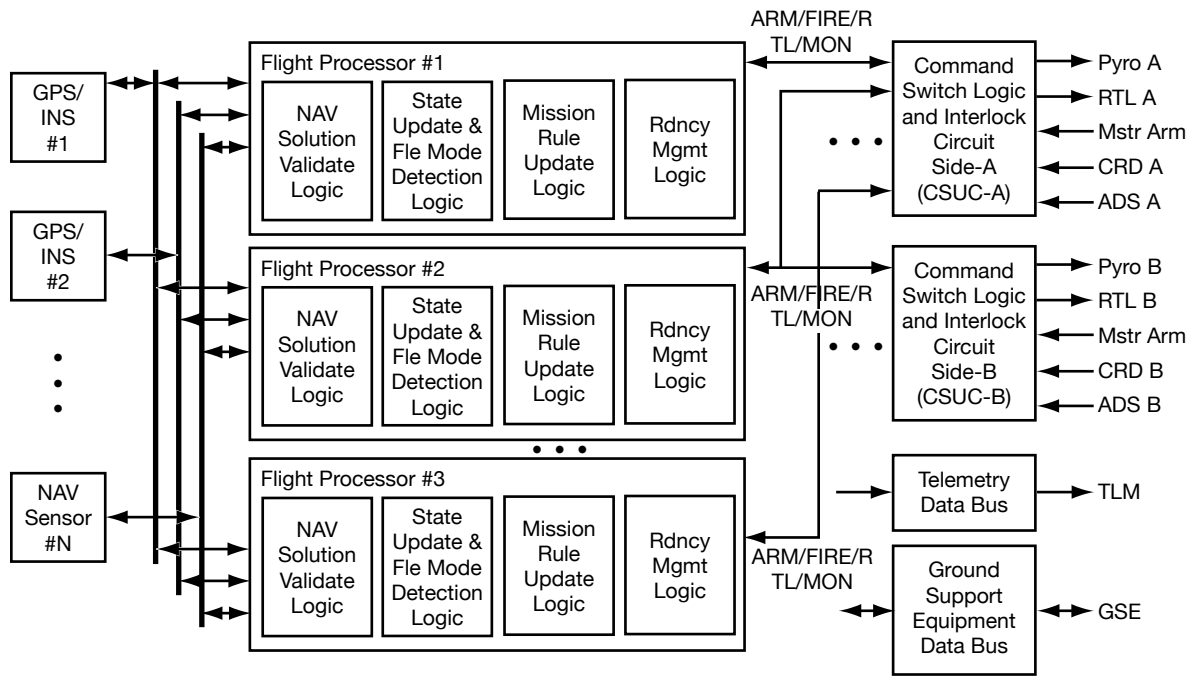
The mission rules are configured for each operation by the responsible Range Safety authorities and can be loosely categorized as follows:

- Parameter Threshold Violation – some trajectory value exceeds an allowed limit.
- Physical Boundary Violation – present position or instantaneous impact point is out of allowed region.
- Two-Point Gate Rule – determines if a specified point (e.g., vacuum impact) has crossed a gate formed by a line between two points or is ahead of or behind the gate.
- Green-Time Rule – how long the missile can safely fly without receiving valid updated tracking data.

Violations are weighted to prevent instantaneous termination due to random erroneous data and to ensure termination after a sufficient number of violations occur within a given time interval. Redundancy management can detect a bad processing string and ignore its output, preventing AFSS from terminating the vehicle with a single-point failure.



AFSS hardware.



Functional baseline of AFSS.

The primary testing will be performed with the hardware in the loop via large-scale Monte Carlo simulations to verify the system's ability to handle as many different failure modes as possible. Preliminary aircraft testing is also scheduled within the next year. Final testing will consist of parallel operations with existing systems during launches. The AFSS team has been in close contact with the Range community during Phases II and III and is soliciting their input for the final design and testing.

#### Key accomplishments:

- 2000: Phase I, Lockheed Martin Space Systems Company Feasibility Demonstration.
- 2002: Phase II, Lockheed Martin Space Systems/KSC and WFF/Dynacs Bench Prototype. Simulation testing performed on dual-sensor/single-processor system against 28 launch scenarios with various failure modes.
- 2003: Phase III, developed new software. Simulation-regression-tested Phase III algorithms against Phase II launch scenarios with various failure modes.

#### Key milestones:

- 2004: Final design of redundant system. Aircraft flight testing of single processor, multisensor system. Simulation testing of final redundant processor, multisensor system.
- 2005: Flight test of AFSS on a high-performance vehicle.

Contacts: B.A. Ferrell ([Bob.A.Ferrell@nasa.gov](mailto:Bob.A.Ferrell@nasa.gov)), YA-D7, (321) 867-6678; J.B. Bull, WFF, (757) 824-1893; and R.J. Lanzi, WFF, (757) 824-2492

Participating Organizations: ASRC Aerospace (J. Marin, S.M. Simmons, and R.D. Zoerner), RSO (J.L. Parks), YA-D7 (Dr. J.C. Simpson and S.A. Santuro), WFF (S.E. Kremer and G.F. Robinson), NSROC (V.M. Anton), LJT & Associates, Inc. (H.C. Chang), and USAF 30th and 45th Range Safety Offices

## Latest Enhancements for the Microwave Scanning Beam Landing System (MSBLS) Flight Inspection System



Space & Air Traffic  
Management System

The Space Shuttle Orbiter uses MSBLS for final approach and landing at end of mission, Continental United States (CONUS), and Transatlantic Abort Landing (TAL) runways. The MSBLS ground station signals (azimuth, elevation, and range) are acquired when the Orbiter is close to the landing site and has turned on its final leg. This usually occurs on or near the heading alignment cylinder, about 8 to 12 nautical miles (9 to 13 statute miles) from touchdown at an altitude of approximately 18,000 feet. The MSBLS ground stations are normally inspected every 2 years using airborne instruments (MSBLS Flight Inspection System [FIS]) that compare a Differential GPS (DGPS) position (truth) to the position signals sent by the MSBLS station to verify the system is within Orbiter-required specifications. The MSBLS antennas are adjusted, if necessary, to achieve the smallest error possible within the specifications.

The MSBLS FIS consists of a computer system with DGPS and MSBLS navigation data and Interrange Instrumentation Group B (IRIG-B) time for data synchronization. The MSBLS FIS computes the error between the two data inputs. Another computer system is used to generate a display for use by the aircraft pilot to fly certain profiles around the runway. The present MSBLS FIS hardware is becoming obsolete and the original equipment manufacturer of the computer operating system software no longer offers support. To continue performing MSBLS flight inspections, a project was started to upgrade the MSBLS FIS and improve its operational requirements. This has led to a NASA/Federal Aviation Administration (FAA) partnership for the next MSBLS FIS.

The FAA Bombardier Challenger 601 aircraft configured to operate with the FAA Automated Flight Inspection System (AFIS) has added MSBLS-flight-equivalent avionics and an L1/L2 GPS receiver to AFIS and added MSBLS and GPS antennas to the aircraft. The AFIS software performs the same function as the MSBLS FIS and produces similar data plots and data statistics. AFIS relies on the aircraft Flight Management System to control the flight profile used for a particular flight test run.

The FAA will have three aircraft configured to support MSBLS flight inspections or commissioning. This relieves NASA from scheduling an aircraft for flight inspection, configuring the aircraft with the MSBLS FIS, and installing antennas and associated waveguide and cables.



*AFIS Control and Display Flight Management System.*





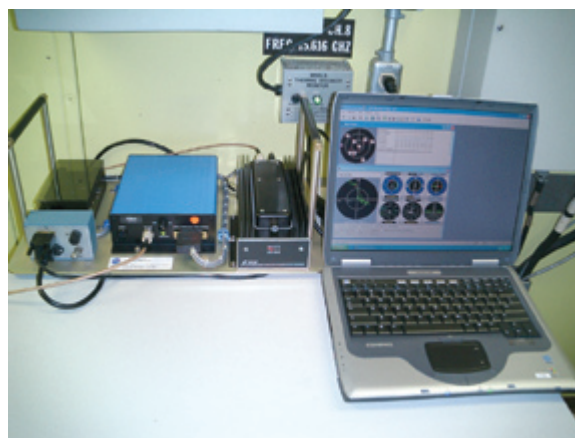
*Reference station GPS receiver and data link antennas.*

NASA and ASRC Aerospace have redesigned and fabricated DGPS reference stations for each MSBLS-supported runway. For redundancy and testing prior to the arrival of the FAA for flight test, there are two complete reference stations at each runway site. The new reference stations use the latest off-the-shelf hardware and software and can be set up, configured, and brought to operational status in less than an hour. While not in use, the reference stations are stored in four moistureproof cases at the runway facilities.

Continuing work on this project will replace the Automatic Gain Control (AGC) Calibration Test Set and downlink the AFIS data to the ground for display. The AGC Calibration Test Set generates MSBLS signals that are used to verify the FAA aircraft. AFIS can support MSBLS flight tests without actual flight testing at a MSBLS runway. The AGC Calibration Test Set is also useful for troubleshooting the MSBLS flight avionics. Downlinking the AFIS data to the ground will eliminate the need to have a MSBLS engineer in the FAA aircraft during the flight test to relay the needed antenna adjustments. The downlink data addition to AFIS will also benefit the FAA on other ground navigational aids it inspects and certifies.

*Contact:* J.J. Kiriazes ([John.J.Kiriazes@nasa.gov](mailto:John.J.Kiriazes@nasa.gov)), PH-F1, (321) 861-3700

*Participating Organizations:* ASRC Aerospace (M.M. Scott and T. Erdogan) and FAA Aviation System Standards (J. Lufkin)



*Reference station GPS receiver and data link transmitter assembly.*

## Real-Time Telemetry Display System (RTTDS)



*TDRSS-Compatible  
Transceiver*

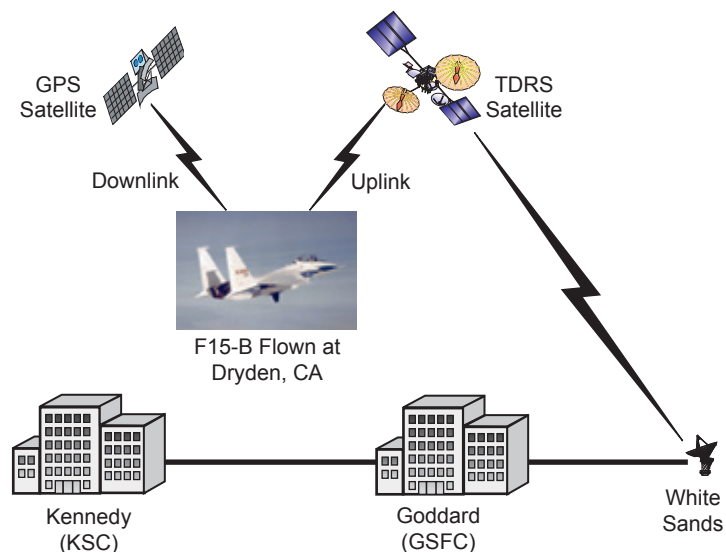
A series of flight tests was performed at NASA's Dryden Flight Research Center (DFRC) in California with an onboard experimental Space-Based Telemetry and Range Safety System in the summer of 2003.

A high-performance F-15B aircraft was used for these flight tests. The KSC RTTDS was designed and successfully used in support of this experiment. The RTTDS displayed the flight information at KSC while the F-15B was flying at DFRC over 2,000 miles away.

The total end-to-end data transmission delay is about 1.5 seconds from the time the F-15B receives GPS data to the time it displays the animation of the aircraft on the Satellite Tool Kit (STK) moving map. The total space data link distance was over 38,000 miles and the landline distance was over 3,000 miles.

The RTTDS user interface display is used for observing the actual flight telemetry graphically, enabling the user to make observations and decisions during the flight. The engineers and scientist involved in the flight testing can watch a 3-D display of the flight from a remote location and not have to be at the actual test site. Flight-test-related decisions can be made in real time and relayed to DFRC. This system can receive telemetry data from anywhere in the world and display the telemetry data at KSC. The system can also receive any source of telemetry data and display the data in a graphical manner for real-time evaluation.

In this particular flight test, the downlink telemetry, including GPS navigation data, was sent from the F-15B to an earth station at White Sands, New Mexico, via the Tracking and Data Relay Satellite System (TDRSS). The telemetry data



*Data path of the RTTDS.*

was sent to KSC over landlines through Goddard Space Flight Center (GSFC). At KSC's Range Technologies Development Laboratory, a Veridian Telemetry Decommutator Board was installed in a PC, which decommutates the telemetry data and makes it available to other applications.

LabVIEW by National Instruments was used to develop software code to display the health and status of the onboard flight system. LabVIEW receives the health and status data by linking to a Veridian software library. The health and status data display resides on the same PC as the decom board.

GPS position data is stripped out of the telemetry data bit stream and sent over the network using User Datagram Protocol (UDP). On another PC running STK, a graphical simulation and analysis tool, a C/C++ program was written to read the incoming position data using a UDP socket, verify its checksum, and send the data to STK. On STK the position data is sent to the F-15B scenario, as external ephemeris data. STK displays an animation of the aircraft movement in near real time over the maps while displaying position and movement data. External maps of the DFRC area were added to enhance the visualization.

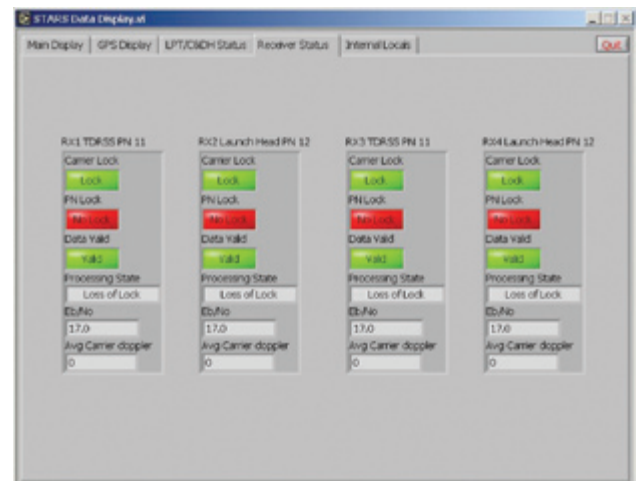
The advantage of this RTTDS is its versatility since it was not developed for a specific application and can be used with various scenarios. The RTTDS can receive any position and attitude telemetry data from any flight system or a terrestrial vehicle located anywhere and display it in near real time.

Contact: L.M. Valencia ([Lisa.M.Valencia@nasa.gov](mailto:Lisa.M.Valencia@nasa.gov)), YA-E6, (321) 861-7682

Participating Organization: ASRC Aerospace (R.B. Birr, R.D. Zoerner, and Dr. C.D. Immer)



Real-time display showing the simulated F-15B and the "real" F-15B.



LabView display showing health and status.

# Advanced Data Description Exchange Services (DDES) for Heterogeneous Vehicle and Spaceport Control and Monitoring Systems



*Seamless  
Command & Control  
Coordination*

These services provide a cross-platform software capability that enables a common semantic for control and monitoring of spacecraft and ground systems by autogenerating semantic processing services from standardized metadata specifications.

Command and Control Technologies Corporation (CCT) has designed and prototyped, as part of the Phase I Small Business Innovation Research (SBIR) project, a generic, platform-independent software capable of exchanging semantic control and monitoring information. In addition, CCT has laid the foundation for autogeneration of semantic construction and interpretation libraries from semantic databases that can be used for message-based communications between loosely coupled systems. Phase I work focused on evaluating approaches to both exchange of semantic information and semantic processing using a new space domain EXtensible Markup Language (XML) metadata standard called XTCE (XML Telemetric Command Exchange schema). We also considered the value of those approaches for both new and legacy systems.

This new capability is significant because it will reduce development, operations, and support costs for legacy and future systems that are part of ground- and space-based distributed command and control systems. It will also establish a space systems information exchange model that can support future highly interoperable and mobile software systems.

The principal Phase I objective was to evaluate the feasibility of creating generic services for control and monitoring information exchange. The Phase I objectives were fully met as shown by the following results and findings.

- Confirmed through analysis of a broad base of legacy space ground systems and processes that semantic description and exchange are not currently standardized and that a significant component of ground systems cost is consumed with customization and adaptation for ingesting mission configuration information.
- Confirmed XTCE is an appropriate and viable standard for telemetry and command description. Custom extensions to XTCE are usually not required but are easy to implement when necessary.
- Determined that autogeneration of XTCE manipulation services does not provide a significant advantage over use of common XML libraries for query, parse, and validate tasks.
- Found that developing a generic approach to autogenerating custom XTCE exchange adapters for legacy systems is difficult and may not be cost-effective.

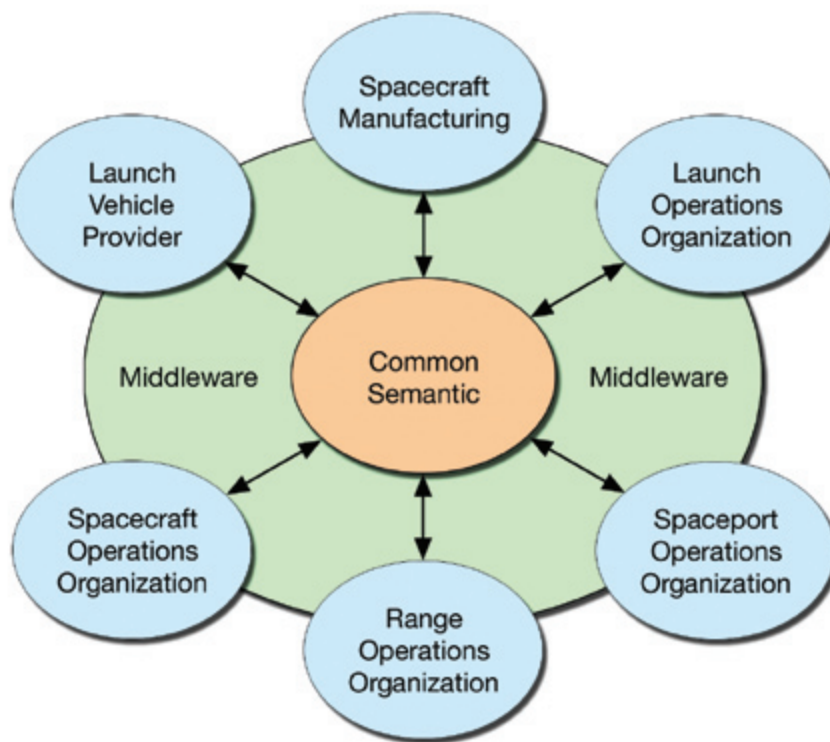


- Determined that autogeneration of semantic processing (AGSP) services for heterogeneous systems directly from XTCE or other metadata specifications is feasible and highly desirable, significantly reducing the amount of custom software required to create new or adapt legacy communications systems.

The findings and results of this research indicate there is a tremendous potential advantage in establishing a common semantic for both spacecraft and ground systems, and the autogeneration of semantic processing services will reduce costs and significantly enhance space systems interoperability.

Contact: Dr. J.J. Amador ([Jose.J.Amador@nasa.gov](mailto:Jose.J.Amador@nasa.gov)), VA-E1,  
(321) 853-9551

Participating Organization: Command and Control Technologies  
Corporation (R.D. Davis)



*XML DDES middleware concept.*

## Emerging Communication Technology (ECT)



*Seamless  
Command & Control  
Coordination*

Range Technology systems currently rely heavily on expensive networks of unique and costly ground-based legacy communication assets to interconnect tracking, communications, and flight termination functions. Much of this aging infrastructure is interconnected through legacy-installed, nonmovable cables. A future vision of a more flexible Spaceport and Range is emerging based on high-speed first-mile/last-mile communication technology implemented with new commercial technologies. Such technologies can seamlessly extend existing legacy Range infrastructure without wires and cables and hold great promise for preserving the utility of existing Range infrastructures while achieving life cycle cost savings and increased operational flexibilities for meeting new Range Communication needs.

The three technologies identified as most promising are Ultra-Wideband (UWB), Wireless Ethernet (Wi-Fi), and Free-Space Optical (FSO). Together, these technologies enable flexible communication at high data rates over the short distances needed for implementing first-mile/last-mile Range Communication connectivity. The predecessor Range Information System Management (RISM) project first identified these three key technologies in a report released in FY 2002 that identified the major communication trends and techniques being developed in the private sector, as well as their likely contributions to meeting future Spaceport and Range needs. The ECT project continued this investigation in FY 2003 through procuring and testing exemplars of these three technologies, culminating in a report released at the end of FY 2003 that detailed testing results for Wi-Fi, narrow-beam auto-tracking FSO systems, and second-generation UWB data communication systems. Based on these data results and identification of additional topics involving these technologies, continued investigations were conducted during FY 2004 into higher-reliability, lower-cost, wide-beam, nonautotracking FSO equipment, as well as into Orthogonal Frequency Division Multiplexed (OFDM) and position-aware functionality of UWB. From these steps, a common view of the future is developing, indicating that increased communication reliability at lower cost can be achieved through the use of commercial hardware, and this approach is feasible and realistic for addressing first-mile/last-mile Range Communication connectivity needs.

Key aspects of the Range Communication vision:

- Mobile, portable, fixed Range/Spaceport requirements.
- High-bandwidth, high-data-rate capability ultimately usable over 3 decades of data rates (10 Mb/s to 10<sup>+</sup> Gb/s) through the use of Wi-Fi, FSO, UWB, and related technologies.
- Seamless connections to today's wired communication infrastructure and future systems.
- Selectable features versus communication capability to best match future needs and provide flexible and quick turnarounds.

During the last year, the ECT project procured wide-beam FSO exemplars and collected measured results using a specially instrumented advanced networking laboratory at KSC to determine the limits of reliable lower-cost FSO technology. Shortcomings of

commercial products were identified, thereby pointing out developments needed for a new generation of commercial products for better meeting future Range Communication needs.

The ultimate outcome of ECT will be to establish selection criteria for best fitting appropriate commercial communication technologies to meet emerging Range Communication needs, while achieving data connectivity over at least 3 decades of data rates. Once the performance limits of these technologies are determined for networking capabilities, it will become possible to introduce operational systems utilizing these commercial technologies to augment future Range capabilities, while increasing Range safety and lowering life cycle costs.

Plans for FY 2005 are to continue investigations into longer-range Wi-Fi (greater than 20 miles), as well as into implementing and testing networking functions in wide-beam FSO systems, extending beyond the point-to-point, single-link FSO limitations tested over FY 2003 to FY 2004.

#### Key accomplishments:

- Successfully identified, procured, and tested a wide-beam FSO system for assessing whether lower-cost, more reliable FSO equipment without autotracking can provide future Range Communication functions. Results indicate up to 4-kilometer FSO systems provide highly satisfactory OC-12 (622 Mb/s) connectivity.
- Supported Advanced Range Technologies Working Group (ARTWG) and Advanced Spaceport Technologies Working Group (ASTWG) development efforts through participation in subgroup teams.
- Identified capability limits of UWB technology in addressing position awareness functions.

#### Key milestones:

- September 2003: Submitted ECT Phase II final report detailing testing results for Wi-Fi, UWB, and narrow-beam, autotracking FSO communication equipment.
- September 2004: Submitted ECT Phase II final report detailing testing results for wide-beam, nontracking FSO communication equipment.

Contact: R.A. Nelson ([Richard.A.Nelson@nasa.gov](mailto:Richard.A.Nelson@nasa.gov)), YA-D7, (321) 867-3332

Participating Organization: ASRC Aerospace (Dr. G.L. Bastin, W.G. Harris, T. Erdogan, and W.D. Haskell)

#### Comparison of leading candidate communication technologies.

Key Range Communication Attributes	Medium Data Rates (10 Mb/s – 100+Mb/s)	High Data Rates (100 Mb/s – 1,000+Mb/s)	Highest Data Rates (1,000 Mb/s – 10,000+Mb/s)
Candidate Technology	Wireless Ethernet (Wi-Fi)	Ultra-Wideband (UWB)	Free-Space Optical (FSO)
Typical Range	< 0.5 km (802.11b) < 32 km (LR Wi-Fi)	< 0.5 km	> 0.2 km, < 5 km
Selectable Data Security	Yes	Yes	Yes
Portable, Mobile, Fixed	Yes	Yes	Yes

## Four-Channel IRIG-106 Telemetry Decoder on a PC-104 Plus Card



*TDRSS-Compatible  
Transceiver*

A four-channel IRIG-106 telemetry decoder on a PC-104 Plus card was designed to accomplish required space and complexity reductions for the Spaced-Based Telemetry and Range Safety (STARS) Project Command and Data Handler (C&DH) Assembly (see the figure). The card is designed to meet most of the IRIG-106 Class 1 PCM specifications. A header provides data and clock differential inputs for each channel. Internal programming provides decoding NRZ-L, NRZ-M, NRZ-S, Bi-ØL, Bi-ØM, and Bi-ØS. The card does not support RNRZ-L formats or 33-bit-sync words and operates up to 1-Mbps data rates per channel. An in-house design was implemented only when an acceptable commercial equivalent could not be found.

The STARS project is a proof of concept demonstrating the feasibility of a space-based range system. STARS utilizes existing space platforms such as Tracking and Data Relay Satellite System (TDRSS) and GPS for flight termination, vehicle tracking, and telemetry for Range Safety and Range Users. A STARS-like system will save money by reducing the need for ground-based infrastructure and Downrange assets required to support Range operations. Studies have shown that a space-based range system could save the Air Force and NASA a combined \$50 million a year. To prove the concept, STARS will conduct three flight demonstrations.

The first C&DH utilized single-channel SAM/DEC/005 PCM decoder cards by ACRA Control Inc. These PC cards, or PCMCIA as they were once called, worked very well and are small by themselves. However, once four were mounted (one for each channel input) in a PC-104 carrier card and electrically connected, the additional protrusion added 2 inches along one axis, requiring a large amount of dead space inside the assembly.



*PC-104 Plus IRIG-106 decoder card prototype.*



The new card uses 5-volt and 3.3-volt power. PC-104 interrupts INTA, INTB, INTC, or INTD may be selected through onboard jumpers. IDSEL and clock lines are also selectable through onboard jumpers. Estimated power consumption is 2 watts. All components are rated for -40 to +80 °C operation.

Configuration data, mapped as I/O, for the desired minor frame is written to the card over the PCI bus, and a software reset is caused by writing to a status word address initializing the new configuration data. Minor frame data is stored in a paging scheme to allow reading by a processor while another minor frame is being stored. The page data is memory-mapped within the host system.

Upon storing a complete minor frame, an interrupt is provided to notify the processor that new minor frame data is available for reading. The status word is then read to determine which channel interrupt is set. A prioritization scheme must be established in the processor software program to handle multiple channel interrupts simultaneously. Each channel interrupt is reset immediately after reading the first data address. See the table for page data.

Testing has been limited to the requirements for the C&DH, and no drivers have been developed for a particular operating system. A knowledge of the PCI Bus and PC-104 Plus standards is required to set up and communicate with the card in a PC-104 stack.

Interest has surfaced for the card and may develop into other hardware versions such as a PCI card.

#### Key accomplishments:

- Fabricated and programmed a second prototype card.
- Conducted C&DH flight demonstration 1 on June 3, 2003.
- Reduced the size of the C&DH by approximately 50 percent.
- Passed acceptance testing on C&DH flight unit 2.

#### Key milestones:

- Conduct flight demonstrations 2 and 3 (scheduled for March 2005 and FY 2006, respectively).
- Complete a third and final version of the PC-104 card (July 2005).

Contacts: R.L. Morrison ([Robert.L.Morrison@nasa.gov](mailto:Robert.L.Morrison@nasa.gov)), YA-D5, (321) 867-6687; and E.C. Denson, YA-D8, (321) 867-6537

Participating Organizations: YA-E (L.M. Valencia and C.S. Forney) and YA-D (D.L. Hornyak)

Page data.

Address	Data			
	Upper 2 Words		Lower 2 Words	
	31	16	15	0
0	Sync Word			
1	DATA WD1		DATA WD2	
2	DATA WD3		DATA WD4	
254	DATA WD508		DATA WD509	
255	DATA WD510		DATA WD511	

# Spaceport Structures and Materials

Advanced structures and materials are critical to achieving the goals of reduced costs, increased reliability, and higher flight rates for future spaceports. Spaceport structures and materials technology development areas include corrosion abatement, static charge dissipation, nondestructive evaluation (NDE), reduction of vibroacoustic loads during launch, and nonflammability. Sources of corrosion and material degradation include humid saltwater environments surrounding launch structures and aggressive ozone and hard radiation environments of Earth orbit. Static charge buildup on payloads, spacecraft, and launch structures can present significant safety issues for personnel and equipment. NDE technologies are critical to obtaining rapid status analysis of flight hardware. Passive sound mitigation techniques to replace active noise reduction methods such as water suppression systems are desirable for future launch vehicle pads. Advanced nonflammable materials are desirable to enhance the safety of crew and ground personnel during operations. Since materials are ubiquitous in spaceflight, the reach of this technology thrust area will encompass launch structures, payload processing, spacecraft design, and vehicle maintenance.

Technology focus areas include the following:

- Launch Structures and Mechanisms
- Corrosion Science and Technology
- Electromagnetic Physics
- Materials Science and Technology
- Nondestructive Evaluation

The goals and objectives of Spaceport Structures and Materials include the following:

- Ensure safe, efficient, and reliable structures techniques
- Enhance reliability and reduce maintenance cost of infrastructure
- Improve safety and reliability of operations through detection, mitigation, and prevention of electrostatic generation on equipment
- Develop specialty materials in support of future structures and materials initiatives

*For more information regarding Spaceport Structures and Materials, please contact Dr. Carlos Calle ([Carlos.I.Calle@nasa.gov](mailto:Carlos.I.Calle@nasa.gov)), YA-C2-T, (321) 867-3274.*

## Pressure Dependence of Insulator-Insulator Contact Charging

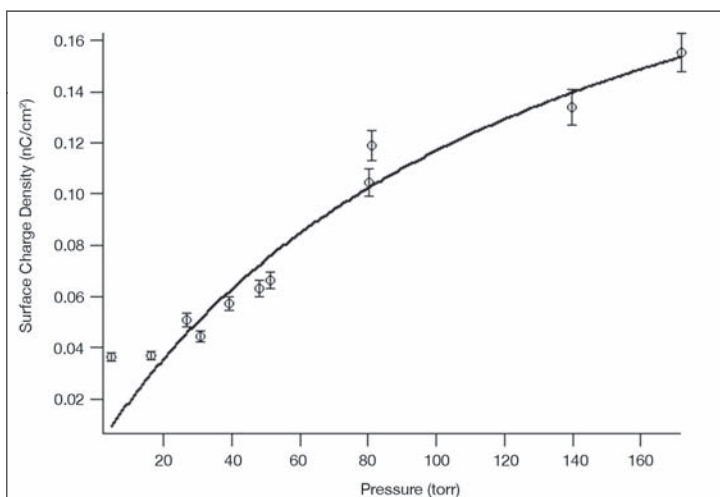


Contamination  
Detection/Reduction/  
Cleaning

The mechanism of insulator-insulator triboelectric (contact) charging is being studied by the Electrostatics and Surface Physics Laboratory at KSC. The hypothesis that surface ion exchange is the primary mechanism is being tested experimentally. A preliminary two-phase model based on a small partial pressure of singly charged ions in an ambient neutral ideal gas in equilibrium with a submonolayer adsorbed film will provide predictions about charging as a function of ion mass, pressure, temperature, and surface adsorption energy. Interactions between ions will be considered in terms of coulombic and screened potential energies. This work is yielding better understanding of the triboelectrification of insulators, which is an important problem in space exploration technology. The work is also relevant to important industrial processes such as xerography and the application of paints and coatings. A better understanding of the fundamental mechanism of insulator-insulator triboelectrification will hopefully lead to better means of eliminating or at least mitigating its hazards and enhancing its useful applications.

Metal-metal and metal-insulator contact charging are well-known phenomena with good to fair theoretical understanding. In spite of its great importance in industrial processes, insulator-insulator charging is the least understood triboelectric phenomenon. Insulator-insulator charging is also of great concern for spacecraft in deep space or on planetary surfaces.

Surface impurities, which can be mostly ionic in nature, can play a role in the charging of insulators. Ion transfer in metal-insulator charging has been advocated by several researchers to account for charge exchange. Ions can exist on the surface of an insulator either in weak bonds caused by intermolecular forces while residing in vibrational energy states or as solvated ions in a thin surface water layer.



Curve fit of new experimental data for HDPE with two-phase equilibrium model.

Since atmospheric pressure and surface moisture layers play a major role in surface charging, a preliminary model is presented in which the surface of the insulator is in equilibrium with its external environment. Equilibrium is used because charge transfer occurs rapidly during triboelectrification. The surface is modeled as having localized states with a certain adsorption energy,  $-\xi_0$ , for the surface particles. The particles are considered to be a vapor of noninteracting ions of single polarity in

equilibrium with an adsorbed submonolayer on the surface. The chemical potential of the vapor is determined using the grand canonical ensemble and then equated to the chemical potential of the submonolayer to determine vapor pressure. By assigning a charge (assuming single ionization) to the vapor particles, the surface charge resulting from the adsorbed monolayer can be calculated as a function of pressure. Including the effective electrostatic potential felt by the gas-phase particles from the surface charge gives an equation for surface charge density in terms of ion mass, pressure, adsorption energy, and temperature:

$$\sigma = \frac{q_e N}{A} \frac{P_v}{(k_B T)^{5/2} E_2(\alpha/z_0) \left( \frac{m}{2\pi\hbar^2} \right)^{3/2} e^{-\xi_D/k_B T} + P_v} \quad (1)$$

where  $N$  is the total number of surface states available,  $A$  is the surface area,  $P_v$  is the vapor pressure,  $k_B T$  is the particles' thermodynamic energy,  $\xi_0$  is the adsorption energy, and  $\hbar$  is Planck's constant divided by  $2\pi$ .  $\alpha$  is a characteristic distance found by dividing the electrostatic energy by the thermal energy of a particle and solving for the radius, and  $z_0$  is the distance from the surface.  $E_2(\alpha/z_0)$  is the second-order  $E_n(x)$  function with  $\alpha/z_0$  as the argument.

Experimental surface charge versus pressure data was taken for several polymers. This data was curve-fit to the model equation for each polymer. An example of these curve fits is shown for high-density polyethylene (HDPE) in the figure.

Future work will include more experimentation to expand the data set for polymers. To reproduce previous experimental data on metal-metal and metal-insulator triboelectric charging by others and to validate the experimental techniques for insulator-insulator triboelectric charging, triboelectric experiments will be performed using oriented metal samples of known work function.

#### Key accomplishments:

- Developed preliminary physical model.
- Studied initial surface charge density versus pressure experiments on polymers.
- Revised preliminary model to include effective coulombic and screening potentials.
- Performed initial curve fits of theoretical equation to experimental data. Good correlation was shown.

#### Key milestones:

- Perform additional insulator-insulator triboelectric experiments.
- Perform metal-metal and metal-insulator triboelectric experiments.
- Continue to improve theoretical model and determine its physical limitations.

Contacts: M.D. Hogue ([Michael.D.Hogue@nasa.gov](mailto:Michael.D.Hogue@nasa.gov)), YA-C2-T, (321) 867-7549; and Dr. C.I. Calle, YA-C2-T, (321) 867-3274

Participating Organization: University of Central Florida (Dr. E.R. Mucciolo and Dr. R.E. Peale)



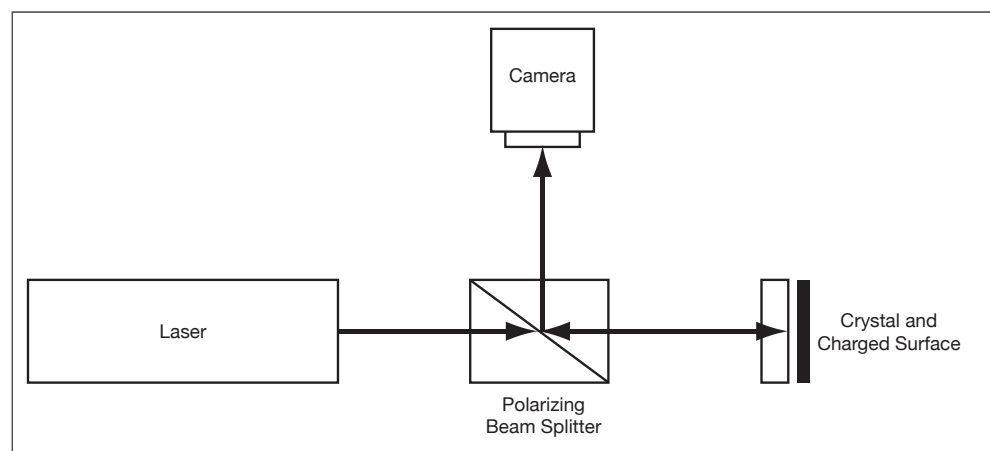
## Electro-Optic Method of Surface Charge Measurement



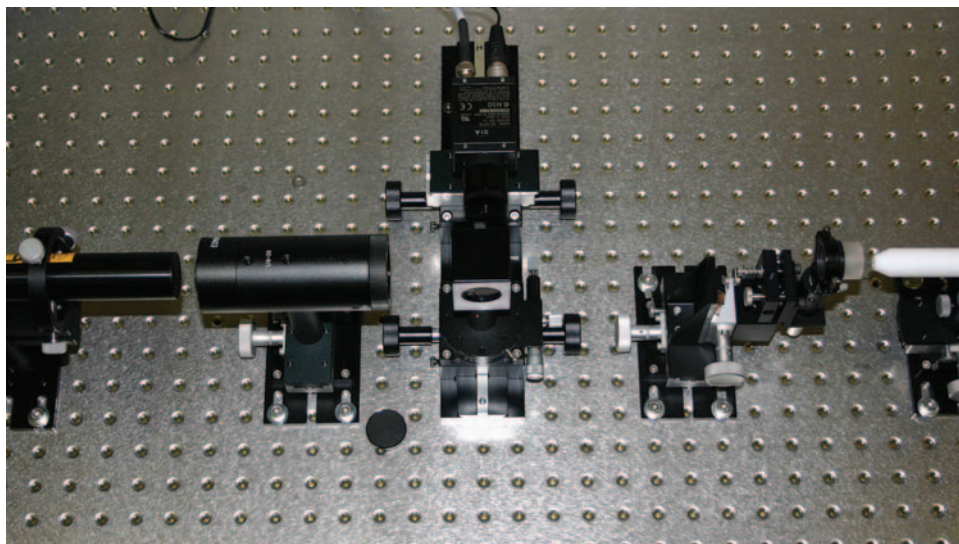
Contamination  
Detection/Reduction/  
Cleaning

Current methods for charge measurement are either impractical for field measurements or do not give a true value of charge distributed over a surface. A current option for charge measurement is to use a Faraday cup. With this device, the total amount of charge developed on a surface can be measured, but the surface charge density on the material cannot be determined. Also, the material to be measured must fit within the cup, which makes it impractical for determining the charge on the surface of large objects. Furthermore, only a single average value is reported to describe the charge accumulation on the material. Electrometers are also sometimes used to determine the amount of charge accumulated on a surface; however, electrometers only give an average reading of the electric field over an area and are greatly affected by any surrounding grounded or metallic materials. Again, this method only gives a single value to describe the electric field characteristics of the materials.

An electro-optic method to visualize electrostatic charge developed on insulator surfaces is being investigated. Certain birefringent crystals undergo an electro-optic effect known as the Pockels effect. In these crystals, the phase of light changes as a function of the potential difference across the faces of the crystal. By bringing a charged surface near or in contact with the crystal surface, the electric field across the crystal is modified. This in turn changes the direction of polarization of the light traveling through the crystal. If the light is polarized in a known direction before it travels through the crystal, then the polarization of the light will shift after exiting the crystal. Passing the light back through the same polarizer that was used to initially polarize it will result in some light being blocked. Therefore, we can measure the magnitude of the electric field across the crystal by measuring the change in intensity of the light after it passes back through the linear polarizer. This system will allow us to determine how charge is distributed over a surface and will allow us to identify both positive and negative charge.



*Experimental setup concept.*



*Actual experiment setup (same as drawn diagram).*

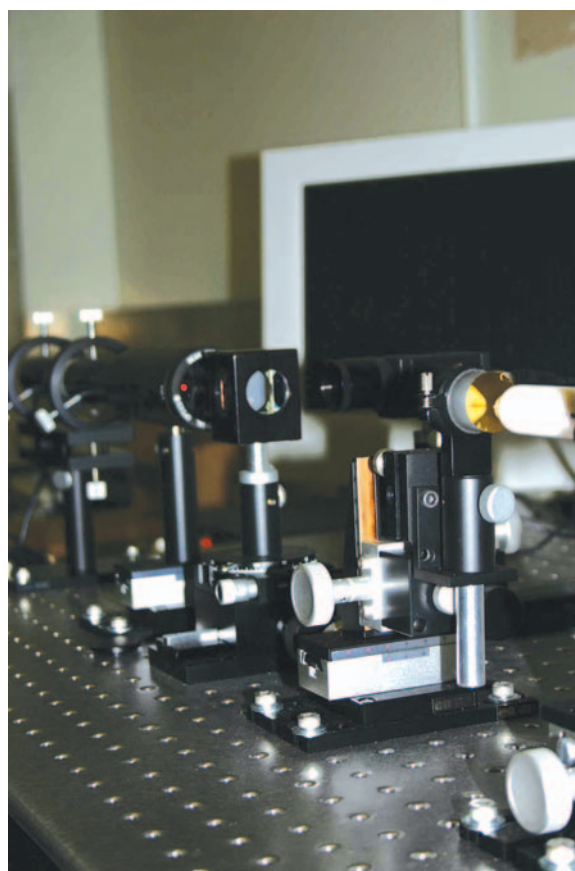
The goals of this project are to develop an instrument to visualize surface charge on insulators for material characterization and to calculate the minimum obtainable resolution to determine if the system can detect defects on either insulator or conductor surfaces.

#### Key accomplishments:

- Completed an optical board layout of components and an image acquisition system for a laboratory-based device.
- Developed an image processing program for the reduction/elimination of interference patterns in acquired images.
- Performed intensity shift calculations to calibrate the crystal's response to electric fields.
- Made initial measurements with  $\text{LiNbO}_3$  crystal and observed intensity shift with applied electric field.
- Initiated computer modeling (using FEMLAB) to compare the sensitivity of current electrometer systems for charge measurement to the expected sensitivity of the optical system.

Contacts: Dr. C.I. Calle ([Carlos.I.Calle@nasa.gov](mailto:Carlos.I.Calle@nasa.gov)), YA-C2-T, (321) 867-3274; and E.E. Arens, YA-C2-T, (321) 867-4861

Participating Organization: ASRC Aerospace (A.W. Nowicki)



*Side view of setup. The crystal can be seen in the image (gold disk). One side of the crystal has a thin gold coating on it in order to ground one side so the electric field across the crystal will be more significant for measurement purposes.*

## Polyimide Wire Insulation Repair Material



Wire  
Inspection &  
Repair

Electrical wiring, with its associated insulation, is installed throughout all hardware that uses electricity for power and/or signal transmission, including spacecraft, manned or unmanned; the International Space Station (ISS); ground support equipment (GSE); and landers, manned or unmanned. Failure of the wire insulation represents a major prob-

lem that can lead to mission failure and loss of life in manned operations. The current repair procedures follow Boeing Specification ML0603-0004 for Shuttle Electrical System Material Review and Maintenance Procedures – Level II. A significant quantity of wire insulation used in the Shuttle is Kapton, a polyimide that is susceptible to damage by hydrolysis and mechanical stress. Many of the repair procedures use tape with wire ties at each end to cover the damaged insulation. This type of repair is not moisture-tight and does not prevent hydrolysis of Kapton. Many times, when Kapton insulation is damaged near connectors, “ring breaks” occur. Another common repair method uses a clamshell-type clamp to hold a low-softening-point Teflon-type material in place while it is melted with a heat gun. Although this repair is moisture-tight, the heat gun can damage surrounding wire insulation and there are many locations where the gun cannot reach the damaged insulation. These repairs use material with lower melt temperatures than Kapton H, which cannot be used as part of a self-repairing insulation, the long-term goal of this development effort. It is also common to find that two new “ring breaks” appear at the ends of the repaired insulation when the clamshell-type repair is made.

The present project involves developing a method of using polyimide itself to repair damaged Kapton wire insulation. The initial goal of the project is to develop a method to manually repair damaged wire insulation. A second objective is to develop a chemical heating system that can be used in conjunction with the repair materials to accomplish the cure and bonding to Kapton H insulation.

Kapton-type wire insulation is prepared via the reaction scheme illustrated in Figure 1. The starting components include a dianhydride and a diamine. An initial polymer, a poly(amic acid) (PAA), is produced. This polymer, when heated to temperatures above approximately 150 °C, undergoes a molecular condensation/cyclization resulting in the final polyimide. The final polyimide has exceptionally good electrical insulating properties in addition to outstanding high-temperature and chemical resistance. Because of Kapton’s chemical and high-temperature properties, conventional insulation repair techniques are ineffective for this material.

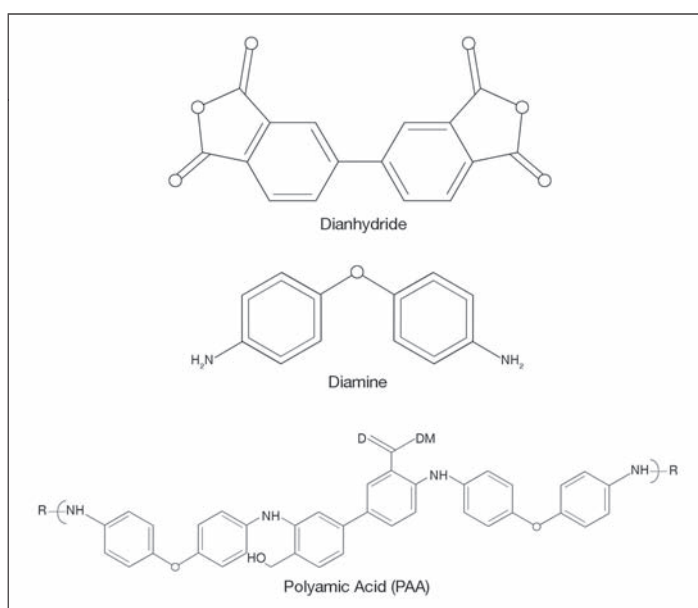


Figure 1. Reaction scheme for Kapton-type wire insulation.

Research to date has centered on the preparation of PAA precursors that have the needed physical properties to allow this material to be applied to damaged Kapton insulation and be heated to a temperature where the PAA could cure in place and simultaneously bond to the original Kapton insulation. Several physical forms of PAA have been prepared in an effort to achieve good adhesion to Kapton after cure. These forms include the preparation of solid microparticulate PAA (5 to 30  $\mu\text{m}$ ), PAA/N-methylpyrrolidinone (NMP) solutions, and PAA/NMP thin films.

Initial adhesion tests to a Kapton film substrate have proven successful. A PAA/NMP solution (approximately 15 percent PAA) was applied as a thin film to a Kapton film substrate and submitted to a ramped temperature cure cycle consisting of an hour at 80 °C, an hour at 150 °C, and a final hour at 200 °C. The resulting bilayer film was flexible and the layers could not be manually separated. This film was submitted for lap shear analysis to see if the two layers could be separated under harsher conditions. The epoxy glue bonds that attached the shear apparatus to the film failed before any separation of the two polyimide film layers was observed (see Figure 2).

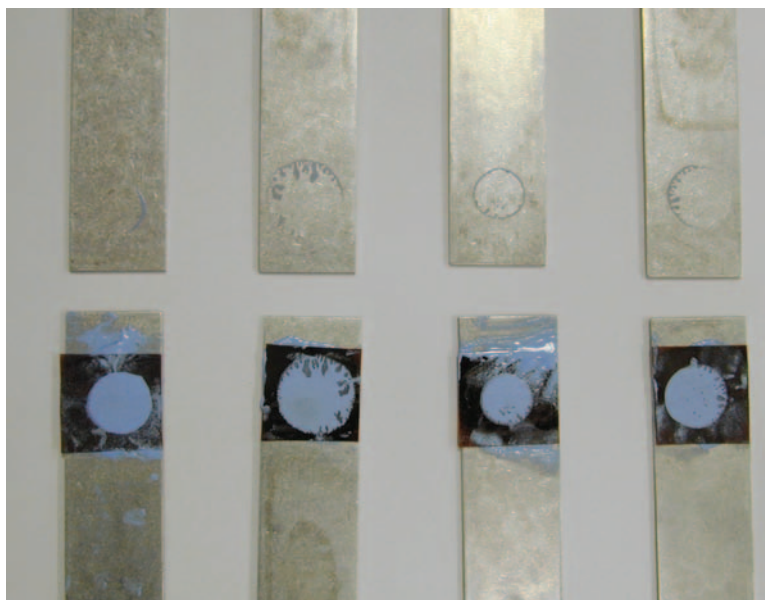


Figure 2. Lap shear testing.

#### Key accomplishments:

- Prepared PAA precursors in various forms.
- Demonstrated outstanding bond adhesion using a precursor PAA that was applied wet and cured in place.

#### Key milestones:

- Demonstrate bonding to Kapton H using PAA precursors.
- Prepare and operate a localized chemical heater to cure PAA precursor materials.

Contact: Dr. C.F. Parrish ([Clyde.F.Parrish@nasa.gov](mailto:Clyde.F.Parrish@nasa.gov)), YA-C3,  
(321) 867-8763

Participating Organization: ASRC Aerospace (Dr. T.L. Gibson  
and Dr. S.T. Jolley)



## Medium-Velocity-Contact Electrification Experiments With Martian Regolith Simulant

NASA has great interest in testing the electrostatic charging of various materials caused by the saltation process near the surface of Mars. It is necessary to know the extent of charging of man-made materials to better plan future Mars missions. A test method that quantifies frictional charging of Johnson Space Center Mars-1 regolith simulant was developed that minimizes variations in initial conditions and produces reasonably consistent results. The “shakerbox” concept involves triboelectrification within a closed system, induced through vigorous motion of a container enclosing a controlled amount of simulant. The interior surface of the container is lined with the test material under consideration. Assuming conservation of charge, the accumulated charge of the simulant, measured in a Faraday cup, will be equivalent but opposite in sign to the charge induced on the surface of the test material. The primary forms of frictional charging that are induced through this method are sliding, rolling, vibration of surfaces at a contact, and impact charging. The variables for this process are surface area, frequency, displacement, and duration.

The test environment was a low-pressure atmosphere (7 mm mercury), composed mostly of carbon dioxide with a low water vapor content, at a mean temperature falling within standard ambient. The materials selected for testing were Teflon, Rulon, G-10, Lexan, and acrylic. Two specific charging processes with differing contact characteristics were investigated. Trial set 1 investigated the effects of a high-frequency, low-displacement orbital (rotary) vibration. Trial set 2 tested the effects of a low-frequency, high-displacement orbital vibration. The total surface area within the closed shakerbox was 94.33 cm<sup>2</sup>. The entire inner surface of the shakerbox came into contact with the regolith simulant during the high-displacement experiments, but during the low-displacement experiments, the surface area impacted by the regolith simulant was a fraction of the total, on the order of 25 to 30 cm<sup>2</sup>. In addition, time-based studies (trial sets 3 through 5), using the Teflon- and G-10-lined shakerboxes, were conducted to investigate the effects of varying the duration, frequency, and magnitude of contact.

The baseline-adjusted results from trial sets 1 and 2 are expressed in terms of nanocoulombs per gram, as shown in Figure 1. For the time-based studies, frictional charging experiments were conducted in durations of 0 to 300 seconds. Trial set 3, as shown in Figure 2, used the same vibration frequency and displacement from trial set 2. Trial sets 4 and 5 used varying displacement and frequency settings to investigate the uncertainty in cumulative charge demonstrated by the Teflon-based material. In addition, trial set 5 investigated the difference in results between the nominal “closed system,” provided by a shakerbox with its lid in place, and results obtained when the experiment was conducted with an open top to the shakerbox. These results are illustrated in Figures 3 and 4. The mechanical characteristics of each trial set are provided in the table.

*Contact:* Dr. C.I. Calle ([Carlos.I.Calle@nasa.gov](mailto:Carlos.I.Calle@nasa.gov)), YA-C2-T, (321) 867-3274

*Participating Organization:* Florida State University (Dr. R. McCown and Dr. F.B. Gross)

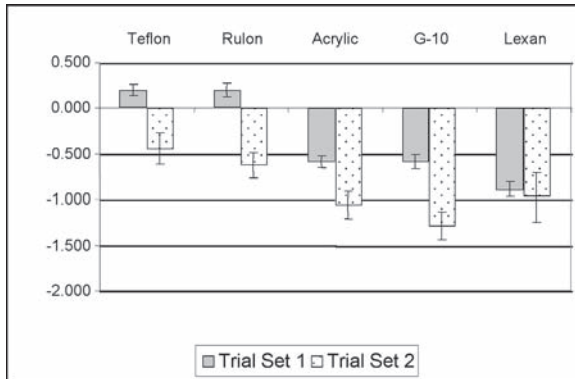


Figure 1. Results of trial sets 1 and 2.

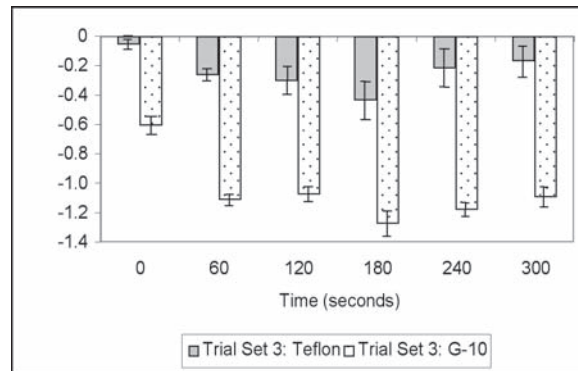


Figure 2. Results of trial set 3.

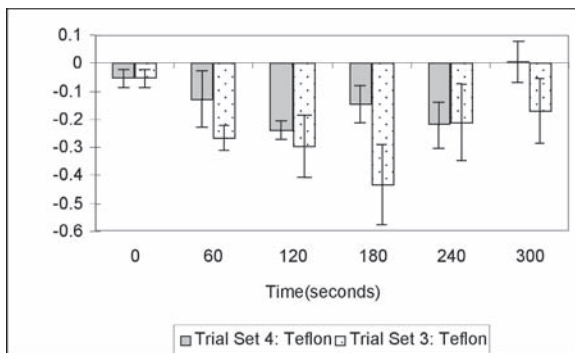


Figure 3. Comparison of trial sets 3 and 4.

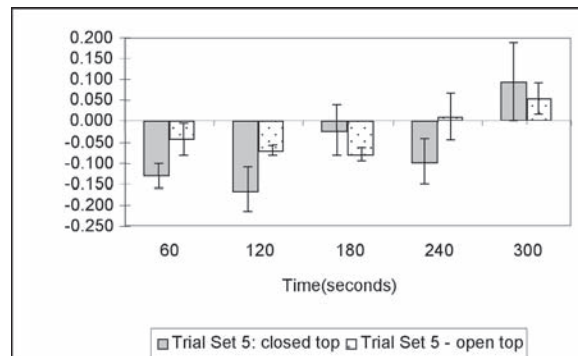


Figure 4. Results of trial set 5.

Experiment mechanical characteristics.

Trial set	Shaker Box Configuration	Displacement (inches)	Hz	Arm Weight (grams)
#1 Full set, 180 seconds	open top, 30 g (average weight)	$\pm 0.063$	22.40	12.47
#2 Full set, 180 seconds	closed top, 65.5 g (average weight)	$\pm 1.250$ (major axis) $\pm 0.600$ (minor axis)	5.20	80.81
#3 Time trials, Teflon and G-10	closed top	$\pm 1.250$ (major axis) $\pm 0.600$ (minor axis)	5.20	80.81
#4 Time trials	closed top	$\pm 0.125$	33.30	30.44
#5 Time Trials	closed and open top	$\pm 0.045$	22.94	16.21

## Development of the Dust Particle Analyzer To Characterize the Size and Charge of Particles Suspended in the Martian Atmosphere



*Contamination  
Detection/Reduction/  
Cleaning*

Some of the latest pictures of the surface of Mars sent by NASA's Spirit rover in early January 2004 show very cohesive, "mudlike" dust layers. Significant numbers of dust clouds are present in the atmosphere of Mars. NASA spacecraft missions to Mars confirmed hypotheses from telescopic work that changes observed in the planet's surface markings are caused by wind-driven redistribution of dust. In these dust storms, particles with a wide range of diameters (less than 1 to 50  $\mu\text{m}$ ) are a serious problem for solar cells, spacecraft, and spacesuits. Dust storms may cover the entire planet for an extended period. It is highly probable that the particles are charged electrostatically by triboelectrification and by ultraviolet irradiation.

To analyze the size and charge distributions of the Mars dust cloud, a Dust Particle Analyzer is being developed by NASA's Electrostatics and Surface Physics Laboratory at KSC in collaboration with the University of Arkansas at Little Rock. This instrument may be developed into a flight instrument that could be used to characterize the size and charge of dust particles suspended in the Martian atmosphere.

The prototype instrument is currently being tested in KSC's Mars Electrostatics Chamber using a Martian dust simulant. To study the contact electrification of the Mars simulant dust caused by erosion of the dust in a storm and the resulting suspension over millions of years in a dry atmosphere, experiments are being performed to characterize the particle size and electrostatic charge distributions of this simulant. Approximately 20 grams of simulant dust sample was contained in a small plastic jar and shaken for 3 minutes to allow the dust to acquire electrostatic charge by friction against itself and by contact with the wall of the plastic jar. Since the wall surface was comparatively negligible compared to the large surface area of the dust particles, and since the container wall was insulating, it was assumed that tribocharging was primarily due to particle-particle collisions.

In the Dust Particle Analyzer, measurements are performed by oscillating particles in an acoustic or electric field or by simultaneous application of both fields. The motion of the particle is measured in real time through the application of Laser Doppler Velocimetry or by using image analysis as shown in Figure 1. In the digitally controlled Dust Particle Analyzer, the ac drive frequency can be varied depending upon the particle size and electrostatic charge distributions to cover particle size from 0.5 to 30  $\mu\text{m}$  and the electrostatic charge from zero to the saturation charge level, which depends upon the particle size and the environmental condition. Figure 2 shows the prototype instrument.

The experiential data presented in Figure 3 shows preliminary results performed with Johnson Space Center (JSC) Mars-1 simulant particles in a laboratory environment at 40 percent relative humidity and at atmospheric pressure. The results demonstrate the possible application of the instrument in a future planetary mission.

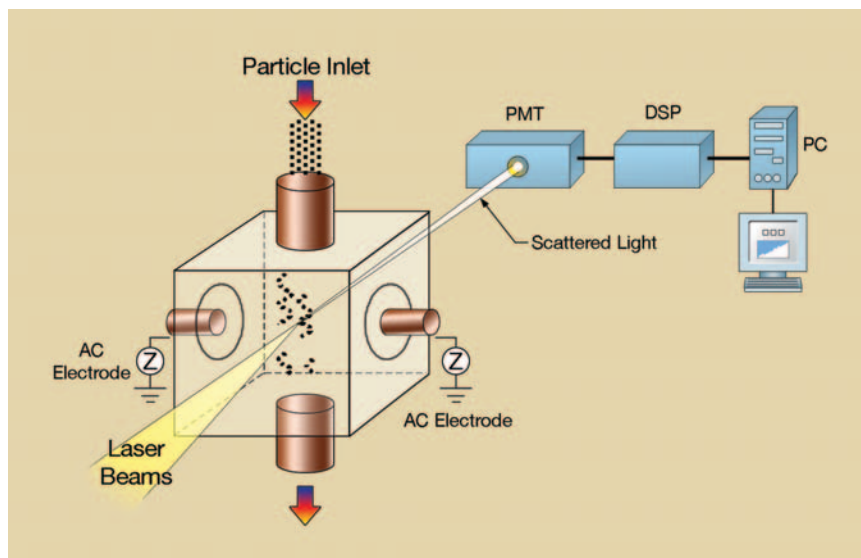


Figure 1. Basic schematic of the ESPART analyzer. The particles are oscillated by an ac drive, and the signal is detected by a photomultiplier tube (PMT) and analyzed by a digital signal processor for particle size distributions and charge-to-mass distributions.

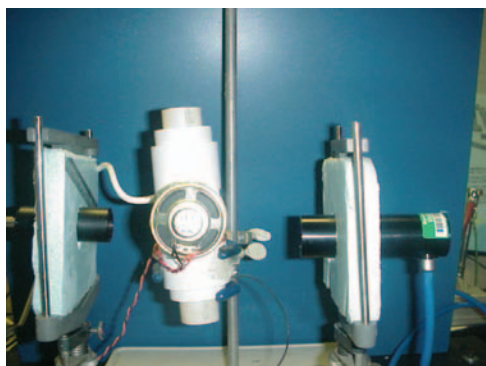


Figure 2. The dust particle analyzer. The integrated version of the instrument will be housed in a small plastic box for its installation within a vacuum chamber for testing under a simulated Martian atmosphere.

Contact: Dr. C.I. Calle ([Carlos.I.Calle@nasa.gov](mailto:Carlos.I.Calle@nasa.gov)), YA-C2-T, (321) 867-3274

Participating Organizations: University of Arkansas at Little Rock (Dr. M.K. Mazumder), Florida Institute of Technology (Dr. J.G. Mantovani), and ASRC Aerospace (Dr. C.R. Buhler and A.W. Nowicki)

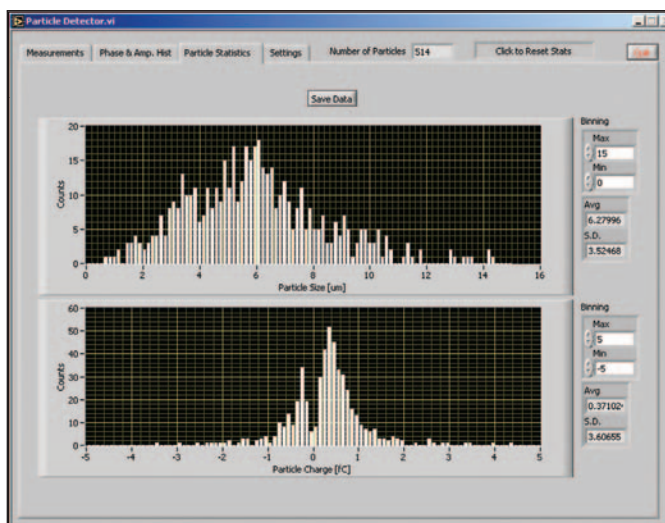


Figure 3. The two histograms show the particle size (top) and electrostatic charge (bottom) distributions of JSC Mars-1 simulant dust. The net Q/M was  $0.37 \mu\text{C/g}$  with a bipolar charge distribution.



## Self-Assembled Monolayers on Aluminum 2024-T3



Corrosion Protection &  
Detection Under  
Paint

Aluminum alloys are commonly used in the aerospace industry because of their high strength. However, the 2000 series aluminum alloys are extremely susceptible to corrosion. New coatings designed to protect these alloys are currently being developed since the traditional chromate conversion coatings are being phased out because of environmental concerns.

Self-assembled monolayers (SAMs) are becoming a common form of surface modification. SAMs have been investigated for their corrosion protection properties, antimicrobial applications, and adhesion. SAMs achieve their properties in a very efficient manner. A SAM forms an organized surface that can be made to expose a specific functionality of the molecule (e.g., hydrocarbon or amine). This makes SAMs ideal for changing surface properties. A small number of total molecules can profoundly impact the surface properties of a material. Previous studies have focused on SAMs deposited on pure metals that have a homogenous surface. In this project, the SAM is deposited on aluminum 2024-T3, a surface that has intermetallic particles and grain boundaries that complicate the deposition procedure.

SAMs of N-decyltriethoxysilane,  $\text{CH}_3(\text{CH}_2)_9\text{Si}(\text{OCH}_2\text{CH}_3)_3$ , (DS) and n-octadecyltriethoxysilane,  $\text{CH}_3(\text{CH}_2)_{17}\text{Si}(\text{OCH}_2\text{CH}_3)_3$ , (ODS) were prepared on aluminum 2024-T3. These SAMs form a very hydrophobic surface because of the exposed hydrocarbon groups. The SAMs were deposited from a dilute solution of the silane in ethanol. The SAM surfaces were characterized with contact angle, infrared spectroscopy, and x-ray photoelectron spectroscopy. The electrochemical and corrosion properties were evaluated with potentiodynamic polarization and electrochemical impedance spectroscopy (EIS).

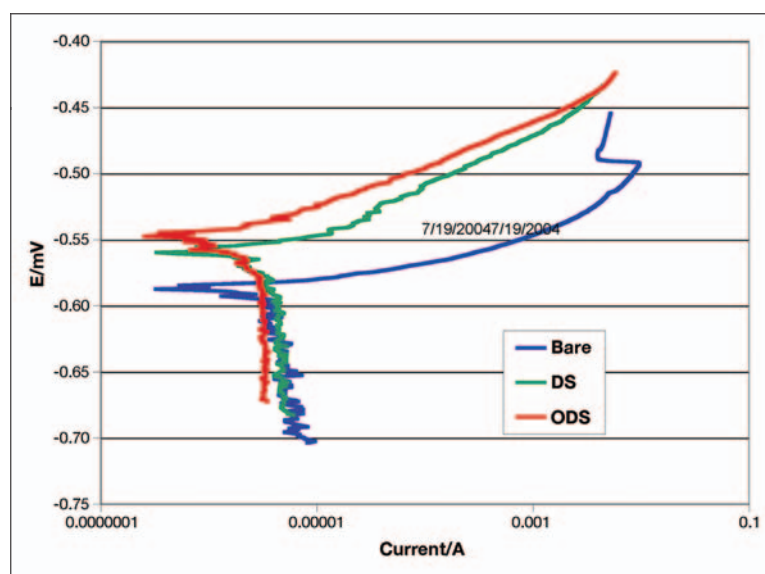


Figure 1. Potentiodynamic polarization measurements for bare and SAM-modified surfaces.

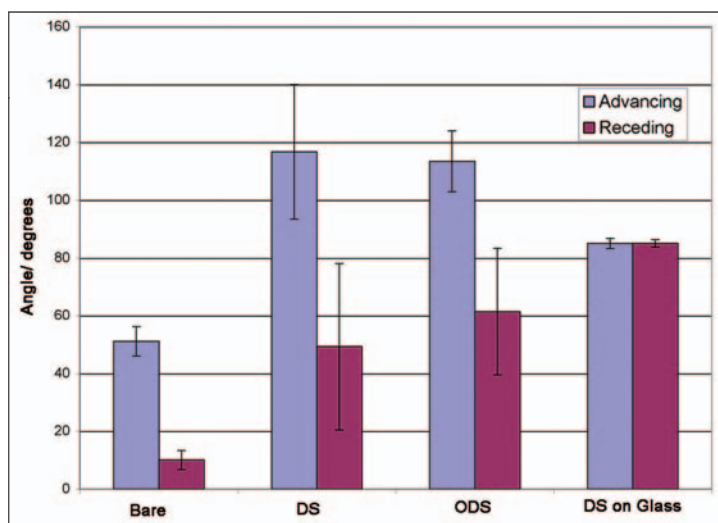


Figure 2. Contact angle of bare and SAM-modified surfaces.

Organosilanes form hydrophobic SAMs with a large number of defects on aluminum 2024-T3. Although there is good coverage on the aluminum oxide surface, the defects are probably centered on copper-enriched particles that are distributed throughout the alloy surface. Electrochemical measurements suggest that the SAM does not provide a great deal of protection from localized corrosion because the copper-rich particles are not protected although the aluminum oxide surface is protected. This behavior can be expected on any surface that does not have a homogeneous surface oxide layer.

It is suggested that the copper-enriched particles must be protected in order for SAM modification to provide significant corrosion protection on aluminum 2024-T3 surfaces. This can be achieved by applying a mixed monolayer that bonds to both the copper particles and aluminum oxide surface or by devising surface preparation techniques that induce more complete SAM coverage. This study of bonding to the aluminum 2024-T3 surface should aid in the development of coatings that are more efficient and can be used as replacements for chromate conversion coatings.

#### Key accomplishments:

- Deposited SAMs on aluminum 2024-T3, making a hydrophobic surface.
- Developed a methodology for evaluating SAM-modified surface, electrochemical, and corrosion properties.

#### Key milestones:

- Presented results at the U.S. Army Corrosion Summit in February 2004 and at the 6<sup>th</sup> International Symposium on Electrochemical Impedance Spectroscopy (EIS-2004) in May 2004.
- Submitted the work for publication in a refereed journal (*Electrochimica Acta*).

Contact: Dr. L.M. Calle ([Luz.M.Calle@nasa.gov](mailto:Luz.M.Calle@nasa.gov)), YA-C2-T, (321) 867-3274

Participating Organization: National Research Council (Dr. P.E. Hintze)

# Prediction of the Long-Term Corrosion Performance of Candidate Alloys for Launch Pad Applications Using dc Electrochemical Techniques



Corrosion Protection &  
Detection Under  
Paint

and the hydrochloric acid present in the Solid Rocket Booster exhaust. The acidic chloride environment is aggressive to most metals and causes severe pitting that can cause cracking and rupturing of high-pressure gas and fluid systems. Such failures can be catastrophic to launch pad personnel in the immediate vicinity. Outages in the systems where failures occur can impact normal operation and Shuttle launch schedules. The use of better tubing alloys for launch pad applications would greatly reduce the probability of failure, improve safety, lessen maintenance costs, and reduce downtime.

The objective of this work was to study the susceptibility to pitting corrosion of several candidate corrosion-resistant tubing alloys to replace the existing 304L SS tubing at the Space Shuttle launch sites. The candidate SS alloys chosen for this investigation were 316L, 317L, AL-6XN, AL29-4C, and 254-SMO. Type 304L SS was included as a control in the study. Corrosion potential, linear, and cyclic polarization data were gathered for the alloys in three different aerated electrolyte solutions: 3.55% NaCl, 3.55% NaCl-0.1N HCl, and 3.55% NaCl-1.0N HCl. Respectively, these solutions were chosen to emulate conditions less aggressive than, similar to, and more aggressive than those found at the launch pads.

A potential range of  $\pm 20$  mV versus open-circuit potential was used for the linear polarization measurements. The scan rate was 0.166 mV/s. A linear graph of potential ( $E$ ) versus current ( $I$ ) was obtained and the polarization resistance ( $R_p$ ) was calculated. This parameter is important because the corrosion rate is inversely proportional to  $R_p$ . Cyclic polarization measurements were started at -250 mV relative to the corrosion potential ( $E_{corr}$ ). The scan rate was 0.166 mV/s. The scans were reversed when the current density reached 5 mA/cm<sup>2</sup>. The

Type 304L stainless-steel (304L SS) tubing is used in various supply lines that service the Orbiter at the KSC launch pads. The chloride content of the atmosphere at the pads is very high, caused by the proximity to the Atlantic Ocean

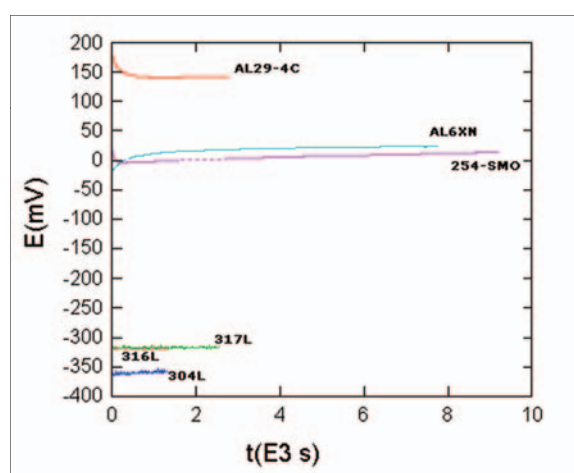


Figure 1. Corrosion potential of SS alloys in 3.55% NaCl-1.0N HCl.

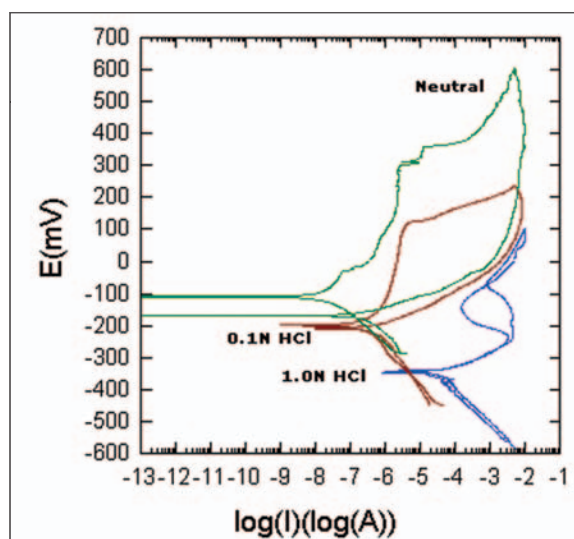


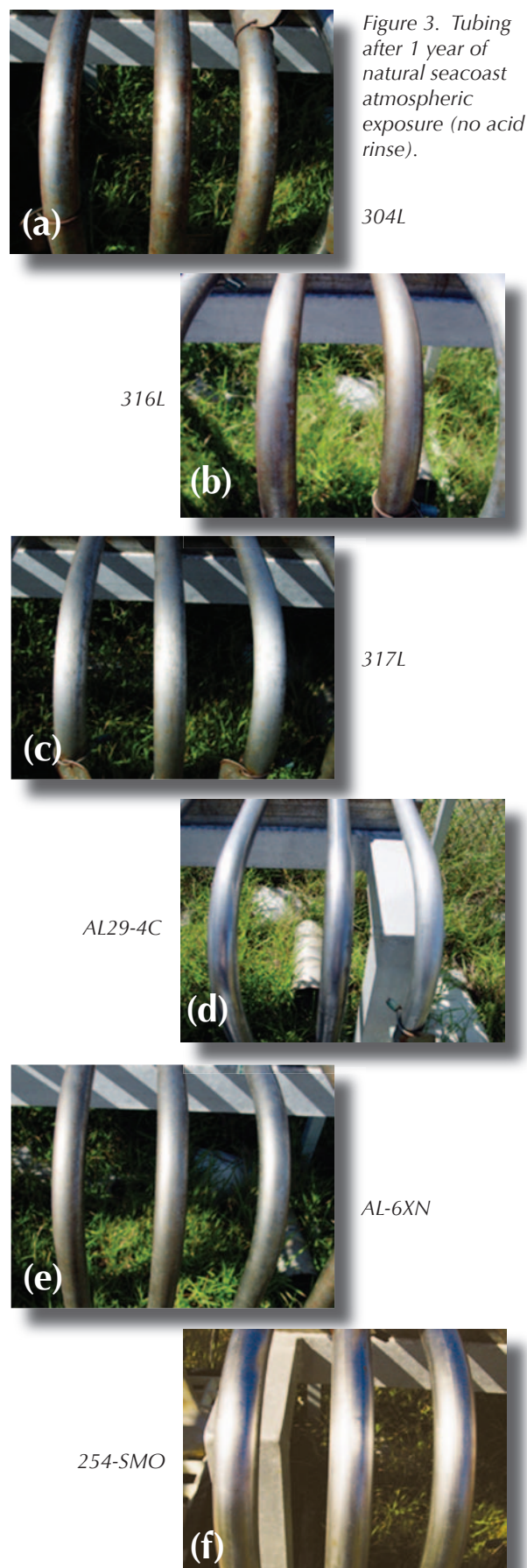
Figure 2. Cyclic polarization scans for 304L in neutral, 0.1N, and 1.0N HCl-3.55% NaCl solutions.

reverse potential scan continued until the potential returned to the starting potential of -250 mV relative to  $E_{corr}$ . A graph of  $E$  versus  $\text{Log}(I)$  was obtained. From this graph, the breakdown potential ( $E_{bd}$ ), repassivation potential ( $E_{rp}$ ), and the area of the hysteresis loop were obtained. Linear and cyclic polarization results were calculated using the SoftCorr III® software. The NASA/KSC Corrosion Technology Testbed atmospheric exposure site near the launch pads was used to evaluate the six alloys for their resistance to localized corrosion under atmospheric conditions similar to those at the launch pad.

The dc electrochemical measurements of the six alloys indicated that the higher-alloyed SS 254-SMO, AL29-4C, and AL-6XN exhibited a significantly higher resistance to localized corrosion than the 300-series SS. The stable corrosion potential values obtained in neutral 3.55% NaCl did not correlate with the performance of the alloys under natural seacoast atmospheric exposure. A correlation was found between the stable corrosion potential values obtained in acidic 3.55% NaCl (Figure 1) and the corrosion performance of the alloys under atmospheric exposure with and without acid rinse. There was a correlation between the corrosion performance of the alloys during a 2-year atmospheric exposure study and the corrosion rates based on polarization resistance values. There was a correlation between the atmospheric exposure data and the susceptibility to localized corrosion that was predicted based on the difference between  $E_{bd}$  and  $E_{corr}$  (Figure 2 shows cyclic polarization data from which these values are obtained). These predictions were in agreement with expectations based on the pitting resistance equivalent number (PREN) calculated for the alloys. The area of the hysteresis loop cannot be used as the sole criterion to predict susceptibility to localized corrosion. Figure 3 shows tubes fabricated with the alloys used in this study after 1 year of atmospheric exposure with no acid rinse. The photographs show the presence of corrosion in the tubes fabricated with the 300-series SS and its absence in those made from the higher-alloyed materials.

Contacts: Dr. L.M. Calle ([Luz.M.Calle@nasa.gov](mailto:Luz.M.Calle@nasa.gov)), YA-C2-T, (321) 867-3278; and L.G. MacDowell, YA-C2-T, (321) 867-4550

Participating Organization: ASRC Aerospace (R.D. Vinje)





# Electrochemical Impedance Spectroscopy of Alloys in a Simulated Space Shuttle Launch Environment



Corrosion Protection &  
Detection Under  
Paint

KSC has one of the highest documented corrosivities of any site in the continental United States.

The naturally occurring oceanfront corrosivity of KSC was the highest among several sites for which corrosion rates were published by the American Society for Metals (ASM) in the 1970s. This high corrosion rate is caused by a combination of factors, such as the proximity to the Atlantic Ocean and the intense Florida sun, rainfall, and humidity. The naturally corrosive environment at the launch pads is aggravated by the approximately 70 tons of hydrochloric acid (HCl) that are produced by the Solid Rocket Boosters during a launch. As a result of these highly corrosive conditions, structures and ground support equipment at KSC will weather or degrade at rates far in excess of those experienced at other locations around the country or even the world. To meet the challenges posed by these high rates of corrosion, KSC has tested materials, coatings, and maintenance procedures, using the atmospheric exposure facility near the launch pads since 1966 during the Gemini/ Apollo Programs. This testing yielded very valuable information. However, as new materials and coatings become available, it is highly desirable to have an alternate laboratory method for material selection that yields results in a matter of weeks as opposed to the several years needed to obtain results from atmospheric exposure. The most important criterion of any laboratory test for corrosion is that it rank alloys consistently with their actual long-term service performance. Electrochemical methods have been used at KSC since 1985 to study the corrosion behavior of coatings and alloys under conditions similar to those found at the launch pads. Both dc and ac electrochemical methods have been employed in the selection of alloys for use at the launch pads. The latest project involved using both techniques to study the corrosion behavior of several candidate alloys to fabricate tubing suitable to replace the existing 304L stainless-steel (SS) tubing used in various supply lines that service the Orbiter at the launch pads.

Type 304L SS is susceptible to pitting corrosion that can cause cracking and rupturing of high-pressure gas and fluid systems. Outages in the systems where failures occur can impact the normal operation of the Shuttle and launch schedules. The use of a more corrosion-resistant tubing alloy for launch pad applications would greatly reduce the probability of failure, improve safety, lessen maintenance costs, and reduce downtime. A study that included 10 alloys was

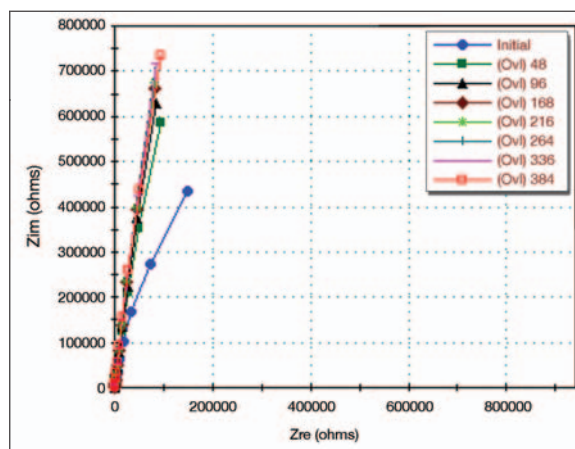


Figure 1. Nyquist plots for 254-SMO in neutral 3.55% NaCl at different immersion times (hrs).

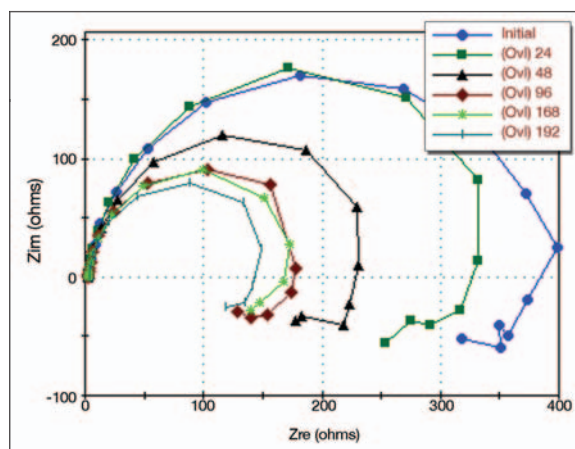


Figure 2. Nyquist plots for 304L SS in 3.55% NaCl-1.0N HCl at different immersion times (hrs).

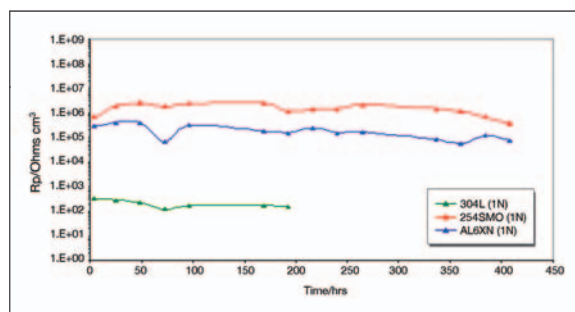


Figure 3. Average  $R_p$  at 3.55% NaCl-1.0N HCl at different immersion times.

undertaken to find a more corrosion-resistant material to replace the existing 304L SS tubing. The study included atmospheric exposure at the KSC outdoor corrosion test site near the launch pads and electrochemical measurements in the laboratory that comprised dc techniques and electrochemical impedance spectroscopy (EIS). This report presents the results from EIS measurements on three of the alloys: AL-6XN (UNS N08367), 254-SMO (UNS S32154), and 304L SS (UNS S30403). Type 304L SS was included in the study as a control.

The alloys were tested in three electrolyte solutions that consisted of neutral 3.55% NaCl, 3.55% NaCl in 0.1N HCl, and 3.55% NaCl in 1.0N HCl. Respectively, these solutions were chosen to simulate environments that were expected to be less aggressive than, similar to, and more aggressive than those present at the Space Shuttle launch pads. The results from the EIS measurements were analyzed to evaluate the corrosion susceptibility of the alloys and their usefulness to predict the long-term corrosion performance of the subject materials. The results from the EIS measurements for the three alloys indicated that the higher-alloyed 254-SMO and AL-6XN exhibited a significantly improved resistance to corrosion compared to the 304L SS as the concentration of hydrochloric acid in the 3.55% NaCl solution was increased. The polarization resistance values obtained from the EIS measurements were consistent with those from linear polarization measurements and were indicative of the actual long-term corrosion performance of the alloys during a 2-year atmospheric exposure study (*KSC Research and Technology 2003 Annual Report*).

The impedance data for the alloys in the three different electrolyte solutions were gathered after the open-circuit potential had stabilized. Nyquist plots of the data, as well as Bode plots, were obtained. It was determined that the response of the alloys with immersion time was more evident in the Nyquist plots. Figure 1 shows Nyquist plots for 254-SMO at different immersion times in neutral 3.55% NaCl. The three alloys showed similar behavior in this environment. The Nyquist plots show an increase in corrosion resistance during the first 48 hours of immersion that remains fairly unchanged thereafter. When HCl was present in the electrolyte solution, the initial increase in the corrosion resistance of the material was followed by a gradual decrease except for 304L SS. This alloy exhibited a significant decrease of its corrosion resistance. Figure 2 shows that the behavior of 304L SS, when the concentration of the acid in the electrolyte was increased to 1.0N, was significantly different from that of the other alloys. There was a significant decrease in its corrosion resistance starting at the initial immersion time. The corrosion resistance is given by the diameter of the semicircle ( $R_p$ ): the greater the magnitude of  $R_p$ , the lower the corrosion rate.

Figure 2 shows the Nyquist plots for 304L SS in an acidified chloride solution at different immersion times. It is evident from the figure that, as the time of immersion increases, the rate of corrosion increases since the diameters of the semicircles  $R_p$  became smaller.

Figure 3 shows the variation in the average value of  $R_p$  with immersion time for the three alloys. The figure clearly shows that 304L SS exhibits the highest rate of corrosion (lower  $R_p$  values), while AL-6XN and 254-SMO have the lowest (higher  $R_p$  values).

The Nyquist plots obtained from the EIS data exhibited only one capacitive contribution represented by a semicircle. An equivalent circuit consisting of a parallel resistor capacitor arrangement in series with the solution resistance,  $R_s$ , simulated the data. The  $R_p$  values obtained from the equivalent circuit simulation at the early immersion times were consistent with those obtained by dc electrochemical measurements (see accompanying article, "Prediction of the Long-Term Corrosion Performance of Candidate Alloys for Launch Pad Applications Using dc Electrochemical Techniques") and were in agreement with the long-term corrosion performance of the alloys as determined in the atmospheric exposure study.

One year in the natural marine environment at the KSC outdoor exposure facility near the launch pads is more aggressive to 304L SS than immersion for up to 408 hours in the neutral 3.55% NaCl electrolyte solution. It was concluded that 254-SMO and AL-6XN are suitable alloys to replace the 304L SS currently used at the launch pads.

*Contacts:* Dr. L.M. Calle ([Luz.M.Calle@nasa.gov](mailto:Luz.M.Calle@nasa.gov)), YA-C2-T, (321) 867-3278; and L.G. MacDowell, YA-C2-T, (321) 867-4550

*Participating Organization:* ASRC Aerospace (R.D.Vinje and Dr. M.R. Kolody)

## Nanotechnology for the Protection of Reinforcing Steel in Concrete Structures



Corrosion Protection &  
Detection Under  
Paint

Facilities at KSC are particularly susceptible to corrosion-related problems. The proximity to the Atlantic Ocean causes an increase in corrosion of ordinary building materials such as steel and concrete. The acidic exhaust deposited by the Solid Rocket Boosters of the Space Shuttle is another problem for the structures.

The objective of this investigation is to develop an innovative method for the corrosion protection of reinforcing steel (rebar) in concrete. This new technology has the potential to lower the cost of maintenance of facilities at KSC, as well as other areas where increased corrosion damage occurs. If proven successful, the technology developed in this project could be applied to building materials in all coastal environments, as well as cold-weather locations that use chloride-containing road salts in the winter.

This research centers upon the use of nanoscale materials as an admixture to concrete. The first corrosion-inhibiting mechanism relies on the nanoscale inhibitor's ability to increase the pH of an acidic species entering through the pores of the concrete. This protects the alkalinity of the porous concrete matrix. Consequently, the acidic species is effectively neutralized.

The second corrosion-inhibiting process utilizes a sacrificial process in which the nanoscale material corrodes prior to the structural steel. When a corrosive species, such as chloride ions, enters through the porous concrete, it is possible that the smaller nanoscale materials will sacrificially protect the rebar. This results from the corrosion of the particles that swell to block the pores, thus preventing further infiltration of corrosive species.

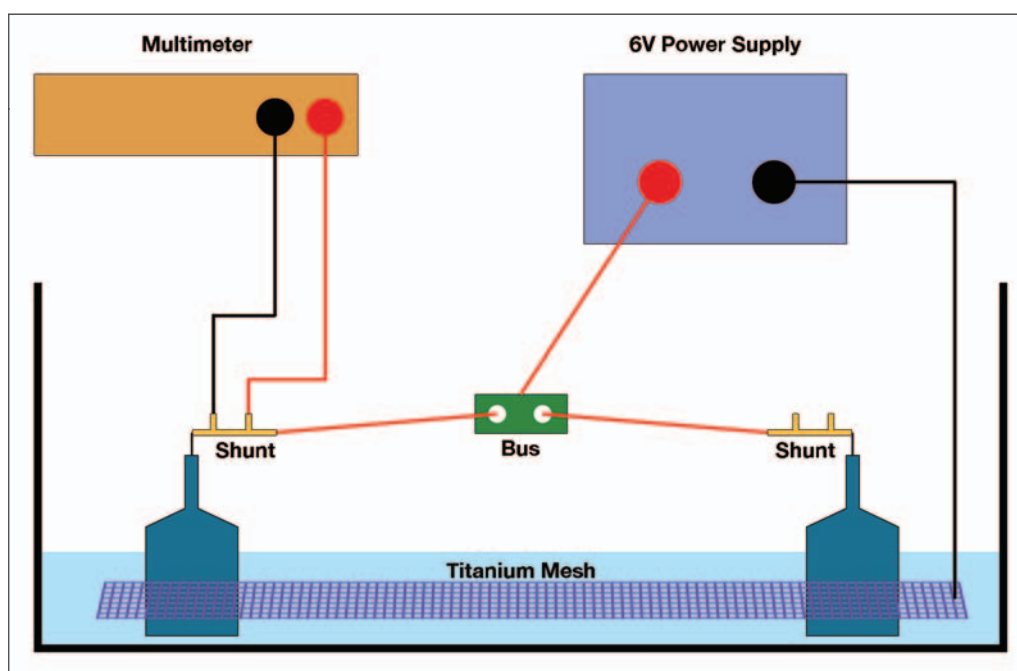


Figure 1. Schematic of the apparatus used for accelerated testing of reinforced concrete.

Various electrochemical methods exist to evaluate an inhibitor's ability to protect reinforcing steel from corrosion. These include but are not limited to open-circuit potential measurements, linear polarization, and electrochemical impedance spectroscopy. These methods provide very useful information though long exposure times are usually needed to suitably degrade the reinforcing steel. Therefore, an accelerated method was employed to evaluate the inhibitors. This method uses a 6-volt driving potential to accelerate corrosion of the rebar electrochemically. Corrosion products form at the surface of the rebar, which swells to an increased volume. This forms a crack that allows for the unimpeded entry of a 5% NaCl solution in which the samples are immersed. A shunt (resistor) through which a voltage drop is measured is attached to the rebar. A large increase in the voltage drop across the shunt signifies failure of the sample. A schematic describing the apparatus used to perform this test is shown in Figure 1. Figure 2 shows two samples that were judged to have failed the accelerated corrosion tests.

The voltage drop that is measured across the terminals of the shunt is plotted as a function of time (Figure 3). From this data, the corrosion-inhibiting performance of the admixture is evaluated. The corrosion performance of sample A was superior to the other samples evaluated.

#### Key accomplishments:

- Designed and fabricated the test apparatus for the accelerated evaluation of concrete samples.
- Investigated a series of concentrations of the nanoscale inhibitor.
- Investigated different particle-size inhibitors.

Contacts: Dr. L.M. Calle ([Luz.M.Calle@nasa.gov](mailto:Luz.M.Calle@nasa.gov)), YA-C2-T, (321) 867-3278; and Dr. J.W. Quinn, YA-C3-C, (321) 867-8410

Participating Organizations: YA-C (N.P. Zeitlin) and ASRC Aerospace (Dr. M.R. Kolody)



Figure 2. Failed concrete samples 1 day (left) and 15 minutes (right) after removal from the test apparatus.

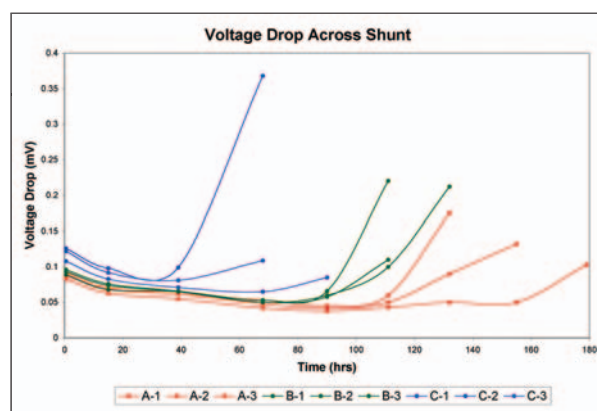


Figure 3. Time to failure (increase in voltage drop) as a function of time for triplicate samples.



## Single-Coat/Rapid-Cure Protective Coatings for Lining Tanks on U.S. Navy Ships



Corrosion Protection &  
Detection Under  
Paint

The NASA Corrosion Technology Testbed and the Naval Research Laboratory Center for Corrosion Science and Engineering formed a partnership to investigate single-coat/rapid-cure coatings for corrosion control of shipboard ballast, fuel, combined holding, and potable water tanks.

Current technology used by the U.S. Navy for the preservation of tanks is limited primarily to two-component, solvent-based epoxy coatings. These coatings have significant disadvantages including:

- Proper curing after application requires 8 to 12 hours of controlled environmental conditions and ventilation.
- The curing requirements place considerable time constraints on adjacent coating application and preservation activities due to risks associated with possible damage to freshly applied coatings in neighboring tanks or spaces.
- The cumulative time requirements associated with curing of these conventional coatings result in impacts to the ship's maintenance availability period.
- Two to three applications (coats) are typically required to obtain the dry-film thickness required for proper corrosion protection.
- The required environmental conditions for proper application and curing are not consistent with the conditions typically found at Navy shipyard locations.

This research program will investigate, test, and evaluate rigid, nonelastomeric epoxy, polyurea, polyurethane, or polyurethane hybrid coating technologies with the following properties:



Figure 1. Ballast tank before new coating application.

- Application using commercially available plural component spray equipment that is commonly used in industrial operations such as general construction and infrastructure maintenance.
- Application using standard industrial surface preparation and coating practices currently present in the shipbuilding and ship repair environment.
- Meet or exceed the performance requirements of MIL-PRF-23236C.
- Cure-to-walk-on time ranging from 20 seconds to 3 hours at 75 °F.
- Completely cured and ready for service in 24 hours at 75 °F.
- Overcoat window greater than 45 minutes at a substrate temperature of 90 °F.
- 100 percent solids, solvent-free.
- Free of aromatic amines (methylenedianiline).
- Minimum of 70 percent edge retention on a 1.0-mm radius at 12 to 20 mils dry-film thickness.
- 1:1, 2:1, 3:1, or 4:1 plural component mix ratios by volume.
- Suitable for immersion service in saltwater ballast, potable water (National Sanitation Foundation NSF-61 approval required), compensated fuel/seawater, diesel fuel, and combined holding transfer fluids.
- Self-priming.
- Able to be applied to a dry-film thickness of 20 to 30 mils in a single application and provide optimal performance.
- Availability of a companion repair coating for touch-up of missed or damaged areas.

Candidate coatings will be procured from the manufactures, applied to test coupons, exposed to the required tests, and evaluated against established performance criteria. The test coupons will be photodocumented before, during, and after the test and evaluation period. A test and evaluation plan and report will be prepared and submitted to the Naval Research Laboratory. Following successful completion of all required laboratory tests, the coatings will be scheduled for field trials on U.S. Navy vessels.

A plural component spray unit was received from the Naval Research Laboratory and installed in the KSC Coatings Application Laboratory. Coating applications and testing began during the fourth quarter of 2004.

Contact: L.G. MacDowell ([Louis.G.MacDowell@nasa.gov](mailto:Louis.G.MacDowell@nasa.gov)), YA-C2-T, (321) 867-4550

Participating Organizations: ASRC Aerospace (J.J. Curran and R.A. Anderson) and Naval Research Laboratory (J. Martin)



Figure 2. Ballast tank after new coating application.

## Innovative High-Temperature Noise Reduction Materials

Ground support equipment, launch vehicle, and payload are negatively affected by the more than 140 decibels of sound pressure level (SPL) and temperatures close to 3,000 °F generated during liftoff. The purpose of this project is to develop a material to dampen these massive acoustic and thermal loads. Ultramet, an advanced materials solution company located in Pacoima, California, and the Graduate Program in Acoustics at Pennsylvania State University have teamed up to develop and test such a material for NASA as a Small Business Technology Transfer (STTR) Phase I research project.

This material is intended to be used as the liner for a duct located beneath a rocket exhaust plume. The Trajectory Simulation Mechanism (TSM) (Figure 1) is located at KSC's Launch Equipment Test Facility. This unique structure is owned and operated by the Launch Systems Testbed (LST) and has the capability to simulate nonstationary scaled rocket launch environments. A J-deflector duct (Figure 2) is used in conjunction with the TSM as a passive scheme for launch exhaust management. The liner developed by Ultramet and Penn State is hoped to ultimately be used inside the J-deflector at the LST laboratory.

The unique porous materials being used in this study are reticulated vitreous carbon (RVC) foam and silicon carbide (SiC) foam (Figure 3). These materials have already been proven to withstand temperatures in excess of 3,000 °F and have demonstrated passive broadband sound reduction over a wide range of frequencies. To test and validate the acoustic impedance of the materials, Penn

State constructed a standing wave tube (Figure 4). Preliminary wave tube measurements have already been conducted. Ultramet has supplied the university with test samples of both RVC and SiC foams for the acoustic testing currently underway.



Figure 1. Trajectory Simulation Mechanism.

Figure 4 shows the closed end of the 5-cm by 5-cm by 1.83-m standing wave tube. A compression driver is positioned at the opposite end to create the standing waves. The sides are constructed of glass, and the top and bottom are of polyvinyl chloride (PVC). When equipped with pressure transducers (three are shown), the holes located on the top of the tube are used to measure acoustic pressure as a function of position along the tube. Simultaneous measurements of acoustic pressure and velocity are taken to determine acoustic intensity. Visible at the top of Figure 4, a Laser Doppler Anemometer (LDA) probe is used to measure the acoustic velocity. Small, square foam samples are positioned snugly in the tube in front of the LDA to study narrowband sound absorption.



The acoustic power dissipated through the sample is found by measuring the acoustic intensity just in front of and just behind the sample.

It is hoped these tests will reveal important information concerning the narrowband sound absorption characteristics of the RVC and SiC foams. Upon completion, a proof-of-concept liner will be designed according to the results of the narrowband tests to demonstrate broadband absorption. In this configuration, the standing wave tube will be completely lined with foam. The final outcome should be the development of an acoustic liner that can withstand the thermal and acoustic loads of the rocket exhaust environment.

#### Key accomplishments:

- Fabrication of RVC and SiC foams.
- Preliminary standing wave tube measurements.

#### Key milestones:

- Proof-of-concept duct liner design, fabrication, and testing.
- Data analysis and documentation.
- Exposure to high acoustic loads.
- Phase II duct design and foam-liner-mounting optimization.

Contact: D.M. Ford ([Danielle.M.Ford@nasa.gov](mailto:Danielle.M.Ford@nasa.gov)),  
YA-C2-T, (321) 867-9432

Participating Organization: Ultramet (C.N. Ward and  
E. Stankiewicz)



Figure 2. TSM with J-deflector duct.

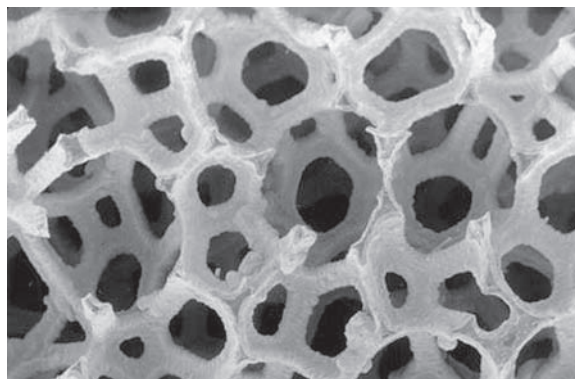


Figure 3. Foam cell structure.

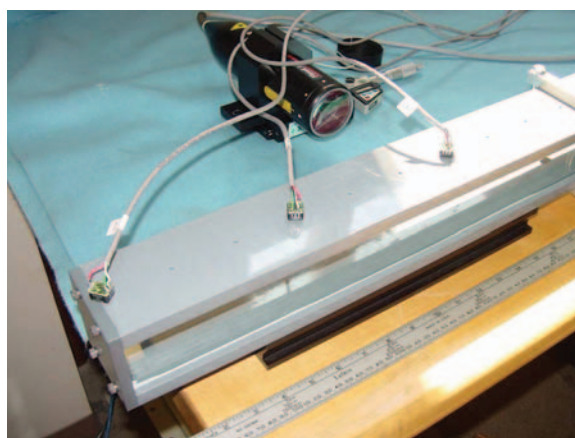


Figure 4. Closed end of standing wave tube.



## Paschen Breakdown Experiments in a Simulated Martian Atmosphere



Contamination  
Detection/Reduction/  
Cleaning

In the dry Martian atmosphere, Martian dust becomes charged because of tribocharging (charging caused by friction) and adheres to surfaces. Spacecraft sent to Mars need to be properly designed to prevent any arcing that can damage electrical systems or potentially ignite explosive materials. To design the spacecraft, the charge levels (voltages) and gap distances at which arcing can occur in the Martian atmosphere need to be known. In addition, knowledge of conditions that can lead to electrical breakdown is required to develop methods to discharge and remove dust for spacecraft, spacesuits, rovers, thermal radiators, and solar panels.

In this project, Martian conditions were simulated in an 18-inch vacuum chamber. Premixed gas designed to emulate the Martian atmosphere, composed of a mixture of 95 percent carbon dioxide, 2.7 percent nitrogen, 1.6 percent argon, 0.13 percent oxygen, and 0.07 percent carbon monoxide, was used. The gas pressure was varied over a wide range. The experiments were conducted at room temperature because electrical breakdown is a function of gas density, not pressure. (Adjusting the gas pressure at constant temperature will vary the gas density.)

A Paschen breakdown curve is a graph of the electrical potential (breakdown voltage) as a function of the product of gas pressure and parallel-plate electrode gap ( $p \cdot d$ ) at which a spark occurs at a constant temperature for a given gas or mixture of gases. A parallel-plate electrode configuration generates a uniform electric field given that gap distances are much smaller than electrode diameters. The typical Paschen curve (Figure 1) initially decreases with decreasing ( $p \cdot d$ ) to a minimum voltage,  $(p \cdot d)_{min}$ , but then sharply increases for  $(p \cdot d) < (p \cdot d)_{min}$ .

Though Paschen breakdown curves have been experimentally obtained for most elemental and molecular gases, including  $\text{CO}_2$ , data are not available for a simulated Martian atmosphere. The Paschen breakdown points were acquired for various combinations of parallel-plate gap distances and gas pressures to obtain electrical breakdown information in the Martian atmosphere. Figures 2 and 3 illustrate the experimental and actual setup.

The Martian atmosphere was simulated at room temperature (20.5 °C) using the following equipment:

- 18-inch-diameter vacuum chamber.
- Mixing manifold designed to mix and introduce various gases.

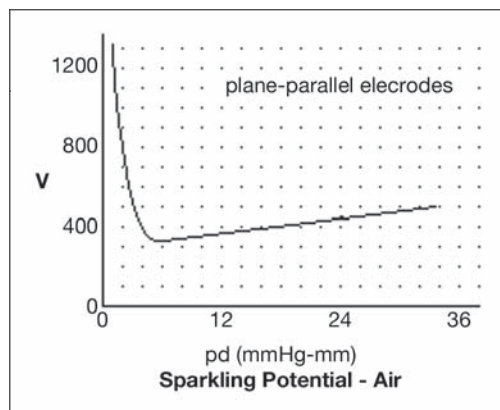


Figure 1. Paschen relationship for air.

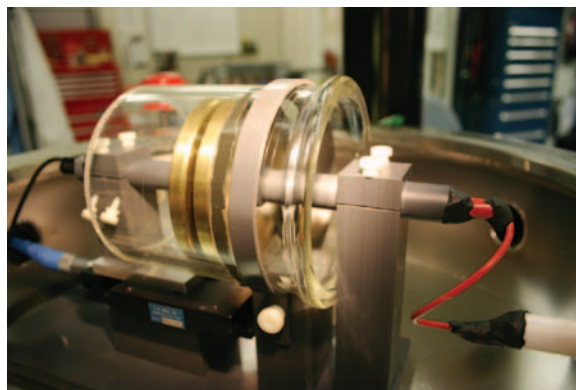


Figure 2. Experimental setup.

- Varian scroll pump (oil-free) to reduce pressure in the chamber and mixing manifold.
- High-accuracy MKS 1000- and 10-torr-range capacitance manometers; utilized because of their ability to accurately indicate pressure regardless of gas composition.
- Bertan 10-kV dc power supply to provide a very low ripple output—important because we are measuring dc breakdown, which can be precipitated at a lower voltage in the presence of any ac components.
- A Stanford Residual Gas Analyzer (RGA) for qualitative analysis of gas components.
- Vaisala relative humidity meter used to measure humidity introduced into the nitrogen component.
- Fabricated bubbling-type humidifier used to add water vapor to the nitrogen component.

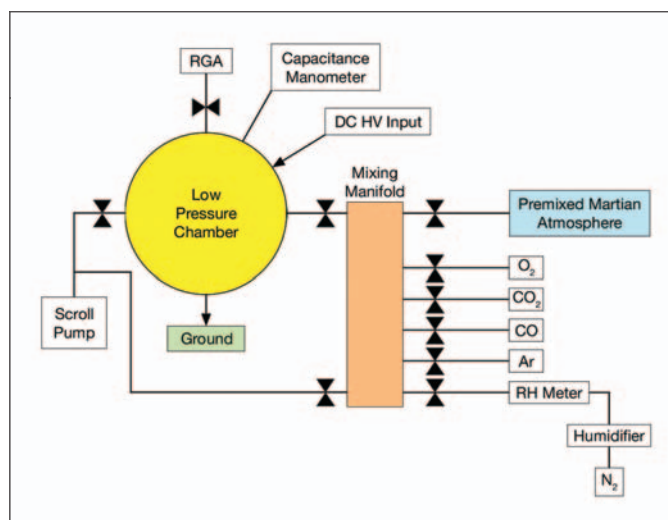


Figure 3. Functional block diagram.

Though statistical and error analysis has not yet been performed on the data gathered, some interesting preliminary conclusions can be drawn. The  $\text{CO}_2$  and Martian gas behaviors are very similar (Figure 4). Obviously, the  $\text{CO}_2$  dictates the shape characteristic of the Martian Paschen curve and is not highly affected by the presence of the minor gases. The Martian breakdown voltages were equal to or slightly lower than  $\text{CO}_2$  in all cases—by an average of 15 volts. While this difference may lie within the error bars of the measurements because the Mars breakdown voltage was always less than  $\text{CO}_2$ , initially we find this statistically relevant. This behavior makes sense since the minor components nitrogen and argon both have lower breakdown voltage strengths than  $\text{CO}_2$ .

Another interesting initial observation illustrated in Figure 5 is the fact that the percentage difference between the  $\text{CO}_2$  and Martian breakdowns increases as  $(p \cdot d)$  decreases, especially for  $(p \cdot d) < (p \cdot d)_{\min}$ . This may be because the nitrogen and argon influence is more strongly felt in this range.

Contact: Dr. C.I. Calle ([Carlos.I.Calle@nasa.gov](mailto:Carlos.I.Calle@nasa.gov)), YA-C2-T, (321) 867-3274

Participating Organizations: Appalachian State University (Dr. J.S. Clements and J. Willis) and ASRC Aerospace (Dr. C.R. Buhler and A.W. Nowicki)

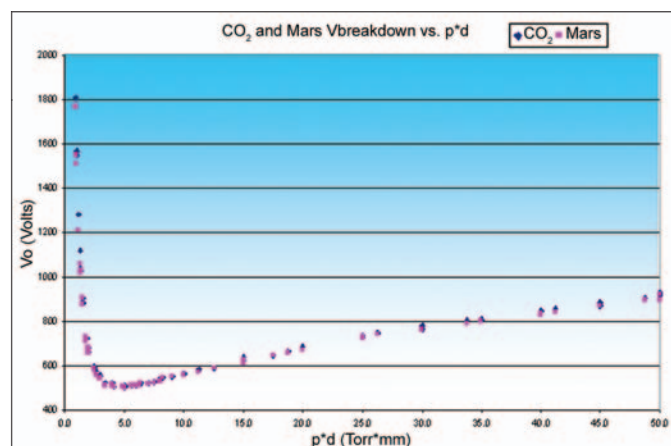


Figure 4.  $\text{CO}_2$  and Mars breakdown voltage versus  $(p \cdot d)$ .

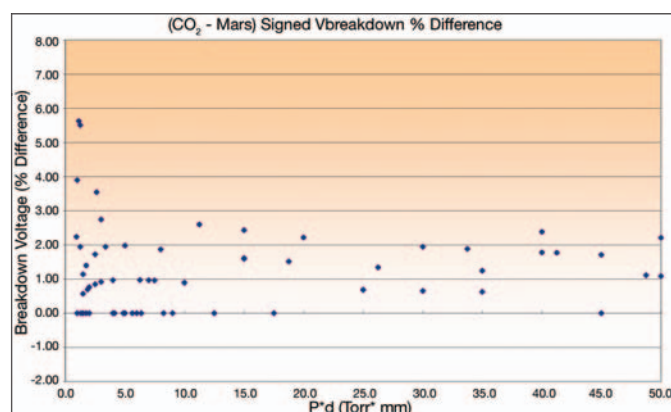


Figure 5. Signed  $\text{CO}_2$ -Mars percentage difference comparison.

## A Wearable Electrostatic Hazard Detection System



*SCAPE Electrostatic  
Discharge (ESD)  
Control Enhancements*

High electric fields lead to electrostatic discharge (ESD) that can injure personnel and damage or destroy sensitive spacecraft apparatus during assembly. Battery-powered, handheld electric field mills are currently used to check workers when they enter the KSC spacecraft assembly facility. This procedure is not convenient and is limited to the detection of high electric potential on workers at points of entry.

In Phase I of this Small Business Innovation Research (SBIR) project, the first wearable system capable of detecting static potentials characteristic of electrostatic hazard at a completely safe distance was demonstrated. The ultrasensitive sensor system is based on a compact electric potential sensor that is at least 100 times more sensitive than prior (nonwearable) technology. The design was optimized by state-of-art E-field modeling.

In the demonstration, the subject system was able to detect a moderate-level static electric voltage (1,000 V) at 1-m distance using a sensor built into a cap. The user was ambulatory, walking past the source of high voltage with the closest approach about 50 cm (Figure 1). This capability should be compared to available handheld static detectors that are only able to detect a 1,000-V source at a distance of 1 cm.

In addition, by incorporating a second sensor the system was able to indicate the direction to the static source. The source location capability was verified by using two sensors mounted on a baseball cap (Figure 2). When both sensors were at the same distance from the source, they had the same response ( $V_1 = V_2$ ), and the difference between their responses  $V_d (=V_1 - V_2)$  was close to zero. However, when the sensors were at different distances from the source, the response amplitudes were different. From the ratio of two detected signals, the subject was able to determine the direction of the source.

Applications for this system include:

- Monitoring electrostatic hazards to both humans and machinery.
- Detecting and measuring electrostatic potential and charge distribution generated on payloads, spacecraft, and landers.
- Monitoring electrostatic hazards around volatile chemicals and fuels.
- Monitoring charge buildup on astronauts.

Key accomplishments:

- Demonstrated the first wearable sensor suite capable of detecting the high voltage associated with electrostatic hazards at a completely safe distance.
- Verified the feasibility of detecting the direction of the source.

Contact: Dr. C.I. Calle ([Carlos.I.Calle@nasa.gov](mailto:Carlos.I.Calle@nasa.gov)), YA-C2-T, (321) 867-3274

Participating Organization: Quantum Applied Science and Research, Inc. (Dr. Y. Zhang)

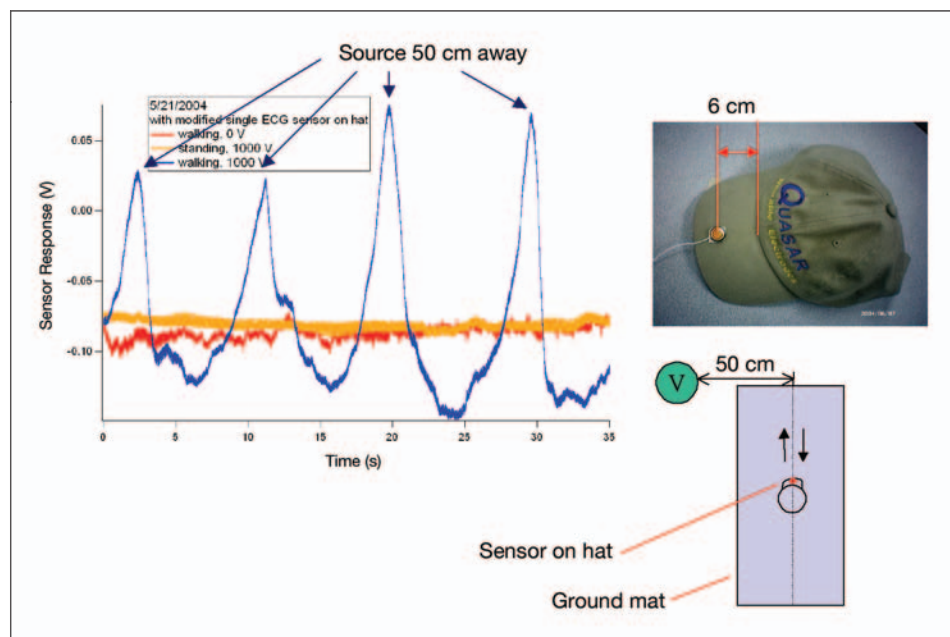


Figure 1. Response of a sensor mounted on a person's cap. The person is walking back and forth on a grounded mat of 1 by 1.8 m. The closest distance between the person and the voltage source (1 kV) is about 50 cm.

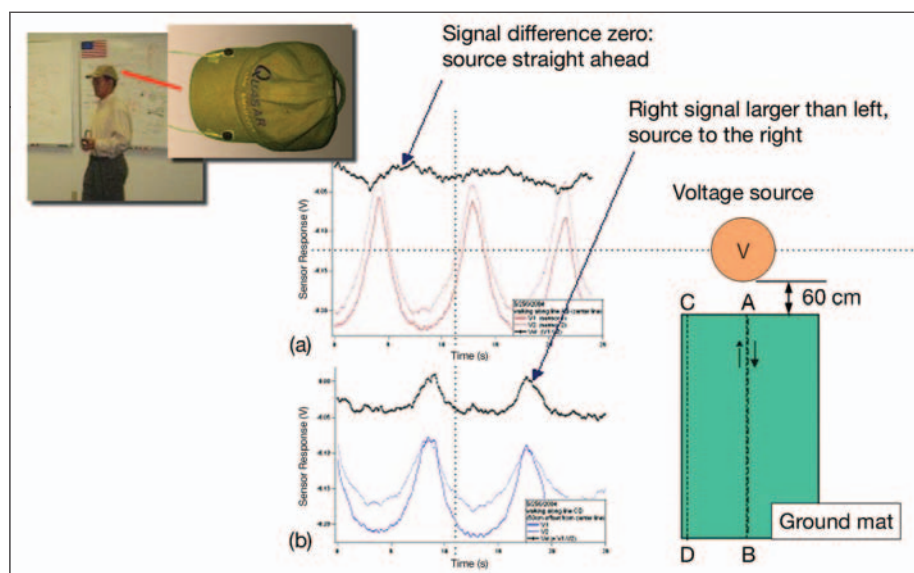


Figure 2. Detecting the direction of an electrostatic hazard. Response of the two sensors on a cap and their difference (black) when subject walked back and forth along line AB (red curves) or CD (blue curves).



## Development of Rocket Acoustic Prediction Tool (RAPT)



*Mission Data  
Feedback &  
Analysis*

The prediction of acoustic loading provides a necessary input for the determination of vibration loads on the vehicle. Recently, the Launch Systems Testbed (LST) at KSC conducted a series of acoustic tests on scaled supersonic nozzles. The data collected from these tests can be used to predict acoustic loading. Several groups at Wright-Patterson Air Force Research Laboratory, including the payload, airframe, and subsystems groups, are interested in such data and their incorporation in predicting acoustic loads.

The NASA SP-8072 method, developed on the basis of extensive rocket test data, appears to be the only documented method to predict noise from an isolated supersonic jet (Figure 1). Methods to estimate the noise produced by multiple rocket engines by the principle of superposition of individual jets work satisfactorily for noninterfering jets (widely spaced nozzles). In the other extreme case of very closely (tightly) spaced jets, the noise produced is occasioned primarily by the combined flow of a single equivalent nozzle. In such circumstances, the effects of clustering are empirically taken into account by an equivalent diameter so that the NASA SP method can be utilized. In both of these extreme cases, the spectral sound pressure level is characterized by a single peak frequency, which is dependent on the characteristic nozzle diameter.

In the case of clustered rocket engines with intermediate spacing between the nozzles, the hydrodynamic interaction among the exhaust jets is such that the individual jets radiate noise independently but ultimately combine into a single effective stream. The resulting complexity of the flowfield significantly modifies the acoustic near-field (typically within 40 jet diameters or about 300 feet from the launch mount) because of the changes in the strength and distribution of the turbulent noise sources. Under such conditions, the noise spectrum is due to both the individual jets and the combined flow. As a consequence, the equivalent diameter approach does not hold. A major limitation of this highly simplified method based on equivalent diameter is that it fails to predict the multiple-peaked spectrum of sound in the near-field, which can affect the resonant vibration modes of the nearby structures. Furthermore, it typically produces an uncertainty of approximately 10- to 15-dB noise level. Thus, it is imperative to develop an improved method to estimate the acoustic effects of clustered rocket thrusters.

A calculation procedure was implemented to predict acoustic levels from large clustered rockets. Test cases were identified to signify the role of ground reflections and hydrodynamic interactions between the neighboring jets. It is shown that the ground reflects the acoustic levels by as much as 5 dB, and the ground reflections seem to increase the peak frequency. For intermediate spacing of clustered rockets, two peak frequencies in the sound spectrum are evident, which correspond to the isolated zone (noninterfering jets) and the mixed zone. Satisfactory agreement was noted between the predictions and the data in assessing ground reflections and the jet interaction effects.

RAPT is designed to offer users a friendly graphical user interface (GUI) environment where they can interactively specify various input parameters for the acoustic estimation (Figure 2). This important feature allows design engineers to conduct parametric studies. The GUI is accomplished with the aid of Visual Basic (VB). In addition, the dynamic link library (DLL) from the main prediction program, coded in C++ or Fortran, will be called from the GUI to eliminate all the command-line options. The computed value for the sound pressure level spectra for the isolated zone and the mixed zone indicates two distinct peak frequencies corresponding to their respective characteristic length scales (Figure 3).

Although the test case considered provides a satisfactory comparison with the test data, it is merely a good starting point. More extensive comparisons with a large range of test data are required to further validate the prediction models.

Key accomplishments:

- Completed the two-zone method to capture multiple peaks in the spectral sound power level for clustered nozzles.
- Results are documented and reported to the Air Force Research Laboratory.

Key milestones:

- Present the study at summer faculty meeting.
- Begin the development of multiple-nozzle testing.

Contacts: Dr. B.T. Vu ([Bruce.T.Vu@nasa.gov](mailto:Bruce.T.Vu@nasa.gov)), YA-C2-T, (321) 867-2376; and S.M. Hauss, SA-B1, (321) 867-3266

Participating Organization: Sierra-Lobo, Inc. (Dr. M. Kandula)

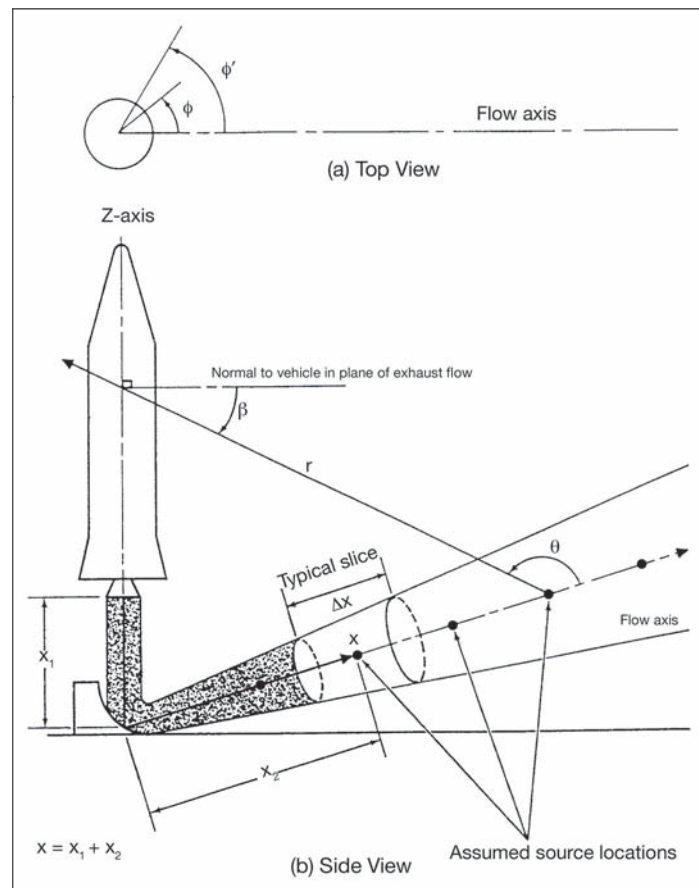


Figure 1. Schematic of the source allocation method due to Eldred (1971).

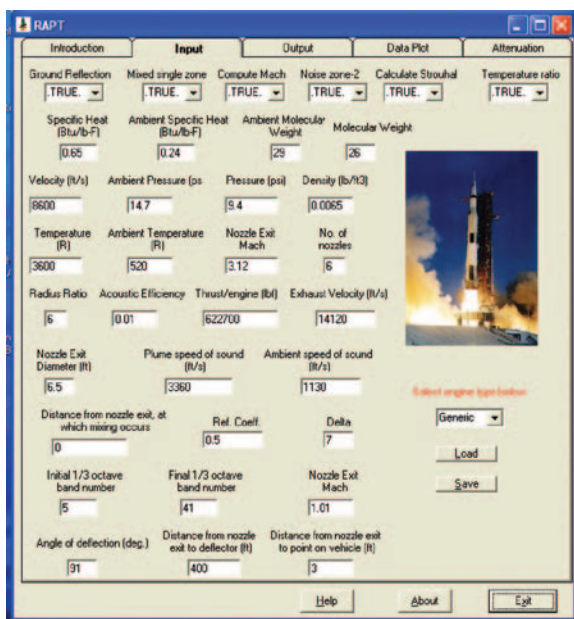


Figure 2. RAPT input.

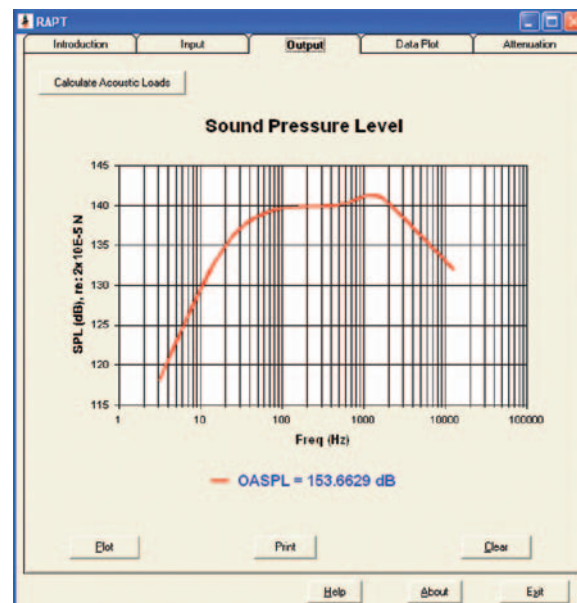


Figure 3. RAPT output.

## Moisture-Resistant Thermal Protection System (TPS) Materials



TPS Process  
Enhancement/  
Automation

The objective of this project is to create a closed-cell foam system that could replace an existing TPS without requiring waterproofing or the use of ablatives. In Phase I, the research dealt with overcoming the initial complications of synthesis, as well as showing the various enhanced properties of the systems. The two synthesis methods chosen for the two portions of the TPS were thermal pyrolysis of a preceramic polymer-containing mixture and the thermal spray of a metal-ceramic mixture. The proposed foam and low-density Thermal Barrier Coatings (TBC) could replace a portion of the foam insulation on the Solid Rocket Booster (SRB) and External Tank (ET), as well as provide a backup TBC to protect current and future space transportation system structures in the event of localized insulation failure.

The first method (thermal pyrolysis) is used to form tiles from a polymer-based slurry mixture. This precursor could be used to form thin or thick films. In fact, the preceramic polymer forms solid ceramic phases more easily in thinner applications. Still, through the processing work done in Phase I, discs of amorphous carbon/silicon carbide (C/SiC) foam were made up to 1-inch thick and 2 inches in diameter. These tiles had approximate thermal conductivities of 0.17 watt per meter kelvin (W/mK).

The second method (thermal spray of metal-ceramic mixture) was used to form moistureproof thermal barriers on aluminum and aluminum enhanced thermal barrier (AETB) surfaces. The choice of type of thermal spray, between plasma and oxy-acetylene flame, was made. The composition was a nominal baseline, though still with a large (60 percent) volume fraction of the ceramic microspheres. The adhesion was quite good because of the metallic Ni-Al matrix, especially on the aluminum substrate. Still, the AETB served as a good substrate. The thermal conductivity of this coating has not yet been tested. As greater fractions of the porous ceramic spheres (the circular black regions in Figure 1) are included in the precursor, the conductivity will drop.



Figure 1. Microscope image of the 0.025-inch-thick layer of Ni-Al with microspheres encapsulated within the coating.



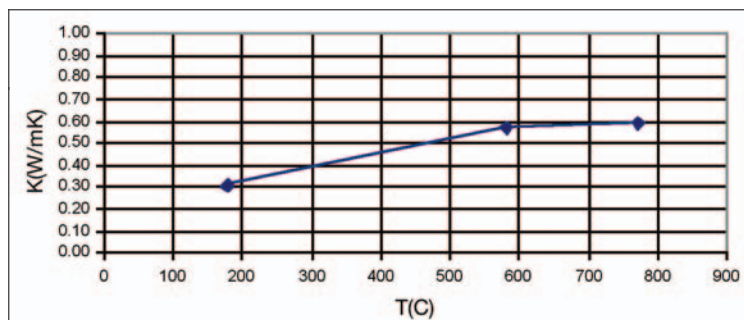


Figure 2. Thermal conductivity of a 1-inch-thick disc, from room temperature to 800 °C.

Initial thermal conductivity was conducted on one of the foam tile samples, and the conductivity was much lower than the standard available, making the reading a little higher than actual. Still, the results were quite good for baseline samples (Figure 2).

The plot of thermal conductivity in the foam disc versus temperature shows that, as temperature increases, the increase in conductivity gets smaller. The change in slope indicates that the thermal conductivity will reach a maximum value and level off, even with increasing temperature. This shows that the foam has great potential as a high temperature insulation.

In addition, the foam has excellent resistance to thermal shock (Figure 3). An acetylene-oxygen torch was applied to each of the foam samples until the region around the contact area began to glow red hot. There was no physical damage to either sample, and, upon removal of the flame, the samples quickly returned to room temperature. Also, at room temperature, the foams have intrinsic water resistance (Figure 4) where water beads up on the surface of the foams, despite having large and small open pores.

Contact: Dr. G.M. Henderson ([Gena.M.Henderson@nasa.gov](mailto:Gena.M.Henderson@nasa.gov)), EA-C, (321) 867-4261

Participating Organization: Powdermet, Inc. (P. Patel)

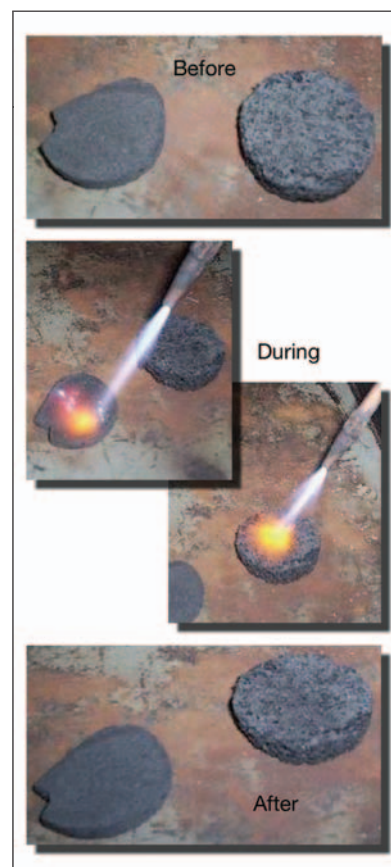


Figure 3. Two foams before, while, and after being hit with a torch.



Figure 4. Water beaded up on the surface of two foam discs, with different types of porosity.



# Process and Human Factors Engineering Technologies

Process and Human Factors Engineering Technologies include research and development of innovative tools and technologies to improve manufacturing and launch site operations safety, efficiency, and effectiveness. Spaceport and range systems have many unique aspects that require development of advanced process, human factors, and industrial engineering technologies. Process and Human Factors Engineering emphasizes the interfaces among people, processes, and hardware/software systems in specific work environments. Process and Human Factors Engineering focuses on the science of process improvement and optimization of the operational phases of complex systems, including current and future space transportation systems. The overall goal of Process and Human Factors Engineering is to develop and apply technologies for designing, implementing, improving, and managing safe and efficient processes, tasks, systems, and work environments that can be quickly adapted to the changing needs of our spaceport and range customers.

The fundamental principles of Process and Human Factors Engineering are:

- All work activities can be represented as processes.
- All processes involve humans.
- All processes can be improved.
- Processes must be measured to be managed and improved.

Process and Human Factors Engineering Technologies directly support NASA's goals of safe, reliable, and affordable space access and exploration. Technology projects develop new concepts, methodologies, processes, and/or systems that advance the state of the art in one or any combination of the following technology focus areas:

- Modeling and Simulation
- Human Factors and Ergonomics
- Task Analysis Technologies
- Process and Operations Analysis
- Life Cycle Systems Engineering Tools
- Scheduling and Risk Assessment Technologies
- Management Support System Technologies

*For more information regarding Process and Human Factors Engineering Technologies, please contact Tim Barth ([Tim.Barth@nasa.gov](mailto:Tim.Barth@nasa.gov)), YA-H, (321) 867-6230; or Dr. Gena Henderson ([Gena.M.Henderson@nasa.gov](mailto:Gena.M.Henderson@nasa.gov)), EA-C, (321) 867-4261.*

# Toolkit for Enabling Adaptive Modeling and Simulation (TEAMS)

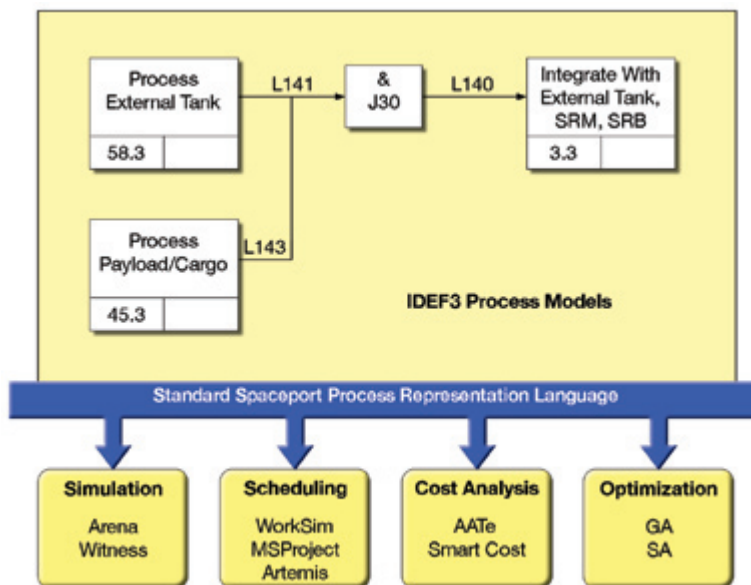


Task/Process  
Modeling &  
Simulation

The increasing complexity of systems has enhanced the use of quantitative operations analysis methods for decision support. The use of operations analysis models facilitates experimentation with real-world systems that would either be impossible or cost-prohibitive otherwise.

In spite of their advantages, however, only a small fraction of the potential practical benefits of operations analysis methods has reached the ever burgeoning user community because of the considerable time, effort, and cost required to build, maintain, and rapidly deploy operations analysis technology. This project targets key central technical challenges associated with Space Transportation System operations analysis, including inadequate methods and tools for cost-effective operations analysis model development, deployment, and maintenance.

The main goal of this project is to design, develop, and demonstrate a Toolkit for Enabling Adaptive Modeling and Simulation (TEAMS), a decision support tool that facilitates quantitative space transportation operations and maintenance process analysis. TEAMS provides Space Transportation System designers a knowledge-based infrastructure for quickly and easily developing, maintaining, and reconfiguring operations analysis models. The technical approach involves defining TEAMS application requirements, designing TEAMS architecture, developing focused TEAMS applications, testing and validating TEAMS applications, and transitioning TEAMS technology. TEAMS provides valuable decision information to Space Transportation System stakeholders, analysts, and designers.



TEAMS solution concept.

The main TEAMS applications that have been developed and demonstrated are (1) a collaborative process modeling and process knowledge management toolkit and (2) an operations planning and schedule analysis application. Potential TEAMS benefits include the ability to affordably explore a large number of Space Transportation System decision alternatives; higher-quality Space Transportation System designs; and reduced spaceport development, operations, and maintenance costs.

The figures illustrate the high-level model concept as well as sample outputs showing facilities utilization and product flow times for different process assumptions.

### Key accomplishments:

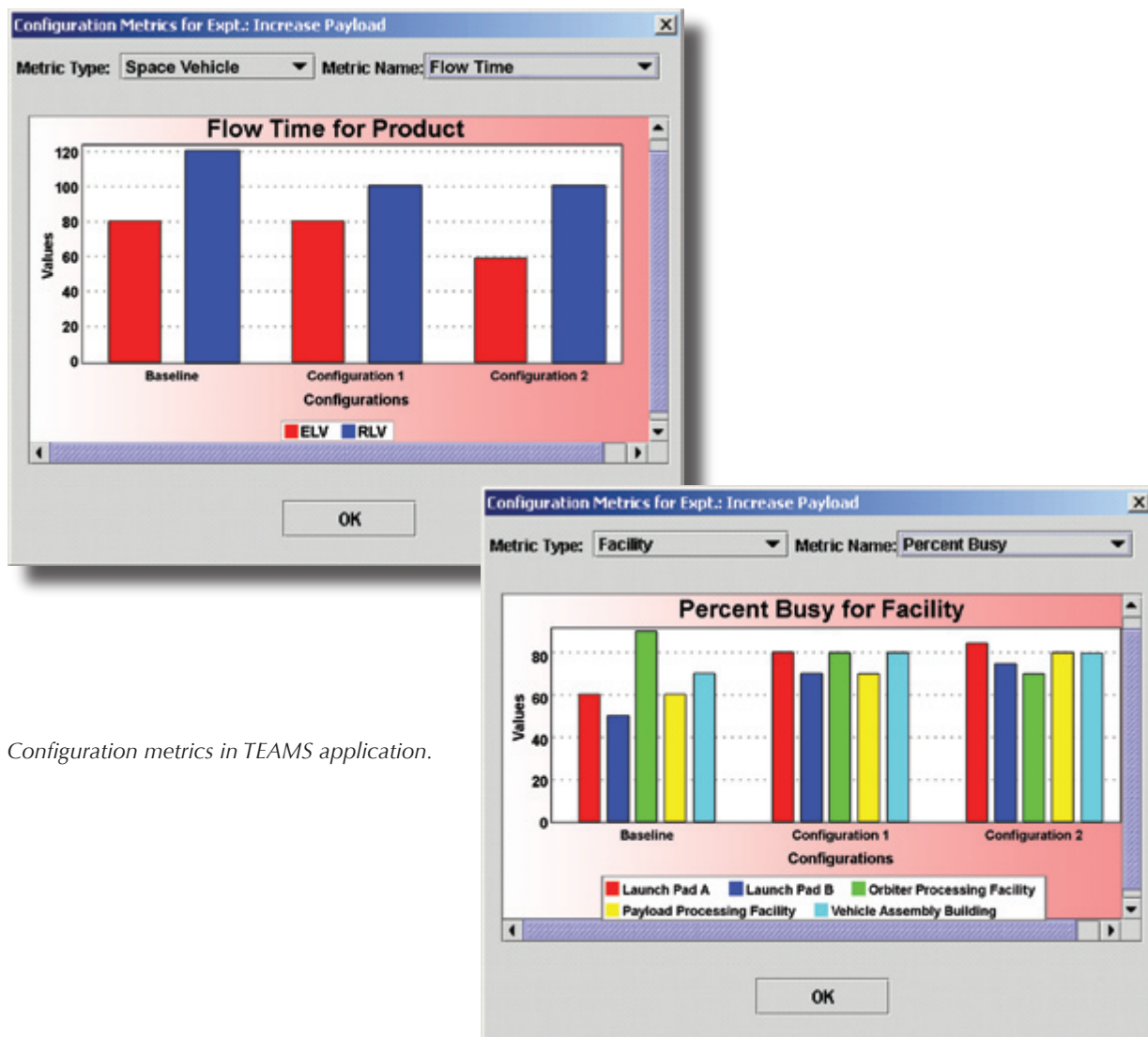
- 2002: Start of Phase II project and identification of TEAMS application focus areas.
- 2003: Definition of TEAMS application requirements; refinement of TEAMS architecture; identification of application test data; and design of test operations analysis models.
- 2004: Testing and validation of TEAMS applications; completion of TEAMS application software; completion of Phase II final report; and completion of TEAMS technology transition.

### Key milestones:

- 2004/2005: Potential follow-on efforts sponsored by Government and/or industry.

Contact: G.R. Rhodeside ([Glenn.Rhodeside@nasa.gov](mailto:Glenn.Rhodeside@nasa.gov)), UB-X, (321) 867-7910

Participating Organization: Knowledge Based Systems, Inc. (Dr. P.C. Benjamin)



Configuration metrics in TEAMS application.

# Human Factors Investigation Refinements

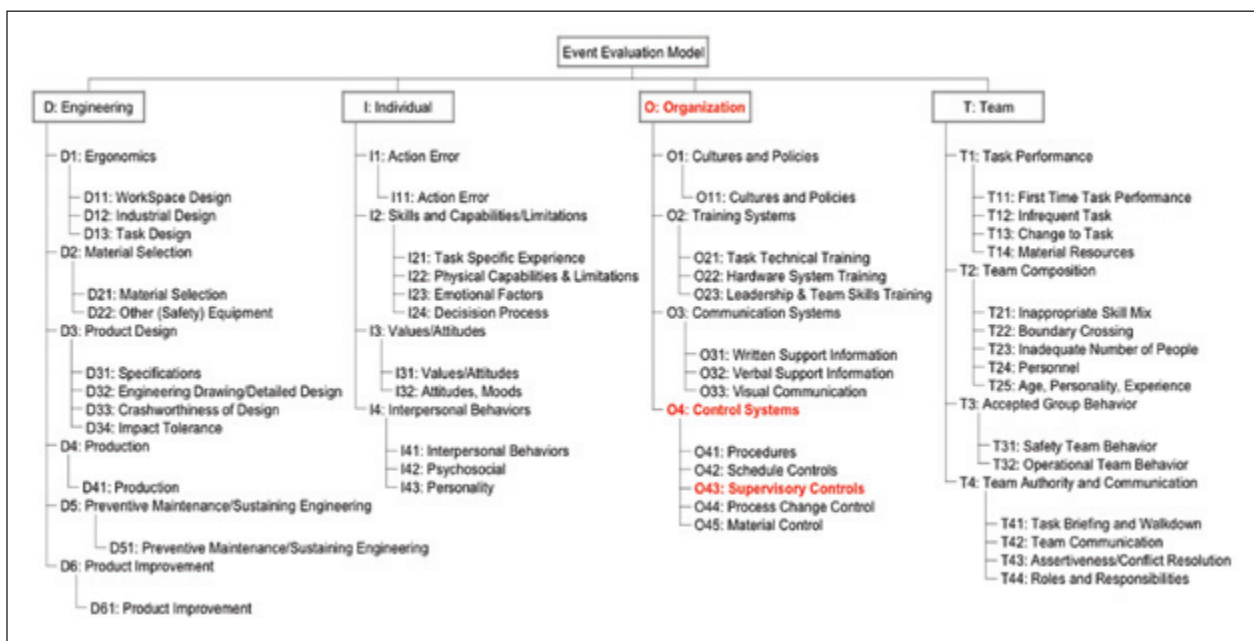


Intelligent Work  
Instructions/Work  
Control Systems

At KSC, Space Shuttle processing involves complex human actions and/or interactions with hazards and equipment. Accordingly, a viable mishap investigation process is a critical key to safety and the improvement of human performance. In response to an April 2000 independent assessment of United Space Alliance (USA) processing of the Shuttle, the USA Industrial and Human Engineering (I&HE) Department launched a substantial standardization effort that included the following actions:

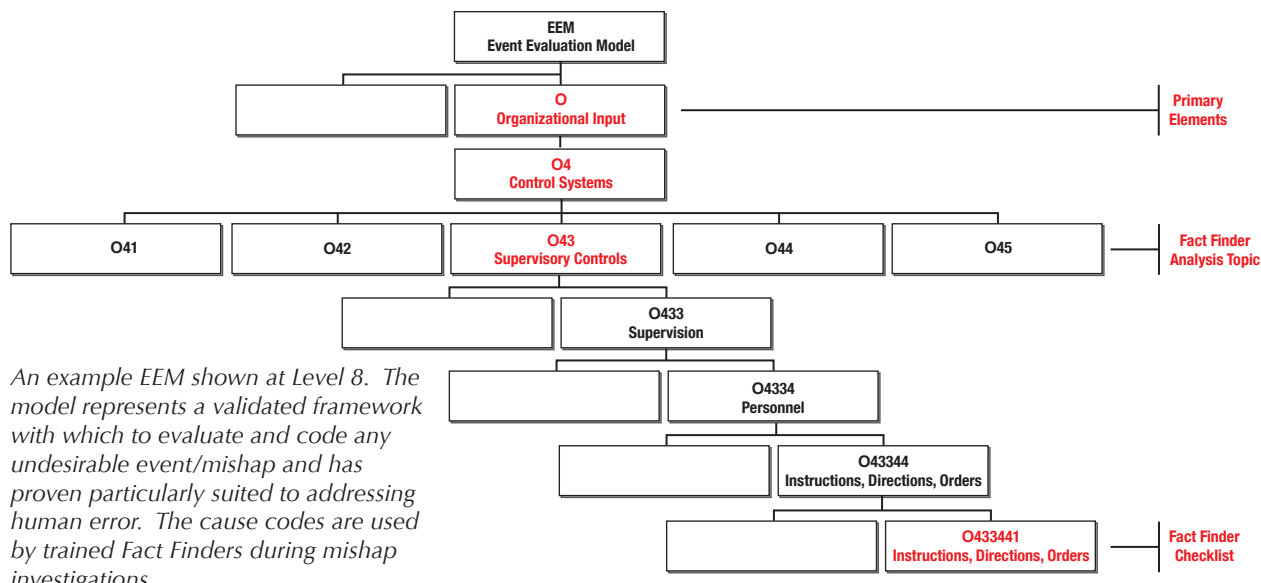
- Standardized investigation reports and management presentations.
- Developed and implemented a standardized investigation protocol and methodology.
- Refined the USA Human Factors Event Evaluation Model (EEM) and Cause Codes (USA003628), which include an investigation checklist.
- Developed and implemented a Fact Finder on-the-job training (OJT) course and certification process for human factors investigators.
- Assisted in the standardization of the Standing Accident Investigation Boards (SAIBs).
- Developed a methodology/database to collect and store all pertinent facts from human factors investigations, as well as a reporting methodology for investigative teams.
- Developed a standard set of metrics for reporting systemic issues.

As part of the Human Factors EEM, the collaboration of KSC, Ames Research Center, and the U.S. Air Force, together with the Team Effectiveness and Leadership Model designed by Dr. Robert Ginnett of the Center for Creative Leadership, supplied the foundation for coding mishap data and provided the framework for the I&HE Human Factors Mishap Investigation Database (HFMID). The database is hierarchically structured for ease of data entry. Causes, contributors, and observations of human error can be recorded and coded through eight progressive levels that offer a finely detailed analysis. These human factors input variables impact the work process phase and the work output phase. Since human errors are a consequence, the preceding causal factors must be identified to explain why the



The HFMID records and codes eight levels of cause, contributor, and observation inputs in four categories: organizational, team, individual, and engineering. In the eighth level, 275 different codes are available.





human error occurred. For example, a decision error (coded I2-4) may be the result of minimal hardware knowledge (coded O2-2) and an assignment to an unfamiliar task (coded O4-3). The latter two would be classified as contributing causes, whereas the decision error or decision process (I2-4) would be classified as the root cause.

Focusing on fact finding rather than fault finding, Fact Finder training emphasizes procedural familiarization, training courses, investigative performance, and standardized operations for interviews and SAIBs. Procedural familiarization emphasizes NASA procedures and guidelines for mishap reporting, mishap investigation techniques, human factors considerations, Root Cause Analysis (RCA), Human Factors EEM, REASON RCA software, and the Five Stop Rules of causation. The Fact Finder OJT package comprises courses in the following: mishap investigation (Florida Safety Council), flight hardware accident prevention, human factors awareness, task team roles and responsibilities, and REASON RCA software.

It is the goal of USA I&HE to improve the quality of mishap investigations and data analysis. Accordingly, investigations and Fact Finder training are viewed as living processes, allowing enhancements to be made and distributed to all certified Fact Finders for implementation, while continuing to improve the ability of USA's investigations to provide insight and proactive accident prevention.

Key accomplishment:

- Developed and implemented a comprehensive program of standards for reporting, investigating, and analyzing mishaps and human errors.

Key milestones:

- Finalize database user refinements and implement a Web-based application for certified Fact Finders.
- Develop an "Expert System" for automating metrics and reports, as well as a statistical package for systemic analysis.
- Develop Fact Finder training software.

Contact: M.M. Groh-Hammond ([Marcia.M.GrohHammond@nasa.gov](mailto:Marcia.M.GrohHammond@nasa.gov)), PH-O, (321) 861-0572

Participating Organization: United Space Alliance (J.R. Ewald, G.P. Sweeney, K.M. Pisula, H.W. Riley, D.J. Frankos, P.A. Hollis, and J.H. Toney)

## Schedule and Activity Generator/Estimator (SAGE)



*Task/Process  
Modeling &  
Simulation*

SAGE is a software tool for operations analysis. Built on extensive Shuttle data, expertise, and lessons learned, SAGE allows the user to compose a system part by part, and from the resulting description, a set of processing times is generated. The system under study is the flight and ground system that composes a Space Transportation System. SAGE is a GUI-type tool, completely compiled in Visual Basic. Even though SAGE integrates another KSC database, the Root Cause Analysis (RCA) Database reflecting subsystem-detailed activities and their durations, Microsoft Access is not required.

The following are among SAGE's key capabilities:

- Adds detail to operations analysis.
- Estimates turnaround times for reusable Space Transportation System elements.
- Maintains ease of analysis.
- Leverages off of the Shuttle RCA Operations Database.
- Allows innovative subsystem and system definition.
- Explores improved maintainability, integration of parts, shared subsystems architectures, and simpler designs with fewer parts.
- Explores improved reliability and supportability.
- Integrates with existing simulation tools.

SAGE was developed by the NASA KSC Systems Engineering Office and Blue Frog Technologies <<http://blue-frog.biz/main/projects.htm>>. Further information on SAGE is available at <[http://science.ksc.nasa.gov/shuttle/nexgen/SAGE\\_main.htm](http://science.ksc.nasa.gov/shuttle/nexgen/SAGE_main.htm)>.

Key accomplishments:

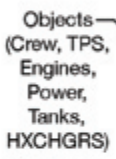
- Completed SAGE development and initiated first practical application in limited availability.

Key milestone:

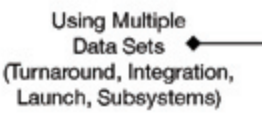
- Release SAGE for full availability to Government, industry, and academia upon request.

Contact: E.Z. Zapata ([Edgar.Zapata-1@nasa.gov](mailto:Edgar.Zapata-1@nasa.gov)), YA-D4-A, (321) 867-6234

Participating Organizations: Blue Frog Technologies (Dr. A.J. Ruiz-Torres) and YA-D4-A (C.M. McCleskey)



Spaceport  
(Reliability  
Safety Factors  
Approach)



*SAGE output screen.*

## Generic Simulation Environment for Modeling Future Launch Operations (GEM-FLO)



*Task/Process  
Modeling &  
Simulation*

GEM-FLO is a generic but powerful simulation of launch operations processing for space transportation systems. By means of a graphic user interface, an underlying Arena discrete-event simulation (DES) is populated with a description of the system being analyzed. GEM-FLO provides insight for operations, process improvement, and system definition improvement and analysis.

With GEM-FLO, a user does not have to undergo the tedious process of creating simulation models, flow diagrams, interactions, or logic. An operations expert, who might not be a simulation expert, can use this tool and quickly produce valuable insight. The generic model, applicable to a broad range of concepts, takes care of this automatically. The basic concept is that the processing of any space transportation system has certain generic processes. These processes may vary in details, such as resources and time, but the relationships are generic and applicable to many flight and ground system architectures.

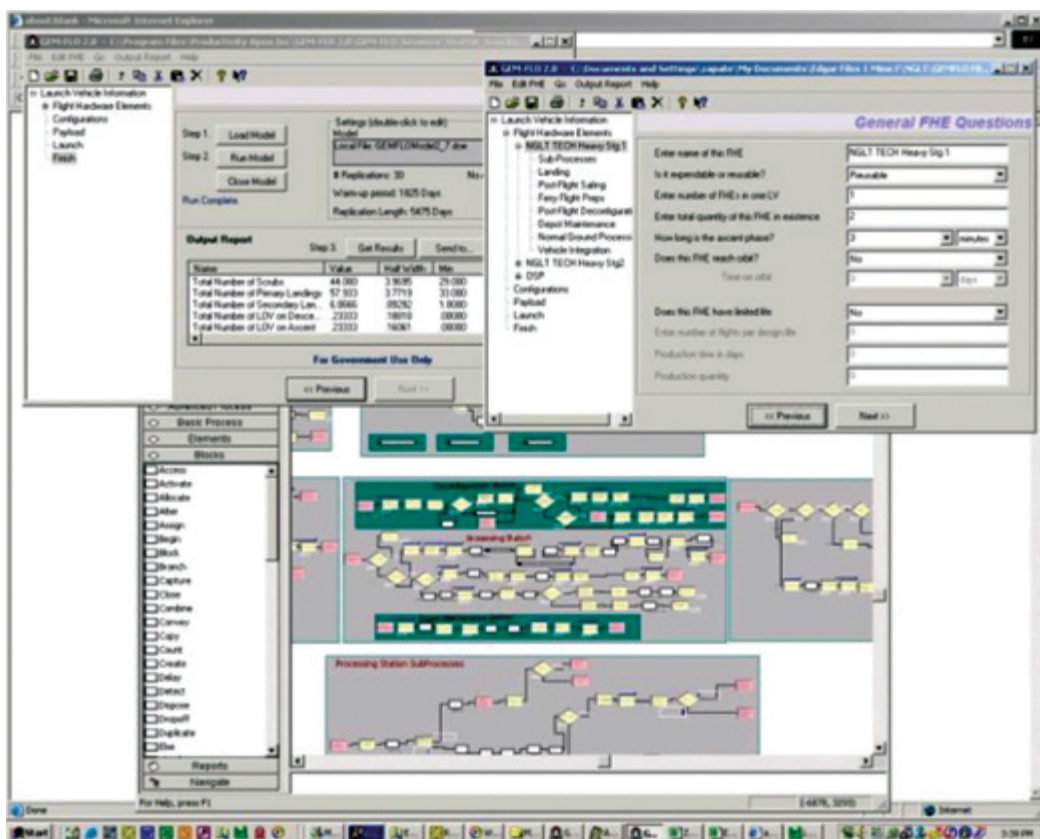
The required input for GEM-FLO includes process times (such as landing, turnaround, depot cycles, integration sequence of stages, integration time, and time on the pad), probabilities (for events such as loss of vehicle or emergency use of alternate landing sites), and resources (such as the number and type of certain facilities or the number of vehicles in a fleet). The addition of optional inputs for resource reliability and maintainability increases the fidelity of results.

In early 2004, GEM-FLO upgrades were finalized, resulting in Release 2.0. This release enhanced the simulation model's algorithms, features, capability, and overall ease of use. Furthermore, it was integrated with SAGE (Schedule Activity Generator Estimator), another tool for operations analysis. In addition, GEM-FLO-OSP, a variant of GEM-FLO, was developed to more specifically address expendable launch vehicles carrying crewed transportation systems. The GEM-FLO tool was used in 2004 in support of major NASA programs such as the Next Generation Launch Technology Program, the Orbital Space Plane, and the Crew Exploration Vehicle (CEV).

*Contacts:* Dr. M.J. Steele ([Martin.J.Steele@nasa.gov](mailto:Martin.J.Steele@nasa.gov)), YA-D4-A, (321) 867-8761; and E.Z. Zapata, YA-D4-A, (321) 867-6234

*Participating Organization:* Productivity Apex, Inc. (Dr. M. Mollaghasemi)





GEM-FLO input, output, and model screens.

## Shuttle Operations Simulations



Task/Process  
Modeling &  
Simulation

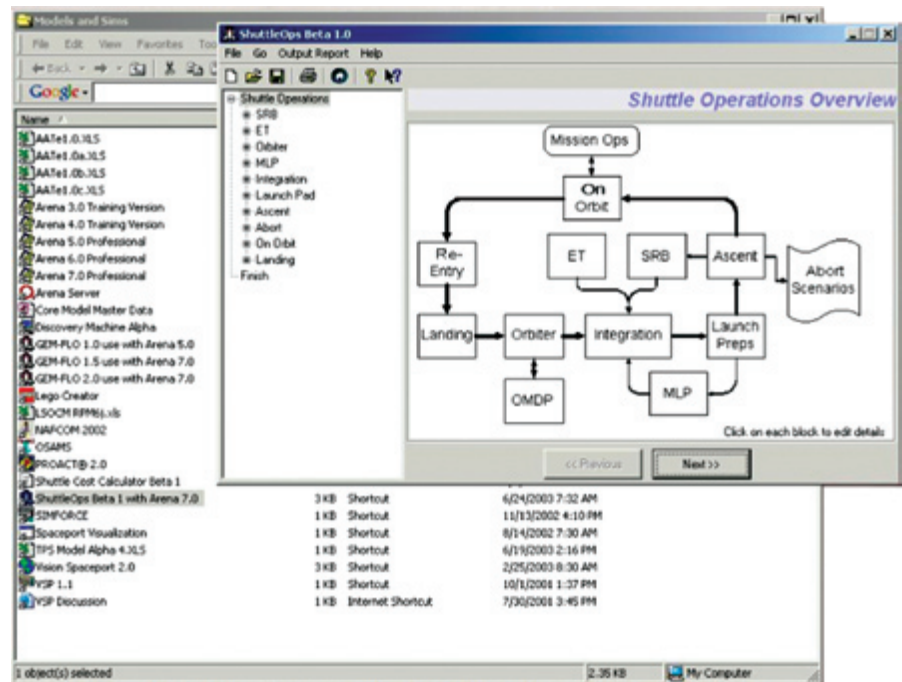
The Shuttle-Ops software tool is a friendly but powerful discrete-event simulation (DES) of the Space Shuttle ground processing operation. By means of a graphical user interface, an underlying Arena DES is populated with the Shuttle data for operations analysis.

Shuttle-Ops can be used to explore changes to the Shuttle ground operations process, yielding answers within minutes for a multitude of factors, such as facility usage, vehicle fleet size, and off-nominal probabilities, including loss of vehicle or landing at alternate locations.

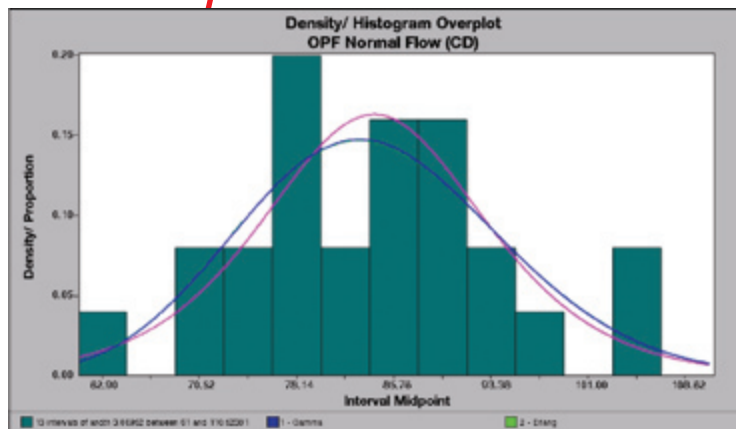
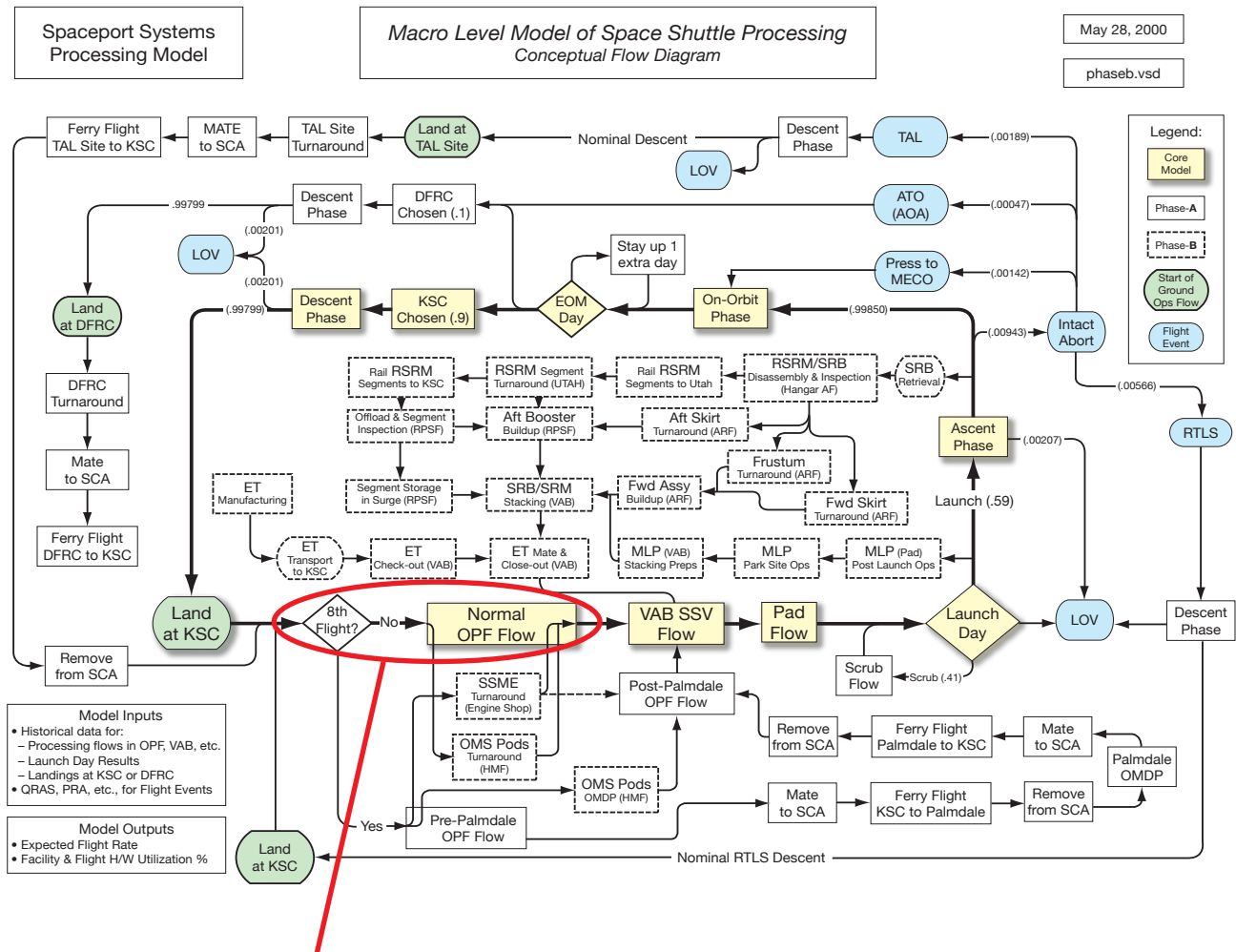
Early in 2004, the Shuttle-Ops 1.0 upgrade was completed, significantly enhancing previous overall capabilities by adding an entirely new graphical user interface for ease of use, increasing verification and validation, and enhancing algorithms.

Shuttle-Ops can be populated with over 200 variables defining system processes or resources, such as landing, turnaround, depot cycles; integration time; time on the pad; numbers of engines; and numbers of Orbital Maneuvering System (OMS) pods.

It can accept anywhere from one to hundreds of inputs per stage, depending on what the user is studying. Statistical outputs such as flights per year, facility utilization, and time in system promote higher-fidelity operations analysis, process improvement, and system definition improvement and analysis.



Shuttle-Ops input screen.



Shuttle-Ops model structure.

For more information, visit [http://science.ksc.nasa.gov/shuttle/nexgen/Shuttle-Ops\\_main.htm](http://science.ksc.nasa.gov/shuttle/nexgen/Shuttle-Ops_main.htm).

Contacts: Dr. M.J. Steele ([Martin.J.Steele@nasa.gov](mailto:Martin.J.Steele@nasa.gov)), YA-D4-A, (321) 867-8761;  
and E.Z. Zapata, YA-D4-A, (321) 867-6234

Participating Organization: Productivity Apex, Inc. (Dr. M. Mollaghasemi)

# Shuttle Operations Root Cause Analysis Database



*Task/Process  
Modeling &  
Simulation*

The Shuttle Root Cause Analysis (RCA) Database is a fundamental research study addressing the design root causes of two conditions: why it costs so much to operate the Shuttle design system and why it takes so long to process the Shuttle.

The RCA Database was a collaboration of the KSC Systems Engineering Office, the KSC Shuttle Processing Directorate, and Lockheed-Martin Corporation personnel at KSC. Users are encouraged to derive new views from the database as well as share enhanced or distilled forms of the data with the space transportation design and operations community.

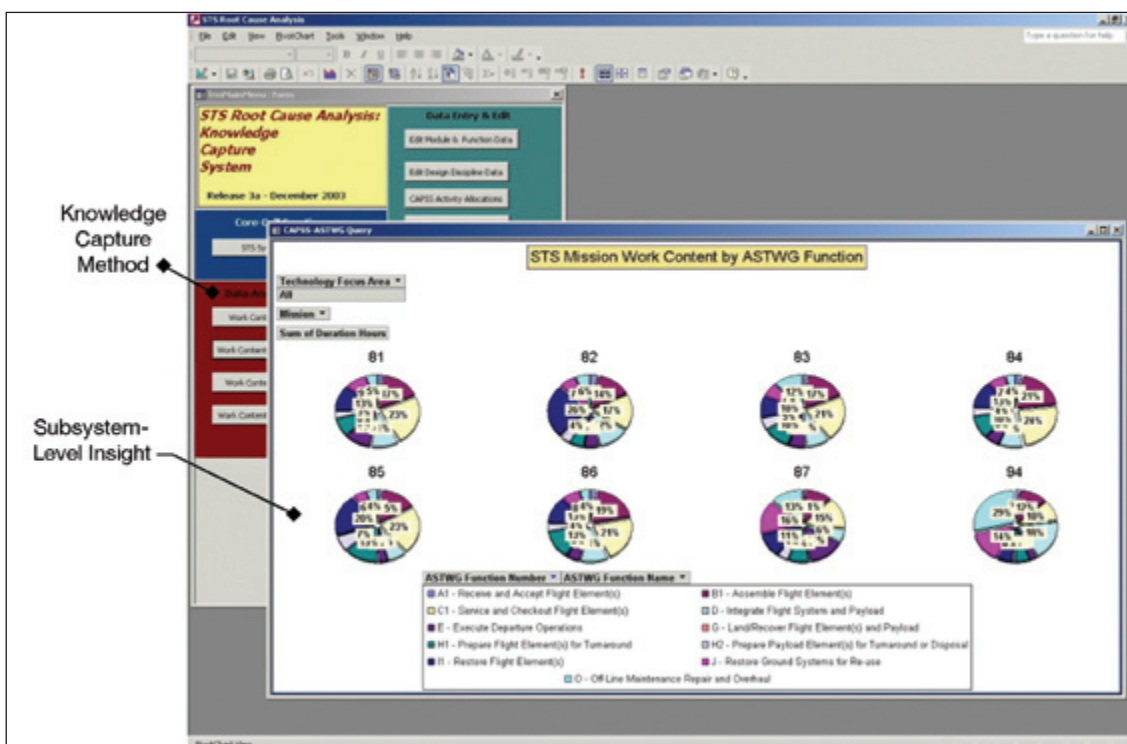
The objective here is an understanding of what can make space transportation flight or ground system designs safer, more affordable, and more routine by identifying the problems, issues, and fundamental roadblocks in operational real-world systems. KSC Space Shuttle Systems engineers contributed expertise and knowledge to the raw, less useful activity sets of data to categorize, understand, and add useful value to each of the thousands of activities defined in the Shuttle processing flow. Knowledge capture of existing Shuttle Systems Engineering (Shuttle Processing Directorate) created an invaluable data set useful for improving the design and operability of future systems.

In 2004 the RCA Database was matured to include multiple flows of data, an enhanced user interface, and significantly enhanced data validity and verification processes, creating value for current and future Space Transportation System operators. Types of data include ground processing activities, duration of activities, type of activity, activity assignment by subsystems, causes of activity, and number of planned and unplanned activities.

Further information on the RCA Database is available at [http://science.ksc.nasa.gov/shuttle/nexgen/RCA\\_main.htm](http://science.ksc.nasa.gov/shuttle/nexgen/RCA_main.htm).

Contacts: C.M. McCleskey ([Carey.M.McCleskey@nasa.gov](mailto:Carey.M.McCleskey@nasa.gov)), YA-D4-A, (321) 867-6370; and E.Z. Zapata, YA-D4-A, (321) 867-6234





Shuttle RCA screen display.

## Integrated Human Factors Toolkit Comparison Matrix

The Integrated Human Factors Toolkit is intended to assist expert and novice practitioners in employing Human Reliability, Safety, and Mission Assurance analysis tools and techniques during all phases of the program/project life cycle. Systems engineers and developers, regardless of their expertise in human factors analysis, need to consider human limitations and capabilities in their designs, whether the human interaction is in operation, testing, or maintenance of the system. The Integrated Human Factors Toolkit promotes these considerations by providing a set of validated and reliable human factors tools, methods, and techniques, along with a decision support system that can be used to select and implement the tool.

This phase of the project involved development and population of the Comparison Matrix. The Comparison Matrix is the data structure that stores information about each tool. It includes descriptive information such as vendor contacts, license availability, hardware and software requirements, and references. More important, it includes analytical criteria that systems engineers can use to select the most appropriate tool for specific analytical requirements. The decision support process is shown in Figure 1.



Figure 1. Filtering criteria for the Comparison Matrix.

In the initial step of the project, human factors tools, methods, and techniques were compiled from a variety of sources, including NASA, contractors, DOD, other Government agencies, private vendors, and the public domain. These tools were evaluated for the following criteria in relation to NASA products and processes:

- **Validity:** The extent to which the tool has been validated through independent research, vendor studies, and extensive use in the field.
- **Reliability:** The degree to which the tool will yield comparable results when used by different analysts to evaluate the same system or multiple systems with the same risk profile.
- **Appropriateness:** The extent to which the tool is designed for systems typical of those used by NASA.

Once the included tools were identified, a set of criteria was devised through which engineers could select which tool best matched the needs of the system being developed. These criteria fell into five categories:

- **System Life Cycle Stage:** The stages of the NPR 7120.5B system life cycle in which the tool is most appropriate to be used.
- **Tool Output:** The format in which the results are provided, such as risk scores, intervention strategies, and objective physical measurements; and the ability of these results to diagnose and ultimately enhance the system design.

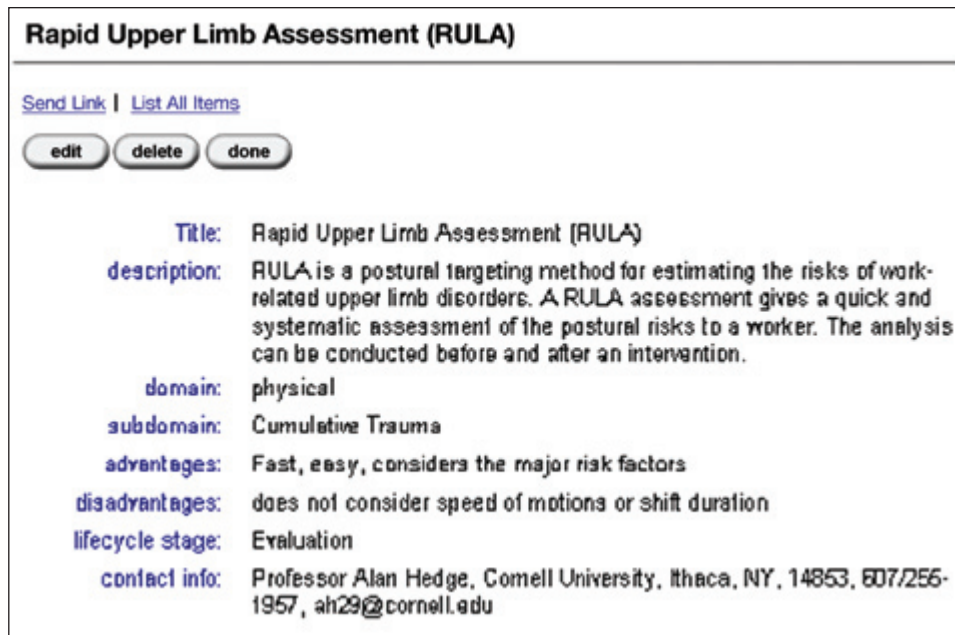


Figure 2. Screen display of a tool description in the Human Factors Toolkit.

- Expertise Requirements: The degree of expertise within the specific human factors domain being analyzed and the familiarity with the requirements of the task being analyzed that are necessary to use the tool effectively.
- Resource Requirements: The time required to conduct a typical evaluation; the requirement for participation of an operator or subject matter expert to use the tool; and the design fidelity required to use the tool.
- Tool Characteristics: Hardware on which the tool runs (if any); software or operating systems on which the tool runs (if any); and licensing requirements.

These criteria are intended to help the systems engineer select the most appropriate tool for the specific requirements of the project. By filtering the Comparison Matrix using these criteria, the systems engineer can ensure the tool can be used given the constraints of the project.

After the tools have been filtered, there may be more than one tool available that matches the requirements of a project. The decision of which tool should be used is supported through the tool differentiation fields. These are lists of advantages and disadvantages of the tools relative to others within the same human factors domain. Using this advice, the systems engineer can optimize the tool selection process. Figure 2 shows a screen display of a tool output within the Comparison Matrix. Only a subset of the fields is shown.

Contact: Dr. G.M. Henderson ([Gena.M.Henderson@nasa.gov](mailto:Gena.M.Henderson@nasa.gov)), EA-C, (321) 867-4261

Participating Organization: Florida International University (Dr. M.L. Resnick)

## AreaAdvisor – Spatial, Real-Time Resources Intelligence



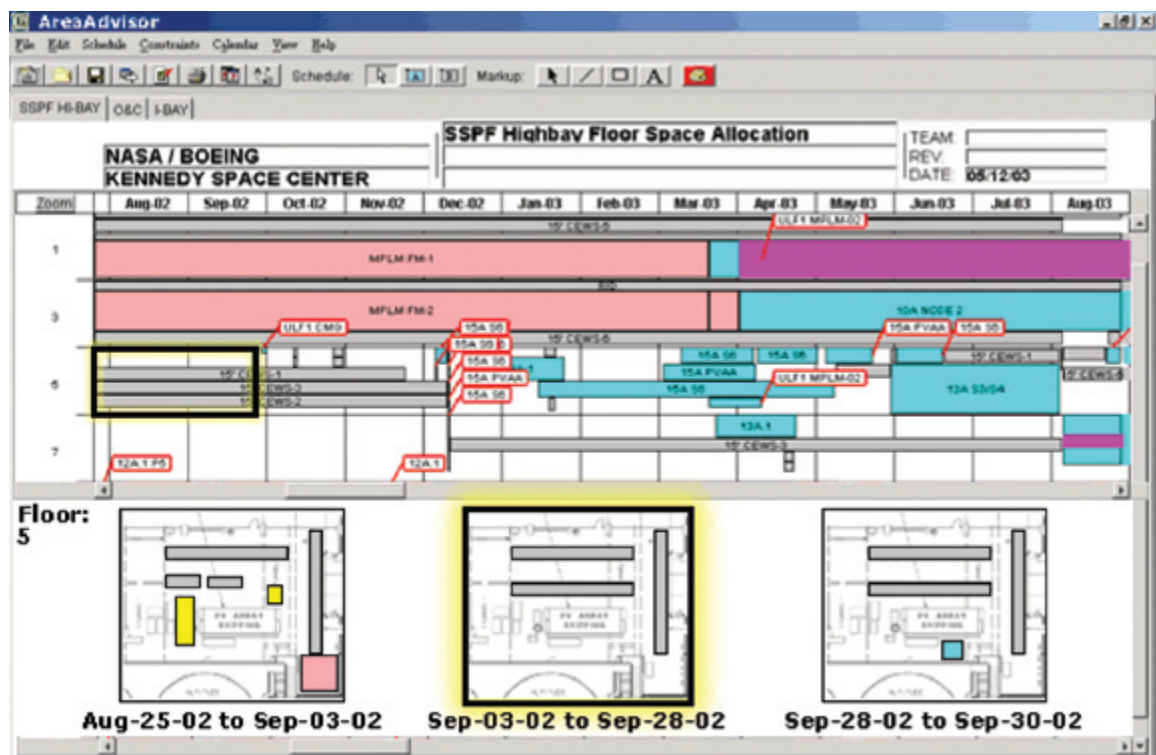
Advanced Planning  
& Scheduling Tools

The AreaAdvisor Phase II system will be an intelligent software application that will make warehousing-related decisions based on the entered knowledge of expert warehouse managers. It takes automated inputs and sends completed transaction data

back to legacy systems, providing a single interface for warehousing and related personnel.

AreaAdvisor will batch tasks that can be done together, select optimum storage and retrieval locations; implement and suggest consolidation and relocation goals; aid in finding lost items; provide dynamic, context-sensitive warehouse utilization visualization; and provide intelligent trending, data mining, and display to help warehousing personnel better manage their processes. This will improve the efficiency, safety, item storage and distribution in the warehouse, warehousing response time, and process and utilization visibility and understanding; reduce errors and lost items; and preserve corporate knowledge relating to managing the warehouses.

AreaAdvisor will accept inputs from a variety of automated sources including the existing GOLD inventory management system; handheld wireless devices; conventional bar codes; smart (MaxiCode) bar codes; KSC ID badges; radio frequency identification tags; and 3-D volumetric scanners. It will output its recommendations in a variety of formats, including through wireless handhelds, PC



Floorspace chart.



graphical user interfaces, and printed reports. It will also export transaction-level information (equivalent to that transmitted from the current PC-based GOLD clients) back to the GOLD warehouse management system. It may also interface to other KSC systems as required for work flow efficiency.

Specific innovations include the following:

- Utilizing artificial intelligence behavior modeling techniques to warehouse management decisions.
- Providing a capability for warehouse personnel to edit and maintain the knowledge the system uses to make decisions, thus changing the decision processes within the software themselves.
- Providing a very high degree of configurability.
- Allowing data mining.
- Noting emergent behaviors (where consolidation effects emerge from a large number of independent storage and retrieval decisions).
- Allowing autonomous goal seeking and dynamic, self-adjusting, intelligent visualization, all applied to the warehouse management system context.

These innovations were proved absolutely in Phase I by developing a prototype that actually implemented the most critical algorithms and showed the utility of the ideas. Furthermore, the prototype served as both a proof and a basis for the Phase II system design. This design proves that the full-scale system can be implemented in Phase II.

Though we will be working with one warehousing group at KSC in Phase II, other warehousing systems at KSC and other NASA Centers have similar warehousing needs and problems. AreaAdvisor will also be of great value to commercial warehouses. Our distribution to them would likely be through warehouse consults, warehouse hardware vendors who have consultants to aid their clients, and warehouse management system vendors. DOD also has unique warehousing requirements relating to both permanent and temporary storage of repair parts, spares, ammunition, etc. DOD's requirements are similar to KSC's and very different from those of most commercial warehouses, so they are also underserved by commercial technology vendors. Contractors involved in the production of weapon systems also have complex warehousing needs best addressed by AreaAdvisor.

Key accomplishments:

- 2004: Developed algorithm and visualization. Demonstrated prototype.

Contact: T.E. Kickbusch ([Tracey.E.Kickbusch@nasa.gov](mailto:Tracey.E.Kickbusch@nasa.gov)), EA-C, (321) 867-2770

Participating Organization: Stottler Henke Associates, Inc. (D. Stottler)

## System Reliability of Multielement Integrated Testing (MEIT)



Task/Process  
Modeling &  
Simulation

The importance of MEIT to estimate total system reliability is relevant since reliability is overestimated because of the lack of knowledge at the interfaces. Too often multielements or three-way failures (hardware-software-human) are not calculated as a first-order interaction of standard reliability.

As a multielement system, the Shuttle launches space exploration experiments in orbit. During a 10-year pilot study, reliability issues were centered on multielement failures, not single element reliability as seen in literature reviews. There were no operational analysis methods to thoroughly analyze the system reliability of such inseparable frameworks. The MEIT of the International Space Station (ISS) program at KSC describes failures of inseparable frameworks from a binary system as operational or failing. For instance, system 1, system 2, and system 3 are composed as a multielement integrated system (Figure 1). System 1 has a hardware failure that is connected to a hardware-software-human failure in system 2. System 2 is connected to a software-human failure in system 3. Although the human element does not come into the scenario until the introduction of system 2, all three systems include a complex integrative system and are connected by the human intervention. Therefore, an operational methodology analysis was developed to characterize and examine all system failures that occur during processing through hypothesis testing on Baker's Generic Classification Scheme (Table 1), Kilgorn's Smirnov's distribution fitting, and Laplace's trend testing.

Baker's Generic Classification Scheme classifies failures of multielement integrated systems within processes as single (human, hardware, software), dual (hardware-software, software-human, human-hardware), and multielements (hardware-software-human) interactions. Table 1 serves as quality and significant contributors in measuring the total reliability of any system. Attribute interactions are comprised from crossing a single element's attributes with those of another single element that create many three-way interactions. The nine consistent dual and two multielement patterns repeatedly shown in the processing test of the ISS are listed in Table 2. The technique (along with distribution fitting and trend testing) provides practitioners with immediate statistical significance of reliability growth or deterioration in a process. The significance of research lies within the inclusion of first-order element interactions of dual and multielements to properly estimate standard reliability.

Table 1. Element attributes for Baker's Generic Classification Scheme.

Hardware	Software	Human
(1) Maintenance	(1) Structural	(1) Mental Acuity
(2) Existence	(2) Logic	(2) Physical Ability
(3) Environment	(3) Coding	(3) Experience
(4) Technology	(4) Input Hypothesis	(4) Training
(5) Warranty		(5) Human-Involved
(6) Compatibility		(6) Nature of Task

Qualitative and quantitative decisions are made to understand mechanisms across simulated and operationally configured tests (Figure 2) (at the system, subsystem, element, element interaction, and element attribute levels, as well as to scrutinize certain problems within steps of various sequenced processes. The analyses mark the first time a logically statistical technique is utilized in an integrated approach to assess total system reliability of simultaneous failures in real field performance. The overall reliability assessment reflects process success rate over the development test time.

This logically statistical technique is applied to the problem reporting system of a processing environment of the ISS program and utilized to classify, identify, analyze, and measure reliability. The nine consistent dual and two multielements patterns repeatedly shown in the processing test of the ISS established reliability metrics that showed growth or deterioration within the process, subsystem, and system. By understanding ISS processing environment, practitioners were able to better understand ground processing phenomena and extend this knowledge to on-orbit tasks for ISS. Although the generic technique can be applied to any system, the space system offers a higher, universal industry domain of a safety-critical and controlled environment. The methodology concentrates on the interface of these elements and their interactions during the life cycle checkout of the MEIT (Phase 1, TC2R) for the ISS program.

Contact: Dr. G.M. Henderson ([Gena.M.Henderson@nasa.gov](mailto:Gena.M.Henderson@nasa.gov)), EA-C, (321) 867-4261

Participating Organizations: SA-C3 (S.C. Bodiford), UB-G6 (R. Franco), University of Central Florida (Dr. Y. Hosni), and Wichita State University (Dr. G. Weheba)

Table 2. ISS significant patterns.

Pattern	Hardware	Software	Human
000	0	0	0
131	1	3	1
614	6	1	4
32X	3	2	
4X6	4		6
61X	6	1	
63X	6	3	
6X4	6		4
X14		1	4
X21		2	1
X31		3	1

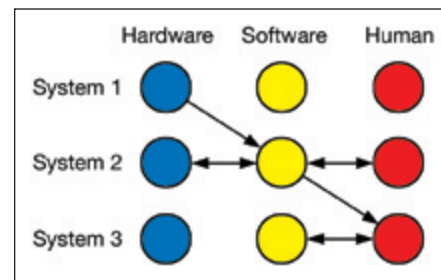


Figure 1. Multielement integrated systems.

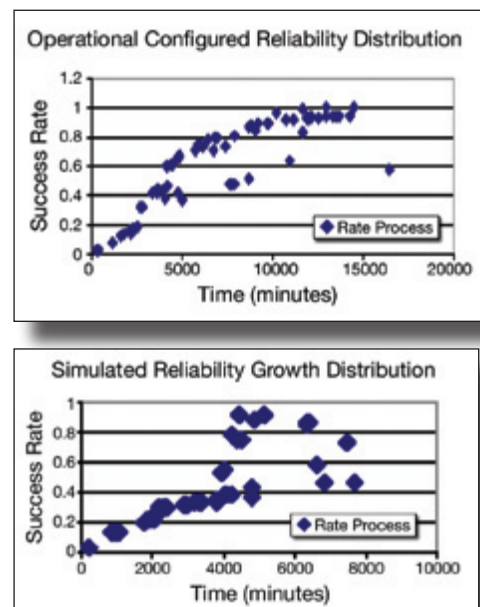


Figure 2. Simulated and configured reliability growth distributions.

## Wing Leading-Edge Structural Subsystems and Reinforced Carbon-Carbon (RCC) Orbiter Processing Facility (OPF) Area/Access Enhancements



Task/Process  
Modeling &  
Simulation

The handling, installation, and removal of RCCs and wing leading-edge hardware at KSC have historically involved considerable physical and technical support with awkward physical positions and manual lifting/lowering. The hardware is bulky, heavy, costly, and nearly irreplaceable. The OPF Level 8 Processing Team was formed to mitigate hazards/risks to personnel when handling hardware. The Columbia Accident Investigation Board (CAIB) report further substantiated a need to improve this area access because of increased inspections, processing, and personnel/equipment traffic.

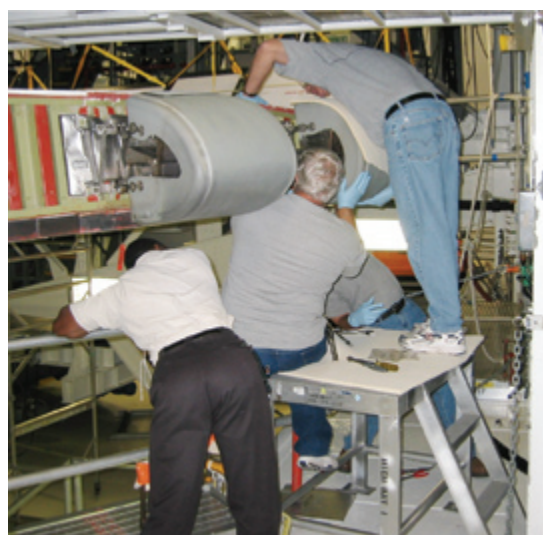
The OPF Level 8 Processing Team, including many members of the Level 8 and Wing Leading-Edge Processing Improvement Team (PIT), United Space Alliance (USA), and NASA personnel, meets to facilitate enhancements, provide status, and participate in design and virtual reality simulation reviews.

NASA Industrial Engineering for Safety (IES) approved FY 2004 funding to USA Ground Operations to support the design efforts for Level 8 platform modifications and additional OPF workspaces. Funding is being requested for implementation in the OPFs. USA is also supporting supplementary operational enhancements: (1) larger platform work stands to accommodate two-person optimum reach to lower RCCs and Leading-Edge Structural Subsystem (LESS) from OPF floors and (2) step-up stands for use on Level 8 to be height-adjustable, larger, and more maneuverable.

Implementation of enhancements was requested for each OPF. Implementations of major OPF facility modifications are dependent on open-bay windows. Centerwide application could include use of an electronic pallet jack in facilities to



*RCC access from OPF floor and Level 8.*



*Limited access to wing leading edge on Level 8.*



eliminate manual handling of hardware or lifting/lowering; work stands to meet height and exceed safety requirements; and articulating/flexible platform edges. The Level 8 Processing Team continues to implement means to reduce personnel and hardware safety risks, reduce schedule and supportability risks, and minimize recovery costs risks.

#### Key accomplishments:

- FY 2004 IES funding granted for 60 percent design of Level 8 platforms to improve access to leading wing edges. Funding also provided design completion of Level 8 platform additions and forward mezzanines for increased processing and storage in OPFs 1 and 2.
- Fabricated and installed toe-board adapter sockets on Level 8 to move handrails closer to the wing leading edge to enable technicians to get closer to RCC panels and the Thermal Protection System (TPS). Moved communication boxes and other items to ensure flight hardware travel path is clear to prevent inadvertent RCC contact.
- Design/efforts are in-work to provide means to transport RCCs and other heavy/awkward hardware from Level 8 to/from each OPF floor, authorize electronic pallet jack for lifting/lowering RCCs and inspection equipment to/from Level 8, and implement pallets that meet OPF fire codes to secure/support RCCs on pallet jacks.

Contacts: S.S. Wilkhu, MK, ([Sandeep.S.Wilkhu@nasa.gov](mailto:Sandeep.S.Wilkhu@nasa.gov)), (321) 861-9085; M.M. Groh-Hammond, PH-O, (321) 861-0572; D.C. Baker, PH-O-A, (321) 861-0407; and M.J. Hoffman, SA-B2, (321) 861-4107

Participating Organization: USA (P.A. Hollis, K.S. Stelges, G.A. Buford, P.D. Hargrove, R.M. Pracek, J.E. Kuhn, J.M. Green, D.R. King, G.L. Grantham, E. Castillo, V.W. Taylor, D.R. Girard, B.A. Lawrence, D.C. Larsen, R.E. Mills, S.L. Cipolletti, J.L. Stirling, L.D. Peck, M.E. LaBrie, M.S. Barnes, C.G. Neely, C.J. Brown, E.J. Deremer-Cook, B.C. Burns, T.D. Adamson, K.R. Wagner, and T.W. Roberts)



*Transporting RCC panels on crowded Level 8.*



*RCC panels on crowded Level 8.*



*RCC processing on OPF floor.*

## TAL Site Heat Shield Removal Study



Task/Process  
Modeling &  
Simulation

Designated lifting equipment or access platforms do not currently exist at the Transatlantic Abort Landing (TAL) sites. In the event of a landing by the Shuttle at a remote site due to an aborted mission, United Space Alliance (USA) would need methods and equipment to perform

Space Shuttle Main Engine (SSME) Dome Heat Shield (DHS) and Engine-Mounted Heat Shield (EMHS) or eyelid removal.

If required today, the conceptual plan for the TAL sites would utilize a labor-intensive system of 30-foot picboards and scaffolding, significantly limiting available floor space. Technicians would have to manually remove heat shields. Rope visual barriers would be used to mitigate fall hazards. Technicians would have to wear fall protection and consider methods for denoting tie-off points. Increased likelihood of trip hazards would exist because of uneven picboards and c-clamps. Scaffolding would (1) pose risks to hardware and personnel because of traversing stairs, (2) limit storage areas, and (3) offer no place to install a mechanical-assist device. Ergonomic concerns would exist with physical energy demands and manual material handling. Likelihood of personnel injury or death and damage to flight hardware exists; thus the development of a designated access platform and means for DHS and EMHS removal at TAL sites were proposed.



*Scaffolding setup for temporary storage in Vehicle Assembly Building (VAB).*



*Scaffolding setup for temporary storage in VAB.*

Process Failure Mode and Effects Analysis (PFMEA) methodology identified requirements and solution alternatives for DHS and EMHS removals at TAL sites. Research and evaluation of several removal methods led to requesting and obtaining NASA Industrial Engineering for Safety (IES) FY 2004 funding to create a virtual reality simulation study. A virtual reality simulation study offers a more cost-effective means to visualize and evaluate the feasibility of multiple versions of hardware or access designs compared to literally designing, manufacturing, and implementing.

The virtual reality 3-D format of the interactive scenes and simulations was available to personnel to view from their desktops. The targeted users viewed the proposed user interfaces and provided appraisal of the most practical and useful interface. This project involved a broad base of users, developers, implementers, and management, including USA and NASA personnel. Since the intent of the study was to develop and eventually implement a practical, useful, and essential system, users' hands-on requirements and preferences guided the research and solution options.



The virtual reality study of the Orbiter aft and potential access equipment assisted in developing safe and efficient recommendations for removing DHSs and EMHSs at TAL sites by providing:

- The equipment and methods to access the heat shields safely and within Occupational Safety and Health Administration (OSHA) guidelines.
- Devices to lift the heat shields away from the Orbiter and to the ground level.
- The process to perform the removals.

In conclusion, the study successfully portrayed options to reduce personnel and hardware safety risks, reduce schedule and supportability risks, and minimize variability in the event SSMEs would need to be removed at a remote landing site.

#### Key accomplishments:

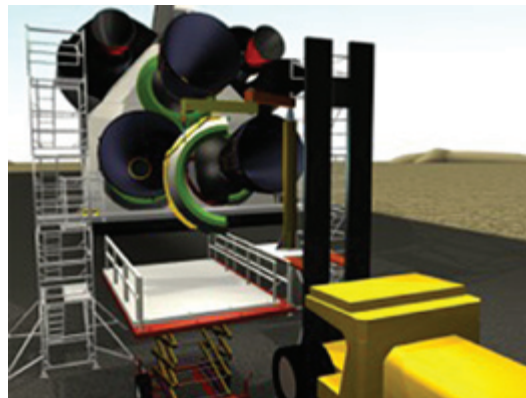
- Conducted PFMEAs and published results. Developed options to consider for SSME removal and two best alternatives to study.
- FY 2004 IES Virtual Reality Study completed by USA, in particular, KSC Advanced Visualization Environments (KAVE). Modeled several PFMEA options and best alternatives.

#### Key milestones:

- Implement an established process, apply lessons learned to other operations, and analyze study recommendations for application for SSME and T-0 access, elevon ferry-lock installation, tail cone access, Thrust Vector Control actuator ferry support installation, engine closeout cover installation, Orbital Maneuvering Subsystem (OMS) pod observer access, and SSME environmental closure installation and removal (Dryden Flight Research Center and KSC).

Contacts: D.C. Baker ([Daniel.C.Baker@nasa.gov](mailto:Daniel.C.Baker@nasa.gov)), PH-O-A, (321) 861-0407; W.R. Carew, PH-J, (321) 867-3271; M.M. Groh-Hammond, PH-O, (321) 861-0572, E.N. Montalvo, PH-G1, (321) 861-3942; and S.S. Wilkhu, MK, (321) 861-9085

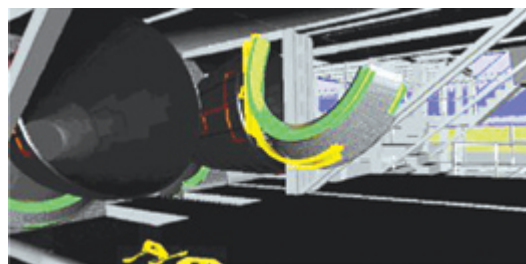
Participating Organization: USA (A.D. Blum, B.C. Burns, S.L. Cipolletti, M.L. Closen, E.J. Deremer-Cook, D.R. Girard, D.J. Gompers, E.W. Hall, P.A. Hollis, E.J. Janda, J.R. Jeffers, M.S. Kelemen, P.L. Kruse, J. Lakaszcyck, D.C. Larsen, B.A. Lawrence, M.L. Linthicum, W.C. Manley, R.E. Mills, P.A. Peabody, L.D. Peck, E.G. Rieck, K.S. Stelges, and J.L. Stirling)



*Simulation option only.*



*Graphically imposed scissor lift near Orbiter at landing.*



*Simulation option only.*

## A Discrete-Event Simulation Model for Spaceport Operations (SPACESIM)



*Task/Process  
Modeling &  
Simulation*

The NASA vision for the spaceport of the future entails transitioning over time from very high-cost, research-oriented space launches with a relatively low frequency of launches to an environment where spaceports are commercialized for the space transportation industry and required to support multiple launches per day in a safe, cost-effective manner. The spaceport of the future may resemble, from an operational perspective, our current airports and seaports and will need to resolve many similar issues to today's transportation hubs. These issues include (1) safe and secure spaceport operations, (2) efficient movement of machinery and people through the spaceport, and (3) cost-efficient, affordable, and timely spaceport operations. Discrete-event simulation is in use to analyze detailed processes at modern-day seaports and airports. Like these more domestic ports, spaceport operations are labor-intensive and require extensive use of personnel and machinery. The efficiency of port operations is improved through proper utilization of port assets. Research for efficient spaceport operations using discrete event simulation can use seaport operations as a foundation toward similar efficiencies. The object-oriented discrete-event simulation system in development will address spaceport operations in the context of aerospace safety, mobility, and efficiency. The simulation system is built upon the Java programming language to provide for maximum portability and utilizes XML for standards-based data interchange. Development of the simulation model provides the underlying basis for follow-on activities such as 2-D and 3-D animation and other visualization capabilities. The overall goal of the spaceport simulation model is to maximize throughput, operational safety, and resource utilization, while minimizing the overall cost of operations.

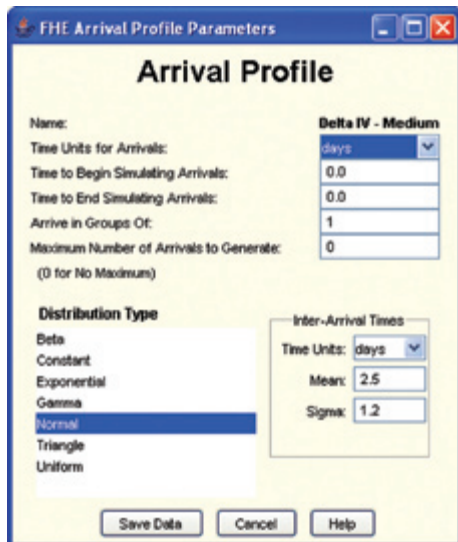
Benefits of this development effort include:

- The ability to play "what if" scenarios in a simulated environment prior to making large capital investments.
- Improved visibility of potential operational problem areas within spaceports.
- Reusable hierarchies of space transportation and ground support objects for modeling integration efforts.
- Significant reduction in operational cost.

The products provided by this project are:

- A Java-based discrete-event simulation engine.
- The SPACESIM Object-Oriented Hierarchy defining spaceport objects.
- The SPACESIM Process Maps defining spaceport processing functions.
- A user interface that will guide the user through the inputs required to run scenarios pertinent to the launch vehicles, spaceports, and schedule options desired (see the figures).





**FHE Arrival Profile Parameters**

**Arrival Profile**

Name: **Delta IV - Medium**

Time Units for Arrivals: **days**

Time to Begin Simulating Arrivals: **0.0**

Time to End Simulating Arrivals: **0.0**

Arrive in Groups Of: **1**

Maximum Number of Arrivals to Generate: **0**  
(0 for No Maximum)

**Distribution Type**

Beta  
Constant  
Exponential  
Gamma  
**Normal**  
Triangle  
Uniform

Inter-Arrival Times

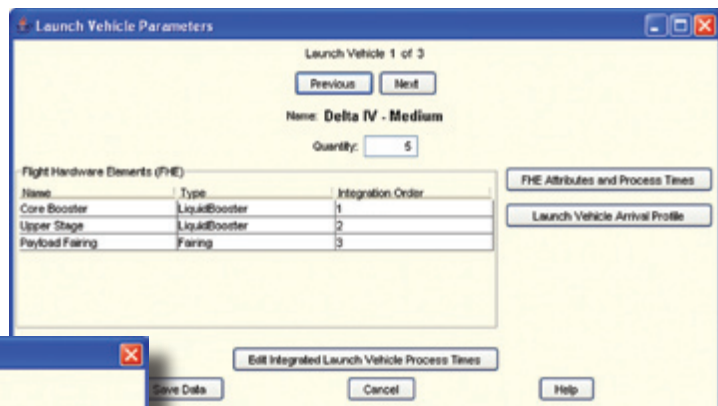
Time Units: **days**

Mean: **2.5**

Sigma: **1.2**

Save Data Cancel Help

Launch vehicle arrival parameters.



**Launch Vehicle Parameters**

Launch Vehicle 1 of 3

Previous Next

Name: **Delta IV - Medium**

Quantity: **5**

**Flight Hardware Elements (FHE)**

Name	Type	Integration Order
Core Booster	LiquidBooster	1
Upper Stage	LiquidBooster	2
Payload Fairing	Fairing	3

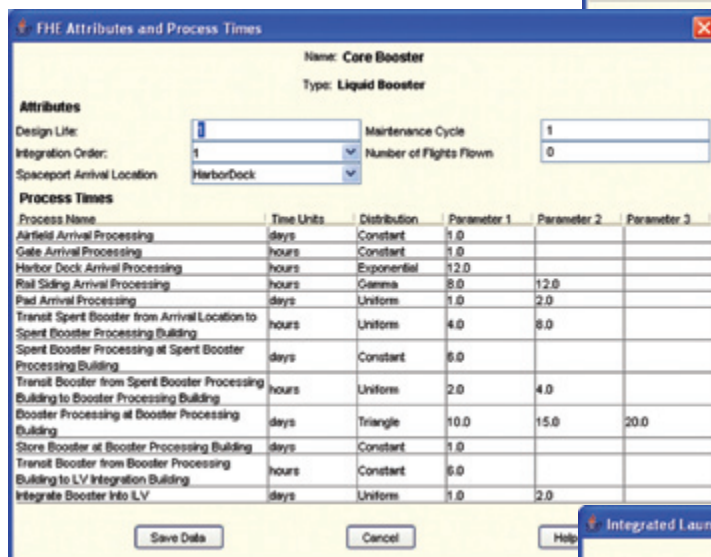
FHE Attributes and Process Times

Launch Vehicle Arrival Profile

Edit Integrated Launch Vehicle Process Times

Save Data Cancel Help

Launch vehicle parameters.



**FHE Attributes and Process Times**

Name: **Core Booster**

Type: **Liquid Booster**

**Attributes**

Design Life: **1** Maintenance Cycle: **1**

Integration Order: **1** Number of Flights Flown: **0**

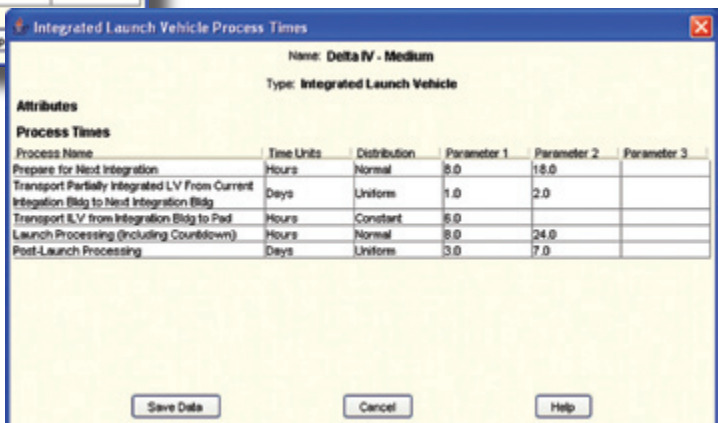
Spaceport Arrival Location: **Harbor/Dock**

**Process Times**

Process Name	Time Units	Distribution	Parameter 1	Parameter 2	Parameter 3
Airfield Arrival Processing	days	Constant	1.0		
Gate Arrival Processing	hours	Constant	1.0		
Harbor Dock Arrival Processing	hours	Exponential	12.0		
Rail Siding Arrival Processing	hours	Gamma	8.0	12.0	
Pad Arrival Processing	days	Uniform	1.0	2.0	
Transit Spent Booster from Arrival Location to Spent Booster Processing Building	hours	Uniform	4.0	8.0	
Spent Booster Processing at Spent Booster Processing Building	days	Constant	6.0		
Transit Booster from Spent Booster Processing Building to Booster Processing Building	hours	Uniform	2.0	4.0	
Booster Processing at Booster Processing Building	days	Triangle	10.0	15.0	20.0
Store Booster at Booster Processing Building	days	Constant	1.0		
Transit Booster from Booster Processing Building to LV Integration Building	hours	Constant	6.0		
Integrate Booster into LV	days	Uniform	1.0	2.0	

Save Data Cancel Help

Flight hardware element parameters.



**Integrated Launch Vehicle Process Times**

Name: **Delta IV - Medium**

Type: **Integrated Launch Vehicle**

**Attributes**

**Process Times**

Process Name	Time Units	Distribution	Parameter 1	Parameter 2	Parameter 3
Prepare for Next Integration	Hours	Normal	8.0	18.0	
Transport Partially Integrated LV From Current Integration Bldg to Next Integration Bldg	Days	Uniform	1.0	2.0	
Transport LV from Integration Bldg to Pad	Hours	Constant	6.0		
Launch Processing (Including Countdown)	Hours	Normal	8.0	24.0	
Post-Launch Processing	Days	Uniform	3.0	7.0	

Save Data Cancel Help

Integrated launch vehicle parameters.

## Virtual Testbed for Spaceport Models



*Decision/Data  
Models &  
Analysis*

The Virtual Testbed (VTB) project from the Spaceport Engineering and Technology Directorate has its foundations in the NASA Ames Research Center (ARC) Intelligent Launch and Range Operations program. Spaceport operations of the present rely on a series of activities and human decisions to plan and support missions, configure systems, conduct flights, and perform space operations analysis. Hundreds of spaceport operations personnel are required to plan and execute all mission-related processes for every scheduled mission.

The objective of the VTB project is to develop a unique collaborative computing environment where simulation models can be hosted and seamlessly integrated. This collaborative computing environment will be used to build a “virtual” spaceport. An important goal of the project is to serve as a technology pipeline to research, develop, test, and validate R&D efforts against real-time operations without interfering with actual operations or consuming the operational personnel’s time.

The VTB project’s ultimate goal is to enable engineers to visualize, interact, collaborate, and play “what if” scenarios with simulations of integrated models representing different elements and processes in spaceport operations. Our approach focuses on customizing the VTB architecture involving visualization components, knowledge-based systems, and specialized kernels for rapid integration of operations-specific models. The project’s impact will promote new ways of doing engineering through interactions with simulations of seamless integrated models, data, and decision-making tools. It also shortens the design cycle and provides intelligent visualization and flow optimization.

The NASA-University of Central Florida (UCF)-All Points Logistics (APL) VTB team focused for the past two years on system issues required to conceptualize and provide form to a system architecture capable of handling the different demands of the Virtual Testbed. Capturing the spaceport complex system of systems (i.e., launch vehicle processing systems, payload processing systems, range systems, and base support [infrastructure and their respective activities]) is no easy task. Spaceports systems are concurrently designed with flight vehicle and flight crew systems.

In FY 2002, the NASA-UCF VTB team began research for the best simulation engine available to accomplish its task. After careful evaluation, the team selected SPEEDES (Synchronous Parallel Environment for Emulation and Discrete-Event Simulation) because of the following attractive attributes:

- U.S. Government-Owned (NASA), thus freeware for NASA
- Scalable object-oriented DES environment (C++)
- Backbone of WARGAME 2002 (Navy) and the Joint Battlespace Info Sphere (U.S. Air Force)
- Open-source-compliant with high-level architecture (HLA)
- Plenty of documentation available, in-house capabilities, maintenance, and expertise
- Handles large and distributed models
- Can be Web-enabled
- Most important, has been proven in other important projects of similar or greater magnitude

In FY 2003, the NASA-UCF VTB team began work on this plan by first studying and analyzing the NASA Shuttle Model that was built in ARENA in 1999-2001 (NASA and UCF). The first subtask

was to convert the NASA Shuttle Model from an older version of ARENA to a newer version of ARENA. The second subtask was to convert from ARENA to SPEEDES, and a third subtask was to validate the SPEEDES model by comparing its output with the output from the ARENA model.

The team developed a “reduced” version of the NASA Shuttle Model and then successfully implemented that version into SPEEDES in April 2003. Then the Shuttle module was completely broken down into modules/objects to allow the conversion of the model to ARENA 7 and the object implementation in SPEEDES. The objects were then added to the reduced SPEEDES model, which can be scaled as time passes and with less complexity. Finally, the validations were done at certain time intervals as the module was considerably enhanced. The complete version of the NASA Shuttle Model was implemented by September 2003.

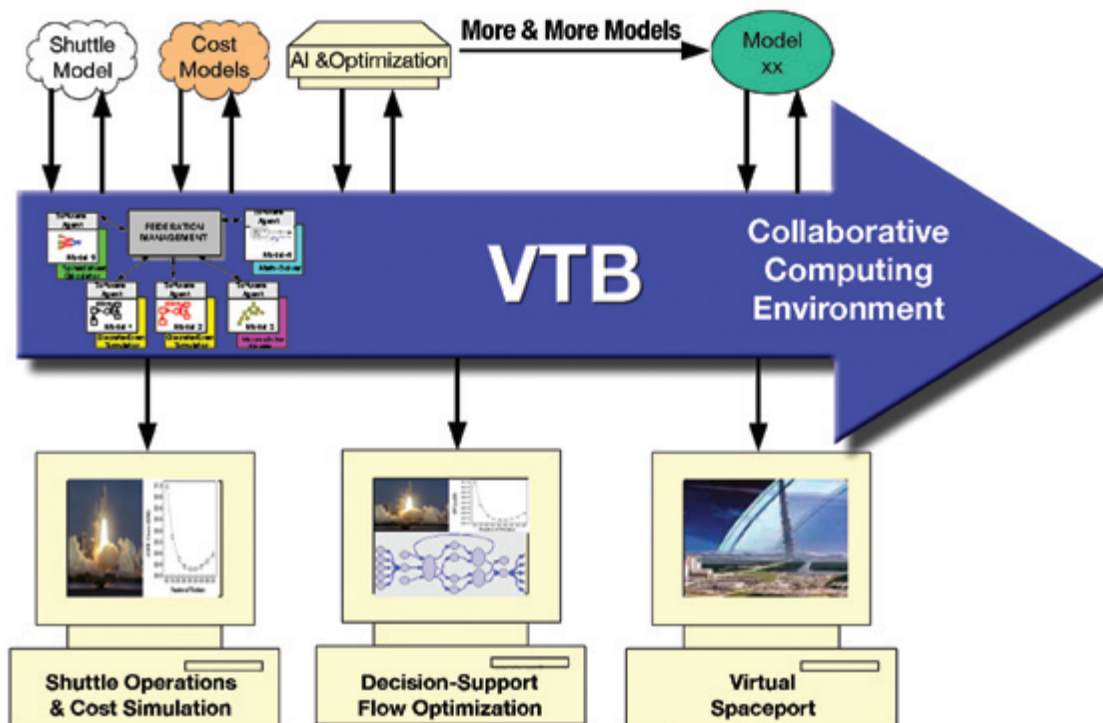
Distributed parallel simulation was demonstrated at ARC, where several geographically distributed modules (ARC and UCF) on different computers successfully simulated the NASA Shuttle Model.

Key accomplishments:

- FY 2003: Distributed across a network a demo experiment of parallel execution of the SPEEDES NASA Shuttle Model on three different computers (two nodes at ARC and one node at UCF). Completed initial spaceport model assessment report.
- FY 2004: Completed integration of virtual range, virtual testbed, and Weather Expert System (WES); and demo experiment of distributed simulation using four computers at UCF. Developed preliminary framework for Usability of Virtual Engineering and Distributed Simulation Environments.

Contact: C.J. Peaden ([Cary.J.Peaden@nasa.gov](mailto:Cary.J.Peaden@nasa.gov)),  
YA-E6, (321) 867-9296

Participating Organization: University of Central  
Florida (Dr. L. Rabelo and Dr. J. Sepulveda)



NASA's Spaceport VTB.

## NASA Faculty Fellowship Program (NFFP) 3-D Modeling



*Task/Process  
Modeling &  
Simulation*

This application project introduced a University of Wisconsin professor and two university students to KSC and yielded a useable product with a valid operational engineering need in a 10-week period. This American Society for Engineering Education (ASEE)/NFFP project was in two phases. Phase I was to complete parts, assemblies, and drawings that could be used by ground support equipment (GSE) personnel to simulate situations and scenarios commonplace to the Space Shuttle Orbiter/External Tank (ET) mate. Phase II was to complete a basic model of the crawler that would include a detailed truck assembly and a chassis representation.

During Phase I, the Orbiter/ET mate takes place in the Vehicle Assembly Building (VAB). These simulations are then used by NASA engineers as decision-making tools.

During the summer of 2003, solid models were collected and translated into Pro/ENGINEER'S .prt and .asm formats. These solid models included computer files of the Orbiter ET, Solid Rocket Boosters, Mobile Launcher Platform, transporter, and VAB. A large number of models came from the Spaceport Engineering and Technology Directorate (YA), whose engineers had updated Orbiter and ET models.

During the summer of 2004, parts were created that defined the Orbiter/ET structural attachment points to the Orbiter. We emphasized building parts and assemblies of the Orbiter sling and related GSE to construct an animation of the Orbiter/ET mate. Emphasis was placed upon assemblies that included the Orbiter/ET forward attachment point (EO-1), aft left thrust strut attachment point (EO-2), aft right tripod support structure attachment point (EO-3), and crossbeam and aft feedline/umbilical supports. These assemblies are used to attach the Orbiter to the ET.

The Orbiter/ET mate assembly was used to compare clearance distances using different Orbiter hang angles for comparison and analysis. A 30-minute arc angle change in Orbiter hang angle affected distance at the tripod strut to Orbiter yoke fitting 8.11 inches.

During Phase II, the Shuttle Crawler Transporter (CT) Model was completed in 4 weeks. A complete CT truck assembly with roller bearing assembly, sprocket assembly, and treads linked was completed. The four trucks were assembled to a block representation of the CT chassis. The models were used in the refurbishment effort of the CT and for making prototypes and engineering aides in operational studies and presentations.

A 3-D solid-model library was established as a result of this project. This library contains parts, assemblies, and drawings translated into several formats of all the models. This library also contains a collection of the following files: .stl for Stereolithography, .stp for neutral file work, shrinkwrap for compression, .tif for Photoshop work, .jpg for Internet use, and .prt and .asm for



Pro/ENGINEER use. This library is available to NASA engineers so they can make angle, load, and clearance analysis studies. These decision-making tools may be used by Pro/ENGINEER users and nonusers. A free .prt or .asm viewer can be downloaded from Pro/ENGINEER for use on a local PC. Work continues to interface the library of models to the YA IntraLink.

Contact: F.J. Kapr ([Frank.J.Kapr@nasa.gov](mailto:Frank.J.Kapr@nasa.gov)), PH-I, (321) 861-3968

Participating Organizations: PH-I (I.F. Velez), YA-D1 (P.A. Schwindt), University of Wisconsin-Stout (Dr. G.S. Godfrey and B. Brandt), and Oregon State University (D. Rorden)



Figure 1. EO1 bipod forward attachment.

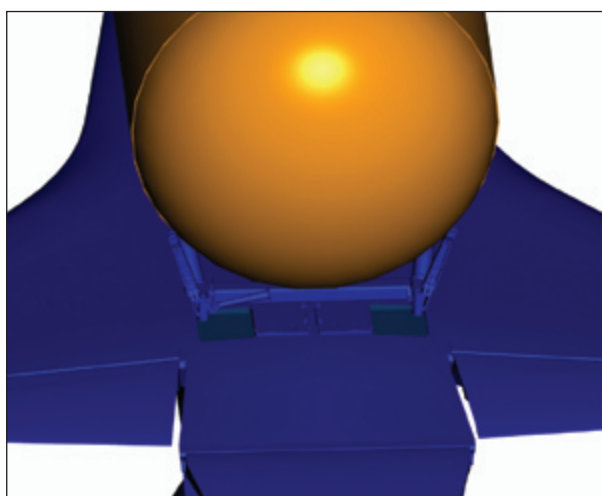


Figure 2. EO2 and EO3 aft Orbiter/ET attach point.

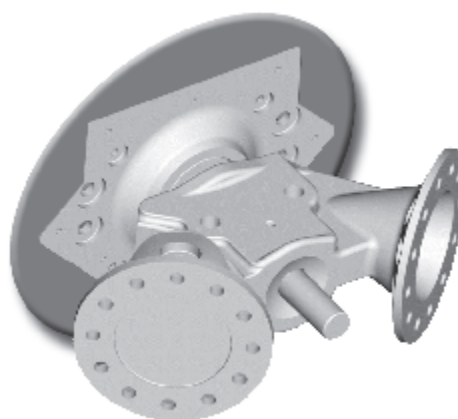


Figure 3. EO1 bipod yoke attached to Orbiter arrowhead bracket.

## External Tank 3-D Model Creation Techniques



Task/Process  
Modeling &  
Simulation

NASA mechanical systems engineers wanted 3-D models to experiment with the process of mating the Orbiter to the External Tank (ET) and to check for clearances in each situation. An ET model had been created by another engineering group and, when we tried to install our models on the aft end of the ET, we discovered they would not fit because it was modeled incorrectly.

To make the models compatible, we received the Export Control release on the formula for the aft-end calculation. Then the ET model was redesigned using the automated features of Pro/ENGINEER software in the following analytical process.

Parametric modeling, using Pro/ENGINEER Wildfire software, was chosen to create 3-D models of Shuttle and ET hardware. Most hardware can be constructed with extruded shapes, cuts, revolved profiles, holes, chamfers, and fillets—all relatively basic geometry. Occasionally, more complex shapes need to be created beyond the limits of basic geometry. In this example, an accurate structural model of the ET was developed to integrate other parts. The aft end of the ET is not spherical but is created from a profile based on a mathematical equation.

An equation was used to create the shape at the bottom of the ET (Figures 1 and 2). This equation represents a variable radius curve.

For Pro/ENGINEER datum curves, equations must be expressed in terms of  $t$ , with  $t=0$  being the start of the line, and  $t=1$  being the end of the line. Since we want our curve to start at  $y=70$  and end at  $y=165.5$ , we must adjust our  $t$  values to cover this range:

$$y = 95.5t + 70 \quad (1)$$

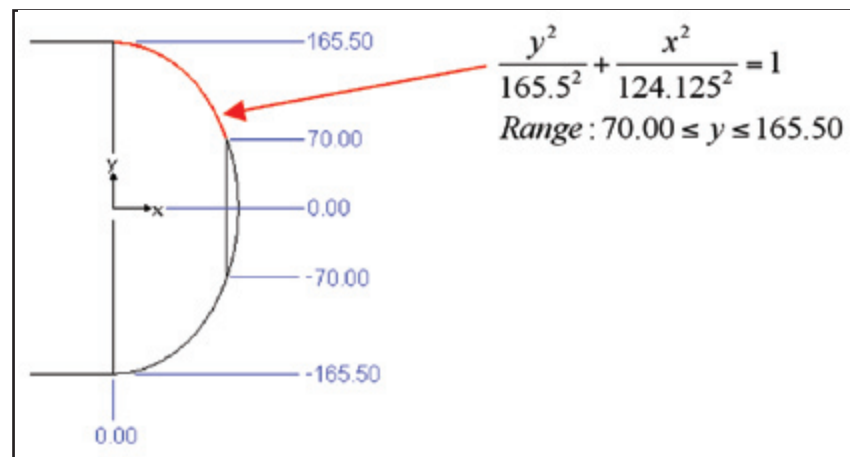


Figure 1. Variable-radius-curve formula.

Since we know our range of values in the  $y$ -direction, we must solve the curvature equation for  $x$  in terms of  $y$  (Figure 3).

With the mathematics defined, the datum curve can now be constructed within Pro/ENGINEER and used to create the bottom of the tank. A revolved protrusion is used to construct the shape, and the datum curve is used to define the profile of the ET's shape.

This example demonstrates a technique for creating advanced geometry to construct accurate models of flight hardware that were not previously available in early 3-D modeling software packages. Beyond this application, parametric modeling allows engineers to build accurate, complex, flexible simulations of flight hardware components and assemblies. These models allow engineers to visualize hardware in 3-D and check dimensions within complex assemblies that would otherwise be rather difficult with paper drawings.

Contact: F.J. Kapr ([Frank.J.Kapr@nasa.gov](mailto:Frank.J.Kapr@nasa.gov)), PH-I, (321) 861-3968

Participating Organizations: PH-I (I.F. Velez), YA-D1 (P.A. Schwindt), and University of Wisconsin-Stout (Dr. G.S. Godfrey and B. Brandt)



Figure 2. ET-120 remodeled curve.

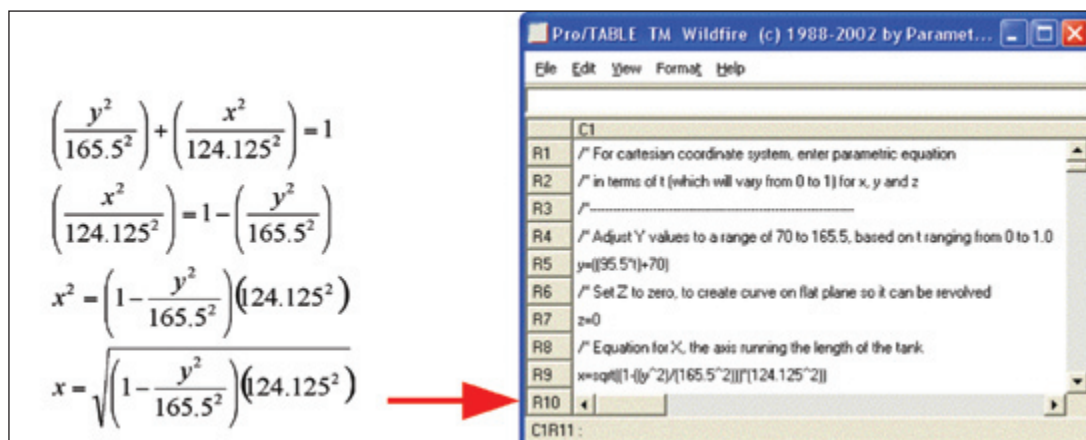


Figure 3. Calculation and Pro/ENGINEER table.

## Orbiter Wing Tip Alignment Tool



*Defect/Damage  
Location & Spacecraft  
Handling Systems*

Space Shuttles are assembled in the integration cells located in the Vehicle Assembly Building (VAB). Over the years, many positioning aids have been developed to help in this complicated assembly process. When the Orbiter is lowered from the VAB ceiling down to the External Tank (ET), it rotates a small amount due to stress relief in the cable. Consequently, the operations personnel try to rotate the Orbiter to compensate while it is at the top of the integration, before it is brought near the other flight elements, so it will end up properly positioned with respect to the ET after being lowered. To do this, operations personnel taped small strings to the wing tips of the Orbiter and attached rulers to the highest platform in the VAB. Then, as the Orbiter passed by, they used line of sight to determine how far the Orbiter needed to be rotated.

Because of parallax, this is a difficult task. When the Orbiter is not properly aligned with the ET, more rotations become necessary. A laser-based system was needed where parallax issues were removed and accurate prerotation was achieved.

To accomplish this, two surveying marks are located on the top platform within the integration cell, one on either side of where the Orbiter will pass. These marks define a reference line to measure the Orbiter rotation. The goal was to develop a system composed of a pair of laser line projectors that produce the desired vertical plane of light that can pass through the desired reference line. The Orbiter could then be prerotated over a range of heights rather than at a specified height defined by the laser beams.

Figure 1 shows one of the two identical units that make up the Orbiter Wing Tip Alignment System. It is composed of an in-house-designed and -constructed laser module situated on top of a survey tripod assembly. The tripod is used to get the laser system off the platform and to locate the laser assembly directly over the surveying mark. Operationally, a centering ring with three axial arms is laid on the platform such that the surveying mark can be seen through the ring. The arms have small indentions at the ends that capture the tripod leg tips, locating the head of the tripod roughly over the centering ring. Then a small interface platform can be moved around on top of the tripod until it is accurately located over the survey mark (Figure 2). This is done using a small site glass. The interface plate is then locked



*Figure 1. The laser assembly and tripod with centering ring for location above a survey mark.*

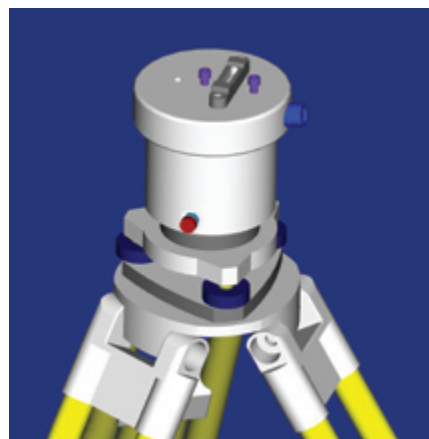


*Figure 2. The laser assembly located on top of the tripod head.*



down, effectively locating the interface platform and the laser directly over the survey mark.

The laser module contains the laser line projector, an accurate level, an on/off switch, and a battery pack. All of this is packaged into a cylindrical shell of delrin and sits on a second delrin piece attached to the interface platform. By pulling on a pair of spring-loaded screws, the delrin shell can be detached and lifted off the second delrin piece allowing access to the battery pack. After the interface platform is located over the survey point, the laser module is leveled by turning three adjustment wheels located in the interface platform. The interface platform has a small level that allows rough leveling, but final leveling is achieved by monitoring the more accurate level located on the top of the laser module.

After leveling the laser module, the laser line generator now projects a vertical sheet of light. The final alignment step is to rotate the laser module until the laser line hits a known mark on the platform or the second laser line projector located on the other side of the integration cell. This rotation is possible because the second delrin piece is attached to the interface platform by a single large coaxial bolt, allowing this piece to rotate on top of the interface platform without translationally sliding.

Figure 3 shows a system in use on the upper platform at the VAB. The Orbiter is shown being lowered off to the right side of the picture. Note the relatively large gap between the Orbiter wing and the platform. Figure 4 shows the ruler attached to the Orbiter wing with the laser line illuminating it.



Figure 3. The Orbiter wing tip alignment tool in operation in one of the VAB integration cells as the Orbiter is lowered.

Key accomplishment:

- Developed a tool to align the wing tips before ET mating to compensate for Orbiter rotations that occur during crane operations.

Key milestone:

- A second alignment tool has been completed and delivered.

Contacts: D.E. Willard ([Doug.Willard@nasa.gov](mailto:Doug.Willard@nasa.gov)), YA-C3-E, (321) 867-8578; and Dr. R.C. Youngquist, YA-C3-E, (321) 867-1829

Participating Organization: ASRC Aerospace (S.L. Parks)

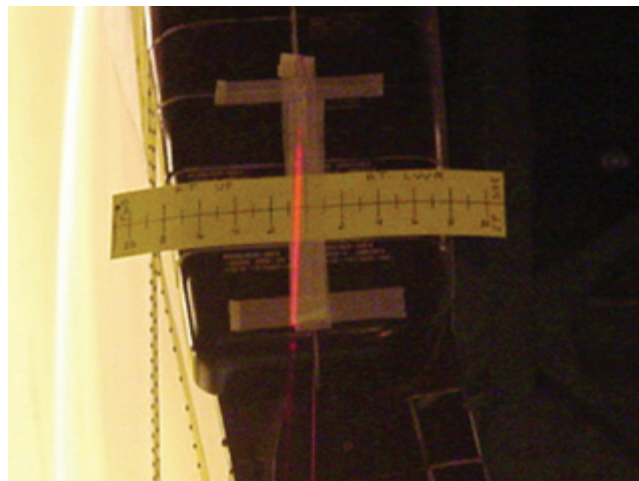


Figure 4. The laser line hitting a ruler taped to the Orbiter wing tip.

# Biological Sciences

The Biological Sciences program at KSC conducts research and technology development in four basic life sciences areas:

- Development of plant systems for food production and regeneration of clean water and oxygen in long-term space missions.
- Ecology and application of microorganisms in water recovery and solid-waste reduction in space.
- Flight hardware development, design, construction, and validation for plant and microbiological experiments.
- Application of results from this research and technology development to the management of agricultural and natural ecosystems on Earth.

Efforts in bioregenerative life support systems research for over 10 years have focused on crop growth and development with the primary emphasis on biomass production under closed conditions. In recent years, the focus has shifted to include the potential use of plants in recycling solid and liquid waste. Another goal for these studies was to determine the stability of microbial communities associated with the plant and recycling systems. The Biological Sciences program initiated significant efforts to understand photosynthetic processes under spaceflight conditions. A series of studies was designed and initiated to determine the response of higher plants to microgravity and to determine if they would remain viable and useful components of a life support system. These experiments required adding new plant flight hardware and refurbishing older flight hardware that had been used for previous plant experiments. Plant flight hardware technology development efforts include investigating the use of light-emitting diodes and their effects on plant growth, using porous tube systems to deliver water and nutrients to the roots of plants, and developing both physical and biological sensors that could give a more complete understanding of the hardware operation and environment during space-flight testing.

Studies to determine the stability and effectiveness of microbial communities with physiological profiling and molecular approaches continued during the past year. The ultimate goal is to develop reactors utilizing microorganisms to recycle solid and liquid wastes, including urine, graywater, inedible plant residues, and trash. The successful demonstration of bioregenerative life support technologies and the ability to evaluate them in the spaceflight environment will permit NASA to estimate the resources needed to design, construct, and test life support systems for future missions. Ultimately, biological life support systems will be required to sustain autonomous human colonies in space. Understanding and optimizing both the biomass production and biological waste recycling concepts for life support, along with their associated reliabilities and costs, will be essential for future exploration of space.

*For more information regarding Biological Sciences, please contact C.D. Quincy ([Charles.D.Quincy@nasa.gov](mailto:Charles.D.Quincy@nasa.gov)), YA-E4, (321) 867-8383.*

## Advanced Life Support Research: Systems Analysis of Waste



*Bioregenerative Life Support  
System Operation/  
Validation/Control*

Waste poses both a great problem and a great potential in space environments: It creates annoyance and hazards for the crew, and it provides a source to potentially replenish resources needed for transit and surface missions.

On Earth, the vast majority of waste is dumped, though in increasingly controlled ways. Radioactive waste is stored until the hazard goes away, and some other wastes are incinerated to produce nonhazardous effluents. In space, waste has been returned to Earth, reentered, dumped overboard, or left onsite. These same approaches can be used for future missions, though the cost of returning waste to Earth from beyond low Earth orbit (LEO) might be prohibitive, and care will be needed to avoid damaging the scientific value of planetary surfaces or contaminating a unique biosphere.

Storage and dumping can remove hazards and annoyances of waste for the crew, but recovery of resources turns out to be a critical reason to, instead, process waste. Water, a factor that limits International Space Station (ISS) crew size while the Space Shuttle is grounded, is plentiful in waste. All the water required for a mission that cannot be recovered must be supplied. About 10 to 20 kg of waste water is produced each man-day and perhaps another half kilogram of water is in the chemical composition of the solid waste produced each man-day. Twenty kg is not a lot of mass, but for a 1,000-day, 6-person mission, it totals about 120 tons.

Water is easy enough to recover: Liquid water can be processed directly, and water content of waste can be driven off by drying and condensing out the resulting water vapor. But processing water for reuse is not necessarily cheap, and many different approaches have been developed. The ISS water processing system (not yet onboard) will require about 600 kg of equipment, 400 W of power and cooling, and filter beds totaling about 2 kg of supplies for every 100 kg of wastewater processed. If we are processing 72 tons of wastewater for a Mars mission, 1.4 tons of supplies would be required. Depending on the mission and the level of contamination of the water, the ISS water processor will regenerate 5 to 10 kg of water per kilogram of equivalent system mass (ESM). Other options that have been investigated are cheaper, with transpiration from crop plants providing from 46 to 454 kg of water regenerated per kilogram of ESM.

Extracting and regenerating water can supply most of the 120 tons of water needed for a Mars mission, providing major cost savings. Then, only 2 to 4 kg of waste per man-day will remain to be disposed of. The volume of the remaining solid waste can be minimized by compacting but still represents about 24 tons of waste for a Mars mission. Some waste can probably be dumped overboard, at least en route to and from Mars. If given a suitable push, the waste will not impact the vehicle or either planet. This will greatly reduce the load on the propulsion system, though this is not a very satisfying approach. Additional water might be extracted through pyrolysis, heating without oxygen, producing additional water vapor and further reducing the mass of solid waste by perhaps 10 percent.

How far should we go in regenerating water? Producing more water than we need is of little value, perhaps providing some additional contingency capability but requiring either storage or disposal. How much water we need depends on a number of issues, including the water content of the food and the closure of other life support systems. The residue will depend on the composition of the waste and the process conditions. Our analyses show that we need to

regenerate wastewater and recover the bulk of the water in solid waste for a transit mission to be in water balance. For a surface mission, with current extravehicular activity (EVA) technologies and a heavy EVA schedule, we would also need to pyrolyze solid waste and recover oxygen from carbon dioxide. Alternatives for surface missions would be to reduce EVA losses and to extract oxygen or water from Martian resources.

Planetary protection is a concern with Mars missions. Pyrolysis is a possible way to ensure that neither microorganisms nor biomarkers from Earth contaminate Mars, rendering the gaseous and solid wastes suitable for dumping or permanent storage on Mars.

In principle, the waste can be incinerated, a disposal method that could protect Mars from terrestrial contaminants. However, incineration requires oxygen and produces carbon dioxide, water vapor, and trace contaminants. Some of these effluents might be dumped, but then we would have to supply the oxygen—about equal in mass to the waste. Regenerating the oxygen to burn the waste would take additional equipment and materials and would be of dubious overall value.

Where waste oxidation does make sense is where we grow most of our own food. With typical crops, about half of the plant material produced is inedible, adding significantly to the primary (unprocessed) waste load. Thus, we would get closure of the air loop by growing about 50 percent of our food on-site. Plants would also purify water at even lower levels of food closure than this, though polishing of the water would be required. As the proportion of food produced locally is increased, the plants will require more carbon dioxide than the crew exhale and would produce more oxygen than they inhale. This sounds like a good thing, but we need to balance crew respiration and plant photosynthesis. Incineration could help balance the gas exchange, using the excess oxygen and producing the additional carbon dioxide that is needed, but would also tend to lock up a lot of plant nutrients in ash, from which the nutrients are difficult to recover. Aerobic digestion, either composting or in an aqueous phase bioreactor, would also balance the gas exchange and might be a good way to oxidize the waste while recovering the minerals. However, the rate of oxidation slows as the waste is destroyed in a bioreactor, and incineration might be a good way to destroy the 50 percent of recalcitrant waste if this is needed to close the carbon cycle.

Thus, dealing with waste is a complex process that interfaces with all life support systems and provides a unique perspective on life support. The best approach depends on trade studies that involve all other life support systems and varies with the mission duration and other constraints.

#### Key accomplishments:

- 2003: Seven studies published.
- 2004: Three studies published, including final report.

Contact: Dr. J.C. Sager  
([John.C.Sager@nasa.gov](mailto:John.C.Sager@nasa.gov)),  
YA-E4-B, (321) 861-2949

Participating Organization:  
Boeing (Dr. A.E. Drysdale)



Stored waste returned to Earth from ISS.



## Advanced Life Support Research: Systems Analysis of Clothing

Clothing makes up about 14 percent of the equivalent system mass (ESM) of the International Space Station (ISS) life support system for the assembly-complete configuration. It has major impacts on both logistics supply and the waste system, and work with North Carolina State University is focusing on reducing these impacts for advanced missions.

For ISS, clothing is shipped to the station. After use, it is either returned to Earth in the Shuttle or reentered in the Progress vehicle. The largest cost involved is delivery (approximately \$20,000 per kilogram); whether clothing is reused is not a significant aspect of the cost. About 0.625 kg of clothing is required per person per day. For a 1,000-day, 6-person Mars mission, this will total almost 4 tons, and there will be additional costs for stowage and disposition after use.

Two ways to reduce this impact have been examined: redesigning the clothing system and washing clothes to allow reuse.

Most ISS clothing is COTS, largely made of cotton. Modern fabrics can probably reduce the mass and improve the functionality. There is a concern that plastics melt on the skin, but some fabrics are more resistant to heat and less flammable than cotton, especially in high-oxygen atmospheres such as those associated with extravehicular activity (EVA). They can be more comfortable, wick sweat from the skin better, and retain less water than cotton. Fibers limiting microbial growth, such as those containing or coated with metallic silver, may allow longer use without unpleasant odors developing.



*Typical ISS clothing stowage.*

Cleaning would allow clothes to be reused, as they are on Earth. As a baseline, we looked at traditional washers, with the washer and dryer sized for the maximum item. There would be challenges laundering clothing in weightlessness. Adequate sealing would be needed, pickup of water from a rotating drum might be difficult, and noise and vibration could be a problem. Rotation of the drum of clothes would tend to rotate a spacecraft in the opposite direction, but that could be prevented by using the motor as a counter mass to the drum. Terrestrial washers and dryers might work adequately on the Moon or Mars, where there is a substantial level of gravity, rather than weightlessness.

We could probably wash clothing 10 to 100 times, depending on the item. This would reduce the mass of clothing that would have to be supplied by a similar factor. The biggest issue would most likely be providing water to wash the clothes. Modern washers are much more efficient than older models, with water ratios of less than 5 kg of water per kilogram of clothing. Still, the water demand in the vehicle would increase by perhaps 20 kg per day.

Water regeneration has been studied for many years. We can calculate the specific performance by dividing the mass of water processed by the ESM required for processing it. The specific performance for delivery, for example, would be less than 1, and clearly it would not be a good idea to provide 5 kg of water rather than 1 kg of clothing. Current water processing system designs have a specific performance from about 10 (for ISS) to over 100 (e.g., for transpired water from food plants). A value of 35 was identified as a reasonable goal, based on a survey of water regeneration technologies.

The Advanced Life Support project metric is the ESM for a mission using ISS technology divided by the ESM for the same mission using advanced technology. (ESM is the sum of the real mass [initial and resupply] and the mass penalties for volume, power, cooling, and crew time.) The goal is to demonstrate an improvement of the metric by a factor of 3 by 2010. By redesigning the wardrobe, we might achieve a metric of 2 for the clothing system with no loss of crew acceptance and an improvement in safety. By washing clothes an average of 40 times, we would achieve a metric of 9. Doing both might allow us to achieve a metric of 18. Further benefits might be possible. Some items not typically considered part of the crew wardrobe, such as liquid-cooled garments and other EVA items, might have their useful life extended by washing. This might increase the washer size somewhat and would certainly increase the washing load for surface mission segments, but the overall benefits would be expected to greatly exceed the cost, especially if washer use were increased.

#### Key accomplishments:

- Annual report for contract NAG 9 1473.
- ICES article in work.
- Outreach Web site: <<http://csil.boeing.ksc.nasa.gov>>.

#### Key milestones:

- January 2005: Second annual report.
- January 2006: Final report.

Contact: Dr. J.C. Sager ([John.C.Sager@nasa.gov](mailto:John.C.Sager@nasa.gov)), YA-E4-B, (321) 861-2949

Participating Organizations: Boeing (Dr. A.E. Drysdale, H.L. Garton, and Dr. S.A. Hasselbrack) and North Carolina State University (Dr. R.L. Barker, Dr. D.B. Thompson, and B.J. Scruggs)

## Porous Tube Insert Module (PTIM) Assembly and Integration: A Modular Tray Supporting Both Porous Tube and Substrate Nutrient Delivery Systems for Plant Studies in Space



Bioregenerative Life Support  
System Operation/  
Validation/Control

A microgravity-based plant culture nutrient delivery system (NDS) is needed for both bioregenerative Advanced Life Support and plant research functions. Providing adequate levels of water (without causing waterlogging)

and oxygen to the root zone is a critical area where previous microgravity systems have had problems. The dominance of the surface tension of water under microgravity conditions has often been found to lead to either severe waterlogging or excessive drying in the root zone. Consequently, differences in plant growth responses between spaceflight experiments and their ground controls are expected based merely upon differences in moisture distribution patterns between the two conditions. The Water Offset Nutrient Delivery Experiment (WONDER) will address the question of comparability of environmental conditions between spaceflight and ground control experiments for both a porous tube plant NDS and a substrate-based NDS by employing three different wetness-level treatments for each of these approaches. It is anticipated that different preset wetness levels than those used on Earth will be required to support optimal plant growth in space. Time-lapsed video recording of the plants will monitor growth over time. At recovery, the plants will be measured, and extensive

tissue analyses relating to gene expression and stress-associated metabolites will be undertaken.

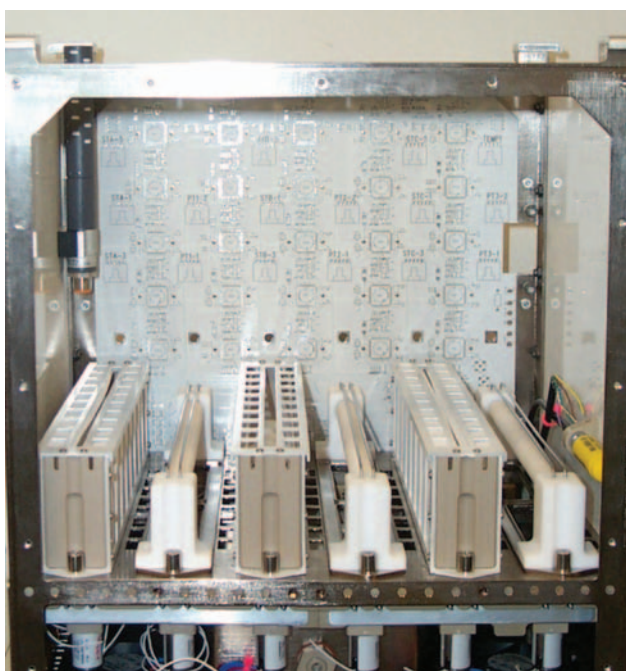


Figure 1. PTIM with alternating bare porous tube and substrate-based NDSs installed. The array of 25 cameras that are to monitor plant growth over time was not yet present on the back wall (circuit board) as shown. A matching wall with the same camera array has been removed for the picture.

PTIM (Figure 1) was designed to fulfill the requirements of this project specifically and to provide a testbed for a multitude of space-based plant studies. PTIM delivers water to both a series of bare porous tubes and to porous tube/substrate compartments. Software will allow the crew to interact with the system's watering initiation protocols. PTIM incorporates moisture sensors to both monitor and control the wetness levels on the three bare porous tubes and within the three substrate compartments contained within the PTIM. A fixed-feed water provision mechanism functions as a backup mode in the event of system failure. Initial payload integration tests have been performed with the fully assembled hardware (Figure 2). Data from the video images (Figure 3) will serve as a diagnostic during flight



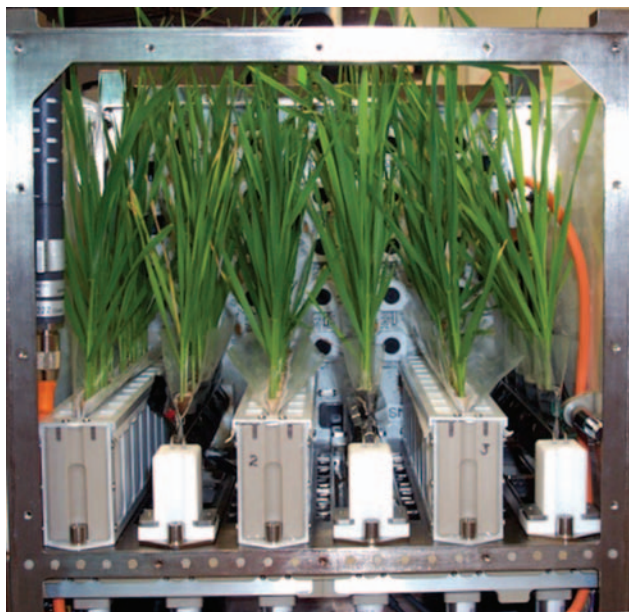


Figure 2. Plants grown during the first PTIM integration experiment on day 21 after planting. The plants have reached the top of the PTIM insert. Some of the 25 cameras arranged on the back wall can be seen behind the plants. For the bare porous-tube NDS, the plant roots encircle the water-providing porous tubes. This approach eliminates the use of particulate substrates, resulting in considerable savings in mass and volume.

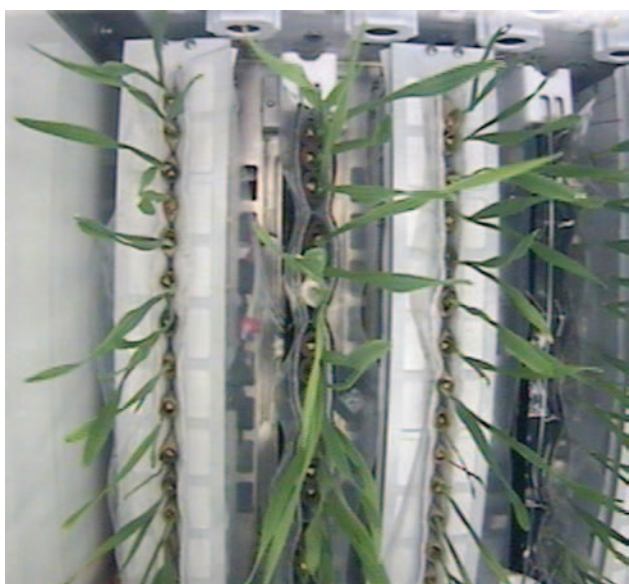


Figure 3. A top-down view of growing wheat plants during the PTIM integration test. These images, in conjunction with those from the side wall cameras, will provide diagnostic and plant assessment functions during the mission.

and a direct measure of the plants and treatment differences.

#### Key accomplishments:

- Completed Phase B review.
- Completed PTIM hardware fabrication and assembly.
- Continued ground studies to define experimental methods and requirements.
- Completed KC-135 testing of fluid behavior in WONDER hardware configurations.

#### Key milestones:

- 2004: Conduct PTIM/Plant Generic Bioprocessing Apparatus Integration ground testing.
- 2004: Conduct KC-135 testing of moisture sensing technology.
- 2004-2005: Conduct high-fidelity Payload Verification Test using flight hardware.
- Targeting 2006: Conduct spaceflight experiment on Space Shuttle.

Contacts: Dr. H.G. Levine ([Howard.G.Levine@nasa.gov](mailto:Howard.G.Levine@nasa.gov)), YA-E4-B, (321) 861-3502; B.P. Leger, YA-E4, (321) 867-3805; and Dr. J.C. Sager, YA-E4-B, (321) 861-2949

Participating Organizations: Dynamac Corporation (J.J. Prenger and D.T. Rouzan-Wheeldon) and Bionetics Corporation (K.A. Burtness, T. Murdoch, A.C. Spinale, and H.W. Wells)



## Plant Lighting Systems



*Efficient  
Lighting  
Systems*

Plants could be an important aspect of future space missions. Plants can produce food, regenerate oxygen, and purify water for space inhabitants. A major challenge to growing plants in space will be controlling and supplying sufficient quantity and quality of light. Conventional lighting technologies would prohibit growing plants on a large scale in space because of low electric power conversion efficiencies. Current lighting research for space-based plant culture is focused on innovative lighting technologies that demonstrate high electrical efficiency and reduced mass and volume. Accordingly, light-emitting diodes (LEDs) are promising technologies being developed to efficiently generate photosynthetic radiation. LEDs can illuminate near the peak light absorption regions of chlorophyll while producing virtually no near-infrared radiation (which is not utilized in photosynthesis). The work in the KSC Space Life Sciences Laboratory, in support of NASA's Advanced Life Support (ALS)/Advanced Human Support Technology Program, gives insight into the feasibility of using LEDs as alternative light sources for plant biomass production.

LED lighting systems are currently being evaluated by Dr. Hyeon-Hye Kim and colleagues at the Space Life Sciences Laboratory. Salad-type plants represent crops that could potentially provide a portion of fresh food as well as psychological benefits to the crew aboard future space transportation vehicles. Experimental data generated with salad-type crops in the presence of various lighting sources will provide important data for modeling and developing future missions.

The combination of red and blue light has proven to be an effective lighting source for producing spinach, radish, and lettuce biomass in controlled environments. However, the addition of green light may have psychological benefits for the crew. Plant leaves readily absorb red and blue light, so absorptance is high and reflectance is low. Therefore, even healthy plants grown under red and blue LEDs alone appear purplish gray to humans. Hence, the addition of green LEDs to red and blue LED arrays would make plants appear normal (green) to the crew. Green light may also promote increased plant growth since green light penetrates the plant canopy better than red or blue light. Leaves in the lower canopy could use the transmitted green light in photosynthesis. For a space mission, highly optimized lighting systems are necessary to conserve power and maximize plant growth, so supplemental green light needs

to be evaluated. Research has begun to evaluate the beneficial aspects of supplemental green light on salad crops in terms of enhancing the aesthetic appeal of plants grown under LEDs and increasing light penetration in the canopy.

Work has been completed with lettuce plants grown in the presence of different lighting sources. First, lettuce plants grown under red and blue LEDs were compared to plants given an additional 5 percent ( $6 \mu\text{mol m}^{-2} \text{s}^{-1}$ ) of green light. Light and  $\text{CO}_2$  photosynthesis response curves were measured along with other physiological parameters, and there was



*Figure 1. Lettuce growing under red and blue LED arrays with green LED supplementation.*

no significant difference between the treatments. The use of green light would be beneficial, since it will not impact plant growth, and provides useful photosynthetically active radiation once it is absorbed, and the plants will appear green and healthy to the crews on space missions. Next, higher levels of supplemental green light were examined. In this study, four light sources were tested: (1) red and blue LEDs (RB), (2) red and blue LEDs with green fluorescent lamps (RGB), (3) green fluorescent lamps (GF), and (4) cool white fluorescent lamps (CWF), which provided 0, 24, 86, and 51 percent of the total photosynthetic photon flux in the green region of the spectrum, respectively. The addition of 24 percent green light (500 to 600 nanometers [nm]) to red (600 to 700 nm) and blue (400 to 500 nm) LEDs (RGB treatment) enhanced plant growth. The RGB treatment plants produced more biomass than the plants grown under the CWF treatment, a commonly tested light source used as a broad-spectrum control. In this study, small fluorescent lamps that emit green light were installed with an array of red and blue LEDs. Considerable commercial interest has been directed toward improving green LEDs, and therefore, green LEDs that have high output and provide the required photon flux are more available now than before. Further studies are needed to determine required levels of green light for optimum plant growth, and more tests with different green peak wavelengths (using green LEDs) with red and blue LEDs would be useful in determining a green-light response spectrum. These findings could then be used to design spectrally balanced LED systems for supporting plant growth, especially for very specialized applications, such as in space.

#### Key accomplishments:

- 1999: Began experiments with growing salad-type plants with LEDs and microwave lamps.
- 2000: Completed initial salad-type plant growth studies with LEDs and microwave lamps. NASA NRA Solicitation 98-HEDS-01 grant to Dynamac Corporation (Dr. Gregory D. Goins) was extended through 2001.
- 2001: Began experiments with mixtures of salad plant species to compare the growth of multiple crops in a common environment/hydroponics system. Testing included characterization of photosynthetic reaction center stoichiometry (photosystem I versus II) in response to light quality.
- 2002: Began experiments to evaluate the beneficial aspects of supplemental green light on salad crops in terms of increasing light penetration in the canopy and enhancing the aesthetic appeal of plants grown under LEDs.
- 2003: Completed initial plant growth and development studies with supplemental green light.

#### Key milestone:

- 2004: Continue the evaluation of supplemental green light at different levels to determine the photobiological effects on salad crops.

*Contacts: Dr. J.C. Sager ([John.C.Sager@nasa.gov](mailto:John.C.Sager@nasa.gov)), YA-E4-B, (321) 861-2949; and Dr. Raymond M. Wheeler, YA-E4-B, (321) 861-2950*

*Participating Organizations: National Research Council (Dr. H.H. Kim), Dynamac Corporation (J.T. Richards, Dr. G.W. Stutte, and N.C. Yorio), and North Carolina A&T State University (Dr. G.D. Goins)*



Figure 2. Installation of new LED lighting system with red LEDs activated (from left, Dr. Gregory Goins and Dr. Hyeon-Hye Kim).

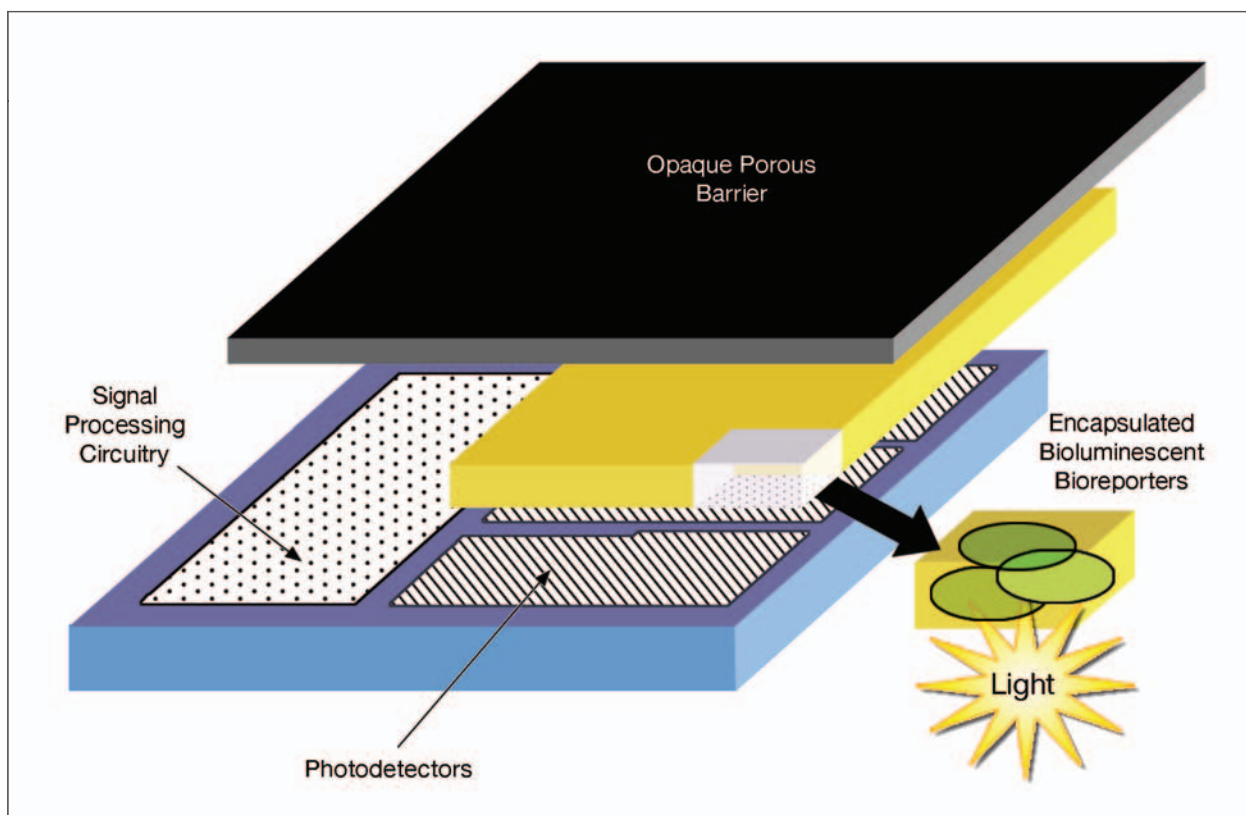
## Bioluminescent Monitoring of Opportunistic Pathogens in the Spacecraft Environment



Remote Plant/  
Microorganism  
Health Sensing

Bioluminescent bioreporters are whole-cell, bacterial biosensors that respond to specific chemical or physical agents in their environment, with the response being manifested by the production of visible light. These bioreporters utilize a genetic construct that consists of the *lux* cassette, derived from the marine bacterium *Vibrio fischeri*. The *lux* cassette contains five genes, *luxA*, *B*, *C*, *D*, and *E*. Inclusion of the entire cassette within a biosensor allows for intrinsic whole-cell bioluminescence, without the addition of any exogenous chemicals or co-factors. This current project focuses on the development of a suite of four bacteriophage-based bioluminescent biosensors for the detection and identification of opportunistic pathogens, with an end goal of deploying the bacterial bioreporters on small, disposable microelectronic chips that will enable online, real-time monitoring within the spacecraft environment. Our collaborators in this effort are the University of Tennessee's Center for Environmental Biotechnology (CEB) and Oak Ridge National Laboratory (ORNL) in Oak Ridge, Tennessee.

Bacteriophages, commonly referred to as "phages," are viruses that infect bacteria; some viruses are species-specific, meaning that they will only infect a certain species of bacteria. Bacteriophage-based bioluminescent bioreporters utilize the pathogen-specific phage infection as a means of inducing bioluminescence



Schematic of the bioluminescent bioreporter integrated circuit (BBIC).



through a modified quorum-sensing signal. The *luxI* gene, which also originates in *V. fischeri*, is inserted into the genome of the phage, resulting in the production of acyl-homoserine lactone (AHL) molecules upon host infection. In these bioreporter systems, the AHL molecules will diffuse into colocated bioreporter cells containing the *luxCDABE+luxR* operon. These AHL molecules bind to the *luxR* protein (the product of the *luxR* gene), and this in turn generates bioluminescence from the *lux* cassette.

The four bioreporters currently being developed and tested are for the detection of the following bacteria: *Staphylococcus aureus*, which causes nasal and skin infections; *Pseudomonas aeruginosa*, which proved to be the causative agent of a urinary tract infection of an Apollo 13 lunar module pilot and was also implicated in material degradation in the Russian space station; *Escherichia coli*, which has been recovered numerous times from crew members during Apollo-Soyuz missions; and *Salmonella*, a leading cause of food-related illnesses, which has not yet been recovered from the spaceflight environment but whose existence on longer manned missions is a very strong possibility.

The CEB is responsible for the construction of three of the four bioreporter systems and for preliminary baseline testing. Scientists on the Life Sciences Service Contract at KSC are constructing the fourth bioreporter system. KSC is also responsible for the majority of the testing of the systems, using environmental samples. Microbial samples have been collected from both the Orbiter 10 to 14 days preflight and the astronaut crew quarters so the bioreporters can be exposed to pathogens from the environments in which they will be used. ORNL is developing and evaluating the integrated-circuit optical transducer (the “microchip”) on which the bioreporter system will be placed.

To date, the bioreporter system for detection of *E. coli* has been fully developed and has undergone preliminary testing at the CEB; more extensive testing is to begin soon at KSC. The bioreporter for the detection of *Salmonella* is nearly complete, and baseline studies have been carried out that indicate its success. The bioreporter for the detection of *P. aeruginosa* is partially constructed; this system is currently being constructed at KSC. Development of the microchip is continuous for the bacterial cells are not needed to design and test the electronic components of the chip.

#### Key accomplishments:

- Constructed bioreporter cell line that responds to AHL molecules.
- Identified and cloned genes necessary for construction of bacteriophage-based system.
- Completed construction of bioreporter for *E. coli*.
- Initiated construction of bioreporters for *Salmonella* and *P. aeruginosa*.

#### Key milestone:

- Encapsulate respective bioluminescent bioreporter systems on integrated-circuit optical transducer (termed a bioluminescent bioreporter integrated circuit or BBIC) that will be capable of real-time, online monitoring of pathogens within the spacecraft environment.

Contact: Dr. J.C. Sager ([John.C.Sager@nasa.gov](mailto:John.C.Sager@nasa.gov)), YA-E4-B, (321) 861-2949

Participating Organizations: Center for Environmental Biotechnology (Dr. G.S. Sayler and Dr. S. Ripp), Oak Ridge National Laboratory (Dr. M.L. Simpson), and Dynamac Corporation (Dr. J.L. Garland and K.A. Daumer)



# Sensing and Control System Development in Support of the Water Offset Nutrient Delivery Experiment (WONDER)



Bioregenerative Life Support  
System Operation/  
Validation/Control

An investigation to determine the microgravity effects upon optimal plant root zone wetness levels is being conducted under the Water Offset Nutrient Delivery Experiment (WONDER). This experiment is being facilitated by the Plant Generic Bioprocessing

Apparatus (PGBA – BioServe Space Technologies) and the Porous Tube Insert Module (PTIM – Bionetics/KSC). Owing to past flight performance and experiment suitability, the PGBA was selected as the primary carrier for WONDER. The PGBA is a Space Shuttle middeck double-locker payload. Within the PGBA double-locker shell, PGBA provides environmental control, data collection, data storage, and user interfaces to the experiment. The PTIM has been developed as an experiment-specific insert to PGBA. It has been designed to fit within the PGBA chamber and provide video imaging; environmental sensing; plant, liquid, and nutrient containment; moisture sensing; and moisture control.

The design of the PTIM control system utilizes distributed processing across an RS-485 data bus and local I<sup>2</sup>C data busses. The RS-485 data bus master is the PGBA CPU. A single WONDER control process developed by Bionetics/KSC and executing on the PGBA CPU is used to sequence through the WONDER experiment, commanding PTIM via the RS-485 bus.

The PTIM has seven individual microcontrollers on this RS-485 bus acting as slave devices. The PTIM controller board is used for control and electrical current sensing of piston pumps and fans. This board's primary microcontroller (resident on the RS-485 bus) does the device switching. A secondary microcontroller on the local I<sup>2</sup>C bus is used to sense the electrical current consumed by each device. Current sensing assists in identification of possible issues with electromechanical device performance, allowing the sequencing software to select the backup pumping device and/or alternate between two questionable or fully functional devices.

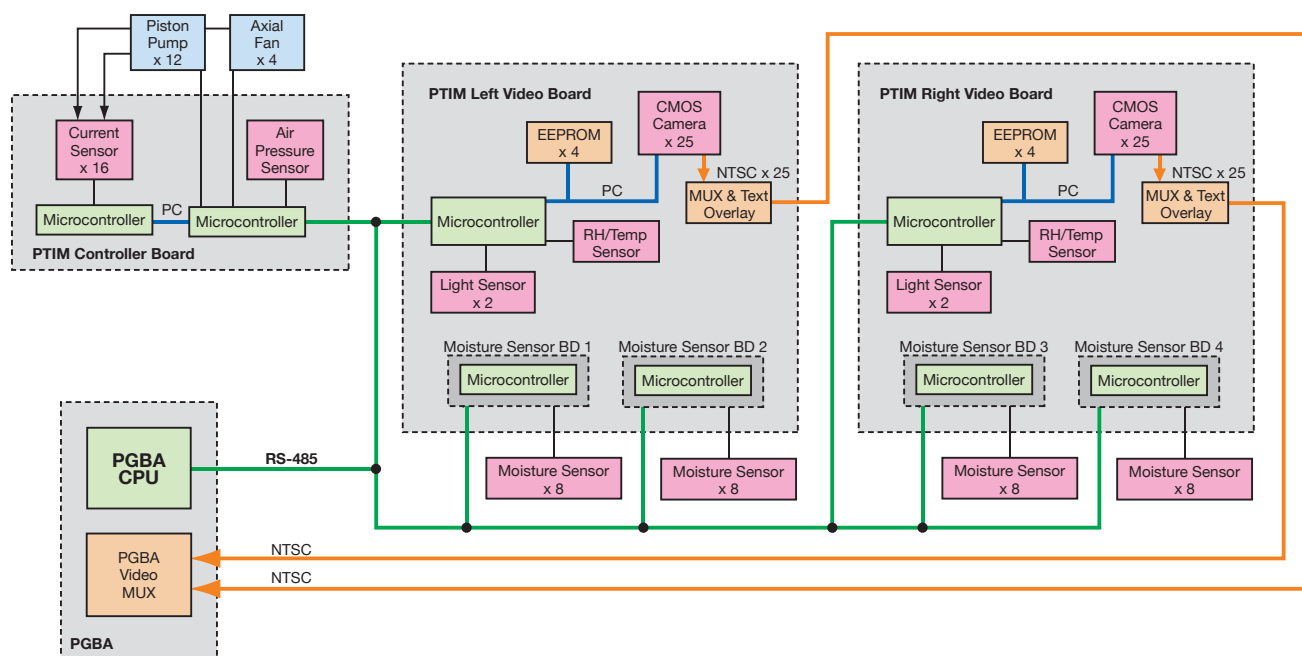


Figure 1. PTIM Sensing and Control System.

Each of the two PTIM video boards includes a microcontroller used to multiplex video and overlay text onto the video. The microcontroller also collects temperature, humidity, and lighting information from onboard digital sensors. Each video board microcontroller resides on the RS-485 bus and communicates with onboard cameras and electrically erasable programmable read-only memories via a local I<sup>2</sup>C bus.

WONDER will nurture approximately 90 wheat plants from seedlings (at launch) through a nominal Space Shuttle (Sortie) mission of approximately 10 to 12 days. Throughout plant development, the PTIM imaging system is required to image the plants, providing enough resolution to accurately measure individual leaf lengths throughout the experiment. Considering the number of plants and the required PTIM hardware (pumps, fans, etc.), a minimal volume was allocated to the video system design. In addition, the video system was required to take pictures of plants from as close as an inch from the lens. Designing a video system with movable cameras would create risk in the areas of damage to plant tissue, possible mechanical failures, and unwanted additional mass and power. The solution was to design the side walls of PTIM as circuit boards, integrating an array of 25 cameras into each side wall. Video board camera spacing was designed to allow camera-to-camera image overlapping of the nearest specimens under test. This solution will allow the investigator to essentially create a mosaic of plants utilizing images from the 25 cameras on each side of the plant chamber.

Each video board also interfaces with daughter boards used for moisture sensing. Each daughter board contains a microcontroller, also on the RS-485 bus. The moisture-sensing microcontrollers are used to control and sense up to eight moisture sensors embedded in the PTIM growth modules.

#### Key accomplishments:

- 2001: Completed science verification test.
- 2002: Conducted KC-135 testing of growth modules and moisture-sensing system.
- 2003: Completed WONDER PGBA/PTIM design reviews. Completed Phase 0/1/2 flight safety reviews.
- 2004: Completed fabrication of PTIM flight hardware. Conducted initial grow-out with PGBA/PTIM flight hardware.

#### Key milestones:

- 2004: Complete flight hardware qualification testing.
- 2005: Complete Phase 3 flight safety review. Conduct payload verification test. Experiment ready for flight.

*Contacts: Dr. H.G. Levine ([Howard.G.Levine@nasa.gov](mailto:Howard.G.Levine@nasa.gov)), YA-E4-B, (321) 861-3502; B.P. Leger, YA-E4, (321) 867-3805; and Dr. J.C. Sager, YA-E4-C, (321) 861-2949*

*Participating Organizations: Bionetics Corporation (K.A. Burtness, T. Murdoch, A.C. Spinale, and H.W. Wells) and Dynamac Corporation (J.J. Prenger and D.T. Rouzan-Wheeldon)*

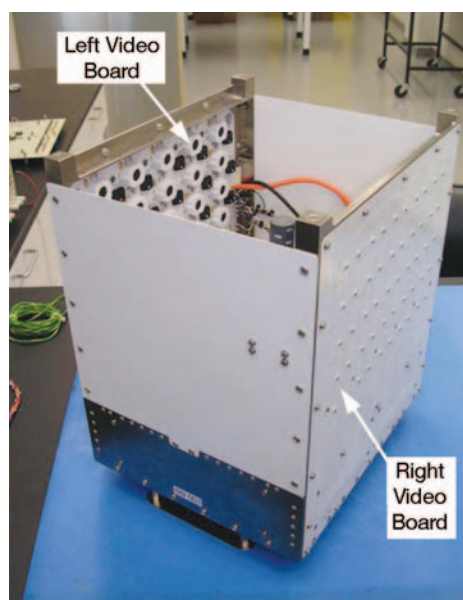


Figure 2. Assembled PTIM.

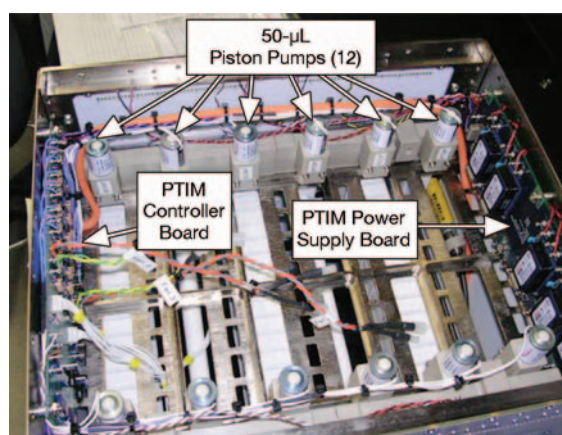


Figure 3. Pumps and circuit boards on underside of PTIM.

## Challenges Utilizing Nonmetallic Materials in the Development of the Advanced Biological Research System (ABRS)



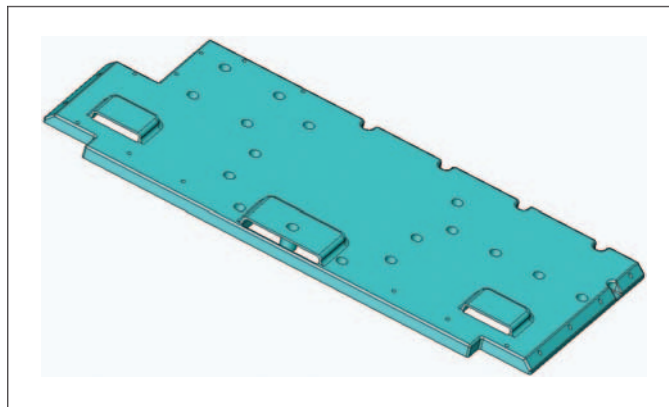
Bioregenerative Life Support  
System Operation/  
Validation/Control

The NASA KSC Biological Sciences Project Office is developing the Advanced Biological Research System (ABRS) for use in conducting microgravity life science experiments in low Earth orbit. The ABRS is being designed as an upgradeable, single middeck locker equivalent (MLE) hardware system to conduct a wide range of biological investigations of both short and long durations with sufficient flexibility to support not only currently planned microgravity studies of higher-order plant, but future, as-yet-unknown investigations of interest. The ABRS will be added to NASA's inventory of generic life science laboratory equipment (LSLE) to be used in NASA-funded investigations. This hardware system provides the ability to automatically control the atmospheric environment within two large, completely separate environmental research chambers (ERCs), each with independent environmental parameter set points (temperature, relative humidity, CO<sub>2</sub>, etc.).

As with many similar systems, polymers are used throughout this hardware assembly. The choice of plastics as an engineering material is a logical decision because of their manufacturing versatility and weight-to-strength ratio. Epoxies are the most widely used polymeric materials for adhesives, sealants, coatings, castings, and encapsulations. Epoxies offer unique versatility in application and performance. Their most desirable properties include high bond strength to a wide variety of different substrates, outstanding gap-filling capabilities, excellent electrical insulation, high chemical inertness, and outstanding resistance to shock and vibration. However, the use of nonmetallic materials in spaceflight hardware to be located in crew-habitable compartments must be done with care. Minimizing the potential safety hazard to the crew and vehicle is the prevailing requirement of any design, and all decisions and engineering trade-offs must be made so this area is not compromised. Issues of flammability, off-gassing, toxicity, and biocompatibility must all be considered prior to selecting a specific material. With these safety-related



*Fan cowling.*



*Air plenum cover.*



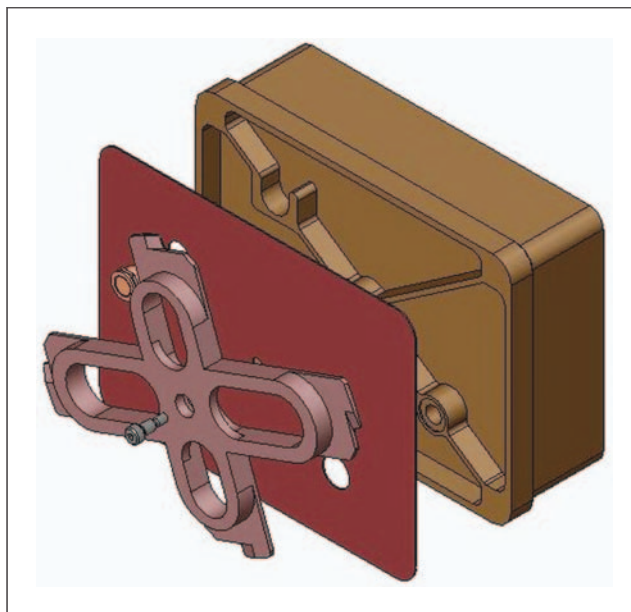
constraints directing the selection process, a two-part, room-temperature-cured epoxy manufactured by Master Bond Inc. (part # EP21FRNS) was chosen as a primary material for a number of components within the ABRs. This particular epoxy was chosen primarily because it is a flame-retardant UL94 V-0-certified system, it is a low-outgassing resin, it has previously been shown to have excellent biocompatibility properties, and its viscosity and working times make it a good material for casting and molding complex parts.

Soft tooling was fabricated and a number of prototype parts were cast using this epoxy, among them, a fan cowling, an air plenum cover, and a growth chamber base (see the figures.) During assembly and testing of these prototype parts, a problem was discovered. The cast parts did not mate correctly to their associated metal work. The parts fabricated from the epoxy were all larger than the engineering drawings called out. It was determined that the parts fabricated from this epoxy were dimensionally unstable. The flammability, offgassing, and biocompatibility properties of this epoxy were too attractive to abandon this material and search for alternatives. Much time had already been invested in this specific epoxy, and the schedule did not permit the research and testing of other materials.

Consultation with technical experts at Master Bond Inc. led to the hypothesis that, during room-temperature curing, free amines in the two-part epoxy system were reacting with water vapor in the ambient atmosphere. These additional water molecules were enough to cause these parts to gain as much as 10 percent in the overall dimension when fully cured. Master Bond chemists felt confident that curing the epoxy at elevated temperatures (150 to 200 °F) would prevent this amine-water reaction from occurring and lead to dimensionally stable parts. New hard tooling was fabricated to withstand these elevated temperatures and new parts were cast. Once the molds were filled with resin, the mold was placed in an oven at elevated temperature and the epoxy allowed to fully cure for more than 24 hours. Parts fabricated utilizing these techniques have proven to be dimensionally stable, and engineers are free to use a material with favorable properties for spaceflight hardware applications.

Contact: F.T. Ahmay ([Frederick.T.Ahmay@nasa.gov](mailto:Frederick.T.Ahmay@nasa.gov)), YA-E4, (321) 867-6044

Participating Organization: Bionetics Corporation (K.F. Anderson)



*Growth chamber base.*



## Transgenic Arabidopsis Gene Expression System (TAGES) Imaging System (TIS)



Remote Plant/  
Microorganism  
Health Sensing

The TIS design was started in November 1999 at the Bionetics Corporation at KSC, and a prototype was up and running by August 2000. The objective was to design a piece of hardware that could collect green fluorescent protein (GFP) expression data in real time aboard the Orbiter. It had to accommodate four square petri dishes in a quadrant and allow a camera transport system to image each petri dish in sequence over a period of time.

To achieve this, it was necessary to design around the following criteria:

- A light source to sufficiently illuminate the plants in the blue region (470 nanometers [nm]) and ensure that no green light (480 nm and above) is present in the illuminated field.
- A camera system capable of seeing small amounts of reflected light in the  $\lambda$  510- to 700-nm region.
- A transport system to move and position the camera along an X,Y axis to be able to image the four petri dishes.
- Computer control of everything to capture images over a period of time for download and retrieval.

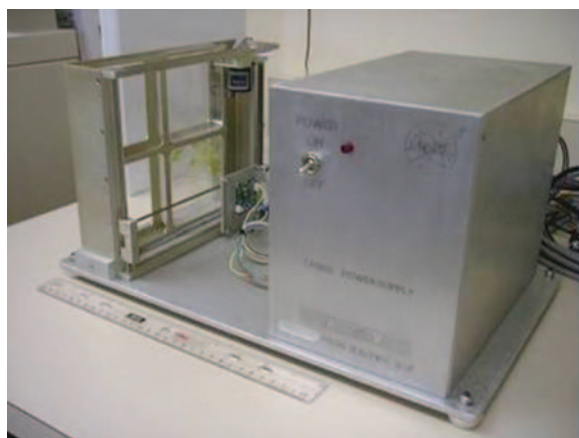


Figure 1. TAGES prototype.



Figure 2. Arabidopsis showing GFP.

The first-generation unit is shown in Figure 1. To achieve the GFP goals, two optical filters had to be designed. The first one had to be a low-pass filter for 470 nm and below. Because blue light-emitting diodes (LEDs) have a certain portion of the green spectrum in them, it was necessary to create a filter with a cut-off of 470 nm. The spectral response of the original design (468 nm  $\pm$  5 percent) cut off the green at 479 nm, which is present in the LEDs. The second filter had to be a high-pass filter allowing 510 nm and above to pass through. This was inserted in front of the charge-coupled device (CCD) and behind the camera lens. This prevented the need to optically coat the actual lens assembly. Also, a low-light CCD camera was chosen for the prototype, providing an excellent spectral response at low light levels.

The low-pass filter had to have a hole cut into it to allow the camera lens to pass through because most of the illumination comes from the front to achieve reflection of the GFP. This proved to be a major task for the glass manufacturer. The glass had to be optically coated on

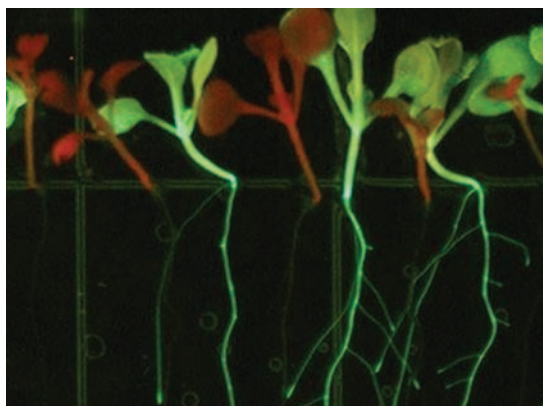


Figure 3. *Arabidopsis* showing GFP and red chlorophyll.

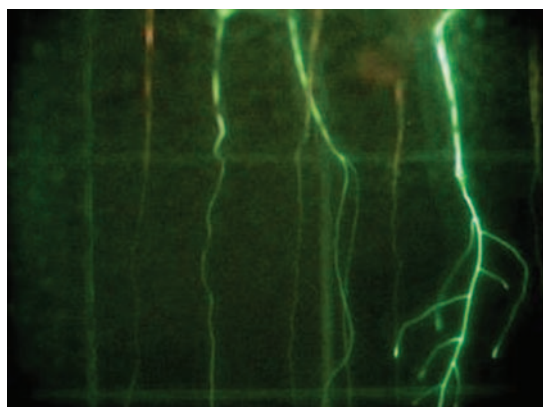


Figure 4. *Arabidopsis* GFP root growth.

both surfaces after cutting and proved to be very fragile to handle in the coating process machines.

Eventually, a compromise was achieved by increasing the thickness of the glass to 0.25 inch. While this resolved one issue, it created another—it required much more light to pass through to give adequate illumination.

The filter for the camera caused no problems and worked the first time. The filter was held in place using an optical adhesive.

One problem encountered was that the camera X,Y transport system jammed, requiring modification to the base hardware and support rails. Once redesigned, the unit was run and tested on several occasions.

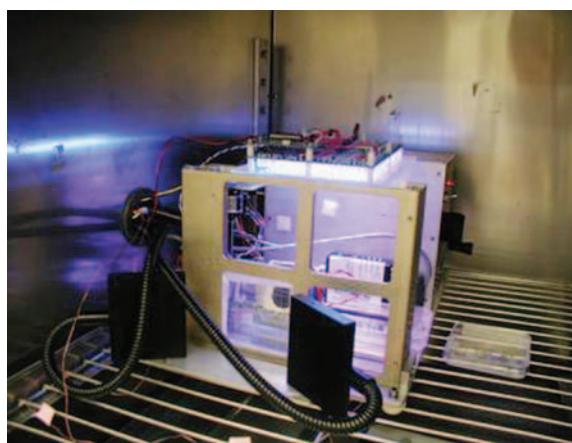


Figure 5. TAGES undergoing testing in the environmental chamber.

The next generation that has been started comprises the following changes:

- A four-camera system that eliminates the motorized transport system. (Depending upon testing, the number of cameras may be increased to obtain higher-fidelity images.)
- An increase in camera resolution to 2,046 pixels (horizontal) by 1,536 pixels (vertical).
- An LED illumination board encompassing all petri dishes with blue and white LEDs for GFP and normal imaging to be accomplished.

Once the hardware was completed, various science verification tests were carried out, with the results appearing in Figures 2 through 5.

Key accomplishments:

- Hardware operating successfully.
- Science verification testing completed.

Key milestone:

- Lessons learned to be implemented in the next-generation unit for flight.

Contact: G.J. Etheridge ([Guy.J.Etheridge@nasa.gov](mailto:Guy.J.Etheridge@nasa.gov)), YA-E4, (321) 867-6369

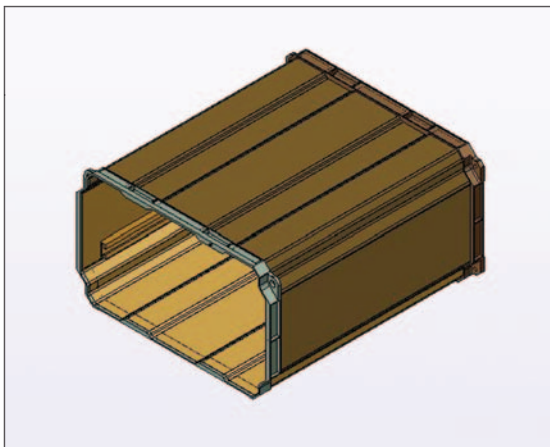
Participating Organizations: University of Florida (Dr. R.J. Ferl and Dr. A. Paul) and Bionetics Corporation (T. Murdoch)

## Role of Finite-Element Analysis Techniques in the Development of Life Science Payloads

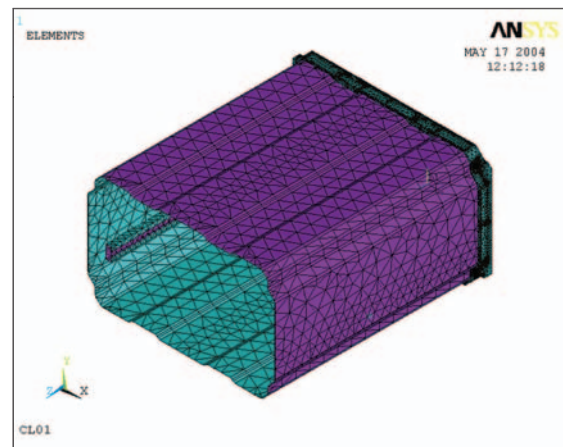
The Life Sciences Support Contract (LSSC) recently added a powerful tool to aid in the development of hardware to fly biological experiments. By their very nature, LSSC experiments require sophisticated hardware to control the environmental conditions. At the same time, Shuttle and International Space Station (ISS) operations impose demanding safety requirements on the hardware. The increasing number of environmental and hardware functions and the priority LSSC places on safety lead to complex mechanical designs where low-mass and high-strength goals must be met.

Finite-element analysis (FEA) techniques originated in the 1950s in response to the need for solutions to the complex structural problems faced by aerospace designers. The availability of ever faster computers fueled FEA development to the stage we see today. Engineers and scientists use commercially available or customized software to solve any number of mathematical models representing a variety of physical systems: structures under complex loading, dynamic response to vibration or shock inputs, thermal response to steady-state or transient heat inputs, interaction between thermal response and structural response, magnetic-structural and electrostatic-structural interactions, micro-electromechanical system (MEMS) behavior, etc. The advantage of such a tool is obvious in that it allows simulation of the system response before costly fabrication and testing.

One recent application of FEA has been the structural analysis of the Advanced Biological Research System (ABRS) hardware, a middeck-locker-sized payload designed to fly powered in the Shuttle middeck to transport live tissue and organisms to the ISS and conduct experiments in the ISS Express Rack. The system incorporates dual chambers with temperature and humidity control, CO<sub>2</sub> and ethylene scrubbing, environmental and video data logging capabilities, and dual banks of light-emitting diodes providing

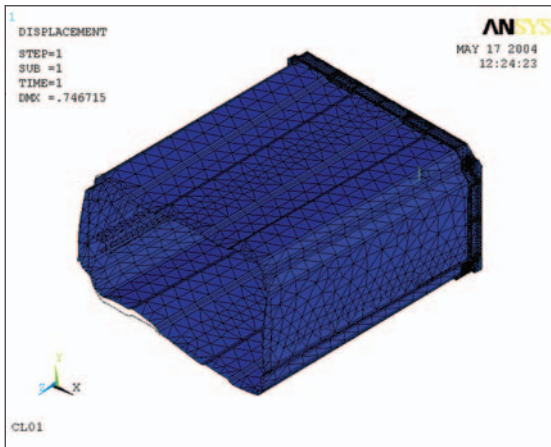


*A solid model is the starting point for the analysis.*



*The geometry is meshed, loads and boundary conditions are applied, and the solution is obtained.*





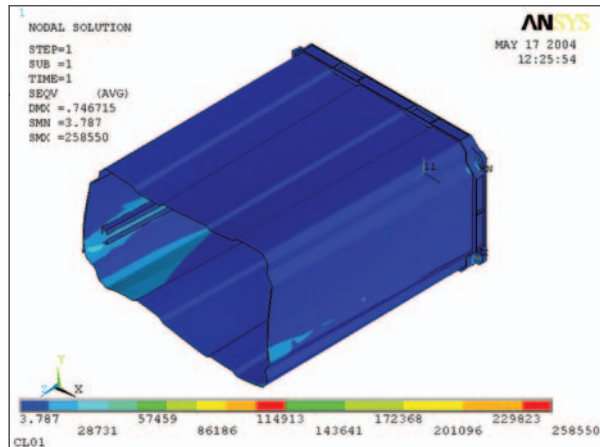
Parts of deformed shapes provide visual information about the model response to the applied loads and boundary conditions.

adjustable intensity and spectral distribution for plant crops.

The limits on weight and center-of-gravity location for middeck locker payloads and the reduced usable volume of the single middeck locker were driving forces in the mechanical design of the payload and the single middeck locker replacement structure that contains it. Using ANSYS, an FEA code with proven reliability and ample capabilities, engineers constructed a computer model of the locker structure, including the fasteners used to attach the payload to the Orbiter and join the different parts of the payload.

The geometry was of such complexity that classical stress analysis solutions would have been either too conservative or too aggressive in predicting the stresses under Shuttle liftoff and landing loads or emergency landing loads. The complete set of loads was composed of eight cases. The results predicted failure of the aluminum rivets joining the skin of the external locker to the mounting plate. The addition of two stiffeners to the inner walls of the locker resolved the problem by more evenly distributing the loads from the locker to the four attachment bolts, adding load-carrying fasteners, and substituting steel fasteners for the aluminum rivets.

Because of the complex loading condition and geometry, it is unlikely this vulnerability would have been identified by other types of analysis.



Stress component plots provide visual information about the ability of the structure to carry the applied loads and areas that are candidates for weight reduction.

Only a test to failure would have shown the problem, and by then the cost and schedule impact would have been all too obvious.

The analysis process starts with a solid model of the locker. An IGES formatter is used to export the geometry to ANSYS. The geometry model is then meshed, and boundary conditions and loads are applied. At this point, it becomes a finite-element model, and the solution is obtained. Plots of deformations and stress components help illustrate the response of the model to the loads applied. The solution files can then be selectively interrogated to obtain numerical solutions at selected nodes or elements.

Key accomplishment:

- Redesigned hardware to sustain specified loads with minimal impact to existing fabricated parts.

Key milestone:

- Extend the use of FEA to other areas of the ABRS payload and to other payloads.

Contact: G.J. Etheridge, ([Guy.J.Etheridge@nasa.gov](mailto:Guy.J.Etheridge@nasa.gov)), YA-E4, (321) 867-6369

Participating Organization: Bionetics Corporation (H.W. Wells)



## Denitrification Composter To Stabilize Space Mission Trash



*Bioregenerative Life Support  
System Operation/  
Validation/Control*

Treatment of solid wastes, or trash, is a critical issue for mid- to long-duration space habitation or transportation. Solid wastes are not stable because they are wet (40 to 90 percent moisture) and contain levels of soluble organic

compounds that can contribute to the growth of undesirable microorganisms with concomitant production of noxious gases and foul odors. The purpose of this research project is to determine the feasibility of using a denitrifying composter to stabilize trash from space habitation (Space Transportation System, International Space Station, and Advanced Life Support) activities. The method of approach starts with design of the denitrification composter, with design criteria derived from experimental variables to be manipulated and variables to be held constant. Key environmental and bioprocess parameters for evaluation are nitrate concentration and rate of addition, oxygen concentration, mixing duration and frequency, and inoculum. Parameters to be held constant are pH, temperature, moisture, carbon-to-nitrogen ratio (C:N), solid-waste feed material, size reduction, gas recirculation rate, trash addition rate, and mode of operation. Important performance parameters to be measured are minimization of undesired products (nitrous oxide, ammonia, and volatile organic compounds) and maximization of desired outcomes (biochemical oxygen demand removal, CO<sub>2</sub> production). The following tasks are required:

1. Design and modify the denitrification composter test stand apparatus.
2. Develop a denitrifying inoculum that is fed simulated space mission food wastes and nitrate with an oxygen-free gas phase.
3. Develop assays to measure key process performance/response variables (chemical and other assay methods for gaseous nitrous oxide, ammonia, and volatile fatty acids [VFAs]).
4. Perform baseline aerobic and denitrifying composter runs with a known feed (alfalfa plus aspen chips) with best estimates for environmental and process parameters.
5. Perform comparative compost runs with simulated space mission trash. Treatments include aerobic, to determine the amount of nitrate needed from CO<sub>2</sub> produced; denitrifying, with nitrate replacing oxygen and with oxygen-free gas recirculation; and both nitrate and oxygen (mixed respiratory conditions – aerobic and denitrifying).
6. Evaluate inocula that have been developed. Treatments include self-inoculated, inoculated with denitrifiers, and inoculated with known fermentative bacteria and dissimilatory nitrate reducers/ammonia producers.
7. Determine the effects of the nitrate addition rate on nitrous oxide production. Treatments include addition of all required nitrate at the start and daily nitrate addition. The amount to be added depends on the expected amount of CO<sub>2</sub> to be produced.
8. Determine the effects of mixing frequency and duration on nitrate distribution and on production of VFAs. Treatments include continuous mixing at 0.5, 1.0, and 2.5 rpm.



*Space Operations Bioconverter, a 28-L, invessel, rotating-drum composting unit.*



*Simulated food wastes before (left) and after (right) 10 days in the denitrifying compost.*

#### Key accomplishments:

- Modified existing 26-L-capacity aerobic compost vessel to meet project requirements.
- Completed the baseline aerobic and denitrifying composter runs with a known feed (alfalfa plus aspen chips) with best estimates for environmental and process parameters. Runs were inoculated with sublitter soil from a local palmetto scrub habitat. These runs demonstrated that an adequate inoculum was lacking.
- Developed both denitrifying and aerobic inocula (consisting of a mixed microbial community) through conventional microbiological enrichment techniques on alfalfa, aspen, and simulated space mission food wastes. These enrichment inocula were grown in bulk, harvested, and stored to provide a consistent, rapidly growing startup culture for each subsequent compost run.
- Continuing the comparative aerobic and denitrifying compost runs with simulated space mission trash. Ten runs have been completed. After four runs it was discovered that the pH of the feed was low, so the starting pH was adjusted to approximately 5.8 by adding sodium bicarbonate. These runs were inoculated with stored mixed microbial community cultures, which were developed as described in task 6.

#### Key milestones:

- Complete the comparative aerobic and denitrifying compost runs with simulated space mission food wastes. Also use these runs to evaluate the inocula that have been developed.
- Complete the remainder of the grant tasks, including the study of nitrate addition rates and the effects of mixing speed on denitrification. Determine the concentrations of undesired products, including nitrous oxide, ammonia, and VFAs.

Contact: Dr. J.C. Sager ([John.C.Sager@nasa.gov](mailto:John.C.Sager@nasa.gov)), YA-E4-B, (321) 861-2949

Participating Organization: Dynamac Corporation (Dr. J.L. Garland, K. Reid, T.J. Rector, M.E. Hummerick, and Dr. R.F. Strayer)

## Development of a VOC Filter Cartridge for Biological Experiments in Space

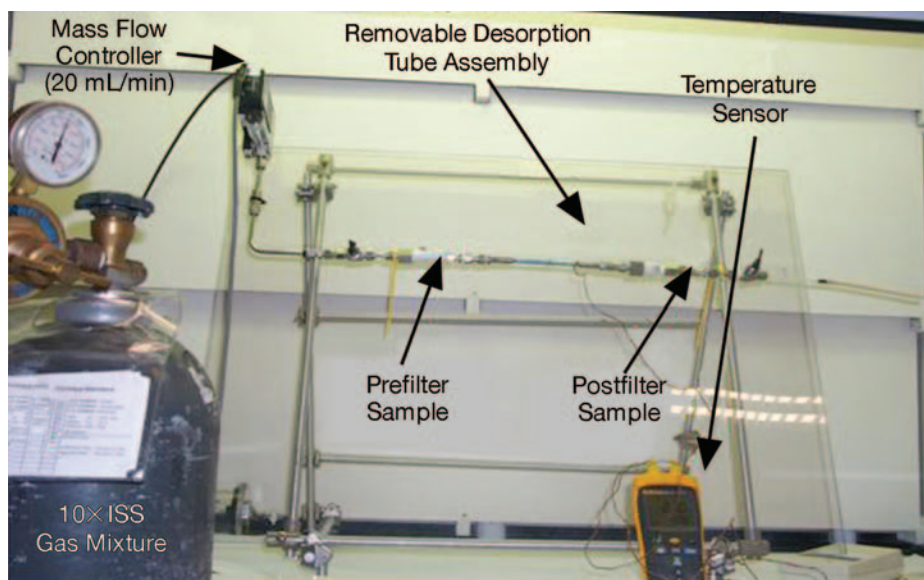


Remote Plant/  
Microorganism  
Health Sensing

The accumulation of volatile organic compounds (VOCs) in spacecraft cabin air can contribute to poor air quality and impose a threat to the health of the crew during long-term missions in space. Furthermore, removal of these VOCs represents an additional load on the air purification systems of the spacecraft. In addition, air quality also affects the quality of the science that can be carried out in spacecraft (e.g., the spacecraft maximum allowable concentration [SMAC] for ethylene is 294 ppm, but plants respond to concentrations of ethylene as low as 25 ppb). These concerns are important to NASA's goal of exploration, whereby humans and biological systems share a common air supply.

Biological (plant/animal/insect) experiments in space are potential sources of VOCs that can introduce trace contaminants into the cabin air of spacecraft. Science in these biological payloads may also suffer from effects caused by VOCs found in spacecraft cabin air.

The project objective is to develop a VOC filter cartridge that is passive (multiple passes over absorbent) and able to reversibly bind the VOCs after long-term storage. The filter cartridge should permit identification and quantification of VOCs and meet flight safety guidelines.



*Benchtop system for VOC filter media characterization.*

The proposed activities span a 2-year effort.

- Filter Media Characterization – select a mixed-bed, multifunction absorbent and determine the filter size and chemical specificity required to meet scrubbing limits required by plant payloads. The challenge is to find a suitable filtering medium to meet the scrubbing requirements of biological payloads in the available volume (FY 2004).
- Filter Cartridge Design – select a mechanical design of the filter cartridge suited to a particular application (FY 2005).
- Efficacy Testing – test the performance of the VOC filter in ground-based and flight plant experiments (e.g., Radish Assimilation in Spacecraft Testbed Atmospheres [RASTA] flight experiment) (FY 2005).

Key accomplishments:

- Organized two laboratories in the Space Life Sciences Laboratory for meeting project requirements.
- Identified several end users of technology (Advanced Life Support Plant Element, BioServe, Jet Propulsion Laboratory, Space Dynamics Lab).
- Designed, built, and tested a benchtop system for filter media characterization experiments.
- Developed and optimized procedures for loading desorption tubes and sampling prefilter and postfilter gas.
- Optimized and calibrated gas-chromatography-based methods for sample analysis of VOCs from the test system.

Key milestone:

- Conducted experiments designed to characterize several adsorbents. A mixture of 10× International Space Station (ISS) cabin air was filtered through 50 to 100 mg of absorbent, and preliminary filter performance data was calculated for seven ISS VOCs (ethylene, ethanol, methanol, dichloromethane, acetone, Freon 22, and acetaldehyde).

Contact: Dr. J.C. Sager ([John.C.Sager@nasa.gov](mailto:John.C.Sager@nasa.gov)), YA-E4-B, (321) 861-2949

Participating Organizations: Dynamac Corporation (Dr. O.A. Monje, J.T. Richards, and I. Eraso) and YA-F2-C (Dr. T.P. Griffin)



## Advanced Life Support (ALS) Project: International Space Station (ISS) Baseline Environmental Crop Studies



Bioregenerative Life Support  
System Operation/  
Validation/Control

The development of a Vegetable Production Unit (VPU) would probably be the first application of food and crop systems used both on ISS and long-duration-transit missions. Such systems, even though restricted in potential

because of their small size and limited power capabilities, would be useful in providing moderate quantities of fresh salad crops to augment the space menu as well as enhance the horticultural practices of the crew in preparation for lunar or Martian habitation. In addition, supplementing a crew's diet on near-term missions to ISS or on interplanetary missions with fresh-grown vegetables could promote positive physiological as well as psychological well being. The VPU would be open to ISS cabin air, making it accessible for the crew, and ambient CO<sub>2</sub> would be used for plant growth. As a result, the need for sophisticated hardware to control environmental parameters is reduced considerably. However, experience with growing salad crops in space, and especially under ISS ambient conditions, is very limited.

Current ALS crop systems research has focused on testing minimally processed crops under typical environmental conditions that would be encountered on ISS or on planetary transit vehicles. Four projects have been actively investigated over the past year in growth chambers located at the new Phytotron in the Space Life Sciences Laboratory. First, radish (*Raphanus sativus* L. cv. Cherry Bomb), onion (*Allium fistulosum* L. cv. Kinka), and lettuce (*Lactuca sativa* L. cv. Flandria) cultivars were grown in monoculture at 25 °C under 150, 300, or 450 μmol m<sup>-2</sup> s<sup>-1</sup> photosynthetic photon flux (PPF) and 400, 1,200, or 4,000 μmol mol<sup>-1</sup> CO<sub>2</sub> (Figure 1). Results indicated that edible yields were strongly influenced by additional incident PPF, as well as by increased CO<sub>2</sub> levels. Second, radish, onion, and lettuce were intercropped as a mixed culture to determine if the growth of crops within a common root and aerial environment affects plant productivity (Figure 2). When data was compared to the monoculture crops, there was no difference in the yields of either cultivar, suggesting allelopathic interactions did not occur in mixed-crop scenarios. Third, cultivar evaluations of fresh vegetables for inclusion in future ISS baseline studies were initiated. Three dwarf tomato (*Lycopersicon esculentum* L. cvs. Florida Petite, Red Robin, and MicroTina) and two dwarf pepper (*Capsicum annum* L. cv. Triton and Hanging Basket) varieties were tested for their growth characteristics under selection conditions of 25 °C, 50 percent relative humidity, 1,200 μmol mol<sup>-1</sup> CO<sub>2</sub>, and 300 μmol m<sup>-2</sup> s<sup>-1</sup> PPF (Figure 3). All varieties yielded high numbers of fruit under the experimental baseline conditions, and a decision on which cultivars will be used for future testing is underway. Fourth, experiments are being conducted to look at the anthocyanin (potential antioxidants) content of red romaine (*Lactuca sativa* L. cv. Outredgeous and Eruption) and red-leaf lettuce (cv. Red Sails) under increasing light intensities.

### Key accomplishments:

- Successfully moved plant growth operations from Hangar L to a new Phytotron in the Space Life Sciences Laboratory.
- Completed all ISS environmental baseline studies and mixed-crop studies under the 25 °C temperature regime.
- Completed dwarf tomato and pepper cultivar evaluation.
- Started light intensity studies for red romaine and red leaf lettuce.
- Selected cultivars for a strawberry baseline study with assistance from several key scientists at the USDA, University of Florida, and University of Maryland.



Figure 1. An example of 21-day-old hydroponically grown radish used in the ISS Baseline Environmental Food and Crop studies. The radish is grown as a monoculture with a recirculating NFT system.



Figure 2. An example of the hydroponic experimental apparatus in the Space Life Sciences Phytotron showing the 0.3-m<sup>2</sup> growing trays planted with a mixed crop of lettuce, radish, and onion plants illuminated with 300  $\mu\text{mol m}^{-2} \text{s}^{-1}$  PPf. Recirculating nutrient reservoirs containing the half-strength Hoagland's solution are located beneath the growing trays, and the solution is recirculated at approximately 1 L per minute per tray.

#### Key milestones:

- Initiate the 28 °C temperature regime for both ISS environmental baseline and mixed-crop studies.
- Initiate a strawberry cultivar evaluation study under hydroponic nutrient film technology (NFT) conditions.
- Initiate dwarf tomato and pepper baseline environmental tests.
- Quantify anthocyanin production in red lettuce cultivars grown under different light intensities.

Contacts: Dr. R.M. Wheeler ([Raymond.M.Wheeler@nasa.gov](mailto:Raymond.M.Wheeler@nasa.gov)), YA-E4-B, (321) 861-2950; and Dr. J.C. Sager, YA-E4-B, (321) 861-2949

Participating Organization: Dynamac Corporation (J.T. Richards, Dr. G.W. Stutte, and N.C. Yorio)



Figure 3. Examples of the dwarf tomato and pepper cultivar evaluation grown in hydroponic systems at the Space Life Sciences Phytotron.



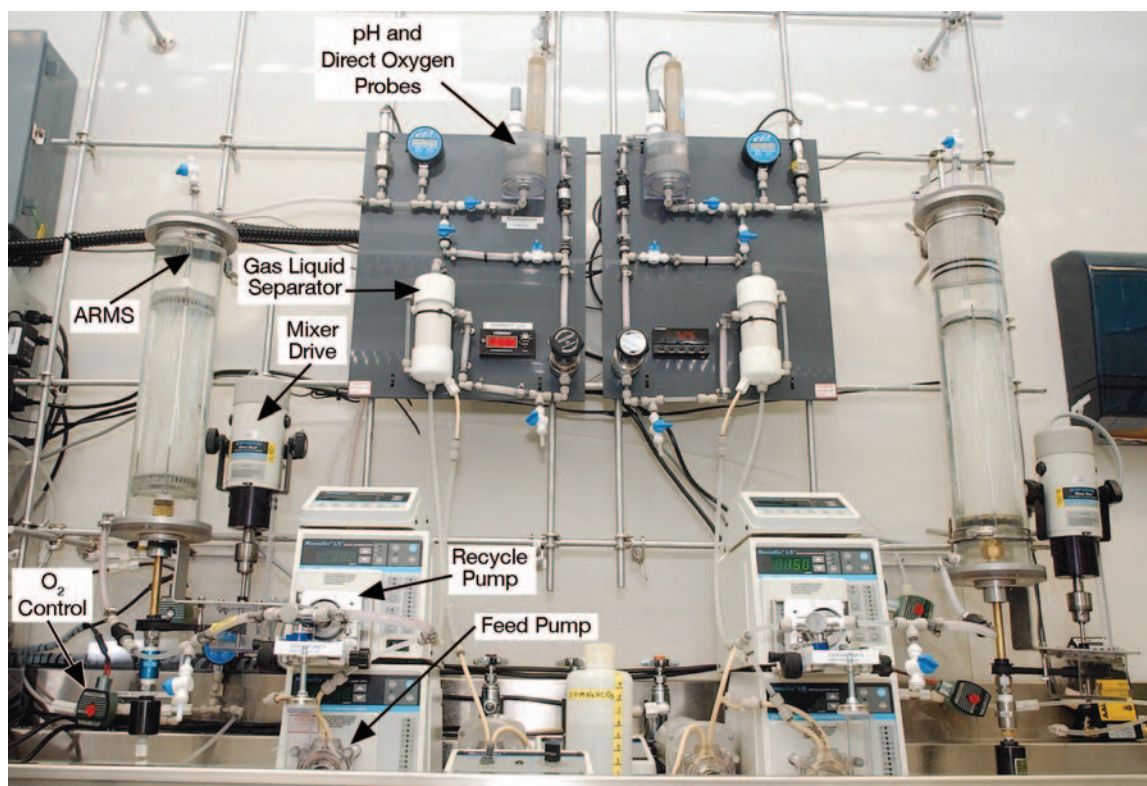
## Evaluation of an Aerobic Rotational Membrane System for the Treatment of Graywater Waste Streams



Bioregenerative Life Support  
System Operation/  
Validation/Control

Biological treatment may be an important component of recycling wastewater (urine, hygiene water, atmospheric condensate) into potable water in Advanced Life Support Systems. Mineralization of organic constituents (e.g., surfactants in hygiene water, short-chain hydrocarbons in the humidity condensate, and creatine and hippuric acid in urine) and conversion of ammonia from human urine to nitrogen gas via microbial processing should substantially improve performance of downstream physiochemical purification systems, such as reverse-osmosis membranes and ion exchange resins.

Ongoing ground research has demonstrated that significant removal of waste constituents can be achieved using biological treatment. Currently, research is focusing on the development of biological reactor systems (bioreactors) that will operate in a gravity-independent environment. The primary concerns in these systems are the separation of gas and liquid streams (oxygen/water) and the ability to keep innocuous by-product gases in solution by pressurization of the reactor vessel. To meet these criteria, membrane bioreactors for the treatment of urine waste streams are being investigated. The integration of membrane-aeration technology with biological water processors has direct application to wastewater treatment in microgravity because of the ability to diffuse gases across the membrane without two-phase interactions (gas-liquid). The current system under evaluation at the KSC Space Life Sciences Laboratory (SLSL) is the Aerobic Rotational Membrane System (ARMS).



ARMS reactor system.

The ARMS uses nonporous silicone membranes to deliver oxygen to bacterial films attached to the outside surface of the cylindrical, hollow-fiber membrane. This technology has been investigated extensively by other researchers; however, the rotation of the membrane fibers in the reactor vessel is novel to ARMS. Rotation of the membrane module containing the hollow fibers allows complete, mixed conditions within the reactor vessel. This complete, mixed environment diminishes gradients with respect to waste constituent concentrations and nutrients, increases mass transfer, and allows for the establishment of a uniform bacterial film layer across the axial length of the membrane surface, preventing wasted area and excess aeration of the bulk liquid.

#### Key accomplishments:

- 2003: Preliminary evaluation of membrane oxygen delivery values to use in determining adequate ARMS design information.
- 2004: Completion of ARMS design, construction, and engineering evaluation, which included hydrodynamic characterization and development of mass transfer correlations. Biological testing of ARMS was also begun in early 2004.

Contact: Dr. J.C. Sager ([John.C.Sager@nasa.gov](mailto:John.C.Sager@nasa.gov)), YA-E4-B, (321) 861-2949

Participating Organization: Dynamac Corporation (Dr. J.L. Garland, M.E. Hummerick, Dr. R.F. Strayer, Dr. M.S. Roberts, Dr. L.H. Levine, and T.J. Rector)



ARMS membrane module containing 115 individual hollow-fiber silicone membranes.



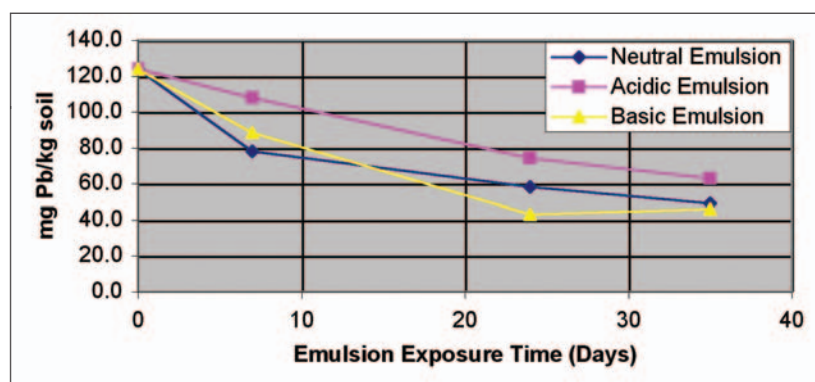
## *In Situ* Heavy-Metal Contaminant Removal Using Emulsified Iron

Of the 1,200 sites in the United States on the National Priority List for contaminated soil treatment, approximately 63 percent contain heavy-metal contamination, including lead, chromium, cadmium, and copper. Once heavy metals reach the environment, from sources including domestic and industrial effluent, they are persistent and cannot be biodegraded. The sediments can act both as sinks for pollutants and as sources of aquatic contaminants. Natural and human disturbances of the sediments can release the contaminants to the overlying water, where bottom-dwelling organisms may be exposed through direct contact, ingestion of sediment particles, or uptake of dissolved contaminants present in the water. Recent studies have shown that approximately 10 percent of the sediment found in the United States is contaminated with heavy metals.

Sediments have proven difficult to remediate *in situ* because traditional remediation techniques generate hazardous by-products. *Ex situ* remediation techniques are often costly, and the agitation caused by dredging the sediments can redistribute the contaminants in the water table.

The use of zero-valent iron ( $\text{Fe}^0$ ) is an *in situ* remediation technique currently under evaluation. The basic mechanism for removal appears to be reduction of contaminant metals followed by the subsequent precipitation of their insoluble forms. Initially,  $\text{Fe}^0$  filings were used to reduce the metal contaminants, but it has been shown that smaller iron particles, such as nanoscale iron, have higher initial reduction rates as well as a higher concentration of contaminant removal per mole of iron. This is because the surface area of the iron particle has a direct relationship to the number of active surface sites on the iron that are available to the contaminant metals. If the size of the particle is decreased, the specific surface area is increased, which leads to an increased rate of reduction.

Emulsion liquid-membrane (ELM) technology has been employed as a remediation technique for the removal of metals from wastewater because both extraction and stripping processes are performed in a single operation. An ELM is made by forming an emulsion between two immiscible liquids, such as oil and water, and is often stabilized by a surfactant. The materials to be transported through the ELM must dissolve in the membrane, diffuse through the membrane, and reverse the dissolution on the other side. Results for the removal of heavy metals from solution using oil-and-water emulsions have been demonstrated and have been shown to concentrate the contaminant in the interior of the emulsion droplet.



Concentration of lead remaining on soil after treatment with EZVI.

We have demonstrated the application of the combination of these two technologies through the use of emulsified zero-valent iron (EZVI) to treat sediments with heavy-metal contamination.

In our demonstration of removal of metal ions in solution by emulsion, microscale iron emulsion (with oil, water, and Span 85, a surfactant) removed 85 percent of lead from solution after 5 days. Similar nanoscale iron emulsion removed 94 percent of lead from solution in the same time.

Emulsion was also found to remove 80 percent of cadmium in 3 days. Our soil studies demonstrated removal of approximately 12 to 13 percent of lead for all emulsion samples. Acidic emulsion samples (pH of 4 to 5) showed the lowest removal at 50 percent after 5 weeks. Basic emulsion samples (pH of 9 to 10) displayed the best results at 65 percent removal after 3 weeks, with no improved removal after that time (see the figure). The results of the soil study using cadmium showed removal levels between 35 and 45 percent after both 1 and 3 weeks, with the basic emulsion showing the best results: 45 percent removal for both time frames. The results of a lead plating study are summarized in the table. The observed lead concentration was determined by analyzing the acid solution by flame atomic absorption analysis. This result was compared with the calculated lead concentration as determined by the amount of lead introduced into the sample, divided by the final sample volume, and adjusted for the percentage of iron recovered from the sample. Assuming even distribution of lead on the iron, analysis documented that 40 to 60 percent of the lead introduced to the sample was found to be on the iron.

The results of this study demonstrate that EZVI is a viable technique for *in situ* remediation of heavy metals in sediments. It has been shown that emulsified zero-valent iron is capable of removing lead ions both from solution and from soil. Further analysis must be performed to ensure all of the lead is plating out onto the zero-valent iron and is then recoverable at the end of the treatment. Additional work includes further investigation into the ultimate fate of the metal in the interior of the emulsion droplet; simulation of more complex environments, including sea water; and a small-scale field test to demonstrate the applicability of this technique in the environment.

Contact: Dr. J.W. Quinn ([Jacqueline.W.Quinn@nasa.gov](mailto:Jacqueline.W.Quinn@nasa.gov)), YA-C3-C, (321) 867-8410

Participating Organization: University of Central Florida (Dr. C.L. Geiger, Dr. C.A. Clausen III, K.M. Milum, and R. DeVor)

*The capture of lead on iron particles in the interior of the emulsion droplet.*

	Exposure (days)	Iron Recovered (g)	Iron Recovered (%)	Final Volume (mL)	Observed Lead Concentration (ppm)	Theoretical Lead Concentration (ppm)	Lead Plated (%)
Control 1a	2	0.4028	79.10	75.0	0.2	0.00	N/A
Control 1b	2	0.4081	80.15	75.0	0.3	0.00	N/A
Control 2a	7	0.4134	81.19	110.0	0.4	0.00	N/A
Control 2b	7	0.3604	70.78	100.0	0.2	0.00	N/A
Sample 1a	2	0.4139	81.28	75.0	0.6	2.17	27.68
Sample 1b	2	0.4484	88.06	75.0	1.0	2.35	42.58
Sample 2a	2	0.3548	69.68	90.0	0.8	1.55	51.67
Sample 2b	2	0.4261	83.68	77.0	1.1	2.17	50.61
Sample 3a	2	0.2684	52.71	75.0	0.8	1.41	56.92
Sample 3b	2	0.3101	60.90	75.0	0.7	1.62	43.10
Sample 4a	7	0.3076	60.41	75.0	0.8	1.61	49.66
Sample 4b	7	0.2655	52.14	75.0	0.8	1.39	57.54
Sample 5a	7	0.2824	55.46	75.0	0.9	1.48	60.86
Sample 5b	7	0.3799	74.61	76.0	1.3	1.96	66.21
Sample 6a	7	0.2629	51.63	76.0	0.9	1.36	66.24
Sample 6b	7	0.3440	67.56	75.0	1.2	1.80	66.61

## Appendix A



### KSC High-Priority Technology Needs

*Note: Articles from the KSC Research and Technology 2004 Report are listed under the applicable technology need.*

#### Hazardous-Leak Detection and Isolation

- Identifying and Quantifying Toxic Vapors Using an Electronic Nose (p. 12)
- Small Gas Analyzer for NASA and Commercial Applications (p.14)

#### Contamination Detection/Reduction/Cleaning

- Implementation of an Automatic Particle Counter Using an Acoustic Transducer (p.10)
- Color-Indicating Wipe for Cleaning Hypergolic Propellant (p. 28)
- Pressure Dependence of Insulator-Insulator Contact Charging (p. 64)
- Electro-Optic Method of Surface Charge Measurement (p. 66)
- Development of the Dust Particle Analyzer To Characterize the Size and Charge of Particles Suspended in the Martian Atmosphere (p. 72)
- Paschen Breakdown Experiments in a Simulated Martian Atmosphere (p. 86)

#### Integrated System Health Management Technologies

- Autonomous Flight Safety System (AFSS) – Phase III (p. 50)

#### Corrosion Protection and Detection Under Paint

- Self-Assembled Monolayers on Aluminum 2024-T3 (p. 74)
- Prediction of the Long-Term Corrosion Performance of Candidate Alloys for Launch Pad Applications Using dc Electrochemical Techniques (p. 76)
- Electrochemical Impedance Spectroscopy of Alloys in a Simulated Space Shuttle Launch Environment (p. 78)
- Nanotechnology for the Protection of Reinforcing Steel in Concrete Structures (p. 80)
- Single-Coat/Rapid-Cure Protective Coatings for Lining Tanks on U.S. Navy Ships (p. 82)

#### Task/Process Modeling and Simulation

- Toolkit for Enabling Adaptive Modeling and Simulation (TEAMS) (p. 96)
- Schedule and Activity Generator/Estimator (SAGE) (p. 100)
- Generic Simulation Environment for Modeling Future Launch Operations (GEM-FLO) (p. 102)
- Shuttle Operations Simulations (p. 104)
- Shuttle Operations Root Cause Analysis Database (p. 106)
- System Reliability of Multielement Integrated Testing (MEIT) (p. 112)
- Wing Leading-Edge Structural Subsystems and Reinforced Carbon-Carbon (RCC) Orbiter Processing Facility (OPF) Area/ Access Enhancement (p. 114)
- TAL Site Heat Shield Removal Study (p. 116)
- A Discrete-Event Simulation Model for Spaceport Operations (SPACESIM) (p. 118)
- NASA Faculty Fellowship Program (NFFP) 3-D Modeling (p.122)
- External Tank 3-D Model Creation Techniques (p. 124)

## **Wire Inspection and Repair**

- Polyimide Wire Insulation Repair Material (p. 68)

## **Intelligent Work Instruction/Work Control Systems**

- Human Factors Investigation Refinements (p. 98)

## **Propellant Loading/Servicing/Storage**

- Highly Reliable Liquid Oxygen (LOX) Pump for Vehicle Loading (p. 30)

## **Resource, Personnel, and/or Foreign Object Debris (FOD) Identification and Tracking**

- Ground Camera Photogrammetry: 3-D Debris Trajectory Analysis (p. 2)
- Ground Camera 3-D FOD Tracking Software (p. 4)

## **Communications Technology Upgrades**

- Utilizing MIL-STD-1553B Digital Data Bus Devices Across an IEEE-1394A Serial Bus (p. 22)

## **Localized Weather Forecasting and Measurement**

- Effect of Clouds on Optical Imaging of the Space Shuttle During the Ascent Phase:  
A Statistical Analysis Based on a 3-D Model (p. 44)

## **Self-Contained Atmosphere Protective Ensemble (SCAPE) Electrostatic Discharge (ESD) Control Enhancements**

- A Wearable Electrostatic Hazard Detection System (p. 88)

## **Nondestructive Composite Material and Bond Evaluation**

## **Decision/Data Models and Analysis**

- Virtual Testbed for Spaceport Models (p. 120)

## **Seamless Command and Control Coordination**

- Real-Time POSIX Threads for Linux (p.16)
- Hexagonal Fractal Multiband Antenna (p. 38)
- Advanced Data Description Exchange Services for Heterogeneous Vehicle and Spaceport Control and Monitoring Systems (p. 56)
- Emerging Communication Technology (ECT) (p. 58)



## **Water Detection**

### **Mission Data Feedback and Analysis**

- Iridium Flight Modem (p. 48)
- Development of Rocket Acoustic Prediction Tool (RAPT) (p. 90)

### **Minimally Intrusive Repair and Self-Healing Systems**

### **Window Inspection**

### **Improved GN<sub>2</sub> Pipeline Gas Filtration**

### **Ding/Chip Tracking and Evaluation**

### **Defect/Damage Location and Spacecraft Handling Systems**

- Orbiter Wing Tip Alignment Tool (p. 126)
- Scaling Device Software for Measuring the Size of Remote Objects (p. 20)

### **Improved Helium Flow Rate and Quantity Measurements**

### **Advanced Planning and Scheduling Tools**

- AreaAdvisor – Spatial, Real-Time Resources Intelligence (p. 110)

### **Hydrogen Vent Recovery**

### **Spaceport/Range Situational Awareness**

### **Helium Recovery and Purge Gas Substitution**

### **Elemental and Gas Composition Sensors**

### **Payload Environment Models**

### **Flight Environment Measurement**

### **Spacecraft Nutation Models**

- Parameter Estimation of Spacecraft Fuel Slosh Mode (p. 26)

## **Risk Assessment Tool**

- Passive Millimeter Wave Imaging (p. 42)

## **Large Material and Equipment Handling**

## **Modular Support Equipment**

## **In Situ Resource Utilization (ISRU)**

## **Radiation Protection Technologies**

- First-Order Image Charge Calculator for Conducting Spheres (p. 8)
- Electrostatic Radiation Shielding (p. 18)

## **TDRSS-Compatible Transceiver**

- Four-Channel IRID-106 Telemetry Decoder on a PC-104 Plus Card (p. 60)
- Space-Based Telemetry and Range Safety (STARS) 2004 (p. 46)
- Real-Time Telemetry Display System (RTTDS) (p. 54)

## **Unmanned Aerial Vehicle Platforms**

## **Space and Air Traffic Management System**

- Aircraft Attitude Drift Correction Using a Heading-Based Reset Function (p. 40)
- Latest Enhancements for the Microwave Scanning Beam Landing System (MSBLS) Flight Inspection System (p. 52)

## **Efficient Lighting Systems**

- Plant Lighting Systems (p. 136)

## **Remote Plant/Microorganism Health Sensing**

- Bioluminescent Monitoring of Opportunistic Pathogens in the Spacecraft Environment (p. 138)
- Transgenic Arabidopsis Gene Expression System (TAGES) Imaging System (TIS) (p. 144)
- Development of a VOC Filter Cartridge for Biological Experiments in Space (p. 150)

## **Bioregenerative Life Support System Operation/Validation/Control**

- Advanced Life Support Research: Systems Analysis of Waste (p. 130)
- Porous Tube Insert Module (PTIM) Assembly and Integration: A Modular Tray Supporting Both Porous Tube and Substrate Nutrient Delivery Systems for Plant Studies in Space (p. 134)
- Sensing and Control System Development in Support of the Water Offset Nutrient Delivery Experiment (WONDER) (p. 140)
- Challenges Utilizing Nonmetallic Materials in the Development of the Advanced Biological Research System (ABRS) (p. 142)
- Denitrification Composter To Stabilize Space Mission Trash (p. 148)
- Advanced Life Support (ALS) Project: International Space Station (ISS) Baseline Environmental Crop Studies (p. 152)
- Evaluation of an Aerobic Rotational Membrane System for the Treatment of Graywater Waste Streams (p. 154)

## **Remote Payload Testing**

## **Payload Mass and Center-of-Gravity (CG) Monitoring**

## **Bird Abatement System**

## **Thermal Protection System (TPS) Process Enhancement/Automation**

- Moisture-Resistant Thermal Protection System (TPS) Materials (p. 92)

## Appendix B

### Florida Space Research and Education Grant Program

The Florida Space Grant Consortium (FSGC) was formed in 1989 when NASA implemented the National Space Grant College and Fellowship Program. FSGC was one of the 16 founding space grant consortia. Currently there are space grant programs active in all 50 states as well as in Puerto Rico and Washington, D.C. When combined with the Land Grant and Sea Grant Programs, Space Grant forms the final leg of a triad of Federally mandated programs addressing critical national needs in education, research, and service.

FSGC is administered through the University of Central Florida (UCF) and the Florida Space Institute, and its main offices are located at the Astronaut Memorial Foundation's Center for Space Education, on the grounds of the KSC Visitor Complex. The consortium is a voluntary association of 16 public and private Florida universities and colleges. The consortium also includes all of Florida's community colleges, as well as the Florida Space Authority, the Higher Education Consortium for Science and Mathematics, KSC, the Astronaut Memorial Foundation, and the Orlando Science Center.

FSGC supports the expansion and diversification of Florida's space industry by providing grants, scholarships, and fellowships to students and educators from Florida's public and private institutes of higher education. FSGC's vision is based on three basic themes: spaceport technology, living and working in space, and remote sensing, all of which directly relate to areas of emphasis for KSC and Florida and provide a framework for education and research programs that capitalize on the excitement and vitality of Florida-based space activities.

FSGC, KSC, and Florida share the following goals:

- Promotion of aerospace education to improve science, technology, engineering, and mathematics education statewide.
- Development of Florida's aerospace workforce.
- Expansion of minority involvement in aerospace programs.
- Expansion of aerospace research capabilities within Florida's colleges and universities.
- Sponsorship of research activities that support NASA and Florida aerospace development priorities.

In advancing these goals, FSGC has emphasized undergraduate and graduate student research and statewide competitive solicitation and peer review of projects for FSGC sponsorship. FSGC has also maximized its leveraging of state funding, KSC resources, and matching investments from academic and corporate partners. NASA's modest investment in FSGC has been multiplied many times through its partnerships.

FSGC's fellowship program provides a prestigious instrument to attract the best and brightest U.S. citizens to space-related graduate studies in Florida. The purpose of its higher-education programs is to provide opportunities for Florida undergraduate students to become actively involved in ongoing research programs. Its research programs support the expansion and diversification of Florida's aerospace industry by increasing statewide academic involvement in space research,



technology development, engineering, education, and training programs. FSGC's pre-college activities fund student experiment and teacher development programs and have added a strong component designed to influence education policy and support systemic reform efforts in the state. FSGC conducts a number of public outreach programs. Visit our public outreach page at <http://fsgc.engr.ucf.edu/index2.html> for a description of the programs.

The Florida Space Research and Education Grant Program (FSREGP), jointly funded by FSGC, the Florida Space Research Institute, and UCF, combines state, Federal, and other funds for competitive award to projects sponsored within, or conducted in partnership with, the state's public and private academic institutions. Funding is intended to support research that will compete for larger sponsored research awards, attract and leverage other Federal or industry funding, produce technologies that lead to commercial opportunities, promote Florida leadership in emerging aerospace technologies, and/or in other ways enhance the technological competitiveness of Florida universities and space industry. Grants are awarded within three broad categories: Spaceport and Range Technology Development (defined by KSC R&D priorities), Space-Based Research and Payload Development, and Space Education and Training Programs. Proposals are judged on scientific/technical merit; relevance to the expansion and diversification of Florida's aerospace industry; potential for continued project development, including commercial or Government support; qualifications of the project team; and soundness of the proposed work plan, budget, and schedule.

The following Spaceport Technology Development projects were funded in 2003 for a total of \$100,000: Automated Inspection of Orbiter Flaws; Simulation Training Tool; Statistical Process Control for Shuttle Maintenance; and Integration Thermal Protection Systems for Reusable Launch Vehicles.

Key accomplishments (1999 to 2003):

- Evaluated 223 proposals.
- Awarded funding of more than \$3.1M to 69 projects, involving 53 graduate students, 17 undergraduate students, 24 industry participants, 12 universities, 2 community colleges, and 81 faculty members.

Contact: L.M. Freeman ([Michael.Freeman@nasa.gov](mailto:Michael.Freeman@nasa.gov)) XA-D1, (321) 867-4035

Participating Organization: Florida Space Grant Consortium (Dr. J. Mukherjee and Dr. S. Durrance)



Florida Space Grant Consortium Web site.

# INDEX

## A

Adamson, T.D., 115  
Ahmay, F.T., 143  
Amador, Dr. J.J., 57  
Anderson, K.F., 143  
Anderson, R.A., 83  
Anton, V.M., 51  
Arens, E.E., 67  
Arkin, Dr. CR., 15

## B

Baker, D.C., 115, 117  
Ballard, K.C., 21  
Barker, Dr. R.L., 133  
Barnes, M.S., 115  
Barth, T.S., 95  
Bastin, Dr. G.L., 43, 59  
Bauman, W.H., III, 45  
Benjamin, Dr. P.C., 97  
Birr, R.B., 47, 49, 55  
Blum, A.D., 117  
Bodiford, S.C., 113  
Botts, C.D., 43  
Brandt, B., 123, 125  
Brown, C.J., 115  
Buford, G.A., 115

Buhler, Dr. C.R., 73, 87

Bull, J.B., 51  
Bundick, S.N., 47  
Burns, B.C., 115, 117  
Burtness, K.A., 135, 141

## C

Calle, Dr. C.I., 63, 65, 67, 70, 73, 87, 88  
Calle, Dr. L.M., 75, 77, 79, 81  
Campbell, T.A., 29  
Carew, W.R., 117  
Carrol, J., 23  
Castillo, E., 115  
Chang, H.C., 51  
Chaos, Dr. M., 11  
Chau, S., 23  
Chen, Dr. R.H., 11  
Cipolletti, S.L., 115, 117  
Clausen, Dr. C.A., III, 157  
Clements, Dr. J.S., 87  
Closen, M.L., 117  
Cook, Dr. R.P., 17  
Cox, R.B., 21  
Crisfulli, J.B., 43  
Curran, J.J., 83

## D

Daumer, K.A., 139  
Davis, R.D., 57  
Day, L., 23  
Denson, E.C., 47, 61  
Deremer-Cook, E.J., 115, 117  
DeVor, R., 157  
Drysdale, Dr. A.E., 131, 133  
Durrance, Dr. S., 165

## E

Eraso, I., 151  
Erdogan, T., 43, 53, 59  
Eryilmaz, Dr. B., 27  
Etheridge, G.J. 145, 147  
Ewald, J.R., 99

## F

Ferl, Dr. R.J., 145  
Ferrell, B.A., 51  
Fitzpatrick, L., 31  
Ford, D.M., 85  
Forney, C.S., 61  
Franco, R., 113  
Frankos, D.J., 99  
Freeman, L.M., 165

# INDEX

- G**
- Gangadharan, Dr. S., 27
- Garland, Dr. J.L., 139, 149, 155
- Garton, H.L., 133
- Gass, T., 49
- Geiger, Dr. C.L., 157
- Gibson, Dr. T.L., 31, 69
- Girard, D.R., 115, 117
- Glasscock, D.O., 47
- Godfrey, Dr. G.S., 123, 125
- Goins, Dr. G.D., 137
- Gompers, D.J., 117
- Grantham, G.L., 115
- Green, J.M., 115
- Griffin, Dr. T.P., 13, 15, 151
- Groh-Hammond, M.M., 99, 115, 117
- Gross, Dr. F.B., 70
- H**
- Haddad, G.F., 11
- Hall, E.W., 117
- Hargrove, P.D., 115
- Harlacher, M., 47
- Harris, W.G., 43, 59
- Haskell, W.D., 21, 43, 49, 59
- Hasselbrack, Dr. S.A., 133
- Haus, S.M., 91
- Henderson, Dr. G.M., 93, 95, 109, 113
- Hintze, Dr. P.E., 75
- Hoffman, M.J., 115
- Hogue, M.D., 65
- Hollis, P.A., 99, 115, 117
- Hongamen, A., 43
- Hooper, J.M., 29
- Hornyak, D.L., 61
- Hosni, Dr. Y., 113
- Houseman, J., 15
- Hummerick, M.E., 149, 155
- Huynh, T., 23
- I**
- Immer, Dr. C.D., 55
- J**
- Janda, E.J., 117
- Jeffers, J.R., 117
- Jolley, Dr. S.T., 31, 69
- K**
- Kandula, Dr. M., 43, 91
- Kap, F.J., 123, 125
- Kelemen, M.S., 117
- Kibelka, G., 15
- Kickbusch, T.E., 111
- Kim, Dr. H.H., 137
- King, D.R., 115
- Kiriazes, J.J., 53
- Klinko, S.J., 3, 4
- Kolody, Dr. M.R., 79, 81
- Kremer, S.E., 51
- Kruhm, D.A., 1
- Kruse, P.L., 117
- Kuhn, J.E., 115
- L**
- LaBrie, M.E., 115
- Lakaszcyk, J., 117
- Lane, Dr. J.E., 3, 4, 7, 9, 19, 21, 41
- Lane, R.E., Jr., 45
- Lanzi, R.J., 51
- Larsen, D.C., 115, 117
- Lawrence, B.A., 115, 117
- Leger, B.P., 135, 141
- Levine, Dr. H.G., 135, 141
- Levine, Dr. L.H., 155
- Linnell, Dr. B.R., 13
- Linthicum, M.L., 117
- Lufkin, J., 53

# INDEX

## M

MacDowell, L.G., 77, 79, 83  
Madura, J.T., 45  
Manley, W.C., 117  
Mantovani, Dr. J.G., 73  
Marin, J., 51  
Martin, J., 83  
Mazumder, Dr. M.K., 73  
McCleskey, C.M., 100, 106  
McCown, Dr. R., 70  
Merceret, Dr. F.J., 45  
Metzger, P.T., 7, 9, 19  
Mills, R.E., 115, 117  
Milum, K.M., 157  
Mollaghasemi, Dr. M., 102, 105  
Monje, Dr. O.A., 151  
Montalvo, E.N., 117  
Morrison, R.L., 61  
Mucciolo, Dr. E.R., 65  
Mukherjee, Dr. J., 165  
Murdoch, T., 135, 141, 145  
Murray, A.J., 49  
Murray, J., 43  
Murtland, K.A., 43

## N

Neely, C.G., 115  
Nelson, R.A., 37, 43, 59  
Nevins, M.R., 119  
Notardonato, W.U., 25, 33  
Novak, Dr. M.J., 31  
Nowicki, A.W., 67, 73, 87

## O

Otero, I.H., 23

## P

Parks, J.L., 47, 51  
Parks, S.L., 127  
Parrish, Dr. C.F., 31, 69  
Patel, P., 93  
Paul, Dr. A., 145  
Peabody, P.A., 117  
Peaden, C.J., 121  
Peale, Dr. R.E., 65  
Peck, L.D., 115, 117  
Pisula, K.M., 99  
Pittman, D.M., 35  
Polk, J.D., 43  
Pracek, R.M., 115  
Prenger, J.J., 135, 141

## Q

Quincy, C.D., 129  
Quinn, Dr. J.W., 81, 157

## R

Rabelo, Dr. L., 121  
Rector, T.J., 149, 155  
Reid, K., 149  
Resnick, Dr. M.L., 109  
Reynold, M., 23  
Rhodeside, G.R., 97  
Richards, J.T., 137, 151, 153  
Rieck, E.G., 117  
Riley, H.W., 99  
Ripp, Dr. S., 139  
Ristow, J., 27  
Rivera, J.E., 21  
Roberts, Dr. M.S., 155  
Roberts, T.W., 115  
Robinson, G.F., 51  
Rorden, D., 123  
Rottmund, M.E., 35  
Rouzan-Wheeldon, D.T., 135, 141  
Ruiz-Torres, Dr. A.J., 100



# INDEX

## S

Sager, Dr. J.C., 131, 133, 135, 137, 139, 141, 149, 151, 153, 155

Sakahara, R.D., 47

Santuro, S.A., 51

Sayler, Dr. G.S., 139

Schafer, E.J., 17

Schwindt, P.A., 123, 125

Scott, M.M., 43, 53

Scruggs, B.J., 133

Sepulveda, Dr. J., 121

Short, D.A., 45

Simmons, S.M., 51

Simpson, Dr. J.C., 41, 47, 49, 51

Simpson, Dr. M.L., 139

Smith, J.A., 47

Sobchak, T.C., 47

Spinale, A.C., 135, 141

Stager, M.A., 47

Stankiewicz, E. 85

Steele, Dr. M.J., 102, 105, 119

Stelges, K.S., 115, 117

Stevenson, C.G., 21

Stirling, J.L., 115, 117

Stottler, D., 111

Strayer, Dr. R.F., 149, 155

Stutte, Dr. G.W., 137, 153

Sudermann, J.E., 27

Sweeney, G.P., 99

## T

Tang, P.W., 39

Tao, Dr. Y.X., 33

Taylor, V.W., 115

Thompson, Dr. D.B., 133

Toney, J.H., 99

## U

USAF 30th and 45th Range Safety  
Offices, 51

## V

Valencia, L.M., 47, 55, 61

Velez, I.F., 123, 125

Vinje, R.D., 77, 79

Vu, Dr. B.T., 91

## W

Wagner, K.R., 115

Wahid, Dr. P.F., 39

Wampler, D.L., 47

Ward, C.N., 85

Waterman, R.D., 1

Weheba, Dr. G., 113

Wells, H.W., 135, 141, 147

Wessells, R.L., 49

Wheeler, Dr. R.M., 137, 153

Whiteman, D.E., 47

Wilkhu, S.S., 115, 117

Willard, D.E., 127

Willis, J., 87

Winters, K.A., 45

## X

## Y

Yorio, N.C., 137, 153

Young, R.C., 29

Youngquist, Dr. R.C., 3, 4, 7, 9, 19,  
21, 43, 127

## Z

Zapata, E.Z., 100, 102, 105, 106

Zeitlin, N.P., 81

Zhang, Dr. Y., 88

Zoerner, R.D., 51, 55